UNIVERSITY OF SOUTHAMPTON

FACULTY OF NATURAL AND ENVIRONMENTAL SCIENCES

OCEAN AND EARTH SCIENCE

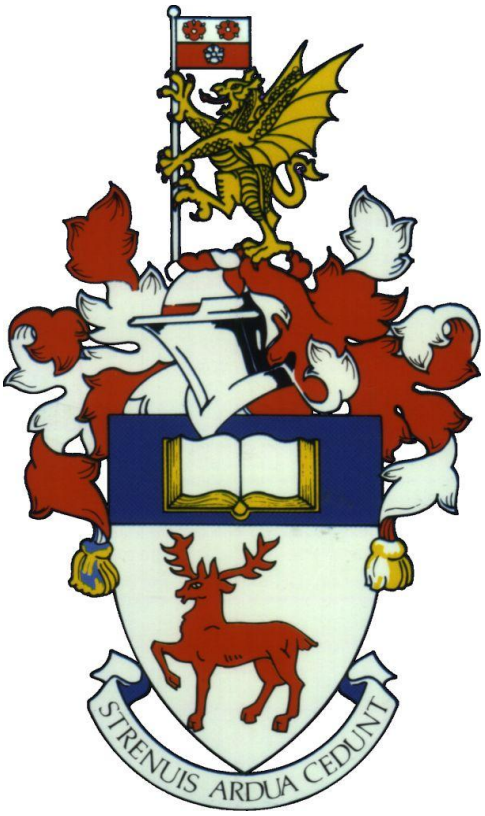

Heme *b* in marine cyanobacteria and the (sub-) tropical North Atlantic

by

David James Honey

Thesis for the degree of Doctor of Philosophy

August 2012

Abstract

Heme *b* is the iron containing prosthetic group to an important pool of iron proteins known as the hemoproteins. Hemoproteins are functionally diverse, playing key roles in photosynthetic and respiratory electron transfer (e.g. cytochrome b_6f, photosystem II, cytochrome bc_1) among other fundamental biological processes. Heme *b* is the most naturally abundant heme structure, but data regarding hemes in the marine environment are limited. An investigation has been conducted to improve our understanding of heme *b* abundance in marine organisms through laboratory monoculture studies of three marine cyanobacteria grown under varying total iron concentration. The unicellular cyanobacteria *Synechococcus* sp. WH7803 was examined under three total iron concentrations: 12 nmol L^{-1} (low), 120 nmol L^{-1} (medium) and 1200 nmol L^{-1} (high). The marine diazotrophs (i.e. nitrogen fixers) *Crocosphaera watsonii* (WH8501) and *Trichodesmium erythraeum* (IMS101) were studied under six total iron concentrations between 0 and 120 nmol L^{-1}. Cultures were analysed for heme *b*, chlorophyll *a*, particulate organic carbon (POC) and particulate organic nitrogen (PON) concentration. Nitrogen fixation rates and biophysical measurements (F_v/F_m and σ_{PSII}) were also obtained for diazotroph cultures. Field data regarding the concentration of heme *b*, chlorophyll *a*, POC and PON as well as nitrogen fixation rates were collected during two research cruises in the subtropical North Atlantic (STNA, D346) and tropical North Atlantic (TNA, D361); an oceanographic region known to demonstrate high nitrogen fixation rates and receive significant dust (iron) deposition from the Saharan and Sahel deserts of Western Africa.

Cultures of *Synechococcus* sp. WH7803 showed evidence of iron stress at low iron treatments via reduced maximum growth rates (μ_{max}), total biovolume and chlorophyll *a* concentration. This was also reflected by a significant reduction in cellular heme *b* content per unit carbon (heme:C) at the lowest iron concentration. An estimated heme *b* requirement between 1.0 and 1.5 µmol mol^{-1} C is proposed for *Synechococcus* sp. WH7803 in order to facilitate μ_{max}. Chlorophyll *a* to heme *b* ratios (chl:heme) were significantly decreased in low iron cultures of *Synechococcus* sp. WH7803, suggesting *b*-type hemoproteins were conserved when iron stressed. Cultures of *Crocosphaera* and *Trichodesmium* were similarly influenced by the availability of iron, with reduced total biovolume and chlorophyll *a* concentration reported at low iron treatments. However, heme:C ratios were maintained at approximately 1.5 and 0.5 µmol mol^{-1} C for *Crocosphaera* and *Trichodesmium* cultures, respectively. A high iron requirement is associated with marine diazotrophs relating to the iron-rich non-heme nitrogenase enzyme complex responsible for nitrogen fixation. Nitrogen fixation rates increased as total iron concentration increased, with *Trichodesmium* demonstrating four-fold higher rates than *Crocosphaera* at corresponding iron concentrations. It has been suggested that relatively low heme *b* contents of *Trichodesmium* cultures resulted from increased nitrogen fixation activity. Furthermore, heme:C ratios of *Crocosphaera* and *Trichodesmium* were typically lower than five eukaryotic phytoplankton previously investigated, potentially related to the allocation of iron for nitrogen fixation. Mean heme:C ratios from cruises in the STNA and TNA were 0.64 and 0.66 µmol mol^{-1} C, respectively. Results could imply the region was iron stressed and/or dominated by cyanobacteria. Evidence is also presented suggesting a possible inverse relationship between nitrogen fixation and heme:C ratio in the TNA which could be attributed to natural populations of *Trichodesmium*.

Contents

Appendix 1

Appendix 2

List of figures

List of tables

Declaration of authorship

I, David James Honey,

declare that the thesis entitled

Heme *b* in marine cyanobacteria and the (sub-) tropical North Atlantic

and the work presented in the thesis are both my own, and have been generated by me as the result of my own original research. I confirm that:

- this work was done wholly or mainly while in candidature for a research degree at this University;
- where any part of this thesis has previously been submitted for a degree or any other qualification at this University or any other institution, this has been clearly stated;
- where I have consulted the published work of others, this is always clearly attributed;
- where I have quoted from the work of others, the source is always given. With the exception of such quotations, this thesis is entirely my own work;
- I have acknowledged all main sources of help;
- where the thesis is based on work done by myself jointly with others, I have made clear exactly what was done by others and what I have contributed myself; and
- the following work has been published:

Honey, D. J., M. Gledhill, T. S. Bibby, F-E. Legiret, N. J. Pratt, A. E. Hickman, T. Lawson, and E. P. Achterberg. 2013. Heme *b* in marine phytoplankton and particulate material from the North Atlantic Ocean. Marine Ecology Progress Series 483: 1-17.

Signed: ……..

Date:……

Acknowledgements

The completion of this thesis would not have been possible without the assistance of countless people over the course of my PhD. Firstly, I would like to offer my sincere gratitude to Martha Gledhill (primary supervisor) who provided constant guidance, tuition, feedback, ideas and enthusiasm and Eric Achterberg (co-supervisor) for his comments, advice and encouragement, as well as his humour! The support of these two individuals was invaluable and something for which I am forever indebted.

I would like to express my appreciation to numerous people working at NOCS who have given their time (often more than I deserve) to help: Duncan Purdie (panel chair), Mark Moore, Sebastian Steigenberger, Christian Schlosser, Joe Snow, Elizabeth Sargent, Mike Bolshaw, Dave Spanner, Tom Bibby, Sophie Richier, Nicola Pratt, Pornsri Mingkwan, Khairul Mohamed, Matt Patey, Shir Akbari, Sinhue Torres-Valdes, Matt O'Shaughnessy, Brian King, Joe Green and the NOCS Stores crew. Also, I am extremely grateful to Richard Geider, Tracy Lawson and Mariella Ragni from the University of Essex, and Bob Head and Malcolm Woodward from Plymouth Marine Laboratory.

Thank you to the scientists and crew onboard the *RRS Discovery* during D346 and D361 for all your assistance and making the cruises enjoyable. In particular, François-Eric Legiret who I had the pleasure of travelling with on both occasions and was always available to help and lighten the mood.

I am extremely thankful to the many friends, new and old, that have offered their continued enthusiasm and encouragement throughout my PhD, helping me relax away from the stresses of work: Chris Wood, Richard Bennett, all my office mates over the years and fellow NOCS PhD students, the NOCS six-a-side football team and the many members of the Southampton University Taekwondo Club (SUTKD), especially my instructors Vince Collins, Colin Jacobs, Cliff Lee and Graham Jones.

I would like to thank the people closest to me. My parents, sister and extended family have always encouraged and supported me in everything I have done, and undertaking a PhD was to be no different. Also, I offer my heartfelt gratitude to Natalie Mestry for her unrelenting support, commitment and love, not to mention hours of proof-reading. Finally, I sincerely apologise if I have forgotten anyone in this section, but know that your assistance was greatly appreciated. Thank you.

Definitions and abbreviations

AC	Azores Current
APX	Ascorbate peroxidase
ASW	Artificial seawater
ATP	Adenosine triphosphate
Chl:heme	Ratio of chlorophyll *a* to heme *b* concentration
Chl:C	Chlorophyll *a* concentration per unit carbon
Chl:N	Chlorophyll *a* concentration per unit nitrogen
CID	Collision-induced dissociation
CO_2	Carbon dioxide
Cyt b_6f	Cytochrome b_6f
DCM	Deep chlorophyll maximum
EA-IRMS	Elemental analysis and isotope ratio mass spectrometry
EDTA	Ethylenediaminetetraacetic acid
EqU	Equatorial Upwelling
ESNAG	East Subtropical North Atlantic Gyre
Fe	Iron
Fe_T	Total iron concentration (nmol L^{-1})
F_v/F_m	Maximum photochemical efficiency of PSII
FRRF	Fast repetition rate fluorometry
FS	Florida Straits
GF/F	Glass microfibre filter
GS	Gulf Stream
H_2O	Water
H_2O_2	Hydrogen peroxide
H_2SO_3	Sulphurous acid
HCl	Hydrochloric acid
Heme:C	Heme *b* concentration per unit carbon
Heme:N	Heme *b* concentration per unit nitrogen
HO	Heme oxygenase
HNLC	High nutrient, low chlorophyll
HPLC	High performance liquid chromatography
HPLC/DAD/ESI-MS	High performance liquid chromatography-diode array detection-electrospray ionisation-mass spectrometry
IdiA	Iron-stress-induced protein to protect PSII from oxidative stress
IsiA	Iron-stress-induced chlorophyll-binding protein
ITCZ	Intertropical convergence zone
Mg	Magnesium
m/z	Mass to charge ratio

N	Nitrogen
N_2	Dinitrogen
NH_3	Ammonia
NH_4^+	Ammonium ion
NO_2^-	Nitrite
NO_3^-	Nitrate
NifH	Gene encoding for the nitrogenase complex
O_2	Oxygen
OGP	Octyl-β-glucopyranoside
PAR	Photosynthetically active radiation
pCO_2	Partial pressure of CO_2
pFe′	-log[inorganic iron]
POC	Particulate organic carbon
POC	Particulate organic nitrogen
ppb	Parts per billion
PSI	Photosystem I
PSII	Photosystem II
σ_{PSII}	Effective functional absorption cross-section of PSII
PsaC	Core subunit of PSI
PsbA	D1 protein of PSII
ROS	Reactive oxygen species
SML	Surface mixed layer
SOD	Superoxide dismutase
SOLAS	Surface Ocean Lower Atmosphere Study
STNA	Subtropical North Atlantic
t_{zero}	Natural abundance (^{15}N), value prior to bioassay
Tg	Teragram (1×10^{12} grams)
TNA	Tropical North Atlantic
TSA	Tropical South Atlantic
μ_{max}	Maximum growth rate
UV	Ultraviolet
V_a	Volume (ml) of acetone in the extract
V_f	Volume (ml) of sample filtered onto GF/F
Vnfix	Nitrogen-specific growth via nitrogen fixation
WSNAG	West Subtropical North Atlantic Gyre

Chapter 1

Introduction

1.1 Background information

For many years, marine scientists have debated the underlying cause(s) for the relatively low phytoplankton biomass in specific areas of the world ocean, despite the vast abundance of macronutrients available. These large expanses are commonly known as high-nutrient, low-chlorophyll (HNLC) regions (Minas et al. 1986, Dugdale and Wilkerson 1991, Cavender-Bares et al. 1999) and incorporate over 20% of the global marine environment (Martin et al. 1994). This unanticipated trend was first documented in the early 1930's by oceanographic researchers in the Southern Ocean (Gran 1931, Hart 1934), which was also referred to as the Antarctic Paradox (El-Sayed 1987). The development of sensitive analytical techniques in the 1970's enabled the determination of extremely low trace metal concentrations in seawater (i.e. sub-nanomolar, Bruland et al. 1979). These advances facilitated the investigation of trace metals with far greater accuracy, including areas of the ocean considered to be 'HNLC situations' (Minas et al. 1986). After the confirmation of low iron concentrations in the Southern Ocean, Martin (1990) suggested that iron deficiency limited primary productivity in the region; a theory commonly referred to as the 'Iron Hypothesis' (Martin et al. 1994). Evidence from Vostok (Antarctic research station) ice cores was also used to show that low atmospheric carbon dioxide (CO_2) concentrations were present during periods of high iron availability over the past 160,000 years, and vice versa (Martin 1990). Low atmospheric CO_2 concentrations were indicative of periods of high photosynthetic activity and, therefore, emphasise the underlying importance of iron in biological productivity.

Despite being the fourth most abundant element in the Earth's crust (5.6%, Taylor 1964), iron is present at extremely low concentrations (<1 nmol L^{-1}) in surface open-ocean waters (Achterberg et al. 2001, Davey and Geider 2001, de Baar and de Jong 2001, Moore and Braucher 2008). In HNLC regions, iron generally exhibits a nutrient-type vertical distribution throughout the water column (Ussher et al. 2004), with reduced concentrations in the surface layer that increase with depth (Johnson et al. 1997). The depletion in surface iron concentrations are related to the biological iron demand of phytoplankton within the photic zone (Pilson 1998). The two oxidation states for which iron (Fe) compounds are naturally found are Fe(II) and Fe(III), also referred to as ferrous

and ferric forms, respectively. In terms of abundance, Fe(III) species dominate oxygenated seawaters due to the formation of oxyhydroxides, which leads to their highly insoluble nature (Wells et al. 1995). In contrast, Fe(II) is thermodynamically unstable resulting in the rapid oxidation to Fe(III) when present in oxygenated seawater (Achterberg et al. 2001, Bowie and Lohan 2009). The biogeochemistry of iron in seawater is extremely complex and not yet fully understood. It is thought that a major proportion of dissolved iron is complexed with organic ligands (Gledhill and van Den Berg 1994, Rue and Bruland 1995) which increase the solubility of iron in seawater (Rijkenberg et al. 2008). However, colloidal iron can also present a substantial fraction of the dissolved iron pool, which is potentially less biologically accessible (Rich and Morel 1990, Wu et al. 2001).

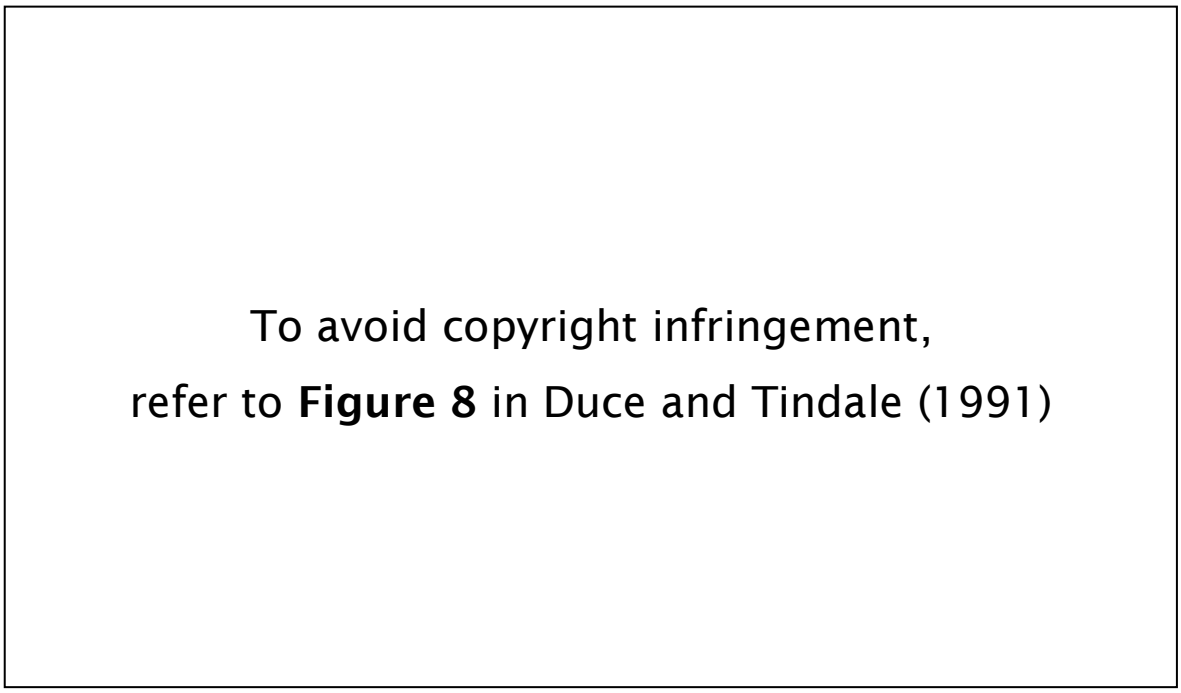

Figure 1.1. Calculated flux of total iron from atmospheric sources to the global ocean; highlighting the predominant fraction of atmospheric iron that enters the ocean via the Northern Hemisphere. Figure from Duce and Tindale (1991); previously modified from Donaghay (1991).

The residence time of iron in deep waters is relatively short (approximately 70 - 200 years, Ussher et al. 2004) compared to ocean circulation time scales, suggesting the input of iron to the marine environment is crucial to the overall availability of iron. Iron enters the marine environment through a variety of pathways including fluvial (riverine), hydrothermal and atmospheric inputs. However, it should be noted that fluvial iron inputs are generally restricted to coastal regions (Poulton and Raiswell 2002) and hydrothermal inputs are quickly precipitated near to the source (Jickells et al. 2005). Taking this into consideration, atmospheric dust could provide the dominant supply of iron to the oceans (Duce et al. 1991, Jickells 1995), particularly in oligotrophic open

ocean areas. The vast majority of dust entering the oceans is derived from the Northern Hemisphere, primarily Northwest Africa and East Asia (Schutz et al. 1990, Jickells and Spokes 2001). It has also been estimated that 43% of total dust inputs to the ocean are received by the North Atlantic (Jickells et al. 2005). The episodic and irregular distribution of atmospheric iron input throughout the global ocean leads to significant variation within and between oceanic basins (Fig. 1.1), with HNLC regions generally receiving the lowest atmospheric iron fluxes.

Over the past two decades, iron has become increasingly acknowledged as an essential resource for numerous biological processes in marine organisms (Geider and La Roche 1994). Before the development of biological life, the Earth's atmosphere was anoxic and contained little free oxygen (Falkowski and Raven 1997) which, in a stark contrast to the present, enabled a large supply of Fe(II) to remain available. The widespread availability of iron for early-evolving organisms is evident from the vast quantity of iron found in sea-bed sediments (Osterberg 1974, Cody et al. 2000). As biological existence increased over time, the highly abundant and accessible iron supply was incorporated into numerous redox reactions as a result (functionality) of iron's two oxidation states. However, as photosynthetic activity increased, rising atmospheric oxygen concentrations oxidised Fe(II) into the relatively insoluble Fe(III). Consequently, despite the reduced bio-availability of iron in the modern ocean, the element is still utilised by organisms for a wide variety of redox reactions today. Understanding the significance of iron in the marine environment has grown through a broad range of biogeochemical studies. Several key processes for which iron is involved include photosynthetic and respiratory electron transfer (Greene et al. 1991, Geider and La Roche 1994), nitrogen fixation (Mills et al. 2004), nitrate reductase activity (Timmermans et al. 1994) and nitrate uptake (Reuter and Ades 1987). Taking these essential roles into account, it has become increasingly evident that iron availability exerts a controlling factor on biological productivity, species composition and trophic structure in planktonic communities in the open-ocean (Sunda 2001).

1.2 Hemes and hemoproteins

The term heme (also spelt haem) refers to the iron-porphyrin complex that acts as the prosthetic group for a wide range of iron proteins known as the hemoproteins. The most commonly recognised hemoprotein is hemoglobin; involved in the transport of oxygen in red blood cells of vertebrates. Hemoglobin was first documented in the mid-nineteenth century due to the oxygen-carrying and chromophore (hemin colour) properties found in human blood (Teichmann 1853). Later that century, MacMunn (1886) described the highly diverse respiratory function of myohaematin and histohaematin in the animal kingdom, although these findings were heavily contested (Hoppe-Seyler 1890, Margoliash and Schejter 1966, Bendall 2005). Myohaematin and histohaematin were later revisited to confirm their central role as respiratory pigments and re-named as cytochromes (Keilin

1925). Since these pioneering studies were conducted, heme functional properties have frequently been investigated. This includes exploring their role in electron transfer (Lemberg and Barrett 1973, Gray and Winkler 1996, Kurisu et al. 2003) and modern ligand biosensing techniques (Chan 2000, 2001), as well as their use in medicine (sickle cell anemia; Pauling et al. 1949). The structure of hemoproteins can vary with regards to polypeptide chain (protein) and heme (non-protein) constituents, enabling a diverse array of biological functions (Chapman et al. 1997). For example, hemoproteins are involved in oxygen transport and storage (hemoglobin and myoglobin, Antonini 1965), oxygen reduction (cytochrome *c* oxidase, Ostermeier et al. 1996), oxidation of organic substrates (cytochrome P450, Ortiz de Montellano 2005), electron transfer (cytochromes *b* and *c*, Gray and Winkler 1996, Scott and Mauk 1996) and hydrogen peroxide utilisation (peroxidases and catalases, Dunford 2010).

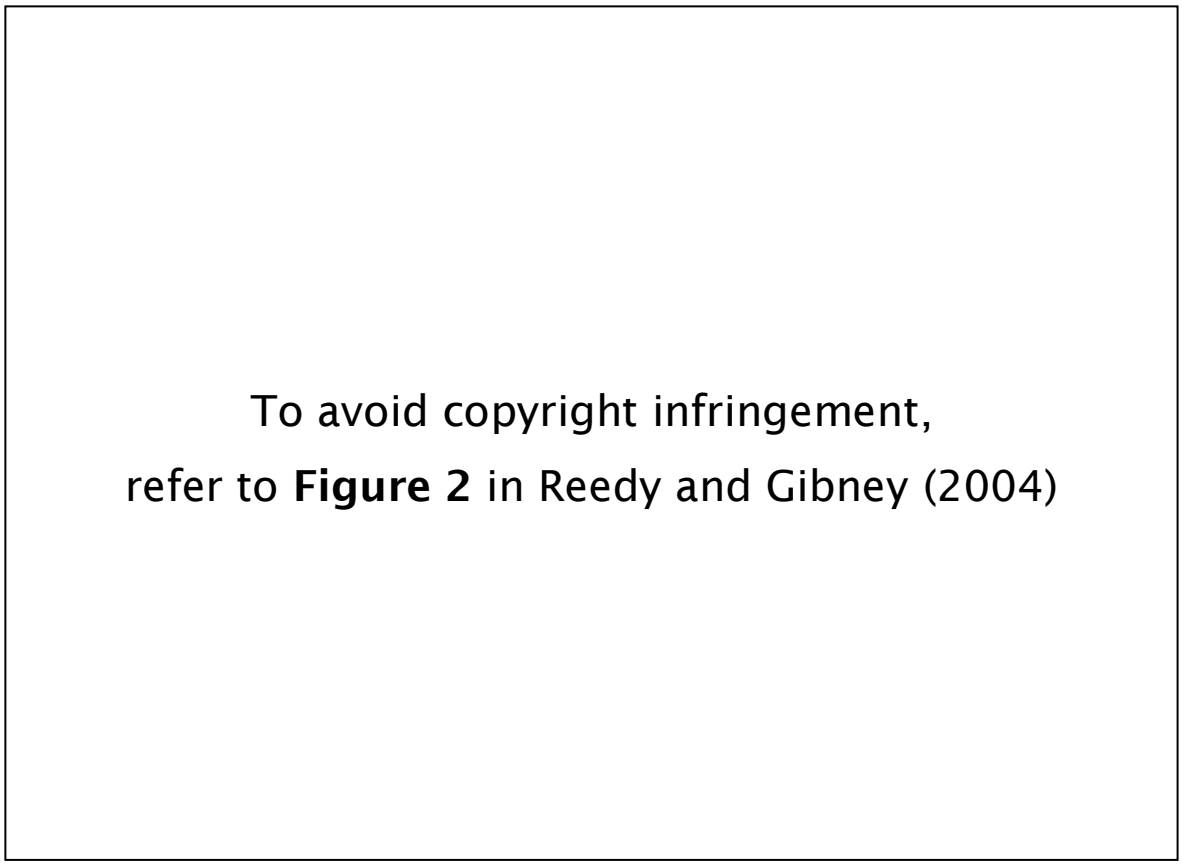

Figure 1.2. Chemical structures of hemes *a*, *b*, *c* and *d*. Notice the similarity within the central iron-porphyrin structure and subtle alterations in side chain groups that differentiate the heme complexes. Figure from Reedy and Gibney (2004).

Four specific heme structures are commonly represented in biology: hemes *a*, *b*, *c* and *d* (Fig. 1.2). Heme *b* (also referred to as Fe(III) protoporphyrin IX) is considered the most versatile form, associated with globins, cytochrome P450, catalases, peroxidases and *b*-type cytochromes (Caughey 1973). The structure of heme *b* is based around an iron-tetrapyrrole macrocycle with methyl groups attached at position 1, 3, 5 and 8, vinyl

groups at positions 2 and 4, and propionic acid groups at positions 6 and 7 (see Fig. 1.2, Reedy and Gibney 2004). The structure of heme *a* differs from heme *b* about positions 2 and 8 of the porphyrin ring, whereby hydroxyfarnesylethyl and formyl groups replace vinyl and methyl groups, respectively. A method to isolate heme *a* was first developed by Warburg and Gewitz (1951), who showed that the complex is actively involved in cytochrome *c* oxidase. Heme *a* has since been examined in further detail to improve chromatographic isolation techniques (York et al. 1967) and assess the structural and functional differences from other heme complexes (Caughey et al. 1975, Yamashita et al. 2005). Heme *c* differs in structure to heme *b* in that the vinyl groups at positions 2 and 4 of the porphyrin ring are replaced by ethyl groups. These ethyl groups are attached to cysteine (amino acid) groups by thioether linkages. Heme *c* has been studied as the prosthetic group for *c*-type cytochromes for the last 50 years (see review by Scott and Mauk 1996). Heme *d* is a less commonly occurring natural heme structure, with complex alterations about the porphyrin at positions 1, 2, 3 and 4 (Timkovich et al. 1985, Murshudov et al. 1996).

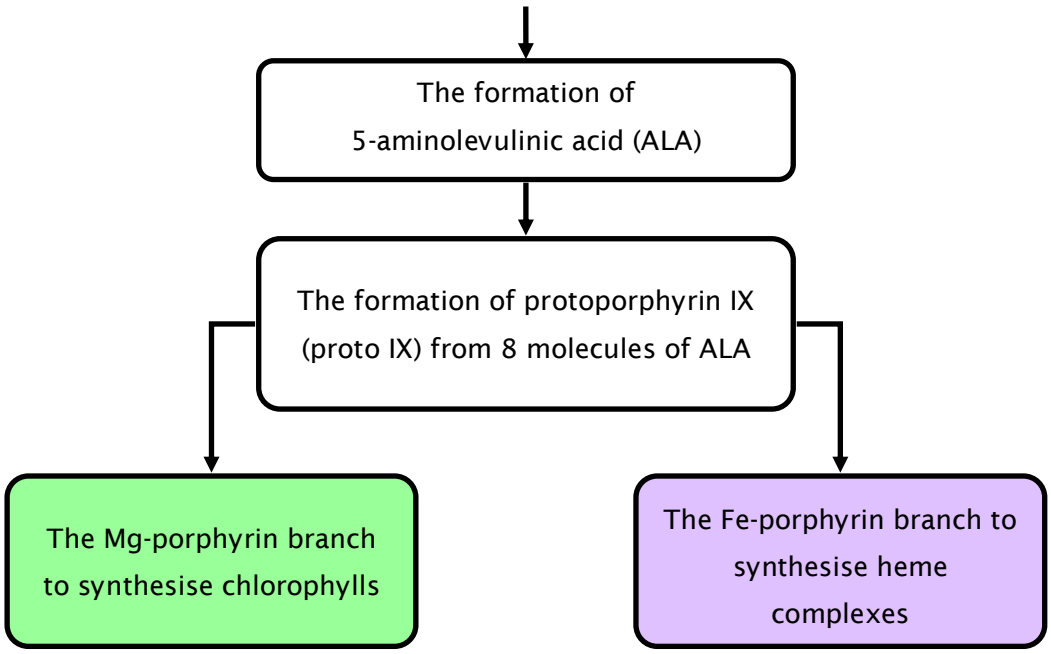

Figure 1.3. Simplified schematic of the chlorophyll and heme biosynthetic pathways according to the four stages described by Papenbrock and Grimm (2001).

Chlorophyll has a cyclic tetrapyrrole structure orientated around a central magnesium atom and is produced along the same biosynthetic pathway as heme; iron is incorporated into heme complexes rather than magnesium. The tetrapyrrole biosynthetic pathway can be characterised into four simplified stages: (1) the production of 5-aminolevulinic acid (ALA) from glutamate; (2) porphyrin synthesis from eight ALA molecules; (3) insertion of magnesium along the chlorophyll synthesis pathway or; (4) insertion of iron along the

heme synthesis pathway (Fig. 1.3, Papenbrock and Grimm 2001). Iron and magnesium (Mg) are chelated into the porphyrin by the enzymes ferrochelatase (Fe-chelatase) and magnesium protoporphyrin IX chelatase (Mg-chelatase), respectively (Papenbrock et al. 1999). A complex feedback mechanism is employed to determine the production of either chlorophyll or heme products (Mochizuki et al. 2010), potentially regulated by adenosine triphosphate (ATP) availability (required by Mg-chelatase, inhibits Fe-chelatase), channelling pools of protoporphyrin IX substrate towards Fe-chelatase or Mg-chelatase activity and gene expression of the two chelatase enzymes (see review by Cornah et al. 2003). The close relationship in structure and synthesis between heme and chlorophyll could suggest that the abundance of heme is of similar importance to the more commonly documented chlorophyll. However, despite their apparent importance, our understanding of hemoproteins in marine organisms is extremely limited.

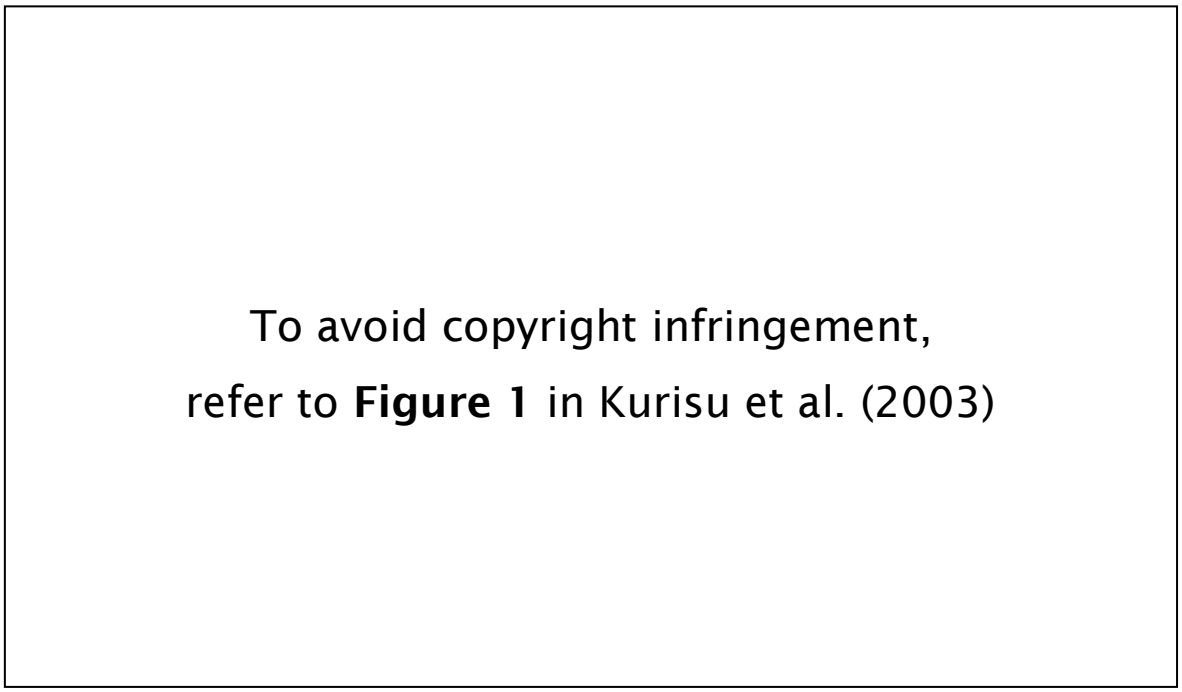

Figure 1.4. Diagram of the membrane-bound protein complexes involved in oxygenic photosynthesis. The intricate reaction series, including electron transport and proton translocation, occurs across the thylakoid membrane between the lumen (*p*-side) and stroma (*n*-side) of photosynthetic organisms to harness light energy. Photosystems I (PSI) and II (PSII); plastoquinol (PQ); cytochrome b_6f (Cyt b_6f); plastocyanin (PC); cytochrome c_6 (Cyt c_6); ferredoxin (Fd); and ferredoxin:$NADP^+$ reductase (FNR). Figure from Kurisu et al. (2003).

Cytochromes can be loosely defined as hemoproteins that function in electron transfer (Lemberg and Barrett 1973), resulting from the reversible valency of iron within the heme structure (i.e. Fe(II) and Fe(III)). Cytochrome *c* oxidase, which contains one heme *a* and one heme a_3 complex, catalyses the last stage of the respiratory electron transport chain through the reduction of molecular oxygen (O_2) to water (H_2O), creating a proton gradient across the membrane (Yoshikawa et al. 2000, Reedy and Gibney 2004). Extensively

studied over the last three decades, the superfamily of cytochrome P450 is believed to catalyse numerous reactions by incorporating one oxygen atom of an O_2 molecule into a substrate, which leads to the simultaneous reduction of the other oxygen atom into H_2O (Groves and Han 2005). Cytochromes are also of particular importance in oxygenic photosynthesis (e.g. cytochrome b_6f, cytochrome c_6 and cytochrome b_{559}) helping to create a transmembrane electrochemical proton gradient to enable the synthesis of ATP. Cytochrome b_6f mediates the link between photosystem I (PSI) and photosystem II (PSII) reaction centres, translocating protons across the membrane (see Fig. 1.4, Cramer et al. 1996, Kurisu et al. 2003). In cyanobacteria, the high-potential cytochrome c_6 transfers electrons from cytochrome b_6f to PSI (Morand et al. 1994, Sawaya et al. 2001, Ho 2005), whilst also functioning in respiration (Schmetterer 1994). The precise function of cytochrome b_{559} remains unclear (Whitmarsh and Pakrasi 1996), although it is thought to protect PSII from photoinhibition and is essential in the assembly of functional PSII complexes (Barber and De Las Rivas 1993, Stewart and Brudvig 1998, Burda et al. 2003).

Several studies have been conducted on the enzyme heme oxygenase (HO), specifically the role of HO in the degradation of hemes. Although not specifically a hemoprotein, HO combines with heme to form a ferric heme-HO complex comparable to natural hemoproteins, including similar absorption spectrums (Yoshida and Kikuchi 1978, 1979). The exact function of HO is unclear, although it is thought the degradation of heme to biliverdin, and subsequently bilirubin, provides an antioxidant defence against oxidative stress (Maines 1988, Kikuchi et al. 2005). Cornejo et al. (1998) suggested that HO regulates the production of phycobilin, a light-harvesting accessory pigment synthesised from biliverdin (IXα), as a result of the availability of iron in cyanobacteria. It was found that in iron-deficient medium, the cyanobacteria *Synechocystis* sp. PCC 6803 increased the level of HO mRNA in a regulatory feedback regarding the cellular demand of phycobilin (Cornejo et al. 1998). Therefore, as the degradation of hemes by HO is influenced by iron availability, hemes could present an indicator of iron deficiency in marine organisms.

Novel variants of hemes *a* and *o* in various cyanobacteria have been successfully detected in archaea bacteria (Lubben and Morand 1994). Extraction of non-covalently bound hemes was achieved through the addition of acetone/hydrochloric acid (HCl, 19:1, v:v) and analysed using High Performance Liquid Chromatography (HPLC) absorption spectrophotometry and mass spectrometry. However, despite the ability to isolate major heme structures and the apparent importance of these complexes, our understanding regarding the influence of iron availability on heme abundance remains largely unresolved. This is specifically the case in the marine environment, where the availability of iron to the biotic community is temporally and spatially sporadic. The situation was addressed by Gledhill (2007) who described a detailed method for the determination of

heme *b* in marine phytoplankton and bacterioplankton, using HPLC with diode array spectrophotometry. The method provides a relatively quick and reproducible technique to quantify the most abundant heme structure; although the study acknowledged the necessity for further exploration of the subject area. Having defined a methodology to quantify heme *b*, Gledhill (2007) provided the first data for heme *b* abundance in laboratory phytoplankton cultures. The marine phytoplankton *Thalassiosira weissflogii*, *Thalassiosira oceanica* (Bacillariophyta, diatoms), *Dunaliella tertiolecta* (Chlorophyta, green algae) and *Emiliania huxleyi* (Haptophyta, coccolithophore) were all measured for heme *b* concentration under nutrient (including iron) replete conditions. Gledhill (2007) calculated that between 3 and 10% of cellular iron quotas corresponded to heme *b* complexes in eukaryotes. These reported percentages are not trivial, further highlighting the significant contribution of hemes, specifically heme *b*, within marine organisms to the total iron protein pool. In addition to eukaryotic organisms, Gledhill (2007) provided heme *b* concentrations for several marine prokaryotes grown under nutrient replete conditions. The concentration of heme *b* in cultures varied between 0.153 nmol L^{-1} (*Synchococcus* sp. WH8102) and 2.62 nmol L^{-1} (*Roseobacter denitrificans*), although insufficient data restricted further analysis of the prokaryotes. However, it has been suggested that prokaryotes, which include the well-documented marine cyanobacterial genera *Synechococcus*, *Crocosphaera* and *Trichodesmium*, have a higher iron requirement for growth (Fe:C ratio) compared to eukaryotes (Raven 1988, 1990, Brand 1991). Therefore, variation in the availability of iron may not only lead to changes in the allocation of iron for different intracellular functions (i.e. heme and non-heme complexes), but could also alter entire phytoplankton community compositions.

Our current understanding of hemoproteins and their abundance in the natural marine environment is limited, despite the reality that hemes are likely to be of significant value in our understanding of marine biogeochemical cycles. The inclusion of hemes in fundamental processes requires further investigation and their specific role(s) could be indirectly linked to the topical subject of global warming, as has been the case with iron (e.g. Jickells et al. 2005, Buesseler et al. 2008, Denman 2008). As hemoproteins are extensively engaged in such a wide variety of redox reactions (Caughey 1973, Moore 1996, Chapman et al. 1997), it could be inferred that their abundance dramatically influences the biological pump and carbon cycling in the oceans. Martin (1990) suggested that low iron availability limits primary production. Therefore, the abundance of hemoproteins could in turn influence the availability of iron for other functions in marine organisms (e.g. nitrogen fixation). Conversely, heme concentrations are likely to be determined by the availability of iron and could provide an indication of iron stress through physiological responses in the synthesis of heme complexes.

1.3 Nitrogen fixation

The global nitrogen cycle is an intricate biogeochemical system that not only incorporates the cycling of nitrogen, but also presents an important link to other key elements (see Fig. 1.5), including oxygen, phosphorus, carbon and iron (Falkowski et al. 1998, Michaels et al. 2001, Gruber 2004). In fact, the diversity of nitrogen oxidation states in marine environments (+5 to -3) makes the element fairly distinct from other nutrients (see Fig. 1.6, Karl et al. 2002, Gruber 2008). Nitrogen is required for life to exist on Earth, providing the essential building blocks for many fundamental cellular components such as nucleic acids, chlorophylls and hemoproteins. The nitrogen cycle encompasses the reversible conversion between molecular nitrogen gas (dinitrogen or N_2) and the pool of fixed nitrogen (Galloway et al. 2004). These biochemically fixed forms of nitrogen (i.e. ammonia and subsequent products of nitrification: nitrite and nitrate) are readily available to the biota for incorporation into structural components. In contrast, a strong triple bond between the two nitrogen atoms of N_2 results in the relatively inert behaviour of N_2 and, therefore, is considered biologically unavailable to the majority of living organisms. This aspect is even more compelling given the fact that the vast majority of nitrogen in the oceans is in the form of N_2 (approximately 94%; Gruber 2008).

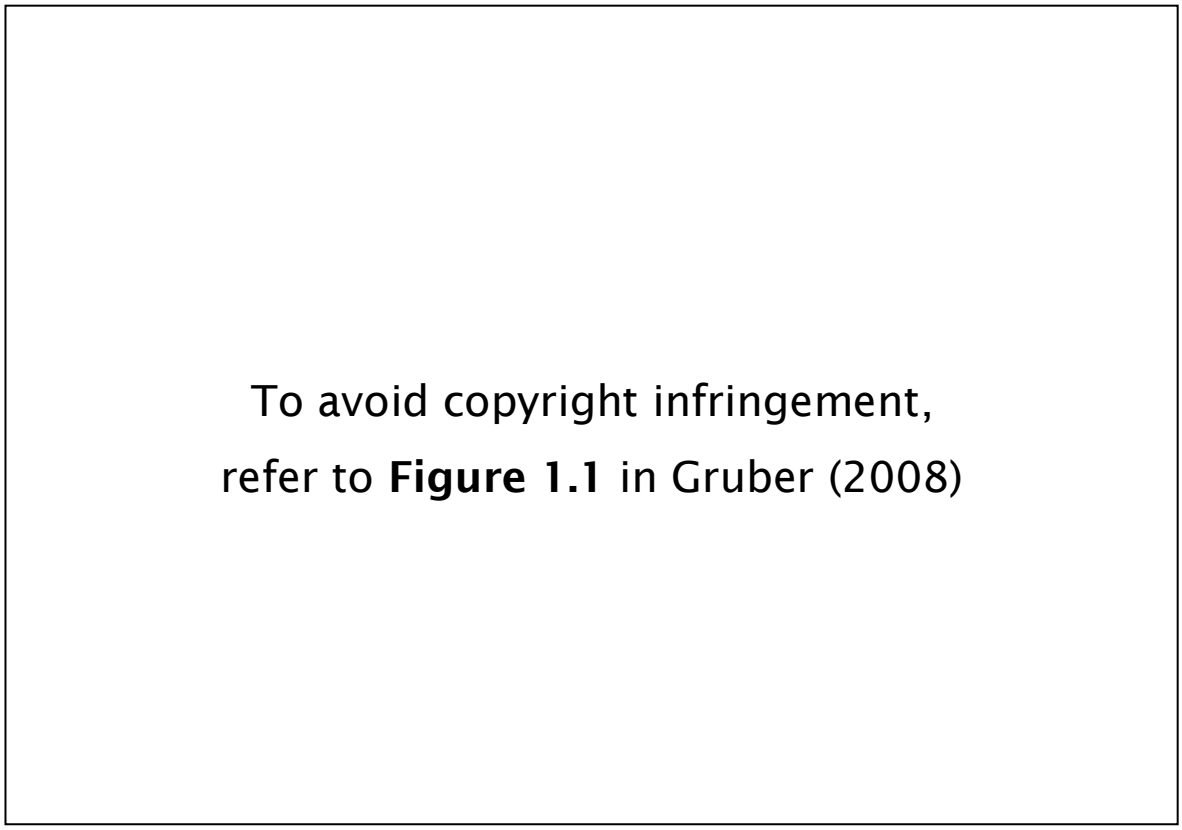

Figure 1.5. An illustration of the marine nitrogen cycle incorporating the relationship with oxygen, phosphorus and carbon cycles. Notice the direct influence each elemental cycle can impose on the local community, leading to a dynamic balance of resources available. Figure from Gruber (2008).

The availability of fixed nitrogen is governed by two crucial input and output processes, commonly referred to as nitrogen fixation and denitrification, respectively (Figs. 1.5 and 1.6). Nitrogen fixation is the process whereby N_2 is reduced (fixed) into ammonia (NH_3 or the ammonium ion NH_4^+), which can be biologically driven or the result of high-energy abiotic factors (e.g. lightening). Ammonia can be readily incorporated into organisms via the synthesis of organic compounds, or oxidised into nitrite (NO_2^-) and nitrate (NO_3^-) (Libes 2009). Biologically mediated nitrogen fixation is an enzyme-catalysed reaction involving nitrogenase (Equation 1). However, the reaction is energetically costly as 8 electrons and 16 ATP molecules are required to reduce each molecule of N_2 (Postgate 1998). Therefore, biological nitrogen fixation typically only takes place in areas that are sufficiently depleted in fixed nitrogen.

$$N_2 + 8H^+ + 8e^- \xrightarrow{\textit{Nitrogenase}} 2NH_3 + H_2 \qquad \textbf{(Equation 1)}$$

$$2NO_3^- + 12H^+ + 10e^- \longrightarrow N_2 + H_2O \qquad \textbf{(Equation 2)}$$

In contrast to nitrogen fixation, denitrification is the process whereby NO_3^- is reduced to N_2 (Equation 2), providing a feedback loop regarding the availability of fixed nitrogen in an ecosystem. The balance between rates of nitrogen fixation and denitrification create a complex dynamic in terms of the spatial and temporal variability of nitrogen species in the ocean (Deutsch et al. 2007; Moore et al. 2009). Another key feature of the nitrogen cycle is anaerobic oxidation of NH_4^+, commonly referred to as Anammox, which provides a chemo-autotrophic (i.e. source of energy) pathway for the removal of fixed nitrogen by combining NH_4^+ and NO_2^- to form N_2 (Strous et al. 1999). Quantification of Anammox in the marine environment remains largely unresolved, although it is currently estimated that 50 % or more of the fixed nitrogen removed from the global ocean is linked to this process (Dalsgaard et al. 2005; Brandes et al. 2007; Van De Vossenberg et al. 2008).

Three main factors were highlighted by Gruber (2008) that have led to the increased interest in the marine nitrogen cycle. Firstly, it appears anthropogenic compounds, such as fertilisers that are high in nitrates, are having a significant and rapid impact on terrestrial, estuarine, riverine and coastal ecosystems (Galloway et al. 2004). Secondly, the extent of marine nitrogen fixation is now believed to be much greater than previously estimated, influencing the residence times of nitrogen in the oceans and heightening the cycle's susceptibility to change. Finally, Gruber (2008) drew attention to the potential role the nitrogen cycle may have in response to future climate change through a series of feedback mechanisms (Michaels et al. 2001). These three points emphasise how the nitrogen cycle potentially dictates our understanding of the overall marine biogeochemical cycle, but also underline the magnitude of what still remains unknown.

The main source of fixed nitrogen to surface waters was traditionally considered to come from deep water upwelling and remineralisation of organic matter. However, marine nitrogen budgets have inferred large inaccuracies in the estimated input of nitrogen to euphotic zones, including the contribution from nitrogen fixation. Lewis et al. (1986) suggested that the physical mixing of seawater alone would be unlikely to meet the nitrogen demands of surface waters and mentioned how nitrogen fixation rates may need to be revised. Only a few decades ago, estimates of marine nitrogen fixation stood at 10 - 20 Tg N $year^{-1}$ (1 Tg = 1 x 10^{12} grams, Capone and Carpenter 1982), although later studies have suggested the flux could be as high as 200 Tg N $year^{-1}$ (Carpenter and Romans 1991, Carpenter and Capone 2008). Therefore, current estimates regarding marine nitrogen fixation suggest a possible contribution of more than 50% to the overall global nitrogen fixation budget. However, these values are often the result of extrapolations from one particular ocean basin to incorporate the entire global ocean. It is widely accepted that a lack of spatial and temporal resolution is currently hampering our ability to accurately define global estimates and models for marine nitrogen fixation (Karl et al. 2002).

Diazotrophs, which are found in terrestrial and marine environments, are specialised nitrogen-fixing organisms that utilise the iron-rich nitrogenase enzyme to convert N_2 to biologically accessible forms of nitrogen. Two protein subunits make up the nitrogenase enzyme complex: (1) an iron protein (nitrogenase reductase) that strongly binds to N_2 and (2) a molybdenum-iron protein (dinitrogen reductase) that provides electrons for the iron-protein (Rees and Howard 2000, Berman-Frank et al. 2001, Berges and Mulholland 2008). Raven (1988) proposed that the high iron content of nitrogenase meant that 78.8 moles of extra iron in the enzyme would equate to the assimilation of only one mole of carbon per second. This led to an estimated iron requirement of approximately 100 times greater than non-diazotrophic phytoplankton to achieve similar growth rates (Raven 1988). However, later studies have suggested that this heavily over-estimated the iron requirement of diazotrophs, with values of only 2.5 - 5.2 times more iron required by diazotrophs in the central (sub-) tropical Atlantic Ocean being projected (Sañudo-Wilhelmy et al. 2001). Nevertheless, it is still considered that an additional limiting stress is imposed upon diazotrophs by the availability of iron (Falkowski 1997, Berman-Frank et al. 2001). It should also be noted that iron incorporated into nitrogenase is not related to heme complexes, highlighting the fact that the iron requirement of nitrogen fixation is additional to basic metabolic functioning of diazotrophs (i.e. respiration and photosynthesis).

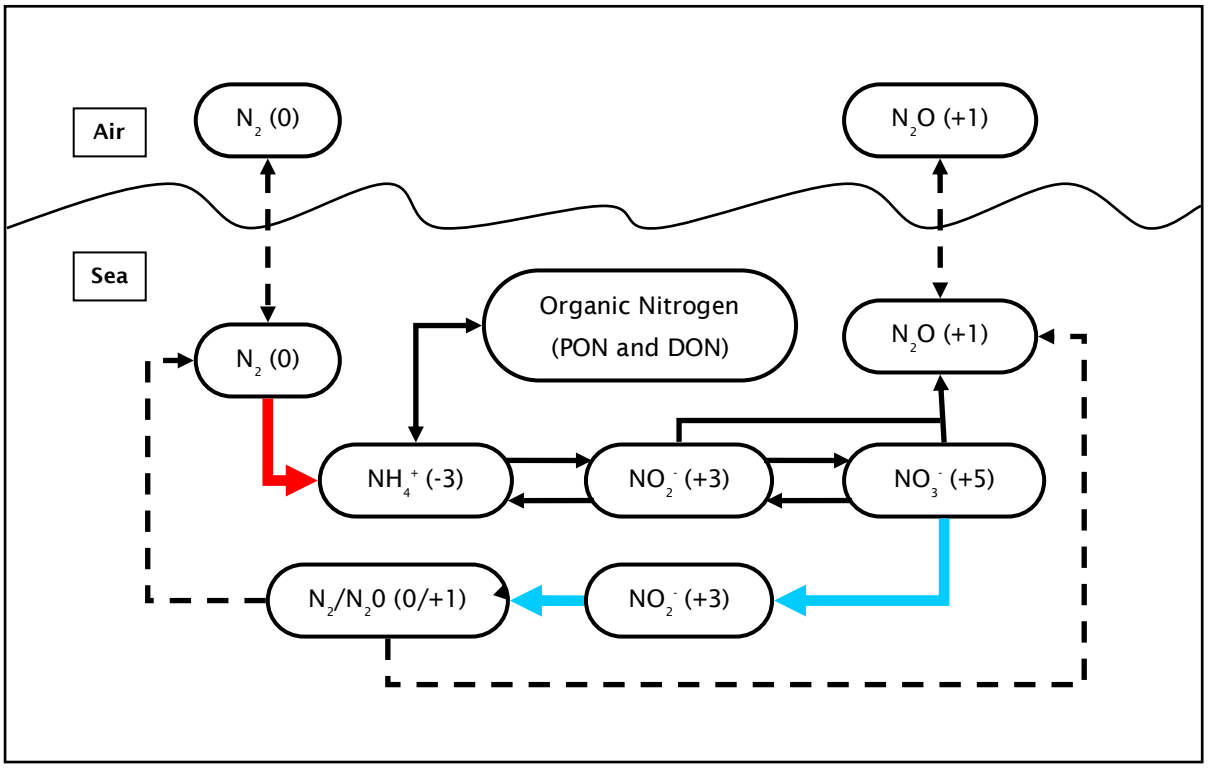

Figure 1.6. A Schematic of the marine nitrogen cycle. Solid lines indicate transformations of nitrogen species by cells or organisms, and dotted lines indicate physical movements of water masses or gas exchange. Red and blue arrows indicate the process of nitrogen fixation and denitrification, respectively. Numbers in parentheses indicate the valence of nitrogen species in each molecule or ion. Notice the range of oxidation states from NO_3^- (+5) to NH_4^+ (-3). Figure modified and redrawn from Karl et al. (2002).

The most documented marine diazotrophs are from the filamentous genera *Trichodesmium* (see Fig. 1.7, Capone et al. 1997) which forms large seasonal blooms in (sub-) tropical regions of the global ocean. A conservatively estimated integrated nitrogen fixation rate of between 1.6 and 2.4 Tmol N $year^{-1}$ (Tmol N = 1 x 10^{12} moles of N) has been attributed to *Trichodesmium* in the North Atlantic alone (Capone et al. 2005). However, despite being considered the dominant diazotroph of the marine environment (Letelier and Karl 1996, Capone et al. 2005), the specific functioning of nitrogen fixation in *Trichodesmium* spp. is still not fully understood. *Trichodesmium* are non-heterocystous which means they do not possess thick cell walls to spatially separate the processes of oxygenic photosynthesis and nitrogen fixation. This intriguing enigma is made all the more significant given that nitrogenase exposure to oxygen, a product of photosynthesis, results in the enzyme becoming permanently inhibited (Milligan et al. 2007). In addition, unicellular diazotrophs are becoming the focus of increased interest given their potential influence on marine nitrogen fixation (Zehr et al. 2000, Montoya et al. 2004, Moisander et al. 2010).

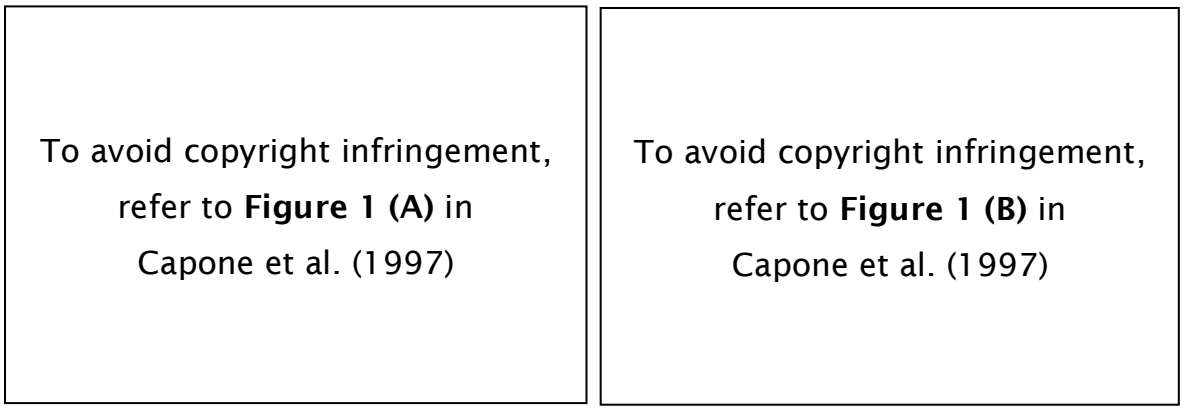

Figure 1.7. Photograph of (**left**) a fusiform (tuft) colony of *Trichodesmium erythraeum* (IMS101) and (**right**) a radial (spherical) colony of *Trichodesmium thiebautii*. Colony length/diameter typically ranges between 2 and 5 mm. Figures from Capone et al. (1997).

1.4 The project, rationales and wider implications

Iron plays a significant role in mediating phytoplankton blooms (e.g. Martin and Fitzwater 1988, Coale 1991, Boyd et al. 2000) and, therefore, potentially influences carbon sequestration to the oceans (Watson et al. 2000). However, it has also been argued that the availability of nitrate (classic 'biological' view) and/or phosphate ('geochemical' view) could exclusively limit or co-limit phytoplankton growth and biomass (Smith 1984, Codispoti 1989, Tyrrell 1999). Thus, in addition to the obvious interest of climate change (e.g. Fig. 1.8), it is interesting to note the significant relationship between iron (including heme complexes) and the nitrogen cycle (non-heme). The analytical technique described by Gledhill (2007) to quantify heme *b* in marine phytoplankton and bacterioplankton has provided an opportunity to explore the abundance of this essential complex in marine microorganisms. Other than the aforementioned study, relatively little is currently known about heme complexes in marine organisms, as well as their abundance in the global ocean. This project aimed to provide further records of heme *b* in three cyanobacterial species, whilst also investigating the abundance of heme *b* in the natural marine environment.

The first cyanobacterium investigated in this study was the physiologically well-defined unicellular phycoerythrin-rich *Synechococcus* sp. WH7803 (e.g. Liu et al. 1999). Given the ubiquitous distribution of the *Synechococcus* genus throughout the global ocean (Zwirglmaier et al. 2008) which dominates the phytoplankton carbon biomass in the (sub-) tropical North Atlantic (Maranon et al. 2000), the investigation of *Synechococcus* sp. WH7803 provided a strong platform for further heme *b* investigation. Furthermore, *Synechococcus* sp. WH7803 offered a non-diazotrophic comparison to the nitrogen fixing cyanobacteria *Crocosphaera watsonii* (WH8501) and *Trichodesmium erythraeum* (IMS101) examined in the second laboratory culture study. All three cyanobacteria have previously been shown to display adaptive responses to iron limitation (e.g. Chadd et al. 1996,

Küpper et al. 2008, Saito et al. 2011), including the induction of the iron stress protein IdiA (Webb et al. 2001). This project aimed to determine whether these physiological responses were also evident when heme *b* abundance was measured at a range of iron concentrations. Iron availability is known to influence photosynthesis (Geider and La Roche 1994) and, therefore, it could be expected that heme *b* associated with the photosynthetic apparatus would offer a similar response. Diazotrophs require an additional supply of iron (non-heme) for nitrogen fixation, which most likely leads to an intricate allocation of iron for heme *b* complexes associated with basic metabolic functioning.

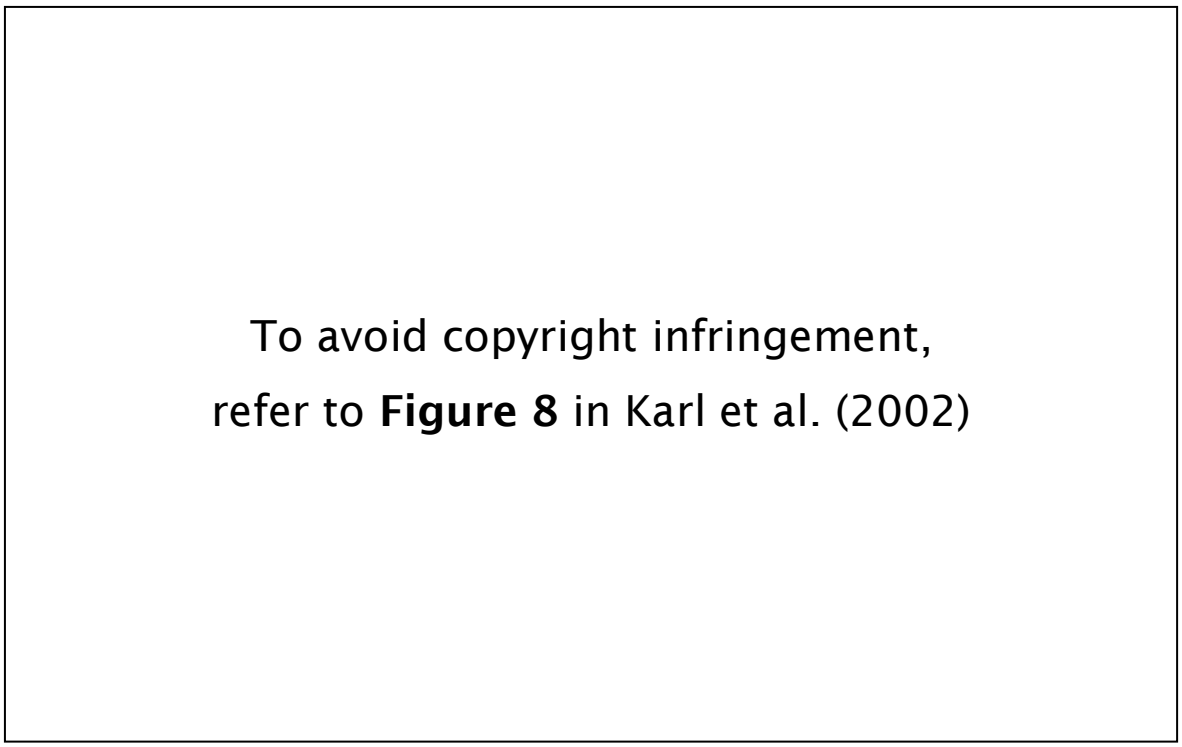

Figure 1.8. Schematic representation of potential feedback mechanisms linking the climate with nitrogen fixation. Figure from Karl et al. (2002); redrawn from Michaels et al. (2001).

Field data were collected from two research cruises in the subtropical North Atlantic (D346) and tropical North Atlantic (D361) in early 2010 and 2011, respectively. The first cruise incorporated several key oceanographic regions, including the Gulf Stream, the oligotrophic subtropical North Atlantic gyre and the upwelling zone towards the eastern boundary of the Atlantic Ocean (Mauritanian coast and Western Sahara). The second cruise incorporated the Senegalese coast of Western Africa and the tropical North Atlantic gyre. The (sub-) tropical North Atlantic is an area known to exhibit high nitrogen fixation rates (Moore et al. 2009) and receives a large atmospheric supply of iron (Jickells et al. 2005), providing an ideal region to compare heme *b* abundance and nitrogen fixation. In addition, the studies of *Synechococcus* sp. WH7803, *Crocosphaera* and *Trichodesmium* provided the baseline of heme *b* measurements for which the two cruises could be

compared. The determination of heme *b* abundance in marine organisms will improve our knowledge of how physiological processes are affected by changing iron concentration, both in the laboratory and the field. In turn, this will help to improve our ability to understand and predict the responses of marine organisms to future climate change and nutrient availability.

Data collected from experiments on *Synechococcus* sp. WH7803 and the subtropical North Atlantic (D346) were presented at the 14th Biennial Challenger Conference for Marine Science (6th - 9th September 2010), and has been accepted for publication in Marine Ecology Progress Series (Honey et al. 2013). The author analysed heme *b* samples collected from the tropical Northeast Atlantic (D326) which is currently being prepared for submission (Gledhill et al. in prep, see Appendix 1). In addition, the author was involved in laboratory-based *Trichodesmium* culture experiments to measure iron-binding photosynethetic and nitrogen-fixing proteins, for which the work has been published in PLoS ONE (Richier et al. 2012).

1.5 Thesis structure

A detailed description of the materials and methods used in this project are provided in **Chapter 2**. Many of the techniques used are relevant to each of the subsequent scientific chapters, hence the decision to incorporate a separate methods chapter. Procedures for the determination of heme *b*, chlorophyll *a*, particulate organic carbon (POC), particulate organic nitrogen (PON), nitrogen fixation rates, biophysical measurements (F_v/F_m and σ_{PSII}) and culturing cyanobacteria are outlined. In addition, details of two research cruises participated in the (sub-) tropical North Atlantic are described.

The first cross-sectional profile of heme *b* in the subtropical North Atlantic (D346) is presented in **Chapter 3**, as well as heme *b* data collected from the tropical North Atlantic (D361). Data presented from both cruises are supported by concurrent chlorophyll *a*, POC and PON concentrations, as well as nanomolar nutrient (nitrate and phosphate) and dissolved iron concentrations from D346 and D361, respectively. An investigation on the unicellular cyanobacteria *Synechococcus* sp. WH7803 is discussed in **Chapter 4**. The study was used to increase the pool of heme *b* data measured from laboratory grown marine organisms, whilst also examining the minimum quantity of heme *b* required to enable basal metabolic functions and maximum growth rates. Concurrent chlorophyll *a*, POC and PON concentrations are presented as well as comparisons to five eukaryotic phytoplankton species previously investigated. **Chapter 5** describes an investigation of the marine diazotrophs *Crocosphaera watsonii* (WH8501) and *Trichodesmium erythraeum* (IMS101) in relation to the influence of iron availability on heme *b* abundance and nitrogen fixation rates. Heme *b* is not directly involved in nitrogen fixation and, therefore, provides an alternative measurement of iron usage in two organisms known to

exhibit relatively high iron demand. Concurrent chlorophyll *a*, POC and PON concentrations are presented, as well as biophysical measurements. In addition, nitrogen fixation rates from the two cruises in the (sub-) tropical North Atlantic are discussed and compared to the laboratory diazotroph cultures.

Finally, **Chapter 6** synthesises the significant conclusions that have been made as a result of this work, whilst also highlighting potential areas for future work.

1.6 References

Achterberg, E. P., T. W. Holland, A. R. Bowie, R. F. C. Mantoura, and P. J. Worsfold. 2001. Determination of iron in seawater. Analytica Chimica Acta **442**:1-14.

Antonini, E. 1965. Interrelationship between structure and function in hemoglobin and myoglobin. Physiological Reviews **45**:123-170.

Barber, J. and J. De Las Rivas. 1993. A functional model for the role of cytochrome b_{559} in the protection against donor and acceptor side photoinhibition. Proceedings of the National Academy of Sciences **90**:10942-10946.

Bendall, D. S. 2005. The unfinished story of cytochrome *f*. Pages 531-542 *in* Govindjee, J. T. Beatty, H. Gest, and J. T. Allen, editors. Discoveries in Photosynthesis. Springer.

Berges, J. A. and M. R. Mulholland. 2008. Enzymes and nitrogen cycling. Pages 1385-1444 *in* D. G. Capone, D. A. Bronk, M. R. Mulholland, and E. J. Carpenter, editors. Nitrogen in the Marine Environment. Elsevier Inc.

Berman-Frank, I., J. T. Cullen, Y. Shaked, R. M. Sherrell, and P. G. Falkowski. 2001. Iron availability, cellular iron quotas, and nitrogen fixation in *Trichodesmium*. Limnology and Oceanography **46**:1249-1260.

Bowie, A. R. and M. C. Lohan. 2009. Determination of iron in seawater. Pages 235-258 *in* O. Wurl, editor. Practical guidelines for the analysis of seawater. CRC Press, Taylor and Francis Group.

Boyd, P. W., A. J. Watson, C. S. Law, E. R. Abraham, T. Trull, R. Murdoch, D. C. E. Bakker, A. R. Bowie, K. O. Buesseler, H. Chang, M. Charette, P. Croot, K. Downing, J. Zeldis, and et al. 2000. A mesoscale phytoplankton bloom in the polar Southern Ocean stimulated by iron fertilization. Nature **407**:695-702.

Brand, L. E. 1991. Minimum iron requirements of marine phytoplankton and the implications for the biogeochemical control of new production. Limnology and Oceanography **36**:1756-1771.

Brandes, J. A., A. H. Devol, and C. Deutsch. 2007. New developments in the marine nitrogen cycle. Chemical Reviews **107**:577-589

Bruland, K. W., R. P. Franks, G. A. Knauer, and J. H. Martin. 1979. Sampling and analytical methods for the determination of copper, cadmium, zinc, and nickel at the nanogram per liter level in sea water. Analytica Chimica Acta **105**:233-245.

Buesseler, K. O., S. C. Doney, D. M. Karl, P. W. Boyd, K. Caldeira, F. Chai, K. H. Coale, H. J. W. de Baar, P. G. Falkowski, K. S. Johnson, R. S. Lampitt, A. F. Michaels, S. W. A. Naqvi, V. S. Smetacek, S. Takeda, and A. J. Watson. 2008. Ocean iron fertilization - Moving forward in a sea of uncertainty. Science **319**:162.

Burda, K., J. Kruk, R. Borgstadt, J. Stanek, K. Strzalka, G. H. Schmid, and O. Kruse. 2003. Mossbauer studies of the non-heme iron and cytochrome b_{559} in a *Chlamydomonas reinhardtii* PSI^- mutant and their interactions with α-tocopherol quinone. Federation of European Biochemical Societies **535**:159-165.

Capone, D. G., J. A. Burns, J. P. Montoya, A. Subramaniam, C. Mahaffey, T. Gunderson, A. F. Michaels, and E. J. Carpenter. 2005. Nitrogen fixation by *Trichodesmium* spp.: An important source of new nitrogen to the tropical and subtropical North Atlantic Ocean. Global Biogeochemical Cycles **19**:GB2024.

Capone, D. G. and E. J. Carpenter. 1982. Nitrogen fixation in the marine environment. Science **217**:1140-1142.

Capone, D. G., J. P. Zehr, H. W. Paerl, B. Bergman, and E. J. Carpenter. 1997. *Trichodesmium*, a globally significant marine cyanobacterium. Science **276**:1221-1229.

Carpenter, E. J. and D. G. Capone. 2008. Nitrogen fixation in the marine environment. Pages 141-198 *in* D. G. Capone, D. A. Bronk, M. R. Mulholland, and E. J. Carpenter, editors. Nitrogen in the marine environment. Elsevier Inc.

Carpenter, E. J. and K. Romans. 1991. Major role of the cyanobacterium *Trichodesmium* in nutrient cycling in the North Altantic Ocean. Science **254**:1356-1358.

Caughey, W. S. 1973. Iron porphyrins - hemes and hemins. Pages 797-831 *in* G. L. Eichham, editor. Inorganic biochemistry. Elsevier, Amsterdam.

Caughey, W. S., G. A. Smythe, D. H. O'Keeffe, J. E. Maskasky, and M. L. Smith. 1975. Heme A of cytochrome c oxidase. The Journal of Biological Chemistry **250**:7602-7622.

Cavender-Bares, K. K., E. L. Mann, S. W. Chisholm, M. E. Ondrusek, and R. R. Bidigare. 1999. Differential response of equatorial Pacific phytoplankton to iron fertilization. Limnology and Oceanography **44**:237-246.

Chadd, H. E., I. R. Joint, N. H. Mann, and N. G. Carr. 1996. The marine picoplankter *Synechococcus* sp. WH7803 exhibits an adaptive response to restricted iron availability. FEMS Microbiology Ecology **21**:69-76.

Chan, M. K. 2000. Heme protein biosensors. Journal of Porphyrins and Phthalocyanines **4**:358-361.

Chan, M. K. 2001. Recent advances in heme-protein sensors. Current opinion in chemical biology **5**:216-222.

Chapman, S. K., S. Daff, and A. W. Munro. 1997. Heme: The most versatile redox centre in biology? Metal Sites in Proteins and Models. Structure and Bonding **88**:39-70.

Coale, K. H. 1991. Effects of iron, manganese, copper, and zinc enrichments on productivity and biomass in the subarctic Pacific. Limnology and Oceanography **36**:1851-1864.

Codispoti, L. A. 1989. Phosphorus vs. nitrogen limitation of new and export production. Pages 377-394 *in* W. H. Berger, V. S. Smetacek, and G. Wefer, editors. Productivity of the ocean: Past and present: Report of the Dahlem workshop. John Wiley and Sons, New York.

Cody, G. D., N. Z. Boctor, T. R. Filley, R. M. Hazen, J. H. Scott, A. Sharma, and H. S. Yoder Jr. 2000. Primordial carbonylated iron-sulfur compounds and the synthesis of pyruvate. Science **289**:1337-1340.

Cornah, J. E., M. J. Terry, and A. G. Smith. 2003. Green or red: what stops the traffic in the tetrapyrrole pathway? TRENDS in Plant Science **8**:224-230.

Cornejo, J., R. D. Willows, and S. I. Beale. 1998. Phytobilin biosynthesis: cloning and expression of a gene encoding soluble ferredoxin-dependent heme oxygenase from *Synechocystis* sp. PCC 6803. The Plant Journal **15**:99-107.

Cramer, W. A., G. M. Soriano, M. Ponomarev, D. Huang, H. Zhang, S. E. Martinez, and J. L. Smith. 1996. Some new structural aspects and old controversies concerning the cytochrome b_6f complex of oxygenic photosynthesis. Annual Review of Plant Physiology and Plant Molecular Biology **47**:477-508.

Dalsgaard, T., B. Thamdrup, and D. E. Canfield. 2005. Anaerobic ammonium oxidation (anammox) in the marine environment. Research in Microbiology **156**(4):457-464.

Davey, M. and R. J. Geider. 2001. Impact of iron limitation on the photosynthetic apparatus of the diatom *Chaetoceros muelleri* (Bacillariophyceae). Journal of Phycology **37**:987-1000.

de Baar, H. J. W. and J. T. M. de Jong. 2001. Distributions, sources and sinks of iron in seawater. Pages 123-254 *in* D. R. Turner and R. J. Hunter, editors. The biogeochemistry of iron in seawater. IUPAC Series on analytical and physical chemistry of environmental systems.

Denman, K. L. 2008. Climate change, ocean processes and ocean iron fertilization. Marine Ecology Progress Series **364**:219-225.

Deutsch, C., J.L. Sarmiento, D.M. Sigman, N. Gruber, and J.P. Dunne. 2007. Nature 445:163-167.

Donaghay, P. L., P. S. Liss, R. A. Duce, D. R. Kester, A. K. Hanson, T. Villareal, N. W. Tindale, and D. J. Gifford. 1991. The role of episodic atmospheric nutrient inputs in the chemical and biological dynamics of oceanic ecosystems. Oceanography **4**:62-70.

Duce, R. A., P. S. Liss, J. T. Merrill, E. L. Atlas, P. Buat-Menard, B. B. Hicks, J. M. Miller, J. M. Prospero, R. Arimoto, T. M. Church, W. Ellis, J. N. Galloway, L. Hansen, T. D. Jickells, A. H. Knap, K. H. Reinhardt, B. Schneider, A. Soudine, J. J. Tokos, S. Tsunogai, R. Wollast, and M. Zhou. 1991. The atmospheric input of trace species to the world ocean. Global and Biogeochemical Cycles **5**:193-259.

Duce, R. A. and N. W. Tindale. 1991. Atmospheric transport of iron and its deposition in the ocean. Limnology and Oceanography **36**:1715-1726.

Dugdale, R. C. and F. P. Wilkerson. 1991. Low specific nitrate uptake rate: A common feature of high-nutrient, low-chlorophyll marine ecosystems. Limnology and Oceanography **36**:1678-1688.

Dunford, H. B. 2010. Peroxidases and Catalases: Biochemistry, Biophysics, Biotechnology, and Physiology, Second Edition. Wiley, New Jersey.

El-Sayed, S. Z. 1987. Biological productivity of Antarctic waters: present paradoxes and emerging paradigms. Pages 1-21 *in* S. Z. El-Sayed and A. P. Tomo, editors. Antarctic aquatic biology. SCAR, Cambridge.

Falkowski, P. G. 1997. Evolution of the nitrogen cycle and its influence on the biological sequestration of CO_2 in the ocean. Nature **387**:272-275.

Falkowski, P. G., R. T. Barber, and V. Smetacek. 1998. Biogeochemical controls and feedbacks on ocean primary production. Science **281**:200-206.

Falkowski, P. G. and J. A. Raven. 1997. Aquatic Photosynthesis. Second edition. Princeton University Press, Oxford.

Galloway, J. N., F. J. Dentener, D. G. Capone, E. W. Boyer, R. W. Howarth, S. P. Seitzinger, G. P. Asner, C. C. Cleveland, P. A. Green, E. A. Holland, D. M. Karl, A. F. Michaels, J. H. Porter, A. R. Townsend, and C. J. Vorosmarty. 2004. Nitrogen cycles: past, present, and future. Biogeochemistry **70**:153-226.

Geider, R. J. and J. La Roche. 1994. The role of iron in phytoplankton photosynthesis, and the potential for iron-limitation of primary productivity in the sea. Photosynthesis Research **39**:275-301.

Gledhill, M. 2007. The determination of heme b in marine phyto- and bacterioplankton. Marine Chemistry **103**:393-403.

Gledhill, M., E. P. Achterberg, D. J. Honey, M. Nielsdottir, and M. Rijkenberg. in prep. Distributions of particulate heme *b* in the Atlantic and Southern Ocean - implications for changes in phytoplankton photosystems (see Appendix 1).

Gledhill, M. and C. M. G. van Den Berg. 1994. Determination of complexation of iron(III) with natural organic complexing ligands in seawater using cathodic stripping voltammetry. Marine Chemistry **47**:41-54.

Gran, H. H. 1931. On the conditions for the production of plankton in the sea. Rapports et proces verbaux des Reunions, Conseil International pour l'exploration de la Mer **75**:37-46.

Gray, H. B. and J. R. Winkler. 1996. Electron transfer in proteins. Annual Review of Biochemistry **65**:537-561.

Greene, R. M., R. J. Geider, and P. G. Falkowski. 1991. Effect of iron limitation on photosynthesis in a marine diatom. Limnology and Oceanography **36**:1772-1782.

Groves, J. T. and Y.-Z. Han. 2005. Models and mechanisms of cytochrome P450 action. Pages 1-44 *in* P. R. Ortiz de Montellano, editor. Cytochrome P450: Structure, Mechanism and Biochemistry. Kluwer Academic Publishers, New York.

Gruber, N. 2004. The dynamics of the marine nitrogen cycle and its influence on atmospheric CO_2 variations. Pages 97-148 *in* M. Follows and T. Oguz, editors. The ocean carbon cycle and climate. Kluwer Academic Publishers, Dordrecht, The Netherlands.

Gruber, N. 2008. The marine nitrogen cycle: overview and challenges. Pages 1-50 *in* D. G. Capone, D. A. Bronk, M. R. Mulholland, and E. J. Carpenter, editors. Nitrogen in the marine environment. Academic Press, London.

Hart, T. J. 1934. On the phytoplankton of the Southwest Atlantic and Bellingshausen Sea 1929-1931. Discovery Reports **8**:1-268.

Ho, K. K. 2005. Cytochrome c_6 genes in cyanobacteria and higher plants. Pages 273-286 *in* M. Pessarakli, editor. Handbook of Photosynthesis: Second Edition. CRC Press.

Honey, D. J., M. Gledhill, T. S. Bibby, F-E. Legiret, N. J. Pratt, A. E. Hickman, T. Lawson, and E. P. Achterberg. 2013. Heme *b* in marine phytoplankton and particulate material from the North Atlantic Ocean. Marine Ecology Progress Series **483**: 1-17.

Hoppe-Seyler, F. 1890. Ueber Muskelfarbstoffe. Zeitschrift fur physiologische Chemie **14**:106-108.

Jickells, T. D. 1995. Atmospheric inputs of metals and nutrients to the oceans: their magnitude and effects. Marine Chemistry **68**:5-14.

Jickells, T. D., Z. S. An, K. K. Andersen, A. R. Baker, G. Bergametti, N. Brooks, J. J. Cao, P. W. Boyd, R. A. Duce, K. A. Hunter, H. Kawahata, N. Kubilay, J. laRoche, P. S. Liss, N. Mahowald, J. M. Prospero, A. J. Ridgwell, I. Tegen, and R. Torres. 2005. Global iron connections between desert dust, ocean biogeochemistry, and climate. Science **308**:67-71.

Jickells, T. D. and L. J. Spokes. 2001. Atmospheric iron inputs to the oceans. Pages 85-121 *in* D. R. Turner and K. A. Hunter, editors. The biogeochemistry of iron in seawater, IUPAC. Wiley.

Johnson, K., R. M. Gordon, and K. H. Coale. 1997. What controls dissolved iron concentrations in the world ocean? Marine Chemistry **57**:137-161.

Karl, D., A. Michaels, B. Bergman, D. Capone, E. Carpenter, R. Letelier, F. Lipschultz, H. Paerl, D. Sigman, and L. Stal. 2002. Dinitrogen fixation in the world's oceans. Biogeochemistry **57/58**:47-98.

Keilin, D. 1925. On cytochrome, a respiratory pigment, common to animals, yeast, and higher plants. Proceedings of the Royal Society, B **98**:312-339.

Kikuchi, G., T. Yoshida, and M. Noguchi. 2005. Heme oxygenase and heme degradation. Biochemical and Biophysical Research Communications **338**:558-567.

Küpper, H., I. Šetlík, S. Seibert, O. Prášil, E. Šetlikova, M. Strittmatter, O. Levitan, J. Lohscheider, I. Adamska, and I. Berman-Frank. 2008. Iron limitation in the marine cyanobacterium *Trichodesmium* reveals new insight into regulation of photosynthesis and nitrogen fixation. New Phytologist **179**:784-798.

Kurisu, G., H. Zhang, J. L. Smith, and W. A. Cramer. 2003. Structure of the cytochrome b_6f complex of oxygenic photosynthesis: Tuning the cavity. Science **302**:1009-1014.

Lemberg, R. and J. Barrett. 1973. Cytochromes. Academic Press Inc. Ltd, London.

Letelier, R. M. and D. M. Karl. 1996. Role of *Trichodesmium* spp. in the productivity of the subtropical North Pacific Ocean. Marine Ecology Progress Series **133**:263-273.

Lewis, M. R., W. G. Harrison, N. S. Oakey, D. Hebert, and T. Platt. 1986. Vertical nitrate fluxes in the oligotrophic ocean. Science **234**:870-873.

Libes, S. M. 2009. Introduction to Marine Biogeochemistry, Second Edition. Elsevier, Academic Press, London.

Liu, H., R. R. Bidigare, E. Laws, M. R. Landry, and L. Campbell. 1999. Cell cycle and physiological characteristics of *Synechococcus* (WH7803) in chemostat culture. Marine Ecology Progress Series **189**:17-25.

Lubben, M. and K. Morand. 1994. Novel prenylated hemes as cofactors of cytochrome oxidases. The Journal of Biological Chemistry **269**:21473-21479.

MacMunn, C. A. 1886. Researches on myohaematin and the histohaematins. Philosophical Transactions of the Royal Society of London **177**:267-298.

Maines, M. D. 1988. Heme oxygenase: function, multiplicity, regulatory mechanisms, and clinical applications. The FASEB Journal **2**:2557-2568.

Maranon, E., P. M. Holligan, M. Varela, B. Mourino, and A. J. Bale. 2000. Basin-scale variability of phytoplankton biomass, production and growth in the Atlantic Ocean. Deep-Sea Research I **47**:825-857.

Margoliash, E. and A. Schejter. 1966. Cytochrome *c*. Pages 113-286 *in* C. B. Anfinsen, editor. Advances in Protein Chemistry. Academic Press Inc., London.

Martin, J. H. 1990. Glacial-Interglacial CO_2 change: The Iron Hypothesis. Paleoceanography **5**:1-13.

Martin, J. H., K. H. Coale, K. S. Johnson, S. E. Fitzwater, R. M. Gordon, S. J. Tanner, C. N. Hunter, V. A. Elrod, J. L. Nowicki, T. L. Coley, R. T. Barber, S. Lindley, A. J. Watson, K. Van Scoy, C. S. Law, M. I. Liddicoat, R. Ling, T. Stanton, J. Stockel, C. Collins, A. Anderson, R. Bidigare, M. Ondrusek, M. Latasa, F. J. Millero, K. Lee, W. Yao, J. Z. Zhang, G. Friederich, C. Sakamoto, F. Chavez, K. Buck, Z. Kolber, R. Greene, P. Falkowski, S. W. Chisholm, F. Hoge, R. Swift, J. Yungel, S. Turner, P. Nightingale, A. Hatton, P. Liss, and N. W. Tindale. 1994. Testing the iron hypothesis in ecosystems of the equatorial Pacific Ocean. Nature **371**:123-129.

Martin, J. H. and S. E. Fitzwater. 1988. Iron deficiency limits phytoplankton growth in the North-east Pacific Subarctic. Nature **331**:341-343.

Martin, J. H., R. M. Gordon, and S. E. Fitzwater. 1990. Iron in Antarctic waters. Nature **345**:156-158.

Michaels, A. F., D. M. Karl, and D. G. Capone. 2001. Element stoichiometry, new production and nitrogen fixation. Oceanography **14**:68-77.

Milligan, A. J., I. Berman-Frank, Y. Gerchman, G. C. Dismukes, and P. G. Falkowski. 2007. Light-dependent oxygen consumption in nitrogen-fixing cyanobacteria plays a key role in nitrogenase protection. Journal of Phycology **43**:845-852.

Mills, M. M., C. Ridame, M. Davey, J. La Roche, and R. J. Geider. 2004. Iron and phosphorus co-limit nitrogen fixation in the eastern tropical North Atlantic. Nature **429**:292-294.

Minas, H. J., M. Minas, and T. T. Packard. 1986. Productivity in upwelling areas deduced from hydrographic and chemical fields. Limnology and Oceanography **31**:1182-1206.

Mochizuki, N., R. Tanaka, B. Grimm, T. Masuda, M. Moulin, A. G. Smith, A. Tanaka, and M. J. Terry. 2010. The cell biology of tetrapyrroles: a life and death struggle. TRENDS in Plant Science **15**:488-498.

Moisander, P. H., R. A. Beinart, I. Hewson, A. E. White, K. S. Johnson, C. A. Carlson, J. P. Montoya, and J. P. Zehr. 2010. Unicellular cyanobacterial distributions broaden the oceanic N_2 fixation domain. Science **327**:1512-1514.

Montoya, J. P., C. M. Holl, J. P. Zehr, A. Hansen, T. A. Villareal, and D. G. Capone. 2004. High rates of N_2 fixation by unicellular diazotrophs in the oligotrophic Pacific Ocean. Nature **430**:1027-1031.

Moore, C. M., M. M. Mills, E. P. Achterberg, R. J. Geider, J. La Roche, M. I. Lucas, E. L. McDonagh, X. Pan, A. J. Poulton, M. J. A. Rijkenberg, D. J. Suggett, S. J. Ussher, and E. M. S. Woodward. 2009. Large-scale distribution of Atlantic nitrogen fixation controlled by iron availability. Nature Geoscience **2**:867-871.

Moore, G. R. 1996. Haemoproteins. Pages 189-216 *in* D. S. Bendall, editor. Protein Electron Transfer. BIOS Scientific Publishers Ltd, Oxford.

Moore, J. K. and O. Braucher. 2008. Sedimentary and mineral dust sources of dissolved iron to the world ocean. Biogeosciences **5**:631-656.

Morand, L. Z., R. H. Cheng, and D. W. Krogmann. 1994. Soluble electron-transfer catalysts of cyanobacteria. Pages 243-269 *in* D. A. Bryant, editor. The Molecular Biology of Cyanobacteria. Kluwer Academic Press.

Murshudov, G. N., A. I. Grebenko, V. Barynin, Z. Dauter, K. S. Wilson, B. K. Vainshtein, W. Melik-Adamyan, J. Bravo, J. M. Ferran, J. C. Ferrer, J. Switala, P. C. Loewen, and I. Fita. 1996. Structure of the heme d of *Penicillium vitale* and *Escherichia coli* catalases. The Journal of Biological Chemistry **271**:8863-8868.

Ortiz de Montellano, P. R. 2005. Cytochrome P450: Structure, Mechanism, and Biochemistry, Third Edition. Kluwer Academic, New York.

Osterberg, R. 1974. Origins of metal ions in biology. Nature **249**:382-383.

Ostermeier, C., S. Iwata, and H. Michel. 1996. Cytochrome *c* oxidase. Current Opinion in Structural Biology **6**:460-466.

Papenbrock, J. and B. Grimm. 2001. Regulatory network of tetrapyrrole biosynthesis - studies of intracellular signalling involved in metabolic and developmental control of plastids. Planta **213**:667-681.

Papenbrock, J., H.-P. Mock, E. Kruse, and B. Grimm. 1999. Expression studies in tetrapyrrole biosynthesis: inverse maxima of magnesium chelatase and ferrochelatase activity during cyclic photoperiods. Planta **208**:264-273.

Pauling, L., H. A. Itano, S. J. Singer, and I. C. Wells. 1949. Sickle cell anemia, a molecular disease. Science **110**:543-548.

Pilson, M. E. Q. 1998. An introduction to the chemistry of the sea. Prentice-Hall, Inc., New Jersey.

Postgate, J. R. 1998. Nitrogen Fixation. Cambridge University Press.

Poulton, S. W. and R. Raiswell. 2002. The low-temperature geochemical cycle of iron: From continental fluxes to marine sediment deposition. American Journal of Science **302**:774-805.

Raven, J. A. 1988. The iron and molybdenum use efficiencies of plant growth with different energy, carbon and nitrogen sources. New Phytologist **109**:279-287.

Raven, J. A. 1990. Predictions of Mn and Fe use efficiencies of phototrophic growth as a function of light availability for growth and of C assimilation pathway. New Phytologist **116**:1-18.

Reedy, C. J. and B. R. Gibney. 2004. Heme protein assemblies. Chemical Reviews **104**:617-649.

Rees, D. C. and J. B. Howard. 2000. Nitrogenase: standing at the crossroads. Current opinion in chemical biology **4**:559-566.

Reuter, J. G. and D. R. Ades. 1987. The role of iron nutrition in photosynthesis and nitrogen assimilation in *Scenedesmus quadricauda* (Chlorophyceae). Journal of Phycology **32**:452-457.

Rich, H. W. and F. M. M. Morel. 1990. Availability of well-defined iron colloids to the marine diatom *Thalassiosira weissflogii*. Limnology and Oceanography **35**:652-662.

Richier, S., A. I. Macey, N. J. Pratt, D. J. Honey, C. M. Moore, and T. S. Bibby. 2012. Abundances of iron-binding photosynthetic and nitrogen-fixing proteins of *Trichodesmium* both in culture and *in situ* from the North Atlantic. PLoS ONE **7**:e35571.

Rijkenberg, M. J. A., C. F. Powell, M. Dall'Osto, M. C. Nielsdottir, M. D. Patey, P. G. Hill, A. R. Baker, T. D. Jickells, R. M. Harrison, and E. P. Achterberg. 2008. Changes in iron speciation following a Saharan dust event in the tropical North Atlantic Ocean. Marine Chemistry **110**:56-67.

Rue, E. L. and K. W. Bruland. 1995. Complexation of iron(III) by natural organic ligands in the Central North Pacific as determined by a new competitive ligand equilibration/adsorptive cathodic stripping voltammetric method. Marine Chemistry **50**:117-138.

Saito, M. A., E. M. Bertrand, S. Dutkiewicz, V. V. Bulygin, D. M. Moran, F. M. Monteiro, M. J. Follows, F. W. Valois, and J. B. Waterbury. 2011. Iron conservation by reduction of metalloenzyme inventories in the marine diazotroph *Crocosphaera watsonii*. PNAS **106**:2184-2189.

Sañudo-Wilhelmy, S. A., A. B. Kustka, C. J. Gobler, D. A. Hutchins, M. Yang, K. Lwiza, J. Burns, D. G. Capone, J. A. Raven, and E. J. Carpenter. 2001. Phosphorus limitation of nitrogen fixation by *Trichodesmium* in the central Atlantic Ocean. Nature **411**:66-69.

Sawaya, M. R., D. W. Krogmann, A. Serag, K. K. Ho, T. O. Yeates, and C. A. Kerfeld. 2001. Structures of cyctochrome *c*-549 and cytochrome c_6 from the cyanobacterium *Arthrospira maxima*. Biogeochemistry **40**:9215-9225.

Schmetterer, G. 1994. Cyanobacterial respiration. Pages 409-435 *in* D. A. Bryant, editor. The Molecular Biology of Cyanobacteria. Kluwer Academic Press.

Schutz, L. W., J. M. Prospero, P. Buat-Menard, R. A. C. Carvalho, A. Cruzado, P. Harriss, N. Z. Heidam, and R. Jaenicke. 1990. The long range transport of mineral aerosols. Pages 197-229 *in* A. H. Knap, editor. The long range atmospheric transport of natural and contaminant substances. Kluwer Academic Publisher.

Scott, R. A. and A. G. Mauk. 1996. Cytochrome *c*: a multidisciplinary approach. University Science Books, Sausalito, CA.

Smith, S. V. 1984. Phosphorus versus nitrogen limitation in the marine environment. Limnology and Oceanography **29**:1149-1160.

Stewart, D. H. and G. W. Brudvig. 1998. Cytochrome b_{599} of photosystem II. Biochimica et Biophysica Acta **1367**:63-87.

Strous, M., J. A. Fuerst, E. H. M. Kramer, S. Logemann, G. Muyzer, K. T. van de Pas-Schoonen, R. Webb, J. G. Kuenen, and M. M. S. Jetten. 1999. Missing lithotroph identified as new planctomycete. Nature 400:446–449.

Sunda, W. G. 2001. Bioavailability and bioaccumulation of iron in the sea. Pages 41-84 *in* D. R. Turner and R. J. Hunter, editors. The biogeochemistry of iron in seawater. IUPAC Series on analytical and physical chemistry of environmental systems.

Taylor, S. R. 1964. Abundance of chemical elements in the continental crust: a new table. Geochimica et Cosmochimica Acta **28**:1273-1285.

Teichmann, L. K. 1853. Ueber die Krystallisation des orpnischen Be-standtheile des Blutes. Ration Med **3**:375-388.

Timkovich, R., M. S. Cork, R. B. Gennis, and P. Y. Johnson. 1985. Proposed structure of heme *d*, a prosthetic group of bacterial terminal oxidases. Journal of the American Chemical Society **107**:6069-6075.

Timmermans, K. R., W. Stolte, and H. J. W. de Baar. 1994. Iron-mediated effects on nitrate reductase in marine phytoplankton. Marine Biology **121**:389-396.

Tyrrell, T. 1999. The relative influences of nitrogen and phosphorus on oceanic primary production. Nature **400**:525-531.

Ussher, S. J., E. P. Achterberg, and P. J. Worsfold. 2004. Marine biogeochemistry of iron. Environmental Chemistry **1**:67-80.

Van De Vossenberg, J., J. E. Rattray, W. Geerts, B. Kartal, L. Van Niftrik, E. G. Van Donselaar, J. S. S. Damsté, M. Strous, and M. S. Jetten. 2008. Enrichment and characterization of marine anammox bacteria associated with global nitrogen gas production. Environmental microbiology **10**(11):3120-3129.

Warburg, O. and H. S. Gewitz. 1951. Cytohemin from the heart muscle. Hoppe-Seyler's Zeitschrift fur physiologische Chemie **288**:1-4.

Watson, A. J., D. C. E. Bakker, A. J. Ridgwell, P. W. Boyd, and C. S. Law. 2000. Effect of iron supply on Southern Ocean CO_2 uptake and implications for glacial atmospheric CO_2. Nature **407**.

Webb, E. A., J. W. Moffett, and J. B. Waterbury. 2001. Iron stress in open-ocean cyanobacteria (*Synechococcus*, *Trichodesmium*, and *Crocosphaera* spp.): Idenitification of the IdiA protein. Applied and Environmental Microbiology **67**:5444-5452.

Wells, M. L., N. M. Price, and K. W. Bruland. 1995. Iron chemistry in seawater and its relationship to phytoplankton: A workshop report. Marine Chemistry **48**:157-182.

Whitmarsh, J. and H. B. Pakrasi. 1996. Form and function of cytochrome *b*-559. Pages 249-264 *in* D. R. Ort, C. F. Yocum, and I. F. Heichel, editors. Oxygenic Photosynthesis: The Light Reactions. Kluwer Academic Publishers.

Wu, J., E. Boyle, W. Sunda, and L.-S. Wen. 2001. Soluble and colloidal iron in the oligotrophic North Atlantic and North Pacific. Science **293**:847-849.

Yamashita, E., H. Aoyama, M. Yao, K. Muramoto, K. Shinzawa-Itoh, S. Yoshikawa, and T. Tsukihara. 2005. Absolute configuration of the hydroxyfarnesylethyl group of haem A, determined by X-ray structural analysis of bovine heart cytochrome *c* oxidase using methods applicable at 2.8 Å resolution. Acta Crystallographica Section D: Biological Crystallography **D61**:1373-1377.

York, J. L., S. McCoy, D. N. Taylor, and W. S. Caughey. 1967. Heme A of cytochrome *c* oxidase. The Journal of Biological Chemistry **242**:908-911.

Yoshida, T. and G. Kikuchi. 1978. Purification and properties of heme oxygenase from pig spleen microsomes. Journal of Biological Chemistry **253**:4224-4229.

Yoshida, T. and G. Kikuchi. 1979. Purification and properties of heme oxygenase from rat liver microsomes. Journal of Biological Chemistry **254**:4487-4491.

Yoshikawa, S., K. Shinzawa-Itoh, and T. Tsukihara. 2000. X-ray structure and the reaction mechanism of bovine heart cytochrome *c* oxidase. Journal of Inorganic Biochemistry **82**:1-7.

Zehr, J. P., E. J. Carpenter, and T. A. Villareal. 2000. New perspectives on nitrogen-fixing microorganisms in tropical and subtropical oceans. Trends in Microbiology **8**:68-73.

Zwirglmaier, K., L. Jardillier, M. Ostrowski, S. Mazard, L. Garczarek, D. Vaulot, F. Not, R. Massana, O. Ulloa, and D. J. Scanlan. 2008. Global phylogeography of marine *Synechococcus* and *Prochlorococcus* reveals a distinct partitioning of lineages among oceanic biomes. Environmental Microbiology **10**:147-161.

Chapter 2

Materials and methods

2.1 Summary

In this chapter, three laboratory cultures of marine cyanobacteria investigated during the project are introduced and the procedures and equipment used are described. Procedures include media preparation, culturing techniques, photophysiology measurements and analytical techniques used to quantify heme *b*, chlorophyll *a*, particulate organic carbon (POC), particulate organic nitrogen (PON) and nitrogen fixation rates. In addition, details of two research cruises in the (sub-) tropical North Atlantic are provided.

2.2 Laboratory cultures

Laboratory culture experiments were conducted on three different species of marine cyanobacteria: the phycoerythrin-rich unicellular cyanobacteria *Synechococcus* sp. WH7803 (CCMP1334) provided by David Scanlan (School of Life Sciences, University of Warwick) and the non-heterocystous diazotrophic cyanobacteria *Crocosphaera watsonii* (WH8501) and *Trichodesmium erythraeum* (IMS101) provided by Tracy Lawson (School of Biological Sciences, University of Essex). Two different media were used to grow cultures in the laboratory: *Synechococcus* was grown in artificial seawater (section 2.2.1, Table 2.1), while *Crocosphaera* and *Trichodesmium* were grown in YBC-II (section 2.2.2, Table 2.2). Refer to Honey et al. (2013) for details on eukaryotic phytoplankton cultures previously studied by Martha Gledhill (School of Ocean and Earth Sciences, University of Southampton).

2.2.1 Artificial seawater medium

Chemicals were reagent grade and purchased from Fisher Scientific UK Ltd, except where otherwise stated. Artificial seawater (ASW) medium defined by Wilson et al. (1996) was used to grow *Synechococcus* sp. WH7803 in batch cultures as initial attempts to grow cultures using f/2 nutrients (Guillard and Ryther 1962, Guillard 1975) with North Atlantic gyre water as the base were unsuccessful. Artificial seawater was modified by removing iron from the trace metal stock solution and added separately (see section 2.2.3). Sodium chloride (NaCl, Table 2.1) was added to a 1 L acid washed (<10% HCl, 7 days)

Compound		Molecular Weight (g)	Primary Stock Solution (g 50 ml^{-1})	Addition	Final Concentration
Name	Formula				
Sodium chloride	NaCl	58.44	-	25 g	0.48 mol L^{-1}
Sodium nitrate	$NaNO_3$	84.99	3.75	10 ml	8.8 mmol L^{-1}
Magnesium chloride	$MgCl_2.6H_2O$	203.31	10	10 ml	9.8 mmol L^{-1}
Potassium chloride	KCl	74.55	5.0	5.0 ml	6.7 mmol L^{-1}
Calcium chloride	$CaCl_2.2H_2O$	147.01	5.0	5.0 ml	4.5 mmol L^{-1}
Magnesium sulphate	$MgSO_4.7H_2O$	246.47	17.5	10 ml	14.2 mmol L^{-1}
Disodium hydrogen phosphate	Na_2HPO_4	141.96	0.6	2.5 ml	172.6 µmol L^{-1}
2-Amino-2-hydroxymethyl-propane-1,3-diol *	$C_4H_{11}NO_3$	121.14	10	5.5 ml	9.1 mmol L^{-1}
Boric acid	H_3BO_3	61.84	-	2.86 g	46.2 µmol L^{-1}
Manganese chloride	$MnCl_2.4H_2O$	197.91	-	1.81 g	9.15 µmol L^{-1}
Zinc sulphate	$ZnSO_4.H_2O$	179.48	-	0.222 g	1.2 µmol L^{-1}
Sodium molybdate	$Na_2MoO_4.2H_2O$	241.95	-	0.39 g	1.6 µmol L^{-1}
Copper sulphate	$CuSO_4.5H_2O$	249.68	0.40	1.0 ml	32 nmol L^{-1}
Cobalt nitrate	$Co(NO_3)_2.6H_2O$	291.07	2.47	1.0 ml	169 nmol L^{-1}
Ethylenediaminetetra acetic acid (EDTA)	$(Na_2)EDTA.2H_2O$	372.24	-	0.5 g	5.0 µmol L^{-1}

Table 2.1. Major salts/macronutrients (**blue**) and trace metals (**red**) of the artificial seawater (ASW) media recipe used to culture *Synechococcus* sp. WH7803; providing the molecular weight, stock solution (g 50 ml^{-1} MilliQ water), quantity added and final molarities of each compound. Note, additions for trace metals refer to preparation of the trace metal stock solution only. * Commonly known as Tris Buffer. Recipe modified from Wilson et al. (1996).

polycarbonate bottle (*A*, Nalgene) and dissolved in 250 ml of high purity water (>18 mΩ cm^{-1}) obtained from a MilliQ water purification system (Millipore, Watford, UK). The remaining major salts of Table 2.1 (blue) were prepared as primary stock solutions using MilliQ water and added to *A*, bringing the volume to 950 ml with additional MilliQ water. The pH of *A* was then adjusted to 8.0 using small additions of 10% HCl. The trace metal stock solution and primary stock solutions of copper sulphate and cobalt nitrate were prepared as described in Table 2.1 (red). The remaining trace metal compounds were weighed and fully dissolved into separate 50 ml polystyrene tubes (Fisherbrand) using MilliQ water. The trace metals compounds were combined in a separate acid-washed (<10% HCl, 7 days) 1 L polycarbonate bottle (*B*, Nalgene) along with 1 ml of copper sulphate and cobalt nitrate stock solutions. The volume of *B* was brought up to 1 L with

MilliQ water and stored at 4 °C. Once the trace metal stock solution was prepared, 1 ml of *B* was added to *A*, followed by various iron additions. The volume of *A* was then brought up to 1 L with MilliQ water. Finally, the contents of *A* were filtered (0.2 µm sterile syringe filter, Minisart, Sartorius) into sterile polycarbonate culture vessels (EasyFlasks, Nunclon, Sigma-Aldrich) and stored at 4 °C prior to use.

Compound		Molecular Weight (g)	Primary Stock Solution (g 50 ml^{-1})	Addition	Final Concentration
Name	Formula				
Sodium chloride	$NaCl$	58.44	-	24.55 g	0.42 mol L^{-1}
Potassium chloride	KCl	74.55	-	0.75 g	10 mmol L^{-1}
Sodium bicarbonate	$NaHCO_3$	84.01	-	0.21 g	2.5 mmol L^{-1}
Boric acid	H_3BO_3	61.84	-	0.036 g	0.58 mmol L^{-1}
Potassium bromide	KBr	119.00	-	0.1157 g	0.97 mmol L^{-1}
Magnesium chloride	$MgCl_2.6H_2O$	203.31	-	4.067 g	20 mmol L^{-1}
Calcium chloride	$CaCl_2.2H_2O$	147.01	-	1.47 g	10 mmol L^{-1}
Magnesium sulphate	$MgSO_4.7H_2O$	246.47	-	6.16 g	25 mmol L^{-1}
Sodium fluoride	NaF	41.98	0.147	1.0 ml	70 µmol L^{-1}
Strontium chloride	$SrCl_2.6H_2O$	266.62	0.867	1.0 ml	65 µmol L^{-1}
Monosodium phosphate	$NaH_2PO_4.2H_2O$	156.02	0.390	1.0 ml	50 µmol L^{-1}
Ethylenediaminetetra acetic acid (EDTA)	$(Na_2)EDTA.2H_2O$	372.24	-	0.745 g	2.0 µmol L^{-1}
Manganese chloride	$MnCl_2.4H_2O$	197.91	0.198	1.0 ml	20 nmol L^{-1}
Zinc sulphate	$ZnSO_4.7H_2O$	287.53	0.058	1.0 ml	4.0 nmol L^{-1}
Cobalt chloride	$CoCl_2.6H_2O$	291.07	0.298	1.0 ml	2.5 nmol L^{-1}
Sodium molybdate	$Na_2MoO_4.2H_2O$	241.95	0.133	1.0 ml	11 nmol L^{-1}
Copper sulphate	$CuSO_4.5H_2O$	249.68	0.112	1.0 ml	1.0 nmol L^{-1}
Thiamine	$C_{12}H_{17}ClN_4OS$	300.81	-	5 mg	0.30 µmol L^{-1}
Biotin	$C_{10}H_{16}N_2O_3S$	244.31	0.025	1.0 ml	2.05 nmol L^{-1}
Cyanocobalamin (B_{12})	$C_{63}H_{88}CoN_{14}O_{14}P$	1355.38	0.025	1.0 ml	0.37 nmol L^{-1}

Table 2.2. Major salts/macronutrients (**blue**), trace metals (**red**) and vitamins (**green**) of the YBC-II recipe used to culture *Crocosphaera watsonii* (WH8501) and *Trichodesmium erythraeum* (IMS101); providing the molecular weight, stock solution (g 50 ml^{-1} MilliQ water), quantity added and final molarities of each compound. Note, additions for trace metals and vitamins refer only to preparation of trace metal and vitamin stock solutions, respectively. Recipe modified from Chen et al. (1996).

2.2.2 YBC-II medium

Chemicals were reagent grade and purchased from Fisher Scientific UK Ltd, except where otherwise stated. The cyanobacteria *Crocosphaera* and *Trichodesmium* were grown in the artificial seawater medium YBC-II defined by Chen et al. (1996), which was developed to culture marine diazotrophs (i.e. no nitrogen source in medium). Similar to the preparation of ASW (section 2.2.1), the recipe iron was removed from the trace metal stock solution and added separately (see section 2.2.3). Sodium chloride (Table 2.2) was added to a 1 L acid washed (<10% HCl, 7 days) polycarbonate bottle (*A*, Nalgene) and dissolved in 250 ml of MilliQ water. Primary stock solutions of sodium fluoride (NaF), strontium chloride ($SrCl_2$) and monosodium phosphate (NaH_2PO_4) were prepared and the remaining major salts were weighed and fully dissolved into separate 50 ml polystyrene tubes (Fisherbrand) using MilliQ water. Each component of *A* was then added as described in Table 2.2 (blue), bringing the volume up to 950 ml with additional MilliQ water. To make the YBC-II trace metal stock solution (*B*), a separate acid-washed (<10% HCl, 7 days) 1 L polycarbonate bottle (Nalgene) was filled with 900 ml of MilliQ water, to which 1 ml of each primary stock solution of Table 2.2 (red) was added. Ethylenediaminetetra acetic acid (EDTA) was weighed and fully dissolved in a 50 ml sterilin tube using MilliQ water, before being added to *B*. The volume of *B* was brought up to 1 L with MilliQ water and stored at 4 °C. To prepare the vitamin stock solution, 40 ml of MilliQ water was added to a 50 ml polystyrene tube (Fisherbrand, *C*), to which 5 mg of thiamine and 1 ml of biotin and cyanocobalamin stock solutions were added as described in Table 2.2 (green). The volume of *C* was brought to 50 ml with MilliQ water, filter sterilised and stored at -20 °C prior to use. Once the trace metal and vitamin stock solutions were prepared, 1 ml of *B* and 1 ml of *C* were added to *A*, followed by various iron additions. The final volume of *A* was made up to 1 L with MilliQ water. The pH was adjusted to between 8.15 and 8.20 with small additions of 10% NaOH. Finally, the YBC-II media was filtered (0.2 µm sterile syringe filter, Minisart, Sartorius) into sterile polycarbonate culture vessels (EasyFlasks, Nunclon, Sigma-Aldrich), stored at 4 °C and allowed to reach room temperature (~2 hours) prior to inoculation.

2.2.3 Iron concentration

Iron (Fe) was omitted from ASW and YBC-II media recipes (see above) and added separately with EDTA via FeEDTA stock solutions (1:1.1 M:M); 1.2 mmol L^{-1} for ASW and 0.4 mmol L^{-1} for YBC-II (total iron concentration). Three differed iron concentrations were prepared for ASW: 12 nmol L^{-1} Fe_T, 120 nmol L^{-1} Fe_T and 1.2 µmol L^{-1} Fe_T; and six different iron concentrations were prepared for YBC-II: 0 nmol L^{-1} Fe_T (no added iron), 4 nmol L^{-1} Fe_T, 10 nmol L^{-1} Fe_T, 20 nmol L^{-1} Fe_T, 40 nmol L^{-1} Fe_T and 120 nmol L^{-1} Fe_T. The concentration of iron not complexed by EDTA, expressed as pFe′ and equal to -log[inorganic iron], was calculated according to Sunda et al. (2005). Concentrations of inorganic iron exceed the solubility of iron in seawater at approximately 0.7 nmol L^{-1} (Sunda and Huntsman 1995),

and thus culture media in this study are thought to have included precipitated iron hydroxides (Sunda et al. 2005). An order of magnitude estimate of inorganic iron was calculated according to Sunda et al. (2005) using the added total iron concentrations. In cultures with no added iron, a nominal iron concentration of 0.5 nmol L^{-1} was used as an estimate of background contamination. The media was not cleaned with Chelex as preliminary studies suggested the chosen iron treatments ranged from iron-replete to iron-stressed conditions, and an understanding of the precise iron speciation was not an objective of this project. Precautions were taken to minimise external contamination of iron, including the preparation of culture media in a laminar flow cabinet and acid-washing (<10% HCl) all polycarbonate bottles for 7 days prior to use (stored in sealed zip-lock bags).

2.2.4 Culturing methods

Batch cultures were monitored in 45 ml of culture medium and acclimatised to the conditions (i.e. iron treatments) for a minimum of five transfers which were conducted every 6 to 10 days during preliminary monitoring. Transfers of *Synechococcus* sp. WH7803 and *Crocosphaera* were carried out in order to obtain an initial biovolume close to 1.0×10^6 µm^3 ml^{-1}; whereas *Trichodesmium* cultures were transferred to an initial trichome (filament) number of approximately 50 ml^{-1}. Cultures of *Synechococcus* sp. WH7803 were grown at 22 °C under 30 µmol quanta m^{-2} s^{-1} light and *Crocosphaera* and *Trichodesmium* were grown at 26 °C under 80 µmol quanta m^{-2} s^{-1} light; all on a 12:12 hour light:dark cycle. Cultures of *Synechococcus* sp. WH7803 and *Crocosphaera* were re-suspended every day by careful inversion of the culture vessels to agitate the 'matt' formed at the bottom. *Trichodesmium* cultures were kept suspended with continuous gentle agitation via an orbital shaker (Stuart, Gyro-rocker SSL3, 60 rpm). Prior to experimental runs, cultures were transferred into 400 ml (EasyFlasks, Nunclon, Sigma-Aldrich) of culture medium before a subsequent transfer in duplicate (400 ml in each culture vessel) during the late exponential phase to commence the experiment. Experiments were conducted over three consecutive 8-day growth cycles; therefore, six growth cycles per iron concentration (i.e. each growth cycle in duplicate).

Growth of experimental cultures was monitored every two days (days 0, 2, 4, 6 and 8) using a Coulter counter (*Synechococcus* and *Crocosphaera*) or light microscope (*Trichodesmium*), as well as photophysiology (F_v/F_m and σ_{PSII}) measurements via fast repetition rate fluorometry (FRRF). Cultures were also vacuum filtered (Fig. 2.1A) using a weak acid-washed (<10% HCl) filtration rig onto glass microfibre filters (GF/Fs, MF300, Fisher Scientific, 0.7 µm) every two days for the determination of heme *b* (10 - 40 ml, section 2.4) and chlorophyll *a* (10 ml, section 2.5) concentration and pre-ashed GF/Fs (450 °C, >12 hours) for particulate organic carbon (POC) and particulate organic nitrogen (PON) concentration (POC/N, 10 - 40 ml, section 2.6). Filtered samples were placed in 1.5

ml eppendorfs and stored at -80 °C prior to analysis. However, samples for the determination of heme *b*, chlorophyll *a*, POC and PON from *Crocosphaera* and *Trichodesmium* cultures were only processed for day 8. Nitrogen fixation incubations for each iron concentration of *Crocosphaera* and *Trichodesmium* cultures were conducted separately during the exponential growth phase (see section 2.7).

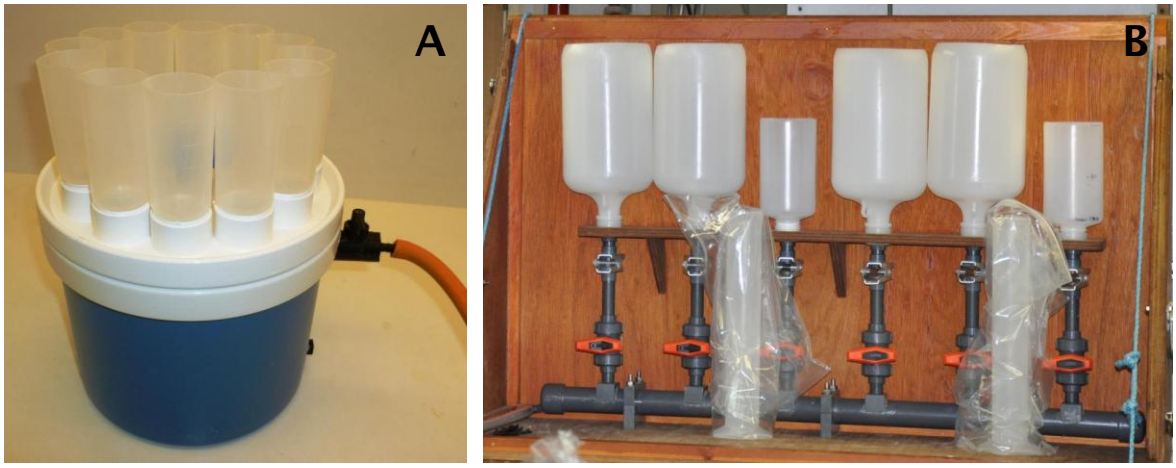

Figure 2.1. Filtration setups used for the collection of heme *b*, chlorophyll *a* and POC/N samples during (**A**) laboratory culture experiments and (**B**) research cruises D346 and D361. A separate filtration rig was used to filter nitrogen fixation samples during the cruises to prevent contamination of POC/N samples which were also used for ^{15}N natural abundance (t_{zero}).

2.2.5 Coulter counter and light microscopy

The diameter of *Synechococcus* sp. WH7803 (~1.5 µm) and *Crocosphaera watsonii* (~3.3 µm) cells enabled cultures to be monitored using a Beckman coulter counter (Multisizer 3, Meritics, Dunstable, UK) with 30 and 70 µm apertures, respectively (Fig. 2.2A). A 3 mol L^{-1} NaCl solution was used as diluent and electrolyte. The number of cells (ml^{-1}, e.g. Fig. 2.2B), mean cell diameter (µm) and total cellular biovolume (μm^3 ml^{-1}) were recorded. *Trichodesmium* trichomes (filaments) varied in length up to approximately 1 mm; hence cultures were not suitable for monitoring using the Coulter counter. Light microscopy (X40 magnification) was used to measure the number of trichomes (ml^{-1}) and mean trichome length (mm) of *Trichodesmium* cultures. After gentle agitation to ensure a representative sample, 1 ml of culture was transferred onto a Sedgewick Rafter counting cell slide (50 rows, 20 cells per row, 1000 cells total). Trichome number was measured by counting the total number of trichomes observed in five consecutive rows on the counting cell in two replicates. The average number of trichomes counted from the replicates was multiplied by 10 to calculate the number of trichomes ml^{-1}. The length (µm) of each trichome counted was also measured.

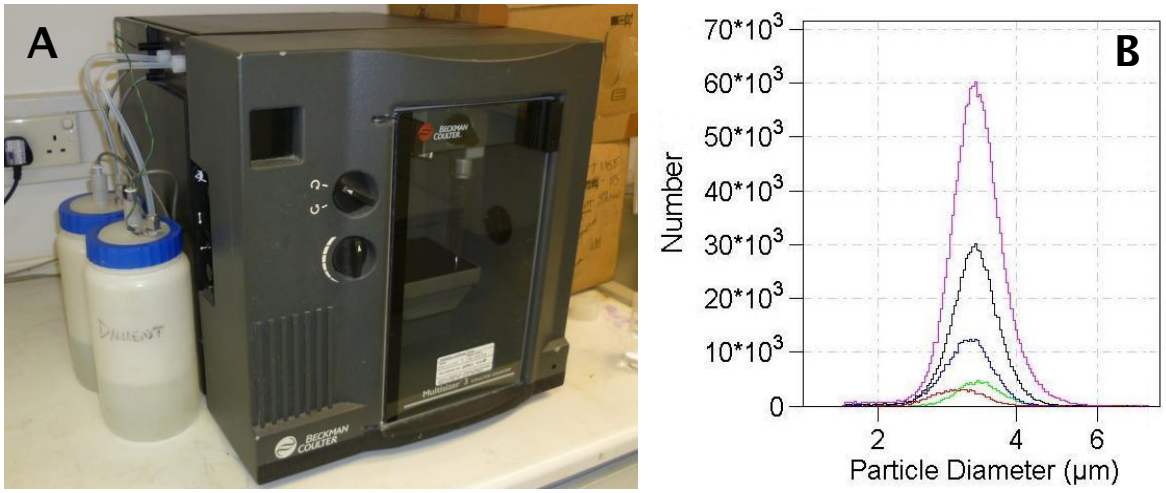

Figure 2.2. (**A**) The Beckman Coulter counter (Multisizer 3) used to monitor cell number, mean cell diameter and total biovolume of *Synechococcus* sp. WH7803 and *Crocosphaera watsonii* cultures and (**B**) an example overlay of peaks (blank subtracted) from one complete 8-day growth cycle used to determine the number of cells (ml^{-1}) from experimental cultures of *Crocosphaera watsonii*. Graph B shows the increase in cell numbers every two days (i.e. days 0, 2, 4, 6 and 8), reaching a maximum of 60 x 10^3 cells ml^{-1} on day 8.

2.3 Research cruises

Field data was collected from two research cruises in the (sub-) tropical North Atlantic during early 2010 (D346, section 2.3.1) and 2011 (D361, section 2.3.2). Both cruises were conducted aboard the *RRS Discovery*. Seawater from depths <200 m was obtained using 20 L Niskin bottles mounted on a stainless steel CTD rosette. Samples from D361 were obtained from pre-dawn CTD casts; however, the timing of sample collection from D346 varied as CTD casts were conducted as soon as the ship reached the next station. Filtered samples were placed in 1.5 ml eppendorfs and stored at -80 °C prior to laboratory analysis, with the exception of chlorophyll *a* filters collected during D361 which were processed during the cruise by Elizabeth Sargent (School of Ocean and Earth Sciences, University of Southampton). Physical parameters (e.g. temperature and salinity) were measured using SEABIRD sensors attached to the CTD during both cruises. See Appendix 2 for cruise metadata (e.g. position, sampling volumes, raw data).

Nanomolar nutrient concentrations from D346 (<200 m depth) were kindly provided by François-Eric Legiret (School of Ocean and Earth Science, University of Southampton). Phosphate and nitrate+nitrite (hereafter referred to as nitrate) concentrations were measured using colorimetric techniques with a standard segmented flow analyser coupled with 2 m liquid waveguide capillary cells (Zhang 2000, Zhang and Chi 2002, Patey et al. 2008). Seawater samples were routinely collected by the author from 20 and 40 m depth using a GOFLO bottle for total dissolvable iron concentration during D346; however, post-cruise flow injection analysis indicated the samples were contaminated (>15 nmol L^{-1}) and

results were consequently discarded. However, dissolved iron (dFe) concentrations have been presented from D361 which were kindly provided by Christian Schlosser (School of Ocean and Earth Science, University of Southampton, Schlosser et al. in prep). Samples for dFe were collected via a continuous towed FISH supply (approximately 2 - 3 m depth) pumped into a trace-metal clean sampling container and dFe determined using flow injection analysis (e.g. Klunder et al. 2011). *Trichodesmium* colony abundance (L^{-1}) during D361 was provided by Joe Snow (School of Ocean and Earth Sciences, University of Southampton), measured from pre-dawn phytoplankton net samples.

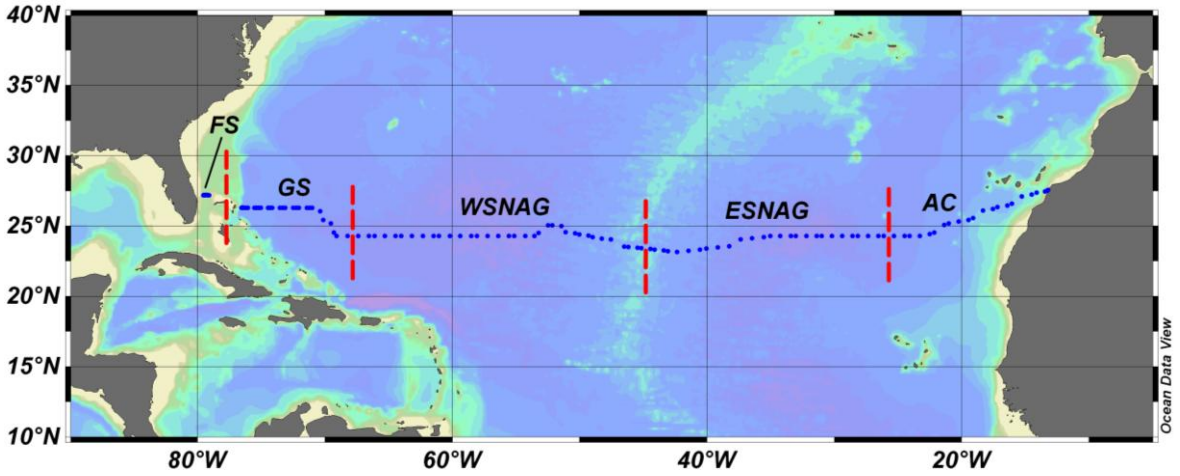

Figure 2.3. Map of station locations (blue dots) from research cruise D346 in the subtropical North Atlantic (STNA). Stations were divided into five oceanographic regions: Florida Straits (FS), Gulf Stream (GS), Western Subtropical North Atlantic Gyre (WSNAG), Eastern Subtropical North Atlantic Gyre (ESNAG) and Azores Current (AC).

2.3.1 Subtropical North Atlantic

The first research cruise (D346) was completed between 5 January and 15 February 2010 along a cross-sectional transect of the subtropical North Atlantic (STNA) from The Bahamas to The Canary Islands (Fig. 2.3). The study area was situated across two biogeographical regions according to Longhurst (1998): the North Atlantic Tropical Gyral Province (NATR) and the North Atlantic Subtropical Gyral Province (NAST). The latter has been used to descriptively distinguish from the second cruise (section 2.3.2). Stations were separated into five oceanographic regions based on the temperature and salinity of the surface mixed layer (SML). The five regions were defined as: Florida Straits (27.2 °N, 79.57 °W to 27.2 °N, 79.10 °W), Gulf Stream (26.3 °N, 76.56 °W to 24.3 °N, 68.24 °W), Western Subtropical North Atlantic Gyre (24.3 °N, 67. 40 °W to 23.43 °N, 45.16 °W), Eastern Subtropical North Atlantic Gyre (23.38 °N, 44.44 °W to 24.31 °N, 26.14 °W) and Azores Current (24.31 °N, 25.32 °W to 27.56 °N, 17.80 °W). Cruise D346 formed part of the CLIVAR programme (Climate Variability and Predictability, www.clivar.org), collecting a full suite of physical and chemical measurements across the subtropical basin at about 24

°N. In total, 133 stations were sampled at up to 3 depths per station (<200 m depth). Seawater was vacuum filtered (Fig. 2.1B) onto GF/Fs (MF300, Fisher Scientific, 0.7 µm) for the determination of heme *b* (1 - 4 L, section 2.4) and chlorophyll *a* (0.5 L, section 2.5) concentration and pre-ashed GF/Fs (450 °C, >12 hours) for the concentration of POC and PON (1 - 4 L, section 2.6). Overall, 388 heme *b*, 399 chlorophyll *a* and 374 POC/N samples were obtained; the number of samples varies due to availability of seawater from the CTD. In addition, 78 nitrogen fixation incubations (see section 2.7) were completed from 39 stations using seawater from two depths per station (surface and chlorophyll maximum).

2.3.2 Tropical North Atlantic

The second cruise (D361) took place between 7 February and 19 March 2011 in the tropical North Atlantic (TNA); forming part of the marine biogeochemical cycles GEOTRACES programme (www.geotraces.org). The cruise was divided into two sections (Fig. 2.4): (1) an East-West (EW) transect from the Senegalese coast of West Africa to south of the Cape Verde Islands (S2 - S9) and (2) a South-North (SN) transect from south of the equator (~7 °S) to northwest of the Cape Verde Islands (S10 - S21). Results examined in subsequent chapters have been described by dividing the stations into five oceanographic regions: Coastal TNA (S2 - S6), Central TNA (S7 - S9, S17 - S18), Equatorial Upwelling Region (EqU, S11 - S16), Tropical South Atlantic (TSA, S10) and East STNA gyre (S19 - S21). In total, 19 stations were sampled at up to 5 depths per station (<200 m depth). Seawater was vacuum filtered (Fig. 2.1B) onto GF/Fs (MF300, Fisher Scientific, 0.7 µm) for the determination of heme *b* (2 - 4 L, section 2.4) and chlorophyll *a* (200 ml, section 2.5) concentration and pre-ashed GF/Fs (450 °C, >12 hours) for the concentration of POC and PON (2 - 4 L, section 2.6). Overall, 127 heme *b*, 127 chlorophyll *a* and 137 POC/N samples were obtained; the number of samples varies due to availability of seawater from the CTD. In addition, 79 heme *b* samples were obtained by vacuum filtration (Fig. 2.1B) between stations from the continuous towed FISH supply (2 - 5 L). Furthermore, 82 nitrogen fixation incubations (see section 2.7) were completed from 17 stations from up to five depths per station.

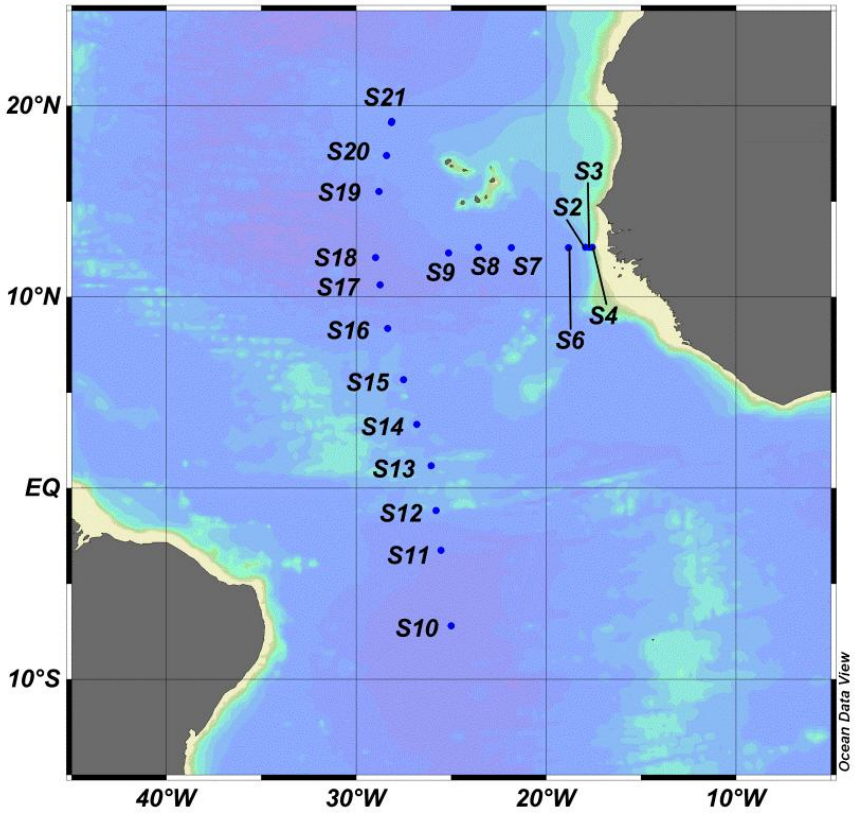

Figure 2.4. Map of station locations (blue dots) from research cruise D361 in the tropical North Atlantic (TNA). Annotations indicate station number (i.e. S2 = Station 2). S4 was closest to the Senegalese coast; followed by S3 and S2. In total, 19 stations were sampled at up to five depths per station. Stations were allocated to one of five oceanographic groups: Coastal TNA (S2 - S6), Central TNA (S7 - S9, S17 - S18), Equatorial Upwelling Region (EqU, S11 - S16), Tropical South Atlantic (TSA, S10) and East STNA gyre (S19 - S21).

2.4 Heme *b*

The quantification of heme *b* was achieved using two analytical techniques during the project. Initially, a previously defined methodology using High Performance Liquid Chromatography (HPLC) with diode array spectrophotometry (Gledhill 2007) was used to analyse heme *b* samples from the STNA (D346) and *Synechococcus* sp. WH7803 experiments (section 2.4.1). Samples obtained from the TNA (D361) and experiments on the marine diazotrophs *Crocosphaera* and *Trichodesmium* were analysed for heme *b* using HPLC-diode array detection-electrospray ionisation-mass spectrometry (HPLC/DAD/ESI-MS, section 2.4.2). HPLC is commonly used in analytical chemistry to separate mixtures enabling the quantification of individual components (e.g. heme *b*), with HPLC/DAD/ESI-MS incorporating the added ability to conduct detailed mass analysis on individual components via mass spectrometry. Therefore, the primary advantage of including HPLC/DAD/ESI-MS relates to the identification of chromatographic peaks with a greater level of certainty as a result of ion molecule fragmentation.

2.4.1 HPLC with diode array spectrophotometry

The zwitterionic detergent EMPIGEN (BB, BioChemika, Sigma-Aldrich) in an ammoniacal (20 mmol L^{-1}) solution was used to extract heme *b* from filtered samples. To prepare the solution, 2.5 ml of EMPIGEN was added to 97.5 ml of MilliQ water, followed by 100 µl of concentrated ammonia solution (i.e. 2.5% v:v EMIPGEN solution). The solution was prepared every 2 - 3 days and stored at 4 °C. Heme *b* samples (GF/Fs stored in 1.5 ml eppendorfs) were removed from the freezer and allowed to thaw at room temperature for 5 minutes, before 1 ml of EMPIGEN solution was added to the eppendorf. Samples were then extracted by means of ultrasonication (15 minutes) followed by centrifugation (Eppendorf, MiniSpin plus, 1300 rpm, 10 minutes). Extracts were filtered (0.2 µm, Minisart, Sartorius) prior to HPLC analysis. Samples were preserved in the instrument autosampler at 4 °C and analysed within 24 hours.

The HPLC system utilised two binary gradient high pressure pumps (Shimadzu, LC-10ADVPµ) to pump the mobile phase and sample through a polystyrene divinyl benzene stationary phase (PLRP-S, 50 x 2.1 mm, 5 µm column, Varian Inc.), operated using the computer program LCsolution (v1.03 SP3) via a controller (Shimadzu, SCL-10AVP). Sample (heme *b* extract) was introduced (100 µl) to the system via an autosampler (Shimadzu, SIL-10ADVP) connected to the pumps. The mobile phases consisted of (*A*) 50:50:0.1% (v:v:v) isopropanol (IPA): acetonitrile (ACN): nonafluoropentanoic acid (NFPA, Sigma-Aldrich) and (*B*) 5:5:90:0.1% (v:v:v:v) IPA: ACN: MilliQ water: NFPA. Fresh solvents were prepared every 2 days. A standard gradient elution was used, starting with 60% *B* to 100% *A* over 15 minutes, followed by a further 5 minutes isocratic elution with 100% *A* prior to return (2 minutes) and re-equilibration (5 minutes) with the starting conditions (see Fig 2.5). The flow rate was 200 µl min^{-1}. Prior to commencing a sample batch, the pumps were purged for 5 minutes (4 ml min^{-1}), followed by 30 minutes at starting conditions (i.e. 60% *B*, 200 µl min^{-1}) to equilibrate the back pressure through the column.

Heme *b* eluted from the column after approximately 5.5 minutes (retention time, Fig. 2.5), with a maximum absorption (λ_{max}) at 400 nm; consistent with the intense absorption band at the 400 nm (UV) region associated with porphyrins (Lim 2002). A background absorbance correction using 450 nm (reference wavelength) was employed to remove baseline fluctuations caused by EMPIGEN. Cellular heme *b* (also referred to as Fe(II) protoporphyrin IX) is present in the reduced iron form; however, iron in heme *b* becomes readily oxidised upon exposure to oxygen, suggesting the peaks measured using this technique are most likely Fe(III) protoporphyrin IX. Therefore, a series of Fe(III) protoporphyrin IX chloride (hemin) standards were used to quantify the concentration of heme *b* (Fig. 2.6). The limit of detection was 1.9 nmol L^{-1}, determined using three times the standard deviation of the lowest hemin standard (i.e. 15 nmol L^{-1}). Pre-concentration

of samples by filtration onto GF/Fs enabled concentrations as low as 0.48 pmol L^{-1} to be reported for seawater samples.

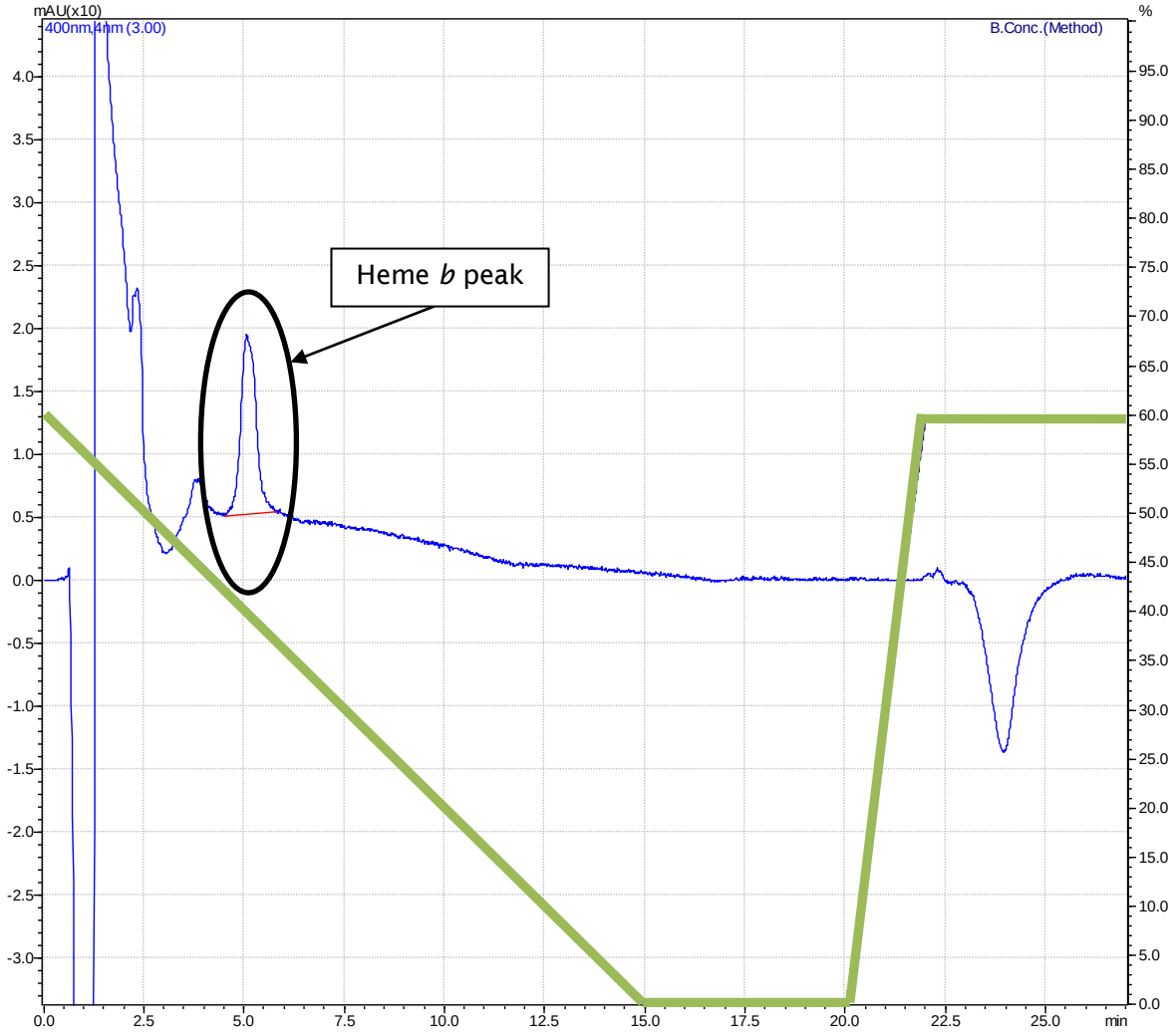

Figure 2.5. Absorption chromatogram (400 nm) showing a hemin standard (46 nmol L^{-1}) peak eluted at approximately 5.5 minutes (blue, left *y*-axis) and an Illustration of solvent gradient elution (green, right *y*-axis). The *x*-axis represents time elapsed (minutes). Plot produced using LCsolution software.

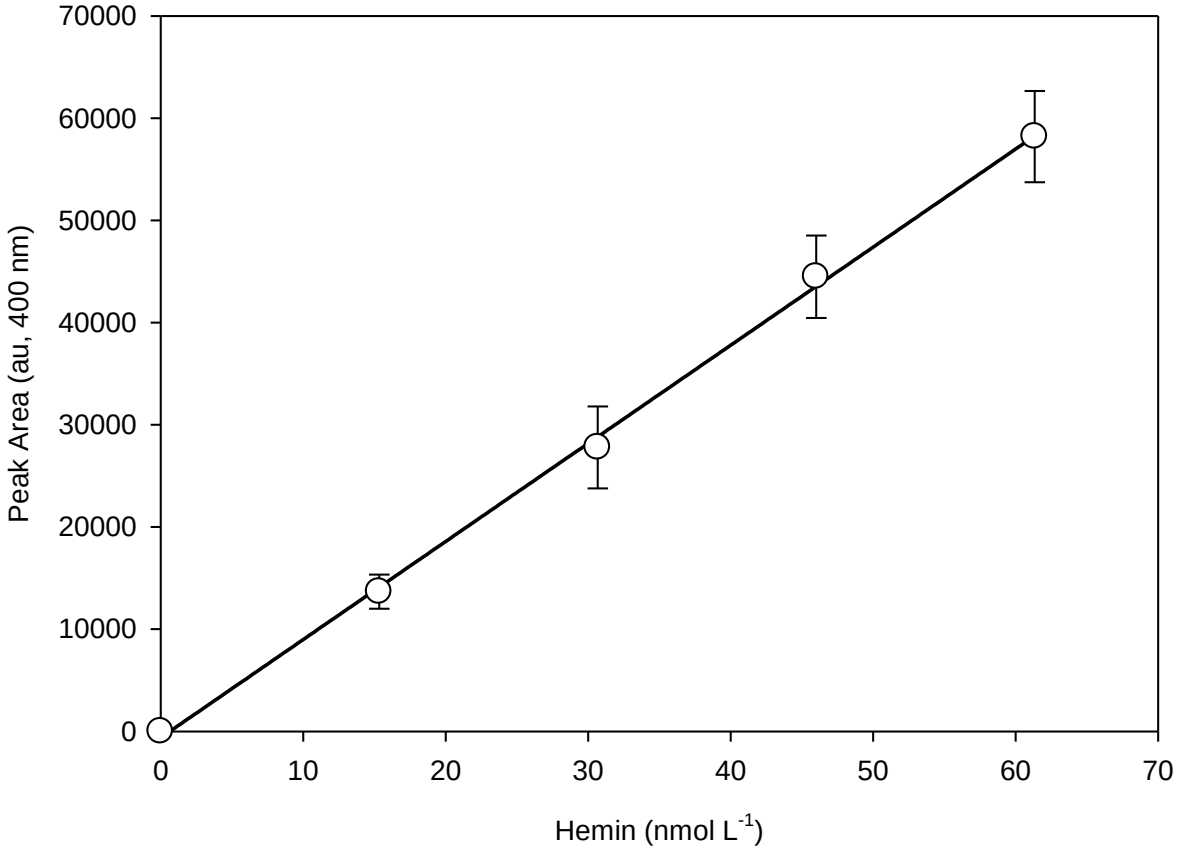

Figure. 2.6. Hemin standard series used to quantify samples for heme *b* concentration. Each point represents the mean peak area from all batch runs for *Synechococcus* sp. WH7803 experiments ($N = 9$) with standard deviation error bars.

2.4.2 HPLC/DAD/ESI-MS

The detergent described in section 2.4.1 (EMPIGEN) interferes with samples during mass spectrometry ionisation; therefore, the non-ionic detergent octyl-*β*-glucopyranoside (OGP, 98%+, Sigma-Aldrich) was used in conjunction with HPLC/DAD/ESI-MS (Keana and Roman 1978, Morandat and El Kirat 2007). An OGP solution (2.5% w:v) was prepared by adding 2.5 g of OGP to 100 ml of MilliQ water, followed by 100 µl of concentrated ammonia solution. Compared to EMPIGEN, OGP is less chemically stable. Therefore, the OGP solution was prepared daily and stored at 4 °C prior to sample analysis. Filters (GF/Fs stored in 1.5 ml eppendorfs) were removed from the freezer, allowed to thaw at room temperature for 5 minutes before 1 ml of OGP solution was added to the eppendorf. Heme *b* was then extracted by ultrasonication (15 minutes) and centrifugation (Eppendorf, MiniSpin plus, 1300 rpm, 10 minutes), after which the extract was filtered (0.2 µm, Minisart, Sartorius) and placed in the HPLC/DAD/ESI-MS autosampler.

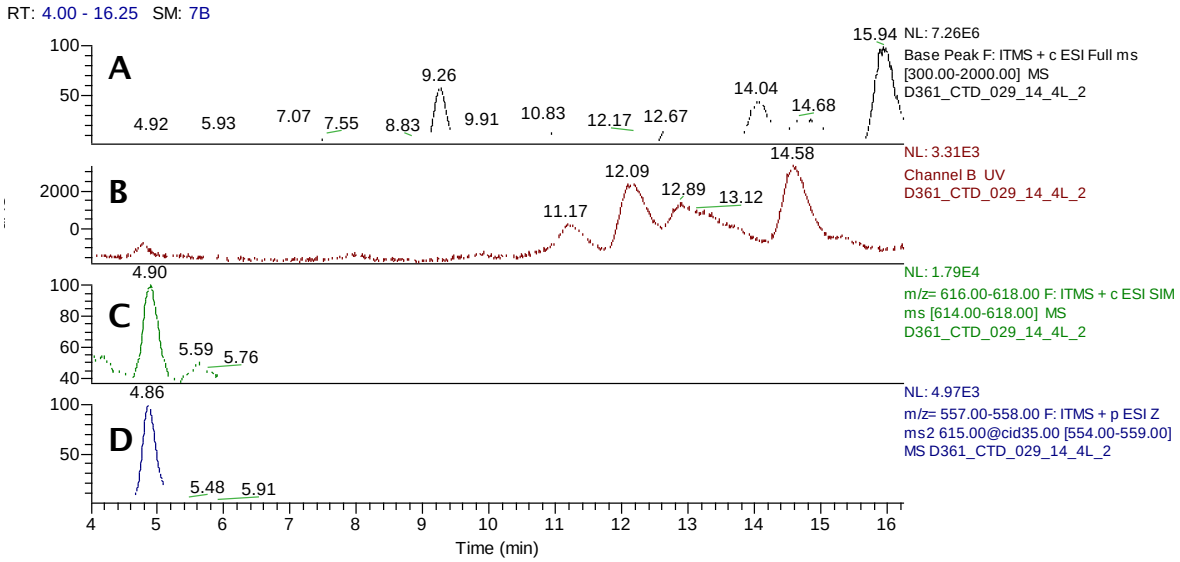

Figure 2.7. Chromatogram (4 - 16 minutes retention time) from a sample collected for heme *b* during cruise D361 (S12, 49.7 m) providing results of (**A**) the base peak (*m/z* 300 - 2000), (**B**) UV signal (400 nm), (**C**) selective ion monitoring (*m/z* 614 - 618) and (**D**) zoom scan mode (*m/z* 554 - 559) for the product ions (MS^2) of CID 616 ± 2.5. Plot produced using Xcalibur software.

Detection of heme *b* by HPLC-DAD-ESI-MS was performed using a quaternary low pressure gradient pump (Thermo Scientific ACCELA 1250 Pump) coupled to a diode array spectrophotometer (Thermo Scientific ACCELA PDA Detector) and a mass spectrometer via a heated electrospray ionisation source (LTQ Velos, Thermo Scientific). Samples were introduced (25 µl) via an autosampler (Thermo Scientific ACCELA Autosampler). Heme *b* was separated on a polystyrene divinyl benzene stationary phase (PLRP-S, 50 x 2.1 mm, 5 µm column, Varian Inc.) using mobile phases and a gradient elution program analogous to those previously described (see section 2.4.1); except the organic solvents used were LC-MS grade (Optima, Fisher Scientific). The flow rate was 200 µl min^{-1}. Data obtained from the mass spectrometer was processed with Xcalibur v2.1 (ThermoQuest) software. Automatic calibration procedures and standard solutions were used to tune and mass calibrate the instrument according to the manufacturer's guidelines using the supplied software (Thermo Tune Plus v2.6.0). To enhance the detection of the mass spectrometer for potential heme *b* peaks, instrument optimisation was conducted by infusing 76.7 nmol L^{-1} (50 µg L^{-1}) hemin (Fe(III) protoporphyrin IX chloride) at 1 µl min^{-1} into a 200 µl min^{-1} eluent flow with a mobile phase consisting of 50:50% (v:v) *A*:*B* (see section 2.4.1) injected from the HPLC system via a built-in syringe pump, a 250 µl syringe (Hamilton 1725N, Reno, CA) and a PEEK Tee union (Upchurch Scientific Ltd., Oak Harbor, WA). The *m/z* 616 (heme *b*) adduct ion was used in the automatic tuning function. To enable a positive ion full-scan range (*m/z* 300 - 2000), the following parameters were set: source temperature, 350 °C; spray voltage, +3.5 kV; capillary temperature, 400 °C; nitrogen sheath gas flow rate, 30 (arbitrary unit); and auxiliary gas flow rate, 10 (arbitrary unit).

Nitrogen zero grade (27009-L, BOC Gases) was used to generate the flow of ions from the heated electrospray ionisation (HESI) source. Helium was used to undertake collision induced dissociation (CID) with an activation energy of 35%.

The duration of each sample run was 27 minutes, split into four unequal segments. The second segment (4 - 9 minutes) coincided with the expected elution of heme *b* (hemin) from the column (approximately 5.5 minutes). In this segment, three specific scan events were conducted: (1) a full-scan of *m/z* 300 - 2000; (2) selective ion monitoring of *m/z* 614 - 618 and; (3) collision-induced dissociation (CID) MS^2 of *m/z* 616 with an isolation width of 5 (± 2.5) using zoom scan mode between *m/z* 554 - 559 (Fig. 2.7). During the remaining three segments (i.e. 0 - 4, 9 - 16 and 16 - 27 minutes), only a full-scan of *m/z* 300 - 2000 was conducted.

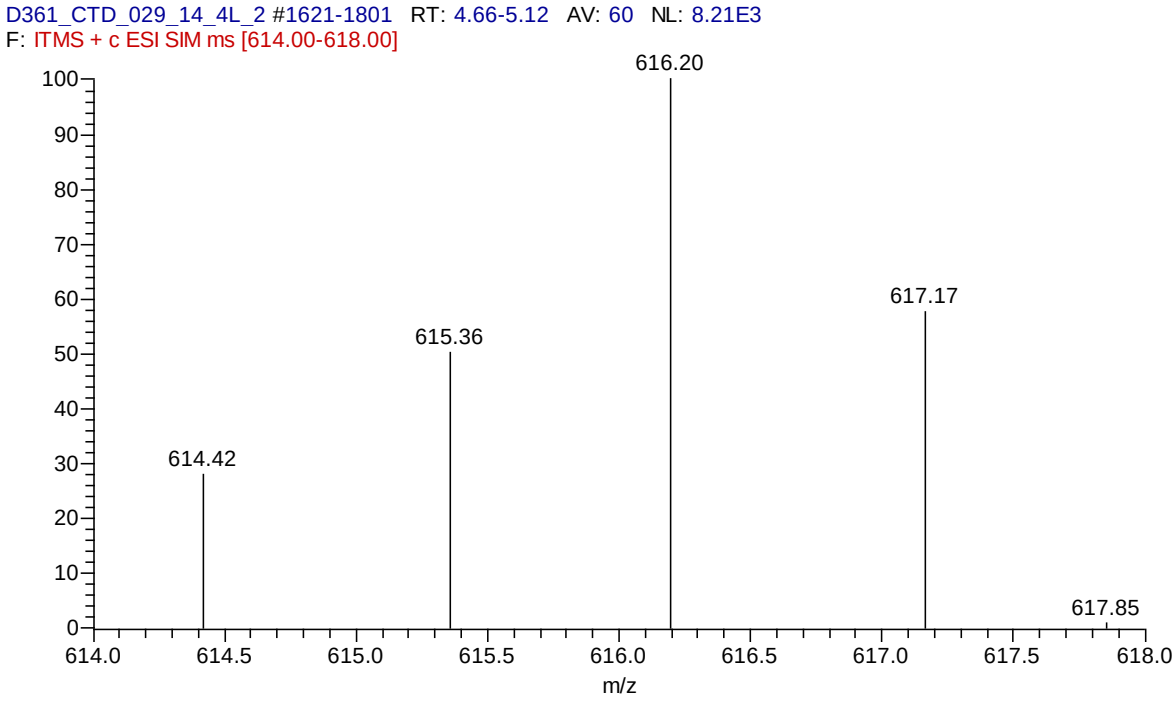

Figure 2.8. Mass spectra for selective ion monitoring of *m/z* 614 - 618 from a sample collected during D361 (see Fig. 2.7C). Mass abundances relative (%) to *m/z* 616.20 (i.e. highest peak). Plot produced using Xcalibur software.

The mass spectra of the peak produced by selective ion monitoring of *m/z* 614 - 618 at approximately 5 minutes (Fig. 2.7C) provides the relative abundance (%) of ions in the sample according to mass (Fig. 2.8). The largest peak was produced at *m/z* 616 (616.20 in the Fig. 2.8 example) which predominantly represents the $^{56}Fe^{3+}$ heme *b* complex. The alternative peaks are characteristic of the same heme *b* structure, produced with different naturally occurring iron (i.e. ^{54}Fe, ^{56}Fe and ^{57}Fe) and carbon (^{12}C and ^{13}C) isotopes, as well as the two different charge states of the ion for the various iron isotopes ($C_{34}\mathbf{H_{32}}O_4N_4\mathbf{Fe^{3+}}$ or $C_{34}\mathbf{H_{33}}O_4N_4\mathbf{Fe^{2+}}$). For example (using Fig. 2.8), *m/z* 614.42 indicates heme *b* comprising

$^{54}Fe^{3+}$ and *m/z* 617.17 indicates heme *b* comprising $^{57}Fe^{3+}$, as well as numerous alternatives (Table 2.3, also refer to Li et al. 1993). However, these mass peaks also include other ions of similar mass to the heme *b* structure. Therefore, CID (MS^2) of *m/z* 616 enabled quantification of heme *b* free from interferences, allowing for the determination of heme *b* via the production of unique fragmentation ions.

Mass Spectra Peak			
m/z 614.42	*m/z* 615.36	*m/z* 616.20	*m/z* 617.17
$^{54}Fe^{3+}$	$^{54}Fe^{3+}$ and ^{13}C	**$^{56}Fe^{3+}$**	$^{57}Fe^{3+}$
	$^{54}Fe^{2+} + H^+$	$^{54}Fe^{2+} + H^+$ and ^{13}C	$^{56}Fe^{3+}$ and ^{13}C
			$^{56}Fe^{2+} + H^+$

Table 2.3. Heme *b* components of each *m/z* peaks from the mass spectra of Fig. 2.8 using iron isotopes (^{54}Fe, ^{56}Fe or ^{57}Fe), carbon isotopes (^{12}C or ^{13}C) and iron charge (Fe^{3+} or $Fe^{2+} + H^+$). The heme *b* structure in bold signifies typically the most abundant form.

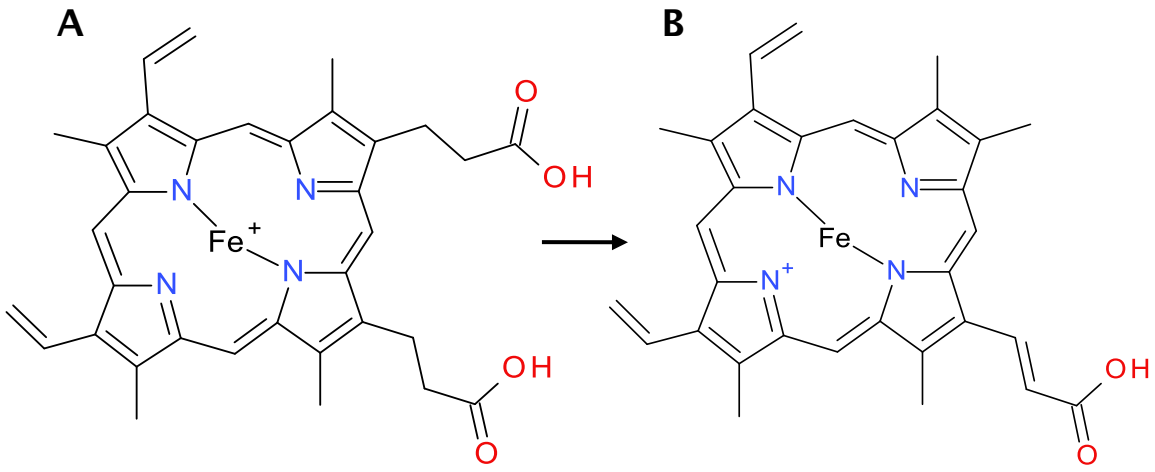

Figure 2.9. Collision-induced dissociation (CID) results in the removal of one ethylcarboxyl side chain (R-CH_2-COOH) from heme *b* (*m/z* 616, **A**) to form a fragment used in the identification of heme *b* (*m/z* 557, **B**).

Molecular ions of *m/z* 616 were accelerated to high speeds and allowed to collide with helium molecules (neutral) in order to fragment the sample (i.e. CID). As shown in Figure 2.9, the dissociation (removal) of one ethylcarboxyl side chain (R-CH_2-COOH) from heme *b* (Fe(III) protoheme IX) leads to the formation of an ion fragment *m/z* 557 (Pashynska et al. 2004). The zoom scan of *m/z* 554 - 559 (Fig. 2.7D) investigated a narrow mass range, but provided an increased resolution of the mass spectra of interest (Fig. 2.10). Therefore, the *m/z* 557 peak was used to measure heme *b* concentrations in samples from research cruise D361 in the TNA and the laboratory cultures of the marine diazotrophs *Crocosphaera* and *Trichodesmium*.

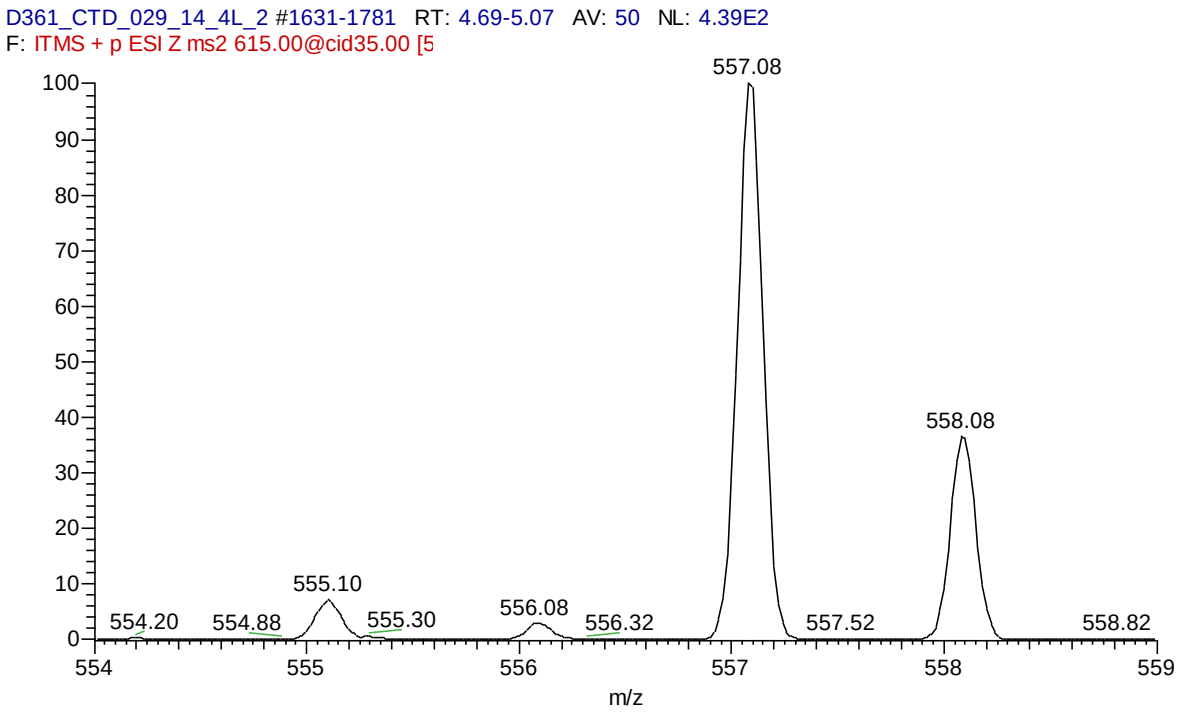

Figure 2.10. Mass spectra for zoom scan mode between *m/z* 554 - 559 from a field sample collected during cruise D361 in the TNA (see Fig. 2.7D). Mass abundances relative (%) to *m/z* 557.08 (i.e. highest peak); a fragmentation of ^{56}Fe(III) heme *b* (see Fig. 2.9). Plot produced using Xcalibur software.

Samples collected for the determination of heme *b* during the cruise D361 in the TNA were quantified using a hemin standard series (0, 15, 30, 46 and 61 nmol L^{-1}); similar to the process described for cruise D346 in the STNA and *Synechococcus* sp. WH7803 culture samples (e.g. Fig. 2.6, see section 2.4.1). However, in addition to the use of a standard series, heme *b* samples obtained from *Crocosphaera* and *Trichodesmium* cultures were quantified using a standard addition technique. Once heme *b* extracts were filtered, the sample was divided into three aliquots; (*1*) 1 ppb hemin stock solution added, (*2*) 2 ppb hemin stock solution added and (*3*) original sample extract with no addition. All samples (including those with standard additions) were analysed by HPLC/DAD/ESI-MS (Fig. 2.11). The limit of detection for samples processed from D361 was 0.19 nmol L^{-1} (three times the standard deviation of the lowest standard); allowing heme *b* concentrations of 0.05 pmol L^{-1} to be determined in pre-concentrated samples from the field. The detection limit of diazotroph culture samples measured via standard addition was 18 pmol L^{-1}; calculated as three times the standard deviation of blank standard noise (i.e. OGP solution only) about the baseline.

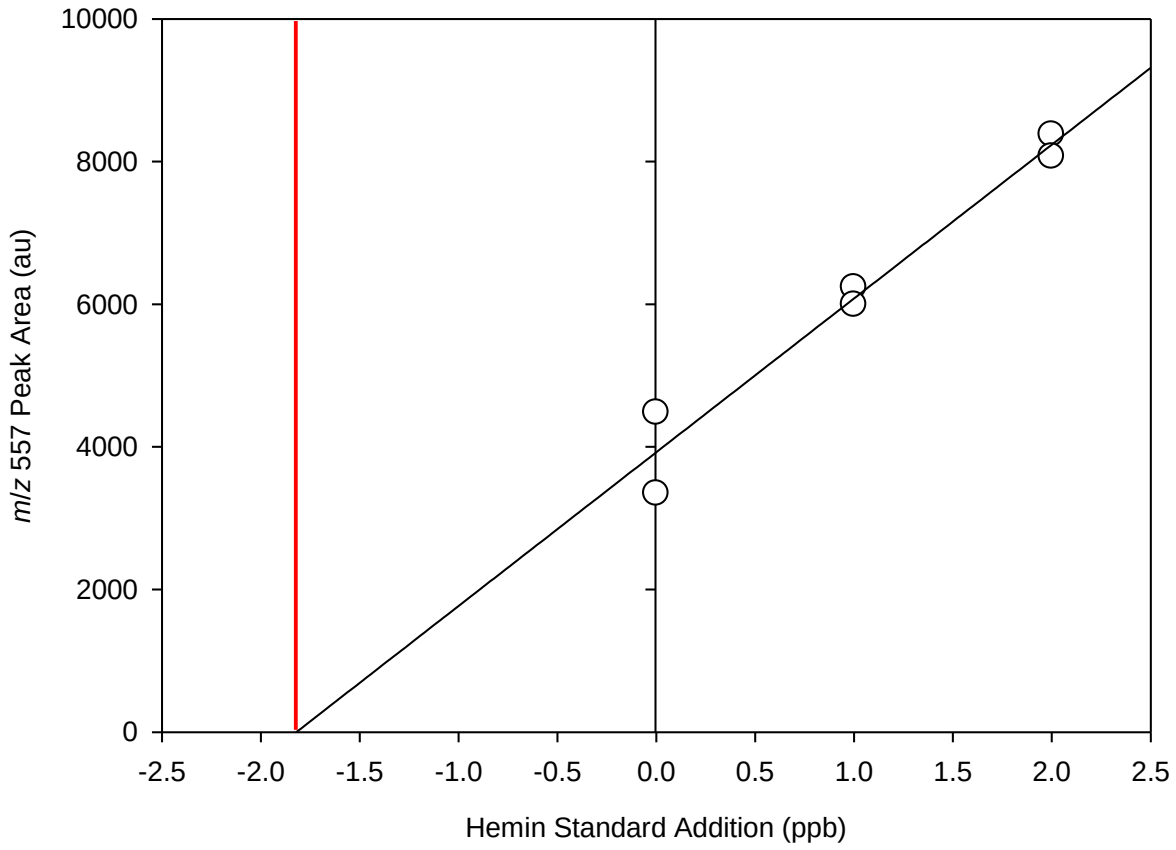

Figure 2.11. Scatter plot of the *m/z* 557 (heme$_{557}$) peak area (e.g. Fig. 2.7D) against hemin standard addition, demonstrating the process used to quantify heme *b* concentration in diazotroph cultures using the standard addition method. Example data obtained from a culture of *Crocosphaera watsonii* grown under 4 nmol L^{-1} Fe_T with 0 ppb (i.e. no addition), 1 ppb and 2 ppb standard additions of hemin stock solution. Red line indicates the *x*-axis intercept (i.e. -heme$_{557}$ *b* concentration).

The peak area of *m/z* 557 (heme$_{557}$) was used to calculate the detection limit for HPLC/DAD/ESI-MS analysis as it provided lower values compared to concurrent UV (400 nm) spectrophotometry (heme$_{UV}$, results not shown). Comparison of samples using the two techniques suggested a strong positive correlation, but the derived heme$_{557}$ concentrations were approximately 30 - 40% lower than the corresponding heme$_{UV}$ concentrations (Fig. 2.12). This indicated a systematic error between concentrations determined using the two techniques, possibly resulting from suppression caused by other ions in samples combined with inefficiencies in ion transfer of CID within the mass spectrometer. In order to account for this error and to utilise the larger data set provided by the heme$_{557}$ technique, resulting from the lower detection limit achieved, heme$_{557}$ concentrations were multiplied by 1.43 (Fig. 2.12A) for cruise D361 and multiplied by 1.52 (Fig. 2.12B) for *Crocosphaera* and *Trichodesmium* culture samples.

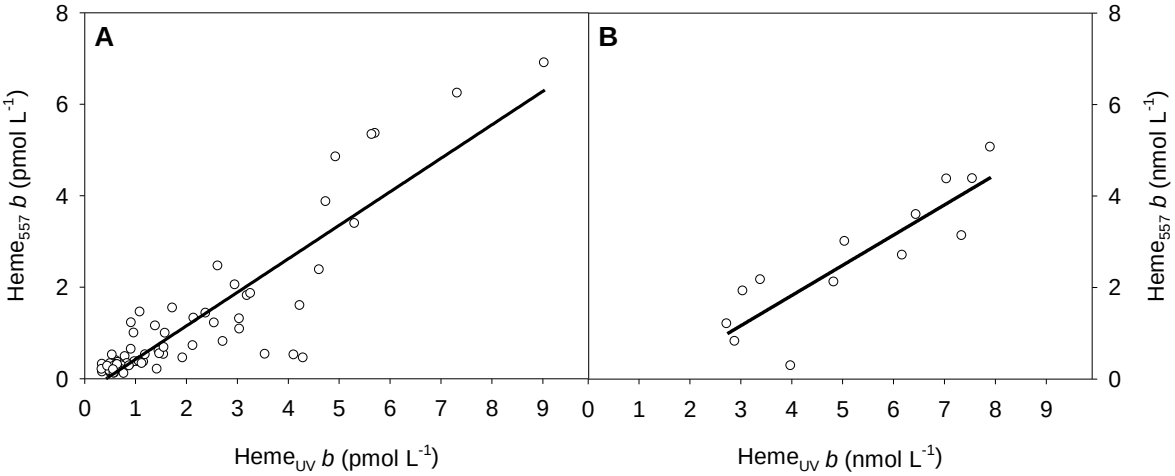

Figure 2.12. Scatter plot of (**A**) heme *b* concentration (pmol L^{-1}) from cruise D361 and (**B**) heme *b* concentration (nmol L^{-1}) from laboratory cultures of *Crocosphaera* and *Trichodesmium* measured using the *m/z* 557 peak ($heme_{557}$) and UV signal ($heme_{UV}$) by HPLC/DAD/ESI-MS. Lines represent correlation between the two techniques (A: $y = 0.732x - 0.309$, $r^2 = 0.801$, $N = 80$; B: $y = 0.660x - 0.814$, $r^2 = 0.771$, $N = 13$).

2.5 Chlorophyll *a*

Filtered (GF/F) samples collected from the STNA (D346) and laboratory culture experiments for the determination of chlorophyll *a* concentration were removed from the freezer and allowed to thaw at room temperature for 5 minutes, prior to transfer (from 1.5 ml eppendorfs) to individual 15 ml centrifuge tubes (Fisherbrand) using clean plastic forceps. Note samples from the TNA (D361) were not stored (-80 °C) upon collection; instead filtered samples were processed immediately. Chlorophyll *a* was extracted into 5 ml of 90% acetone (10% MilliQ water) and dark-refrigerated (4 °C) for 24 hours (i.e. no sonication). A fluorometer (Turner Designs 10-AU) was used to determine the chlorophyll *a* concentration in the extract. The instrument was calibrated using pure chlorophyll *a* spinach standard (Sigma-Aldrich). The spinach standard was dissolved in 90% acetone and the solution was measured via spectrophotometry using absorbance measurements from 664 nm, 647 nm and 630 nm, as well as a wavelength reference from 750 nm. The concentration of chlorophyll *a* (mg L^{-1}) in the spinach solution was calculated using the following equation:

$$[\text{Chlorophyll } a] = (11.85 * A_{664}) - (1.54 * A_{647}) - (0.08 * A_{630})$$

where A_{664}, A_{647} and A_{630} were the absorbance values at 664, 647 and 630 nm, respectively, corrected for absorbance at 750 nm (Parsons et al. 1984). A standard series of the spinach solution was used to calibrate the fluorometer.

To calculate the concentration of chlorophyll *a* in filtered samples (µg L^{-1}), the following equation was used:

$$[\text{Chlorophyll } a] = [\text{Extract}] * V_a / V_f$$

where [Extract] is the concentration of chlorophyll *a* in the extract (i.e. value recorded from the fluorometer), V_a is the volume (ml) of acetone in the extract and V_f is volume (ml) of sample filtered onto the GF/F. A molar mass of 893.1 g mol^{-1} was used to convert chlorophyll *a* concentrations (µg L^{-1}) to molar equivalents (nmol L^{-1}).

2.6 Particulate organic carbon (POC) and nitrogen (PON)

Filtered (pre-ashed GF/F) samples for POC/N analysis were removed from the freezer and allowed to thaw at room temperature for 5 minutes, prior to transfer onto an individual petri dish in batches of 30 samples and several blanks. Each petri dish was carefully placed into a plastic desiccator containing sulphurous acid (H_2SO_3, Thermo Scientific). The desiccator was then evacuated using a vacuum pump and left for 24 - 48 hours to remove inorganic carbon via acidification (H_2SO_3 vapours). The petri dishes were then removed from the desiccator and transferred to a drying oven (50 °C) for a further 24 hours. The filters were then pelleted into pre-ashed (450 °C, 12 hours) 30 mm aluminium discs (D3066, Elemental Microanalysis Ltd) using a custom built sample press, similar to the design described by Hilton et al. (1986). Samples were then analysed using an elemental analyzer (Thermo Finnegan flash EA1112) using acetanilide as the calibration standard (Verardo et al. 1990).

2.7 Nitrogen fixation rates

Nitrogen fixation rates were measured using the ^{15}N technique, originally described by Dugdale and co-workers (Dugdale et al. 1961, Dugdale et al. 1964) and since refined (e.g. Capone and Montoya 2001). In brief, the ^{15}N isotope is introduced to a sample as $^{15}N_2$ and the amount incorporated into PON of the resident organisms over a set period is determined (Mahaffey et al. 2005).

2.7.1 Research cruises

Nitrogen fixation incubations were conducted using seawater samples collected by a CTD from up to five depths per station (<200 m) during research cruises D346 and D361 in the (sub-) tropical North Atlantic. Clear 4.5 L polycarbonate bottles (Nalgene, Thermo Scientific) were carefully filled with seawater direct from the CTD, ensuring no bubbles remained once fastened using septum closures (MPS-159-010V, Fisher Scientific). This was achieved by tilting the bottle at a 45 ° angle and repeatedly turning the bottle whilst filling. A glass gas-tight syringe (5 ml, Hamilton) with 22 gauge steel needle was used to draw 4 ml of $^{15}N_2$ gas (98%+, CK Gas Products Ltd) from the gas bottle manifold. The gas

inside the syringe was equalised to atmospheric pressure and injected through the septum closure of the sample bottles. The bottles were transferred to on-deck incubators maintained at surface seawater temperature using the underway supply for 24 hours. Light film was used to manipulate light levels dependent upon the depth seawater was obtained. The sample was then vacuum filtered (Fig. 2.1B) onto pre-ashed (450 °C, 12 hours) GF/Fs (MF300, Fisher Scientific, 0.7 µm), placed in 1.5 ml eppendorfs and dried for a further 24 hours (50 °C, drying oven).

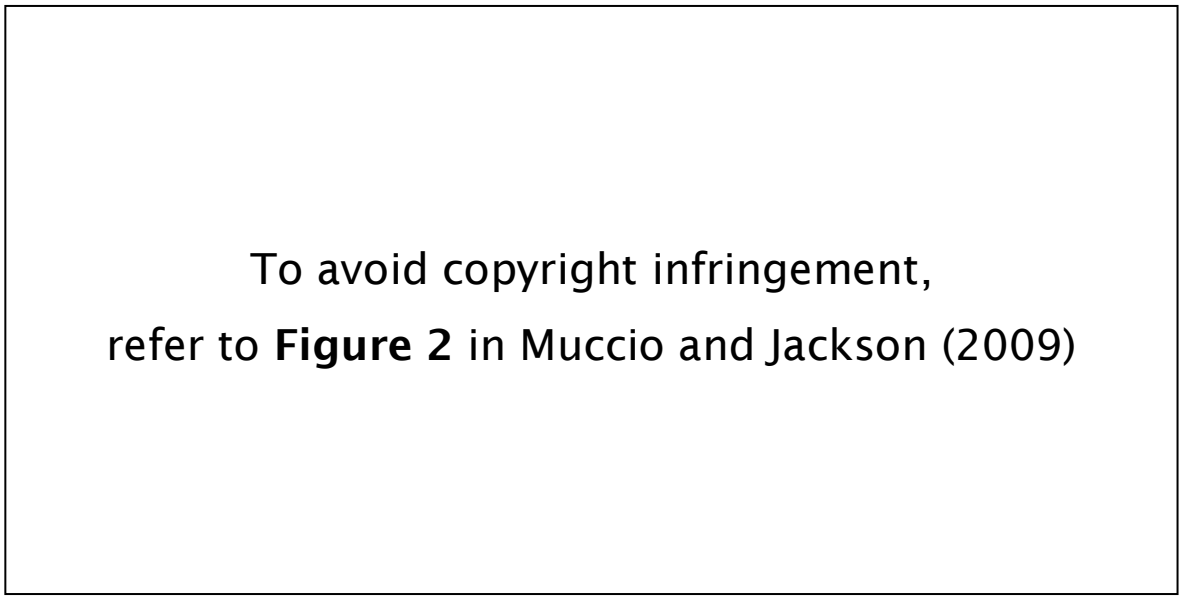

Figure 2.13. Schematic of the elemental analyser used to introduce sample to the mass spectrometer to determine ^{15}N isotopic ratio. An autosampler delivered the sample into a heated combustion oven, which was then transferred through a reduction oven (copper granules) and chemical traps to remove carbon and water. The analyte was then separated and carried by a helium gas stream to the isotopic ratio mass spectrometer (IRMS) along with a reference carbon dioxide gas (nitrogen used in this study). Figure from Muccio and Jackson (2009).

Filters were pelleted in tin capsules (Pelican Scientific Ltd) and analysed by elemental analysis and isotope ratio mass spectrometry (EA-IRMS) via an elemental analyser (EuroEA, EuroVector) and mass spectrometer (GV Instruments, Isoprime). Pelleted samples were flash combusted upon introduction to the elemental analyser with oxygen (Ultrapure, Air Products), and the combusted gas carried to the mass spectrometer by helium (BIP, Air Products) to determine the isotopic composition (Fig. 2.13). Isotopic ratios were reported relative to a reference nitrogen gas (BIP, Air Products). The instrument was routinely calibrated using L-Tyrosine 99%+ (Acros Organics, 7.735% N, $\delta^{15}N = 9.3$) and samples were blank corrected. A small segment (e.g. ¼) of corresponding POC/N filtered sample (GF/F, MF300, Fisher Scientific, 0.7 µm) from the same station/depth were also processed using EA-IRMS to provide ^{15}N natural abundance (t_{zero}) values. Nitrogen fixation samples were then compared to t_{zero} values to calculate nitrogen fixation rates. Note, t_{zero} samples were

vacuum filtered using a separate filtration rig (Fig. 2.1B) to avoid contamination with the ^{15}N isotope from spiked samples.

2.7.2 Laboratory diazotroph cultures

The procedure previously described for the determination of nitrogen fixation rates during research cruises (section 2.7.1) was predominantly followed for laboratory grown cultures of *Crocosphaera* and *Trichodesmium*. Cultures were monitored in 400 ml culture vessels (EasyFlask, Nunclon, Sigma-Aldrich) until the exponential growth phase (day 6) and were then transferred to clear 125 ml polycarbonate bottles (Nalgene, Thermo Scientific) and fastened using septum closures (MPS-159-010V, Fisher Scientific). Bubbles were eliminated by slowly pouring culture medium into the bottle, filling the bottle until it was slightly overflowing and then dropping the septum closure onto the neck of the bottle to remove excess; all conducted in a laminar flow cabinet. Four 125 ml bottles were prepared per iron concentration for both species, with surplus culture medium used to prepare t_{zero} samples. As the volume was less than that used during the research cruises (i.e. 125 ml instead of 4.5 L) and the biomass was much greater, only 0.5 ml of $^{15}N_2$ gas was injected per bottle. Cultures were maintained at 26 °C under 80 µmol quanta m^{-2} s^{-1} light (12:12 hour light:dark cycle) for 24 hours, before the entire bottle contents was vacuum filtered (Fig. 2.1A) onto pre-ashed (450 °C, 12 hours) GF/Fs (MF300, Fisher Scientific, 0.7 µm). Filters were dried (50 °C) for a further 24 hours and analysed by EA-IRMS (see section 2.7.1). As above, t_{zero} samples were vacuum filtered using a separate filtration rig (Fig. 2.1A) to avoid contamination with the ^{15}N isotope from spiked samples.

2.8 Fast repetition rate fluorometry (FRRF)

Photosynthetic physiology measurements for all three cyanobacterial cultures were obtained using a FAST*tracka* II and FASTAct fluorometry system (Chelsea Technologies Group Ltd, West Molesey, Surrey, UK) with FASTpro v2.0.0.1 software. The maximum photochemical efficiency of PSII (F_v/F_m) and the effective functional absorption cross-section of PSII (σ_{PSII}) were measured via fast repetition rate fluorometry (FRRF); a non-invasive technique commonly used to determine the real-time variable fluorescence of marine phytoplankton attributed to chlorophyll *a*. When light levels are low, photosynthetic organisms fluoresce at a constant minimum level, referred to as F_0. As light levels increase, photosynthetic reaction centres begin to close until a point of maximum fluorescence is achieved, known as F_m (i.e. all reaction centres are closed). The variable fluorescence (F_v) is calculated as the difference between minimum (F_0) and maximum (F_m) levels of fluorescence detected. Therefore, F_v/F_m relates to the variability in fluorescence normalised to the maximum fluorescence. σ_{PSII} indicates the rate of increase in fluorescence between F_0 and F_m, inferring the efficiency of an organism to capture light energy (Falkowski and Raven 1997).

A small subsample (approximately 2 ml) of culture medium was transferred to a 15 ml centrifuge tube covered in aluminium foil and dark acclimatised for 30 minutes prior to FRRF analysis. The sample was then introduced to the fluorometer where cultures were subjected to a series of controlled light pulses every four seconds, subsequently measuring the induced fluorescence. An incrementing background irradiance was applied to stimulate F_m in cultures of *Crocosphaera* and *Trichodesmium* (5, 13, 21 and 38 µmol photons m^{-2} s^{-1}), with values reported in Chapter 5 obtained under 21 µmol photons m^{-2} s^{-1} photosynthetically active radiation (PAR) where maximum F_v/F_m was achieved (see Fig. 2.14). Blank YBC-II medium (i.e. no culture) was also measured in order to apply a blank correction to culture samples.

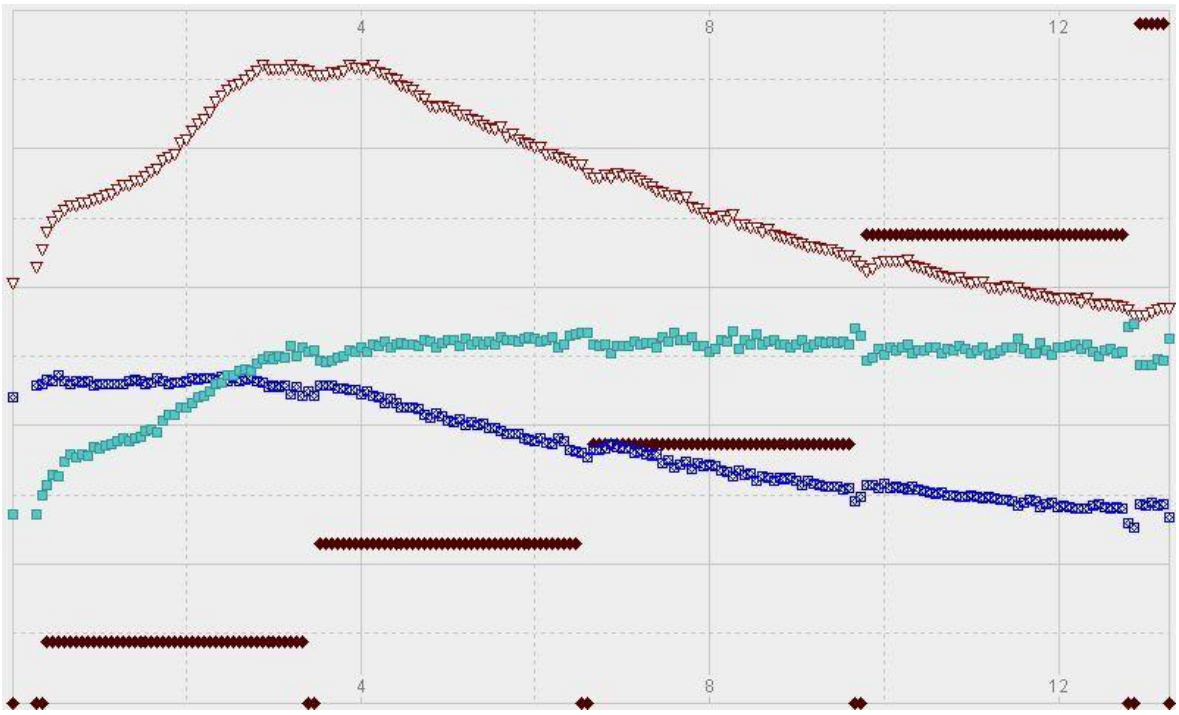

Figure 2.14. Overlay plot of F_0 (dark blue square), F_m (red inverted triangle), F_v/F_m (light blue square) and background irradiance (brown diamond, µmol photons m^{-2} s^{-1} PAR) acquired by fast repetition rate fluorometry (FRRF) for a culture of *Trichodesmium erythraeum* (IMS101) on day 8 of the growth cycle. The *x*-axis indicates time elapsed (minutes). Plot produced using FASTpro software. Notice the increasing F_v/F_m with increased background irradiance until the third light gradient step (i.e. 21 µmol photons m^{-2} s^{-1} PAR) where values plateau.

2.9 Figures and statistics

Graphs presented in this project were predominantly produced using Sigmaplot v11.0, unless otherwise stated. Vertical depth profiles from the marine environment were produced using Ocean Data View v4.3.2 (Schlitzer, R., Ocean Data View, http://odv.awi.de, 2010). All figures taken from the literature have been fully acknowledged.

The statistical analysis used in this project was determined according to Fowler et al. (1998), whilst also using IBM SPSS Statistics v19. Kruskal-Wallis tests (non-parametric) were used to compare the unmatched median of various parameters (e.g. heme *b* concentration) between the different iron treatments used to grow cyanobacterial cultures (i.e. more than two sample groups). These findings were routinely followed by Mann-Whitney *U* tests (non-parametric) to compare the medians of two unmatched groups to determine where, if any, differences were apparent with regards to iron concentration. Partial correlations were also used to assess the influence of two parameters when the variance caused by another parameter is controlled for; their application is explained in further detail when appropriate.

2.10 References

Capone, D. G. and J. P. Montoya. 2001. Nitrogen fixation and denitrification. Methods in microbiology **30**:501-515.

Chen, Y.-B., J. P. Zehr, and M. Mellon. 1996. Growth and nitrogen fixation of the diazotrophic filamentous nonheterocystous cyanobacterium *Trichodesmium* sp. IMS 101 in defined media: evidence for a circadian rhythm. Journal of Phycology **32**:916-923.

Dugdale, R. C., J. J. Goering, and J. H. Ryther. 1964. High nitrogen fixation rates in the Sargasso Sea and the Arabian Sea. Limnology and Oceanography **9**:507-510.

Dugdale, R. C., D. W. Menzel, and J. H. Ryther. 1961. Nitrogen fixation in the Sargasso Sea. Deep-Sea Research **7**:298-300.

Falkowski, P. G. and J. A. Raven. 1997. Aquatic Photosynthesis. Second edition. Princeton University Press, Oxford.

Fowler, J., L. Cohen, and P. Jarvis. 1998. Practical statistics for field biology. 2nd edition. Wiley, Chichester, UK.

Gledhill, M. 2007. The determination of heme b in marine phyto- and bacterioplankton. Marine Chemistry **103**:393-403.

Guillard, R. R. L. 1975. Culture of phytoplankton for feeding marine invertebrates.*in* W. L. Smith and M. H. Chanley, editors. Culture of Marine Invertebrate Animals. Plenum Press, New York.

Guillard, R. R. L. and J. H. Ryther. 1962. Studies of marine planktonic diatoms. I. *Cyclotella nana* Hustedt and *Detonula confervacea* Cleve. Canadian Journal of Microbiology **8**:229-239.

Hilton, J., J. P. Lishman, S. Mackness, and S. I. Heaney. 1986. An automated method for the analysis of 'particulate' carbon and nitrogen in natural waters. Hydrobiologia **141**:269-271.

Honey, D. J., M. Gledhill, T. S. Bibby, F-E. Legiret, N. J. Pratt, A. E. Hickman, T. Lawson, and E. P. Achterberg. 2013. Heme *b* in marine phytoplankton and particulate material from the North Atlantic Ocean. Marine Ecology Progress Series **483**: 1-17.

Keana, J. F. W. and R. B. Roman. 1978. Improved synthesis of *n*-octyl-β-D-glucoside: A nonionic detergent of considerable potential in membrane biochemistry. Membrane Biochemistry **1**:323-327.

Klunder, M. B., P. Laan, R. Middag, H. J. W. de Baar, and J. C. van Ooijen. 2011. Dissolved iron in the Southern Ocean (Atlantic sector). Deep Sea Research II **58**:2678-2694.

Li, Y.-T., Y.-L. Hsieh, and J. D. Henion. 1993. Studies on heme binding in myoglobin, hemoglobin, and cytochrome *c* by ion spray mass spectrometry. Journal of the American Society for Mass Spectrometry **4**:631-637.

Lim, C. K. 2002. Analysis of biosynthetic intermediates, 5-aminolevulinic acid to heme. Pages 95-109 *in* A. G. Smith and M. Witty, editors. Heme, chlorophyll, and bilins: Methods and protocols. Humana Press, Totowa, NJ.

Longhurst, A. 1998. Ecological geography of the sea. Academic Press, San Diego, CA.

Mahaffey, C., A. F. Michaels, and D. G. Capone. 2005. The conundrum of marine N_2 fixation. American Journal of Science **305**:546-595.

Morandat, S. and K. El Kirat. 2007. Solubilization of supported lipid membranes by octyl glucoside observed by time-lapse atomic force microsopy. Colloids and Surfaces B: Biointerfaces **55**:179-184.

Muccio, Z. and G. P. Jackson. 2009. Isotope ratio mass spectrometry. Analyst **134**:213-222.

Parsons, T. R., Y. Maita, and C. M. Lalli. 1984. A manual of chemical and biological methods for seawater analysis. Pergamon Press, Oxford.

Pashynska, V. A., H. Van den Heuvel, M. Claeys, and M. V. Kosevich. 2004. Characterization of noncovalent complexes of antimalarial agents of the artemisinin-type and Fe(III)-heme by electrospray mass spectrometry and collisional activation tandem mass spectrometry. Journal of the American Society for Mass Spectrometry **15**:1181-1190.

Patey, M. D., M. J. A. Rijkenberg, P. J. Statham, M. Mowlem, M. C. Stinchcombe, and E. P. Achterberg. 2008. Determination of nitrate and phosphate in seawater at nanomolar concentrations. Trends in Analytical Chemistry **27**:169-182.

Sunda, W. G. and S. A. Huntsman. 1995. Iron uptake and growth limitation in oceanic and coastal phytoplankton. Marine Chemistry **50**:189-206.

Sunda, W. G., N. M. Price, and F. M. M. Morel. 2005. Trace metal ion buffers and their use in culture studies. Pages 35-64 *in* R. A. Andersen, editor. Algal culturing techniques. Elsevier Academic Press, London.

Verardo, D. J., P. N. Froelich, and A. McIntyre. 1990. Determination of organic carbon and nitrogen in marine sediments using the Carlo Erba NA-1500 analyzer. Deep-Sea Research **37**:157-165.

Wilson, W. H., N. G. Carr, and N. H. Mann. 1996. The effect of phosphate status on the kinetics of cyanophage infection in the oceanic cyanobacterium *Synechococcus* sp. WH7803. Journal of Phycology **32**:506-516.

Zhang, J.-Z. 2000. Shipboard automated determination of trace concentrations of nitrite and nitrate in oligotrophic water by gas-segmented continuous flow analysis with a liquid waveguide capillary flow cell. Deep-Sea Research I: Oceanographic Research Papers **47**:1157-1171.

Zhang, J. Z. and J. Chi. 2002. Automated analysis of nanomolar concentrations of phosphate in natural waters with liquid waveguide. Environmental Science and Technology **36**:1048-1053.

Chapter 3

Heme *b* in the (sub-) tropical North Atlantic

3.1 Abstract

Despite the importance of heme complexes in numerous fundamental biological processes, including photosynthetic and respiratory electron transfer, a lack of data is available regarding the abundance and distribution of heme in the marine environment. As part of this project, samples were collected from two research cruises in the (sub-) tropical North Atlantic for heme *b*, chlorophyll *a*, particulate organic carbon (POC) and particulate organic nitrogen (PON) concentration. This study presents the first cross-sectional profile of heme *b* from the subtropical North Atlantic (STNA), reporting a mean particulate heme *b* concentration of 1.32 ± 0.6 pmol L^{-1} (N = 383). Measurements are also presented from the tropical North Atlantic (TNA) which provided a higher mean heme *b* concentration (2.18 ± 3.2 pmol L^{-1}, N = 90) compared to the STNA; although this was predominantly attributed to elevated heme *b* concentrations in the Coastal TNA region. Chlorophyll *a* concentrations were also higher in the TNA (M = 0.67 ± 1.0 nmol L^{-1}, N = 116) compared to the STNA (M = 0.19 ± 0.1 nmol L^{-1}, N = 396). A significant relationship was observed between chlorophyll *a* and heme *b* in both the STNA and TNA. However, ratios of chlorophyll *a* to heme *b* (chl:heme) concentration were markedly different, averaging 144 ± 76 mol mol^{-1} in the STNA and 553 ± 446 mol mol^{-1} in the TNA. Heme *b* per unit carbon (heme:C) were similar in the STNA (0.64 ± 0.4 µmol mol^{-1} C) and the TNA (0.66 ± 0.6 µmol mol^{-1} C), further highlighting the increased chl:heme ratios of the TNA were primarily linked to increased chlorophyll *a* concentrations, as opposed to reduced heme *b* concentrations. Heme *b* provided a better comparison to POC and PON in the STNA compared to chlorophyll *a*, although chlorophyll *a* provided stronger correlations to both POC and PON in the TNA; thus heme *b* is not considered a better indicator of phytoplankton biomass than chlorophyll *a* in the marine environment. As hemes exert an iron requirement, it is suggested that iron availability may be crucial in the distribution of heme *b* in the (sub-) tropical North Atlantic. Finally, comparison of heme b concentrations obtained during a previous research cruise in the tropical Northeast Atlantic has suggested a temporal variation in heme *b* concentration for the region, potentially associated with atmospheric iron input.

3.2 Introduction

The (sub-) tropical gyre of the North Atlantic is characterised by oligotrophic conditions, yet it plays a significant role in the export of carbon from the euphotic layer (Emerson et al. 1997). With the Gulf Stream in the West (Taylor and Stephens 1998) and Mauritanian upwelling region to the East (Schafstall et al. 2010), the (sub-) tropical North Atlantic is a globally important oceanographic region. The region is continuously stratified and phytoplankton productivity is subjected to regular nutrient limitation (Mills et al. 2004, Moore et al. 2006). Despite being temporally and spatially sporadic, high volumes of atmospheric dust are deposited into the tropical North Atlantic (TNA) and subtropical North Atlantic (STNA) when compared to many other parts of the global ocean. In fact, the North Atlantic in general receives over 40% of the overall annual dust input to the oceans, which totals at approximately 450 Tg $year^{-1}$ (Tg = 10^{12} grams, Fig. 3.1; Jickells et al. 2005). The vast majority of dust deposited into the global ocean is derived from the Northern Hemisphere desert regions, primarily northwest Africa and East Asia (Schutz et al. 1990, Jickells and Spokes 2001). In particular, the Saharan and Sahel deserts of northwest Africa are considered the most prominent aeolian dust sources in the world (see review by Goudie and Middleton 2001).

To avoid copyright infringement,
refer to **Figure 2** in Jickells et al. (2005)

Figure 3.1. Dust fluxes to the world oceans (g m^{-2} $year^{-1}$); model data collated and presented by Jickells et al. (2005). Total atmospheric dust inputs to the oceans estimated at 450 Tg $year^{-1}$. Percentage annual atmospheric dust input is highest in the North Atlantic (43%) and lowest in the South Atlantic (4%).

Dust events provide an essential source of nutrients to the (sub-) tropical North Atlantic, including nitrogen, phosphorus, and perhaps most importantly iron (Eglinton et al. 2002, Ridame and Guieu 2002, Baker et al. 2006). Iron plays a key role in many fundamental

biological processes (Geider and La Roche 1994) and the hemoproteins are an essential group of iron proteins found in all living organisms. Hemoproteins are involved in key biological processes, such as photosynthetic and respiratory electron transfer (Moore 1996). The prosthetic group of hemoproteins, hemes, contain a single iron atom at the centre of the porphyrin-ring structure, creating an obvious iron requirement to enable heme synthesis and functioning. Heme *b*, considered the most versatile form of heme (Caughey 1973), is incorporated into cytochrome b_6f (Kurisu et al. 2003) and photosystem II (PSII, Nelson and Yocum 2006) of the photosynthetic apparatus. Flow injection analysis and chemiluminescence detection were used to measure 'iron-porphyrin-like' complexes from seawater samples obtained from the Southern Ocean (Vong et al. 2007). However, concentrations were typically below the limit of detection (<0.11 nmol L^{-1}) and the author suggested "*a pre-concentration step will be required for analysing open ocean waters*" (Vong et al. 2007). Gledhill (2007) presented an analytical technique using High Performance Liquid Chromatography (HPLC) with diode array spectrophotometry to determine the concentration of heme *b* in marine microorganisms. The study also presented the first measurements of heme *b* content in several different cultures of marine phytoplankton and bacterioplankton (Gledhill 2007). However, our understanding of the distribution of heme *b* as well as other heme complexes in the marine environment remains limited.

As part of this project, the method developed by Gledhill (2007) has been used to measure heme *b* concentration from seawater samples obtained during a research cruise in the STNA (D346). Subsequent samples for the determination of heme *b* collected from a second cruise, predominantly in the TNA (D361), were analysed by HPLC-diode array detection-electrospray ionisation-mass spectrometry (HPLC/DAD/ESI-MS). The TNA region was previously sampled in 2008 (D326, *RRS Discovery*) as part of the SOLAS research program (Surface Ocean Lower Atmosphere Study, www.solas-int.org), investigating the deposition of dust and nutrients into the North Atlantic (Rijkenberg and Achterberg 2008). The mean heme *b* concentration during D326 was 2.24 ± 1.67 pmol L^{-1} (N = 269, Gledhill et al. in prep, see Appendix 1) and the data set offered a close spatial comparison to heme *b* measurements from the eastern STNA (D346) and TNA (D361). Additionally, it should be noted that the SOLAS data set was collected between 5 January and 5 February 2008; the same time of year that cruises D346 and D361 were completed.

The determination of heme *b* in phytoplankton monocultures will potentially provide an insight of physiological responses to changing conditions in the laboratory (see Chapters 4 and 5). However, it is essential that information regarding heme *b* abundance and distribution in the natural marine environment is available for comparison. Atmospheric dust inputs are a significant source of iron for the oceans (Duce et al. 1991, Jickells and Spokes 2001, Jickells et al. 2005) and, as a result, the phytoplankton communities in the

(sub-) tropical North Atlantic are generally considered to be iron-replete compared to the rest of the global ocean (see Fig. 3.1). Therefore, the region posed an ideal location to measure heme *b* concentrations and will provide data upon which following chapters in this thesis will refer. Heme *b* concentrations will be influenced by biomass and, as hemoproteins are nearly ubiquitous in life, bacteria, phytoplankton and zooplankton all will contribute to the total heme *b* pool. In this study, samples were filtered to focus on the >0.7 µm fraction, thereby (largely) excluding bacterial organisms. Comparing heme *b* to chl *a*, which only occurs in phytoplankton, and particulate organic carbon (POC) and particulate organic nitrogen (PON), which will include detrital material in addition to zooplankton, will potentially provide a better understanding of microbial biomass in the oceans.

3.2.1 Aims and objectives

Our current understanding of heme distribution in the marine environment is extremely limited, despite hemes playing vital roles in numerous biological processes. Consequently, the primary aim of the project was to advance our understanding of these complexes, specifically the abundance of heme *b* in the (sub-) tropical North Atlantic. Heme is synthesised along the same biological pathway as chlorophyll (Vavilin and Vermaas 2002, Cornah et al. 2003, Mochizuki et al. 2010) and physiological responses in the environment could be detected through comparison of the two pigments. Additionally, measurements of chlorophyll *a* are routinely used as a simple indicator of phytoplankton biomass; whereas heme *b* abundance could provide a more dynamic assessment of the microbial population. Therefore, the specific objectives of this chapter were:

3.2.1.1 To enhance observational datasets of heme *b* distribution and abundance in the marine environment.

3.2.1.2 To determine the relationship between heme *b* and chlorophyll *a* concentration in the (sub-) tropical North Atlantic.

3.2.1.3 To establish whether heme *b* concentration provides an improved estimation of biomass in the (sub-) tropical North Atlantic compared to carbon measurements.

3.2.2 Hypotheses

The following hypotheses were developed to test the previously described objectives:

3.2.2.1 Heme *b* concentrations will be enhanced close to the African continent as a result of increased atmospheric dust input and benthic-derived iron. The abundance of heme *b* in the marine environment will provide an indication of iron stress.

3.2.2.2 Heme *b* and chlorophyll *a* concentrations will provide a positive correlation throughout the (sub-) tropical North Atlantic. The ratio of chlorophyll *a* to heme *b* concentration (chl:heme) will provide an indication of physiological adaptations in the abundance of heme *b* containing proteins.

3.2.2.3 A significant correlation will be observed between heme *b* concentration and particulate organic carbon (and nitrogen) in the (sub-) tropical North Atlantic. The correlation will provide a stronger explanation of biomass than the relationship found between chlorophyll *a* and particulate organic carbon/nitrogen.

3.3 Research cruises

Samples were obtained from two research cruises in the STNA (D346, Fig. 2.3) and the TNA (D361, Fig. 2.4); both aboard the *RRS Discovery* (section 2.3). Seawater collected from a CTD (<200 m) was vacuum filtered onto GF/Fs (MF300, Fisher Scientific, 0.7 µm) for the determination of particulate heme *b* (1 - 4 L, section 2.4) and chlorophyll *a* (0.2 - 0.5 L, section 2.5) concentration and pre-ashed GF/Fs (450 °C, >12 hours) for POC and PON (POC/N) concentration (1 - 4 L, section 2.6). Pre-dawn CTD casts were conducted during D361, whereas the CTD was deployed at various times during D346. During D361, further samples for the determination of particulate heme *b* were obtained from a continuous towed FISH supply (approximately 2 m depth) by vacuum filtration of seawater (2 - 4 L) onto GF/Fs (MF300, Fisher Scientific, 0.7 µm). Full analytical methodologies and cruise details are described in Chapter 2.

Physical parameters were measured using SEABIRD sensors on a stainless steel CTD rosette frame during both cruises, including temperature and salinity, and seawater samples were collected using 20 L Niskin bottles mounted on the rosette. In addition, nanomolar nutrient concentrations from the STNA (upper 200 m of the water column) were kindly provided by François-Eric Legiret (School of Ocean and Earth Sciences, University of Southampton). Phosphate and nitrate+nitrite (hereafter referred to as nitrate) concentrations were measured using colorimetric techniques with a standard segmented flow analyser coupled with 2 m liquid waveguide capillary cells (see Zhang 2000, Zhang and Chi 2002, Patey et al. 2008). Samples were stored at 4 °C and analysed

within 24 hours of collection. Nitrate and phosphate concentrations were also measured during the TNA cruise (data not shown) by François-Eric Legiret and E. Malcolm S. Woodward (Plymouth Marine Laboratory). Surface dissolved iron concentrations were measured during D361 and were provided by Christian Schlosser (School of Ocean and Earth Sciences, University of Southampton, Schlosser et al. in prep).

3.4 Results

Data collected from two research cruises in the (sub-) tropical North Atlantic are described in two sections. Firstly, results from the STNA (D346) are assessed, with stations allocated to five oceanographic regions: Florida Straits (FS), Gulf Stream (GS), Western Subtropical North Atlantic Gyre (WSNAG), Eastern Subtropical North Atlantic Gyre (ESNAG) and Azores Current (AC). Subsequently, measurements from the TNA (D361) are described, also allocated to five oceanographic regions: Coastal TNA, Central TNA, Equatorial Upwelling Region (EqU), Tropical South Atlantic (TSA) and East STNA gyre. Values typically described as the mean ± standard deviation.

3.4.1 Subtropical North Atlantic (STNA, D346)

3.4.1.1 Temperature, salinity and nanonutrients

A clear thermocline was observed across the STNA basin at approximately 100 m (Fig. 3.2A), which decreased in depth around the eastern margin. The temperature was highest in the upper 50 m of the Florida Straits and WSNAG regions (>25 °C). Surface waters of the Azores Current were lower in temperature (<23 °C) compared to the rest of the cross-sectional STNA transect as a result of cooler deep water upwelling along the West African coast. Salinity ranged from 36.2 to 37.6 with the highest values observed in the gyre regions, particularly the ESNAG, and slightly fresher waters at the eastern and western STNA margins (Fig. 3.2B). Nanomolar nitrate concentrations in the upper 150 m provided a similar spatial distribution to temperature, with the position of the nitracline decreasing in depth towards the Azores Current region (Fig. 3.2C). Above the nitracline, nitrate concentrations were less than 100 nmol L^{-1}; highlighting the oligotrophic conditions of the STNA. Phosphate concentrations were relatively contrasting between the East and the West provinces of the STNA (Fig. 3.2D); once again demonstrating the upwelling of nutrient-rich deep waters along the eastern STNA margin. Low phosphate concentrations (<10 nmol L^{-1}) were observed in the upper 50 m of the Florida Straits, Gulf Stream and WSNAG regions compared to relatively elevated concentrations (>20 nmol L^{-1}) in the Azores Current and part of the ESNAG region.

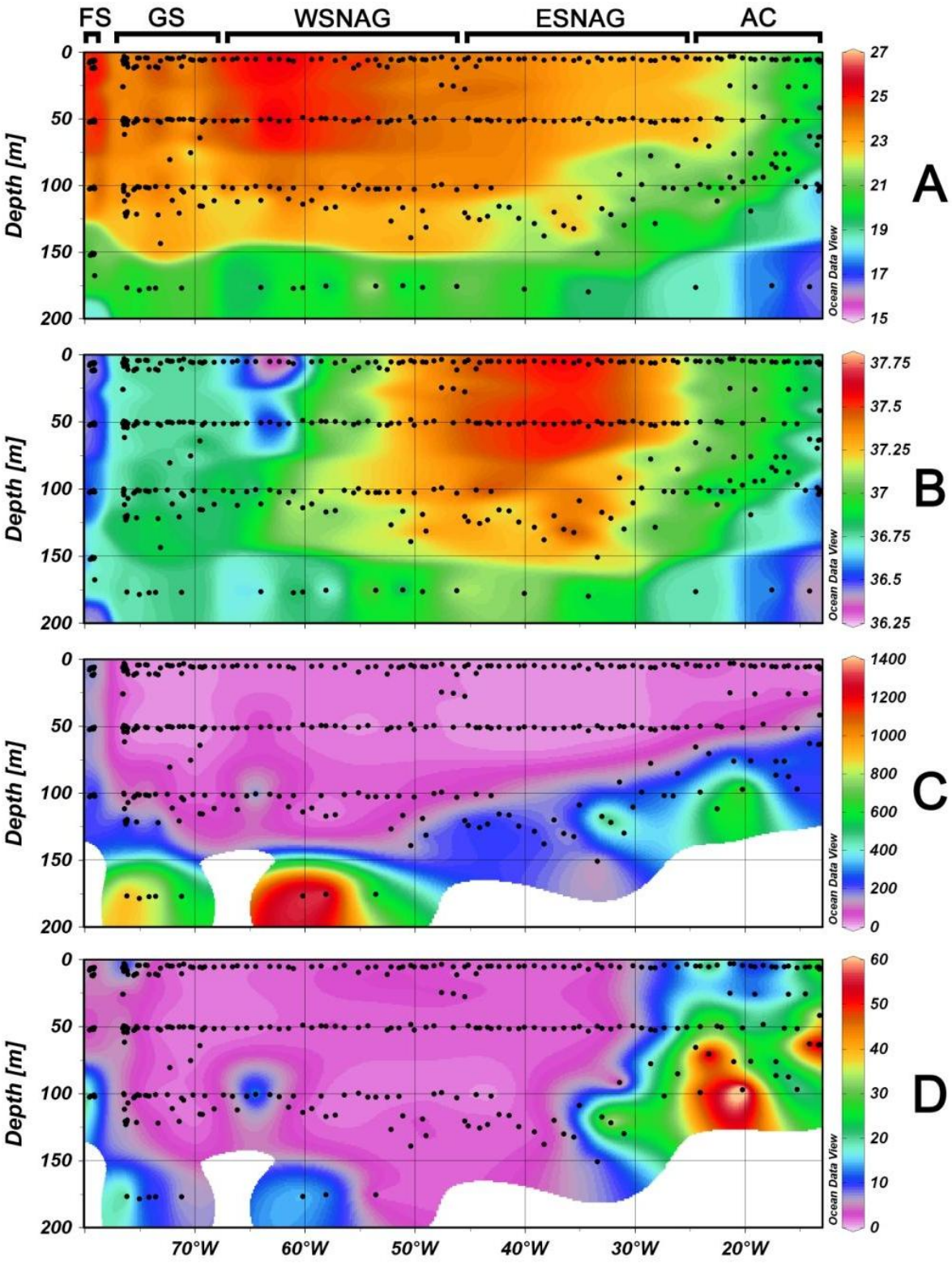

Figure 3.2. Cross-sectional profile (<200 m depth) of (**A**) temperature (°C), (**B**) salinity (psu), (**C**) nitrate concentration (nmol L^{-1}) and (**D**) phosphate concentration (nmol L^{-1}) from the STNA (D346). Note *z*-scales do not start from zero for profiles A and B; ranges from (A) 16 - 26 °C and (B) 35.25 - 36.5 psu. Nanomolar nutrient data (C and D) courtesy of François-Eric Legiret.

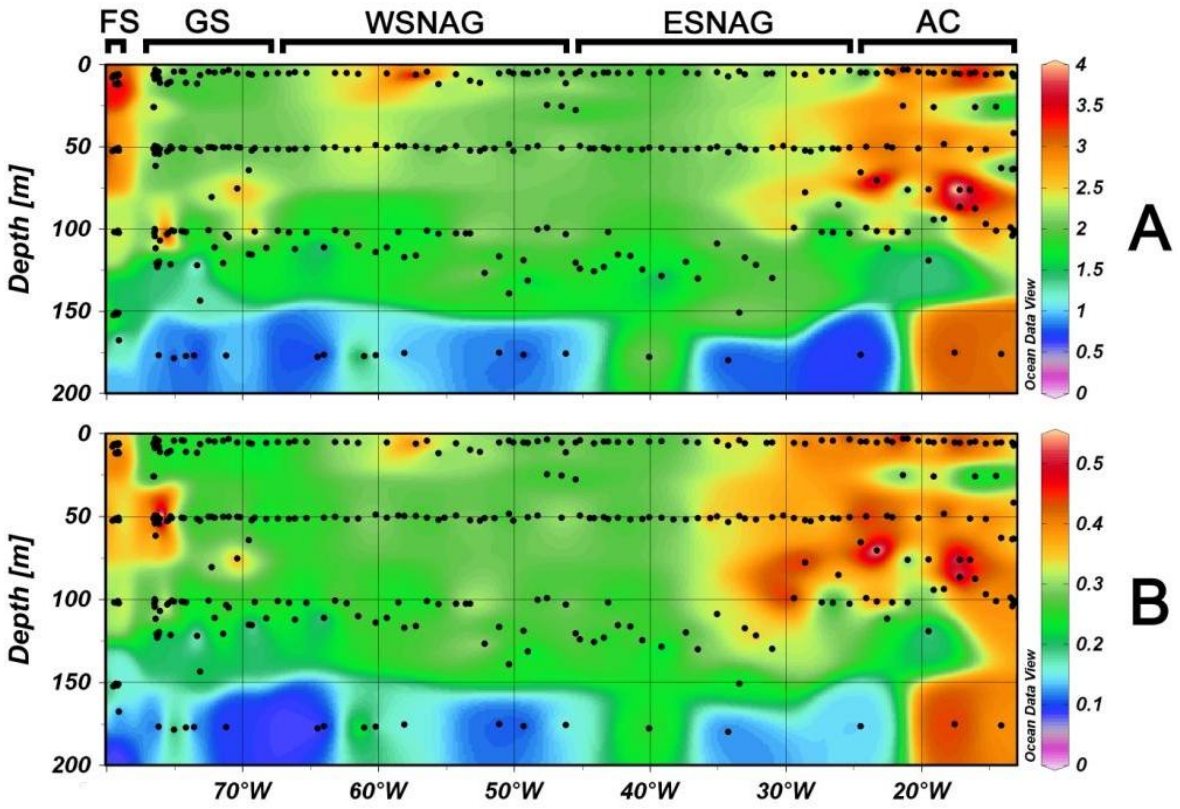

Figure 3.3. Cross-sectional profile (<200 m depth) of (**A**) particulate organic carbon (POC) concentration (µmol L^{-1}) and (**B**) particulate organic nitrogen (PON) concentration (µmol L^{-1}) from the STNA (D346). In total, 374 samples were analysed for POC and PON concentration.

3.4.1.2 Particulate organic carbon (POC) and nitrogen (PON)

The mean POC and PON concentrations across the STNA were 2.26 ± 0.7 µmol L^{-1} (N = 328, Fig. 3.3A) and 0.31 ± 0.2 µmol L^{-1} (N = 328, Fig. 3.3B), respectively. The POC concentration ranged from 0.16 to 7.70 µmol L^{-1}, whilst the PON concentration ranged from 0.05 to 2.66 µmol L^{-1}; with a mean carbon to nitrogen ratio (C:N) of 7.59 ± 1.4 mol mol^{-1}. The spatial distributions of POC and PON were typically analogous, with strong positive correlations between the two measures across the STNA (Table 3.1). The highest mean POC and PON concentrations were observed in the Florida Straits (3.06 ± 0.7 µmol C L^{-1} and 0.36 ± 0.1 µmol N L^{-1}) and Azores Current (2.62 ± 0.88 µmol C L^{-1} and 0.38 ± 0.1 µmol N L^{-1}) regions. In contrast, mean POC and PON concentrations in the Gulf Stream, WSNAG and ESNAG regions were relatively low; suggesting elevated concentrations were associated with the margins of the STNA basin. Below the thermocline, POC and PON concentrations were low, with the exception of several enhanced values in the Azores Current region at >100 m depth. Both POC (p < 0.05) and PON (p < 0.01) were significantly correlated with phosphate concentration when considering the overall STNA cross-section (Table 3.1), although individual regions did not offer any significant relationships. In contrast, nitrate concentrations were not significantly correlated to POC

or PON across the complete STNA transect; whereas specific regions did provide some significant correlations with frequent inverse relationships reported (Table 3.1).

	Variable 2				
Variable 1	Chlorophyll *a*	POC	PON	Nitrate	Phosphate
Florida Straits					
Heme *b*	0.728 (31)**	0.162 (30)	0.188 (30)	0.099 (26)	0.568 (26)**
Chlorophyll *a*	-	0.138 (30)	0.261 (30)	0.187 (26)	0.766 (26)**
POC	0.138 (30)	-	0.844 (30)**	0.238 (25)	0.097 (25)
PON	0.261 (30)	0.844 (30)**	-	0.455 (25)*	0.314 (25)
Gulf Stream					
Heme *b*	0.365 (94)**	0.163 (89)	0.302 (89)**	0.006 (87)	0.054 (87)
Chlorophyll *a*	-	-0.056 (91)	0.087 (91)	0.292 (93)**	0.024 (93)
POC	-0.056 (91)	-	0.730 (91)**	-0.314 (84)**	-0.051 (84)
PON	0.087 (91)	0.730 (91)**	-	-0.386 (84)**	-0.041 (84)
WSNAG					
Heme *b*	0.632 (92)**	-0.029 (81)	0.103 (81)	0.305 (85)**	0.278 (83)*
Chlorophyll *a*	-	-0.370 (83)**	-0.145 (83)	0.270 (89)*	0.190 (87)
POC	-0.370 (83)**	-	0.856 (83)**	-0.152 (76)	0.030 (74)
PON	-0.145 (83)	0.856 (83)**	-	-0.143 (76)	-0.007 (74)
ESNAG					
Heme *b*	0.692 (75)**	-0.088 (63)	0.010 (63)	0.219 (74)	0.133 (67)
Chlorophyll *a*	-	-0.002 (64)	0.220 (64)	0.408 (78)**	0.287 (71)*
POC	-0.002 (64)	-	0.902 (65)**	-0.292 (64)*	0.034 (58)
PON	0.220 (64)	0.902 (65)**	-	-0.059 (64)	0.252 (58)
Azores Current					
Heme *b*	0.484 (64)**	0.096 (60)	0.045 (60)	-0.131 (50)	0.037 (48)
Chlorophyll *a*	-	0.025 (60)	0.077 (60)	0.271 (50)	0.602 (48)**
POC	0.025 (60)	-	0.681 (59)**	-0.175 (48)	-0.105 (46)
PON	0.077 (60)	0.681 (59)**	-	-0.137 (48)	0.137 (46)
STNA (All)					
Heme *b*	0.666 (356)**	0.297 (323)**	0.375 (323)**	0.179 (322)**	0.325 (311)**
Chlorophyll *a*	-	0.184 (328)**	0.289 (328)**	0.362 (336)**	0.377 (325)**
POC	0.184 (328)**	-	0.746 (328)**	-0.17 (297)	0.135 (287)*
PON	0.289 (328)**	0.746 (328)**	-	0.053 (297)	0.364 (287)**

Table 3.1. Results of Pearson Product Moment Correlations (*r*) for heme *b*, chlorophyll *a*, particulate organic carbon (POC), particulate organic nitrogen (PON) and nanomolar nutrient (nitrate and phosphate) concentrations from five oceanographic regions of the STNA, as well as all stations combined from the STNA (D346). Numbers in brackets indicate number of samples. Statistical significance represented by ** where $p < 0.01$ and * where $p < 0.05$.

3.4.1.3 Chlorophyll a and heme b

The mean chlorophyll *a* concentration of the STNA was 0.19 ± 0.1 nmol L^{-1} (*N* = 396), with a maximum value of 0.78 mg m^{-3} (0.87 nmol L^{-1}) measured in the Florida Straits (Station 002, 103 m depth). A distinct chlorophyll *a* maximum was observed across the STNA (Fig. 3.4A), closely linked to the position of the thermocline and nitracline. The highest regional mean chlorophyll *a* concentration was measured in the Florida Straits (0.33 ± 0.13 nmol L^{-1}), followed by the Azores Current (0.24 ± 0.11 nmol L^{-1}). The Gulf Stream and the two central gyre regions provided comparatively reduced mean chlorophyll *a* concentrations (<0.2 nmol L^{-1}). Heme *b* concentrations averaged (mean) 1.32 ± 0.6 pmol L^{-1} (*N* = 383) across the complete STNA transect, ranging from below the limit of detection (0.48 pmol L^{-1}) to 4.98 pmol L^{-1} (Fig. 3.4B). The highest heme *b* concentration was measured in the Florida Straits at the same station and depth as the highest chlorophyll *a* concentration (Station 002, 103 m depth). Heme *b* concentrations were elevated (>2 pmol L^{-1}) at both the western (Florida Straits) and eastern (Azores Current) margins of the STNA, as well as across the central subtropical gyre regions at approximately 100 m depth. Both heme *b* and chlorophyll *a* were significantly correlated to nitrate and phosphate concentration when calculated for all stations in the STNA ($p < 0.01$, Table 3.1).

In general, the cross-sectional profile of heme *b* was spatially similar to chlorophyll *a* concentration, with the deep chlorophyll maximum (DCM) and heme *b* maximum located about 100 m depth across the region. A significant correlation was found between heme *b* and chlorophyll *a* concentration for the complete STNA transect and each of the five oceanographic regions ($p < 0.01$, Table 3.1) as was hypothesised (section 3.2.2.2). However, several clear differences between the spatial distribution of chlorophyll *a* and heme *b* concentration were apparent. This included the relatively low (compared to within the DCM) yet notable heme *b* abundance throughout waters <50 m depth in the central gyre regions, particularly the WSNAG (approximately 1 - 1.5 pmol L^{-1}), compared to very low chlorophyll *a* concentrations (<0.1 nmol L^{-1}). Furthermore, increased heme *b* concentrations associated with the Azores Current were more widespread compared to chlorophyll *a*, particularly in the upper 50 m of the water column. Below the DCM, heme *b* and chlorophyll *a* concentrations were <1 pmol L^{-1} and <0.1 nmol L^{-1}, respectively and these samples were discarded from subsequent analysis.

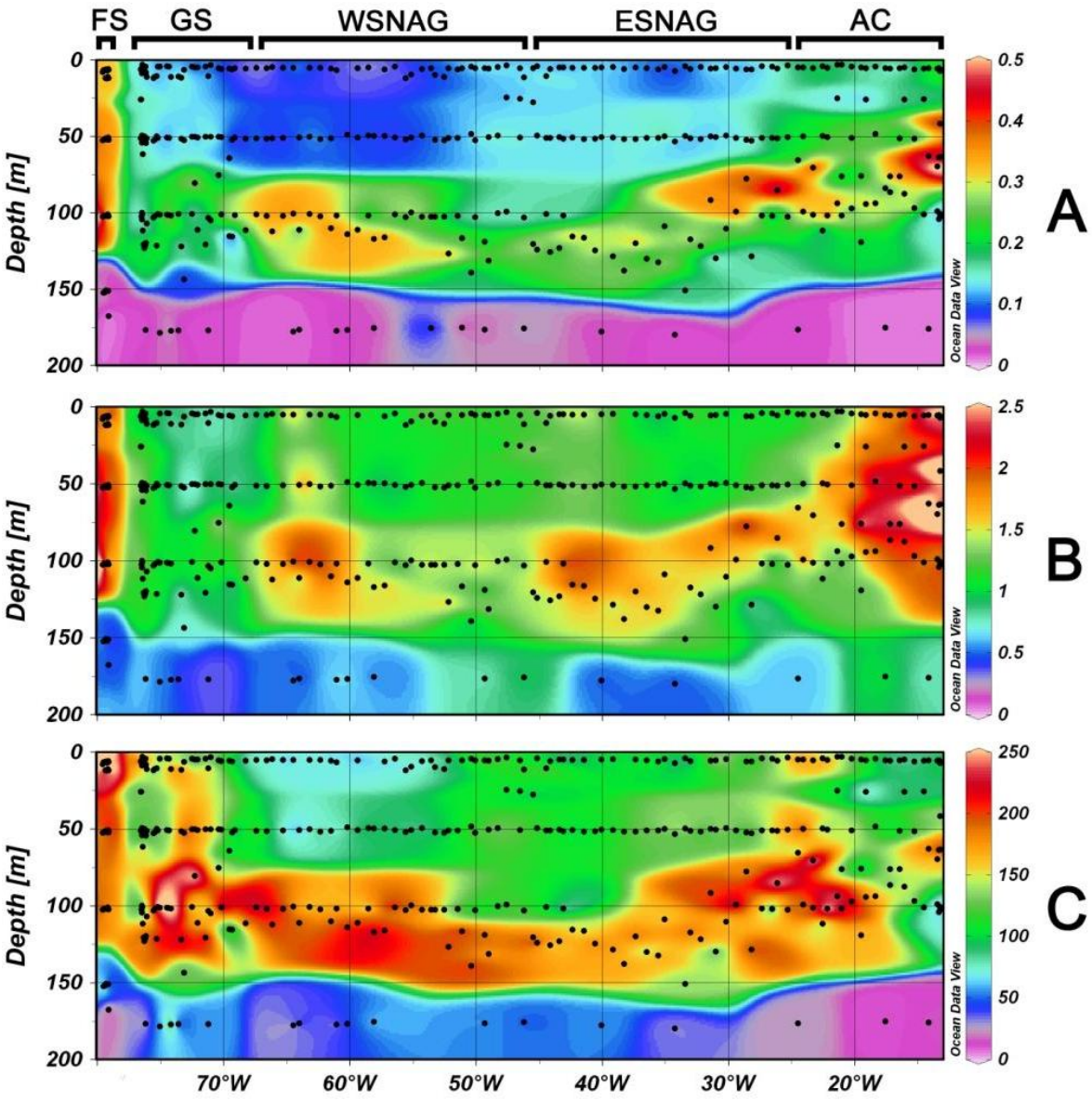

Figure 3.4. Cross-sectional profile (<200 m depth) of (**A**) chlorophyll *a* concentration (nmol L^{-1}), (**B**) heme *b* concentration (pmol L^{-1}) and (**C**) chlorophyll *a* to heme *b* ratio (chl:heme, mol mol^{-1}) from the STNA (D346). In total, 388 heme *b* samples and 399 chlorophyll *a* samples were collected, which enabled 357 chl:heme ratios to be calculated.

The ratio of chlorophyll *a* to heme *b* (chl:heme) ranged from 30.6 to 756 mol mol^{-1}, with a mean ratio of 144 ± 76 mol mol^{-1} (Fig. 3.4C). A notable increase in chl:heme ratio was observed about the position of the DCM, with values generally greater than 150 mol mol^{-1}. The highest chl:heme ratios (>400 mol mol^{-1}) were all observed in the Florida Straits and Gulf Stream regions of the western STNA. The increase in chlorophyll *a* concentration about the DCM compared to the surface mixed layer (SML) was visually more noticeable than the difference in heme *b* concentration between the DCM and SML. Across the complete STNA transect, the mean heme *b* concentration was elevated by 30% within the DCM compared to

Region	SML vs. DCM (Mann-Whitney *U*)	Concentration (SML)	Concentration (DCM)	Change (%)
Gulf Stream				
Heme *b*	541 (60, 33)**	0.94 ± 0.3	1.13 ± 0.3	+20
Chlorophyll *a*	267 (64, 35)**	0.12 ± 0.03	0.19 ± 0.06	+58
POC	755 (57, 33)	2.08 ± 0.3	2.09 ± 1.1	0
PON	931 (57, 33)	0.25 ± 0.04	0.26 ± 0.08	+3
WSNAG				
Heme *b*	480 (57, 35)**	1.15 ± 0.3	1.47 ± 0.4	+27
Chlorophyll *a*	111 (61, 35)**	0.10 ± 0.03	0.26 ± 0.09	+160
POC	370 (54, 29)**	2.21 ± 0.4	1.86 ± 0.3	-19
PON	614 (54, 29)	0.28 ± 0.05	0.26 ± 0.04	-7
ESNAG				
Heme *b*	231 (47, 28)**	1.15 ± 0.3	1.54 ± 0.4	+34
Chlorophyll *a*	102 (51, 28)**	0.13 ± 0.03	0.25 ± 0.10	+99
POC	309 (42, 22)*	2.14 ± 0.3	1.90 ± 0.4	-12
PON	390 (42, 22)	0.32 ± 0.06	0.30 ± 0.09	-7
Azores Current				
Heme *b*	455 (27, 38)**	1.75 ± 0.6	1.89 ± 0.7	+8
Chlorophyll *a*	249 (27, 39)**	0.18 ± 0.05	0.27 ± 0.12	+52
POC	424 (26, 35)	2.67 ± 1.0	2.62 ± 0.8	-2
PON	419 (26, 35)	0.38 ± 0.12	0.38 ± 0.12	+2
STNA (All)				
Heme *b*	6926 (191, 134)**	1.17 ± 0.4	1.52 ± 0.5	+30
Chlorophyll *a*	3044 (203, 137)**	0.12 ± 0.04	0.25 ± 0.10	+97
POC	8833 (179, 119)*	2.22 ± 0.5	2.16 ± 0.8	-3
PON	10269 (179, 119)	0.29 ± 0.08	0.30 ± 0.10	+3

Table 3.2. Results of Mann-Whitney *U* tests (two-tailed) for comparison of the median heme *b* (pmol L^{-1}), chlorophyll *a* (nmol L^{-1}), POC (µmol L^{-1}) and PON (µmol L^{-1}) concentration between the surface mixed layer (SML) and deep chlorophyll maximum (DCM) from four oceanographic regions of the STNA, as well as all stations combined from the STNA (D346). Comparisons were not possible for the Florida Straits as the SML and DCM could not be differentiated. Numbers in brackets (n_1, n_2) indicate the number of samples in the SML (n_1) and DCM (n_2). Statistical significance represented by ** where $p < 0.01$ and * where $p < 0.05$. In addition, mean heme *b*, chlorophyll *a*, POC and PON concentrations for the SML and DCM ± standard deviation and the percentage (%) change in mean concentration between the SML and DCM are presented.

the SML, whereas a 97% increase was calculated for the mean chlorophyll *a* concentration in the DCM (Table 3.2). This trend was also apparent within the five oceanographic regions, particularly the WSNAG which demonstrated a 160% increase in chlorophyll *a* concentration at the DCM compared to the SML; heme *b* concentration was increased by only 27% in the DCM of the WSNAG. Cross-sectional profiles of POC (Fig. 3.3A) and PON (Fig. 3.3B) did not present obvious similarities to chlorophyll *a* and/or heme *b* distribution. In particular, the elevated chlorophyll *a* and heme *b* concentrations about

the DCM were not evident for POC or PON concentration across the STNA basin. Instead, POC and PON were comparatively uniform throughout waters <150 m depth; further highlighted by POC (-3%) and PON (+3%) concentrations remaining relatively similar between the DCM and SML (Table 3.2).

Both POC and PON concentration offered significant correlations with chlorophyll *a* and heme *b* across the complete STNA transect (Table 3.1), despite visual comparisons suggesting dissimilarities between measurements. Heme *b* concentration accounted for slightly more of the variance (r^2) in POC and PON concentration compared to chlorophyll *a*. However, correlations between chlorophyll *a*/heme *b* and POC/PON when separated into five oceanographic regions offered non-significant relationships, with the exception of heme *b* and PON in the Gulf Stream ($r = 0.302$, $p < 0.01$, $N = 89$) and chlorophyll *a* and POC in the WSNAG ($r = -0.370$, $p < 0.01$, $N = 83$, inverse relationship). Partial correlations were used to assess the strength of correlations for the complete STNA between (1) heme *b* and POC/PON and (2) chlorophyll *a* and POC/PON whilst controlling for the variance attributed to chlorophyll *a* and heme *b* concentration, respectively (Table 3.3). Heme *b* remained significantly correlated to both POC and PON concentration when controlled for by chlorophyll *a*. However, the association between chlorophyll *a* and POC/PON concentration while controlling for heme *b* suggested no significant relationship between the variables. Therefore, the relationship between chlorophyll *a* and POC/PON concentrations in the STNA was, at least to some extent, explained by the concentration of heme *b* which offered a stronger correlation as hypothesised (section 3.2.2.3).

	Variable 2	
Variable 1	Heme *b*	Chlorophyll *a*
Controlling for heme b		
POC	-	0.004 (320)
PON	-	0.089 (320)
Controlling for chlorophyll a		
POC	0.239 (320)**	-
PON	0.261 (320)**	-

Table 3.3. Results of Partial Correlation Coefficient (*r*) tests from STNA (D346) samples for heme *b* concentration vs. POC/PON concentration and chlorophyll *a* concentration vs. POC/PON concentration, while controlling for chlorophyll *a* and heme *b* concentration, respectively. Numbers in brackets indicate degrees of freedom. Statistical significance represented by ** where $p < 0.01$ and * where $p < 0.05$.

The mean heme *b* concentrations per unit carbon (heme:C, Fig. 3.5A) and per unit nitrogen (heme:N, Fig. 3.5B) for the STNA were 0.64 ± 0.4 μmol mol^{-1} C ($N = 323$) and

4.61 ± 1.7 μmol mol^{-1} N (N = 323), respectively. The heme:C and heme:N profiles were spatially similar, with increased ratios towards the eastern margin (Azores Current) as well as several areas within the subtropical gyre regions. The highest mean heme:C ratio was observed in the Azores Current region (0.76 ± 0.7 μmol mol^{-1} C, N = 60) and the highest mean heme:N ratio was calculated for the Florida Straits (5.22 ± 2.3 μmol mol^{-1} N, N = 30). Chlorophyll *a* content per unit carbon (chl:C, Fig. 3.5C) averaged 89.0 ± 71.5 μmol mol^{-1} C (N = 329), with a mean chlorophyll *a* content per unit nitrogen (chl:N, Fig. 3.5D) of 635 ± 326 μmol mol^{-1} N (N = 329). Profiles of chl:C and chl:N ratio were spatially analogous to that of chlorophyll *a* concentration (Fig. 3.4A), with enhanced values about the DCM. One noteworthy difference between heme *b* and chlorophyll *a* content (i.e. per unit C or N) profiles was the clear reduction in chlorophyll *a* within the SML of the WSNAG region, compared to the low but detectable heme *b* concentrations. Statistical analysis (Mann-Whitney U tests) revealed that median heme:C (U = 5024, p < 0.01) and heme:N (U = 6032, p < 0.01) ratios were significantly different between the SML and the DCM across the overall STNA transect. In addition, the median chl:C (U = 2910, p < 0.01) and chl:N (U = 3340, p < 0.01) ratios were also significantly different between the SML and DCM. This trend of increased chlorophyll *a* and heme *b* contents within the DCM was also observed within each oceanographic region of the STNA (see Table 3.4).

Region	Variable			
	Heme:C	Heme:N	Chl:C	Chl:N
Gulf Stream	452.5** (57, 32)	587.5** (57, 32)	336** (58, 33)	417** (58, 33)
WSNAG	236** (52, 29)	324** (52, 29)	54** (54, 29)	63** (54, 29)
ESNAG	157.5** (41, 23)	213** (41, 23)	81.5** (42, 22)	89** (42, 22)
Azores Current	368** (26, 34)	389** (26, 34)	273** (26, 35)	278** (26, 35)
STNA (All)	5024** (176, 118)	6032** (176, 118)	2910** (180, 119)	3340** (180, 119)

Table 3.4. Results of Mann-Whitney U tests (two-tailed) for comparison of the median heme *b* concentration per unit carbon (heme:C) and per unit nitrogen (heme:N) and chlorophyll *a* concentration per unit carbon (Chl:C) and per unit nitrogen (Chl:N) between the surface mixed layer (SML) and deep chlorophyll maximum (DCM) from four oceanographic regions of the STNA, as well as all stations combined from the STNA (D346). Comparisons were not possible for the Florida Straits as the SML and DCM could not be differentiated. Numbers in brackets (n_1, n_2) indicate the number of SML (n_1) and DCM (n_2) samples. All comparisons suggested a significant difference between the SML and DCM at the p < 0.01 level (**).

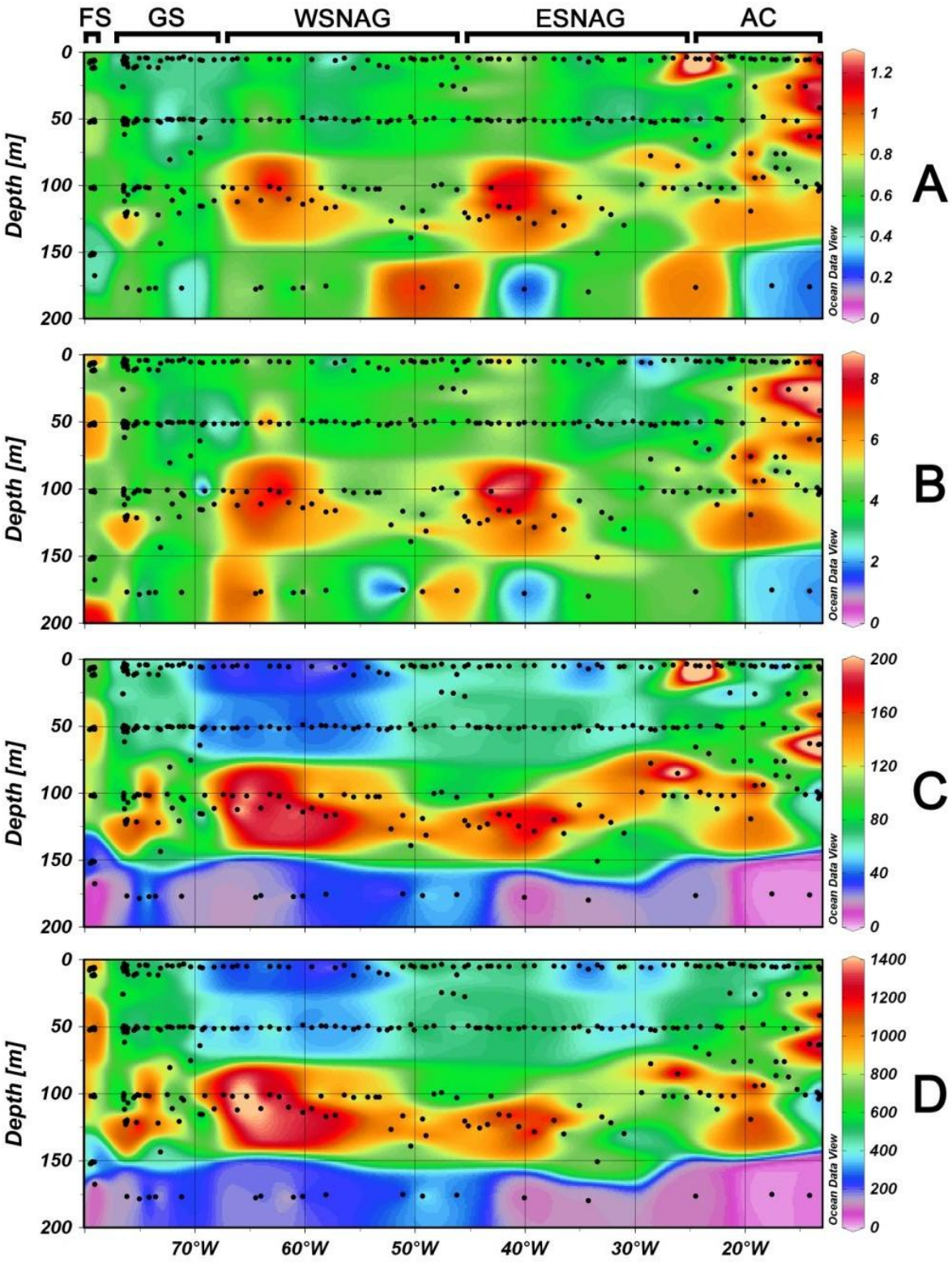

Figure 3.5. Cross-sectional profile (<200 m depth) of (**A**) heme:C ratio (µmol mol^{-1} C), (**B**) heme:N ratio (µmol mol^{-1} N), (**C**) chl:C ratio (µmol mol^{-1} C) and (**D**) chl:N ratio (µmol mol^{-1} N) from the STNA (D346). In total, 345 heme:C and heme:N ratios and 348 chl:C and chl:N ratios were calculated.

In summary, all hypotheses previously described were supported by results collected from the STNA during cruise D346. Heme *b* concentrations were elevated close to the African continent, potentially owing to increased iron input (section 3.2.2.1) and chlorophyll *a* and heme *b* concentrations were significantly correlated throughout the region (section 3.2.2.2). Finally, partial correlations revealed a significant relationship between heme *b* and POC/PON when controlling for chlorophyll *a,* but the relationship between chlorophyll *a* and POC/PON was non-significant when controlling for heme *b*. This demonstrated the correlation between heme *b* and POC/PON provided a stronger explanation of biomass than the relationship found between chlorophyll *a* and POC/PON (section 3.2.2.3).

3.4.2 Tropical North Atlantic (TNA, D361)

3.4.2.1 Temperature, salinity and nanonutrients

The temperature profile of the East-West (EW, Fig. 2.4) transect of the TNA cruise (D361) provided a similar pattern to the STNA (D346, Fig. 3.2A) as the position of the thermocline became increasingly shallow towards the Senegalese coast (Fig. 3.6A). The highest temperatures (>24 °C) were measured in the upper 30 m of S8 and S9 of the Central TNA region. Surface temperatures between 20 and 22 °C in the Coastal TNA were similar to those previously reported in the Azores Current region of the eastern STNA (D346); the result of cold deep water upwelling along the eastern boundary of the North Atlantic. Seawater salinity was relatively homogenous throughout the EW transect (35.5 - 36), with the exception of increased measurements (>36) at >80 m depth from S9 of the Central TNA region (Fig. 3.6B). Compared to the Azores Current region of the STNA (36.5 - 37, Fig. 3.2B), seawater was slightly fresher along the EW transect of the TNA. Nitrate and phosphate concentrations were high throughout the upper 100 m of the Coastal TNA, once again as a result of nutrient-rich deep water upwelling in the region (>0.1 μmol L^{-1}, data not shown). Towards the Central TNA region of the EW transect, nitrate decreased to concentrations <20 nmol L^{-1} in seawaters <100 m depth; typical of an oligotrophic environment. However, phosphate concentration remained relatively high further offshore at approximately 20 nmol L^{-1}; similar to the increased phosphate concentrations observed in the Azores Current and ESNAG regions of the STNA (Fig. 3.2D).

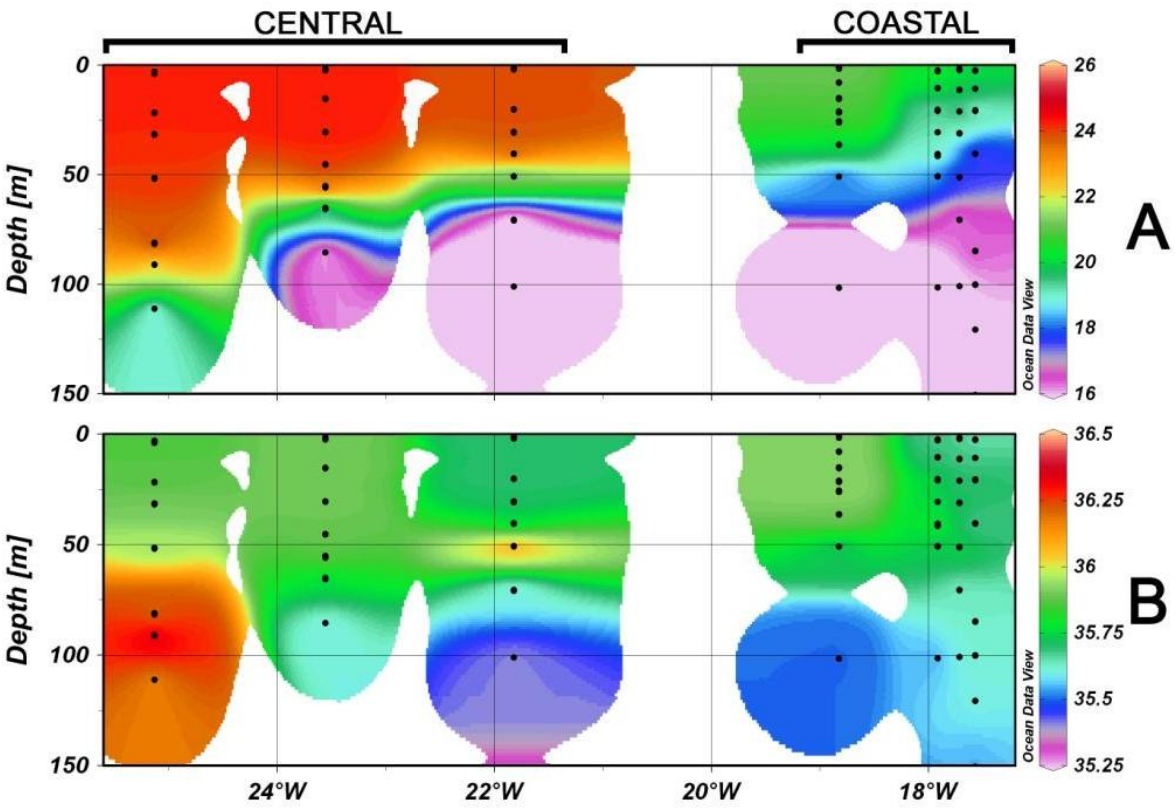

Figure 3.6. Cross-sectional profile (<150 m depth) of (**A**) temperature (°C) and (**B**) salinity (psu) from the EW transect of the TNA (D361).

A distinct thermocline was evident from the temperature profile of the South-North (SN, Fig. 2.4) transect of the TNA cruise (D361, Fig 3.7A), shoaling to approximately 60 m depth as a result of cold deep water upwelling within the EqU region (~5 °N). The position of the thermocline deepened in the TSA and East STNA gyre regions to approximately 100 m depth. The temperature above the thermocline gradually decreased as the SN transect progressed northwards, with temperatures >27 °C in the TSA and EqU regions compared to <24 °C in the East STNA gyre region. The temperatures of the East STNA gyre region (D361) were comparable to the ESNAG previously described from cruise D346 (Fig. 3.2A). The salinity profile showed increased values at the margins of the SN transect (i.e. >36.25), with fresher seawater in the middle section (Fig. 3.7B). In particular, salinity values were markedly decreased in the upper 20 m of S14 in the EqU region (35.01). Rain events occurred whilst crossing the Intertropical Convergence Zone (ITCZ), resulting in an increased freshwater input to the EqU region. In general, nitrate and phosphate concentrations were very low above the thermocline (<30 nmol L^{-1}) throughout the SN transect (data not shown).

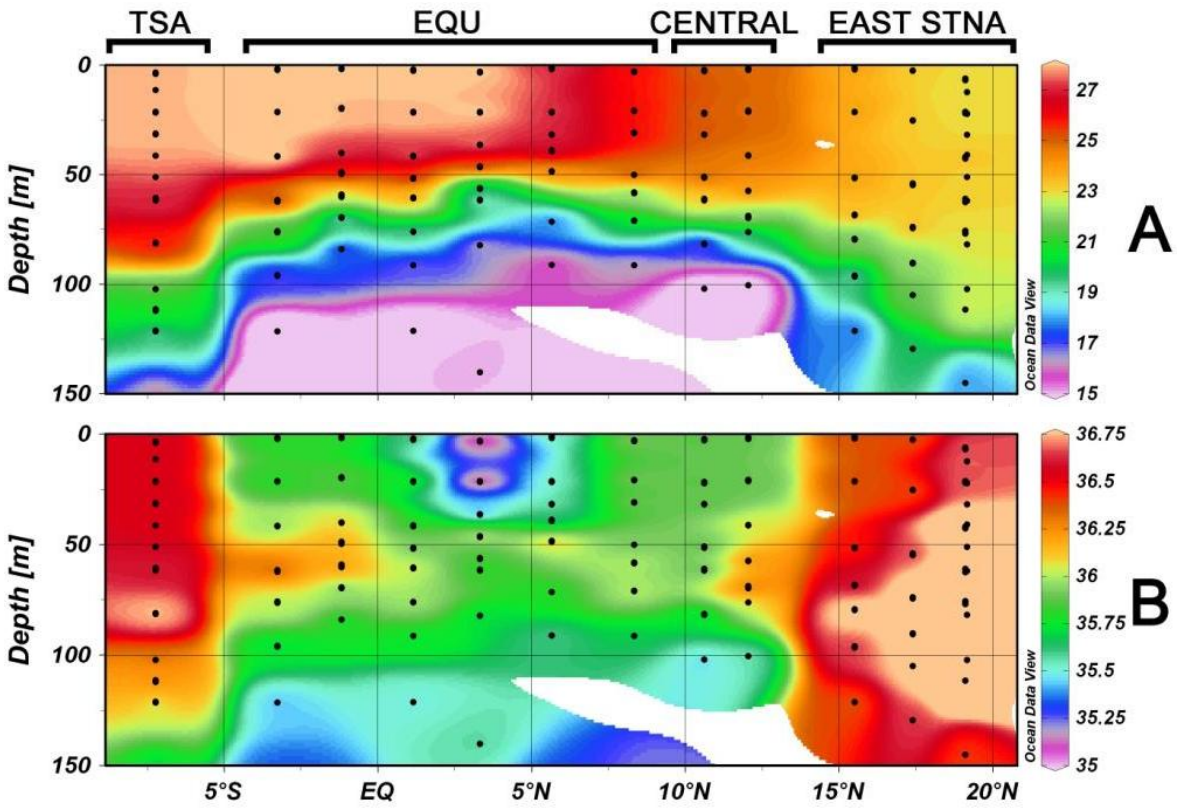

Figure 3.7. Cross-sectional profile (<150 m depth) of (**A**) temperature (°C) and (**B**) salinity (psu) from the SN transect of the TNA (D361).

3.4.2.2 Particulate organic carbon (POC) and nitrogen (PON)

The mean POC concentration of the TNA was 3.57 ± 4.9 µmol L^{-1} (N = 114), ranging from 0.58 to 22.6 µmol L^{-1}. Particulate organic carbon concentrations typically decreased with depth in the Coastal TNA region, with the highest concentrations measured in the upper 20 m of the water column. The highest regional mean POC concentration was observed in the Coastal TNA (M = 11.3 ± 6.1 µmol L^{-1}, N = 24, (Fig. 3.8A), with the highest sample concentration measured at the station closest to the Senegalese coast (22.6 µmol L^{-1}, S4, 2.6 m depth). Concentrations of POC in the Central TNA (M = 1.80 ± 0.6 µmol L^{-1}, N = 27), TSA (M = 1.11 ± 0.4 µmol L^{-1}, N = 4), EqU (M = 1.58 ± 0.8 µmol L^{-1}, N = 36) and East STNA gyre (M = 1.08 ± 0.2 µmol L^{-1}, N = 24) regions were relatively uniform throughout the upper 160 m of the water column (Fig. 3.8B-D), with the exception of S16 of the EqU region which demonstrated a marked increase to 4.98 µmol L^{-1} at 58 m depth.

The mean PON concentration of the TNA was 0.46 ± 0.6 µmol L^{-1} (N = 114), ranging from 0.07 to 2.72 µmol L^{-1} and provided a mean C:N ratio of 7.72 ± 1.7 mol mol^{-1}. The spatial distribution (depth profiles) of PON were similar to POC (data not shown); also demonstrating notably high concentrations in the Coastal TNA (M = 1.45 ± 0.7 µmol L^{-1}, N = 24). Mean POC and PON concentrations in the four offshore TNA regions were similar compared to the STNA (D346, Fig. 3.3), particularly the Azores Current region. However,

POC/N concentrations in the Coastal TNA region were distinctly elevated compared to the STNA, including the Azores Current region of the eastern STNA. Statistical analysis (Mann-Whitney *U* tests) showed that POC/N concentrations in the Coastal TNA were significantly higher than the Central TNA, TSA, EqU and East STNA gyre regions of cruise D361 ($p < 0.01$, Fig. 3.9).

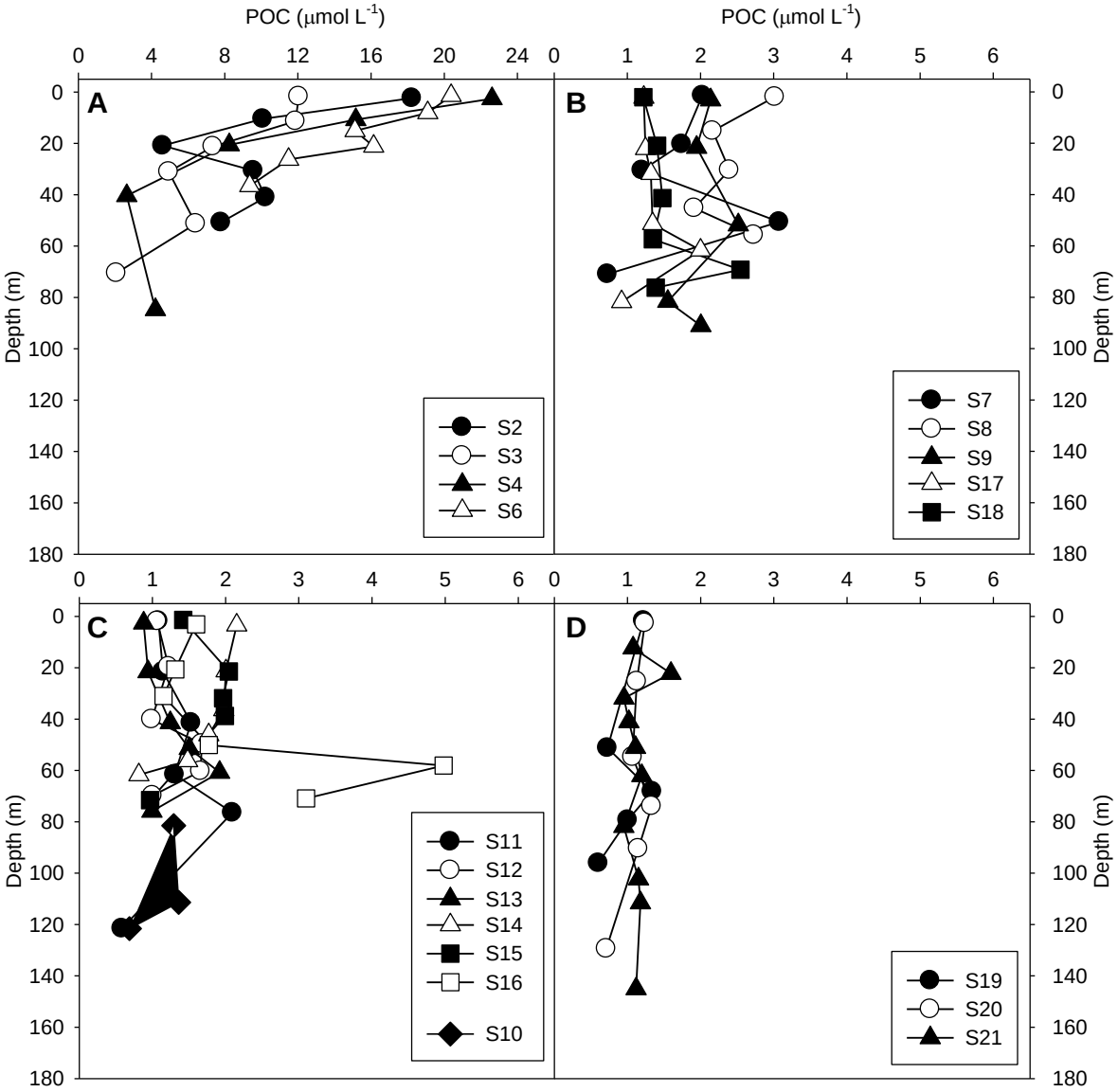

Figure. 3.8. Depth profiles (<180 m depth) of particulate organic carbon (POC) concentration (µmol L^{-1}) from (**A**) the Coastal TNA, (**B**) the Central TNA, (**C**) the TSA and EqU and (**D**) the East STNA gyre regions of the TNA (D361). Note the different *x*-axis scale of A.

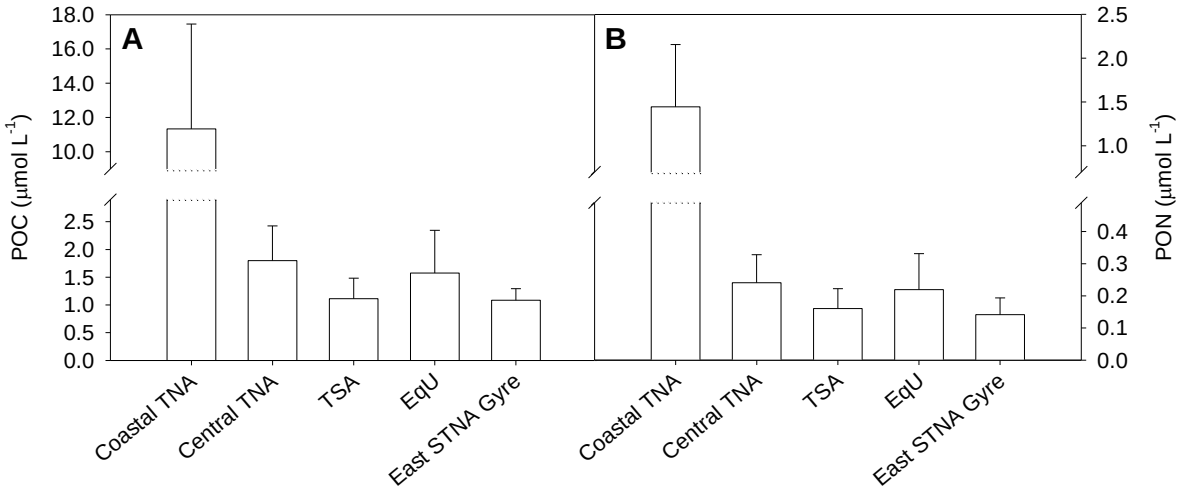

Figure 3.9. Mean concentration of (**A**) particulate organic carbon (POC, µmol L^{-1}) and (**B**) particulate organic nitrogen (PON, µmol L^{-1}) for five oceanographic regions of the TNA (D361).

3.4.2.3 Chlorophyll a and heme b

The mean chlorophyll *a* concentration of the TNA was 0.67 ± 1.0 nmol L^{-1} (*N* = 116); a three-fold increase compared to the STNA (D346, *M* = 0.19 ± 0.1 nmol L^{-1}). Chlorophyll *a* concentrations ranged from 0.05 to 6.61 nmol L^{-1} throughout the TNA, with the highest concentration measured in surface waters (2.6 m depth) of S4 in the Coastal TNA region. The comparatively increased mean chlorophyll *a* concentration of the TNA was predominantly attributed to the very high concentrations measured in the Coastal TNA region (*M* = 2.18 ± 1.3 nmol L^{-1}, *N* = 23). These elevated chlorophyll *a* concentrations were linked to the increased nutrient supply from nutrient-rich deep water upwelling about the eastern boundary of the North Atlantic. Relatively similar chlorophyll *a* concentrations were measured in the Central TNA (0.34 ± 0.2 nmol L^{-1}, *N* = 26), TSA (0.17 ± 0.1 nmol L^{-1}, *N* = 6), EqU (0.33 ± 0.3 nmol L^{-1}, *N* = 36) and East STNA gyre (0.22 ± 0.1 nmol L^{-1}, *N* = 25) regions of the TNA (D361) when compared to the STNA (D346). Depth profiles of chlorophyll *a* in the Coastal TNA were similar to POC and PON concentration, with increased values at the surface that decreased with depth (Fig. 3.10). Increased chlorophyll *a* concentrations were measured between 50 and 100 m depth throughout the SN transect of the TNA, showing a similar spatial distribution to the position of the thermocline (Fig. 3.7A). Chlorophyll *a* concentrations were significantly correlated to POC and PON concentration in the TNA, with the exception of the comparison between chlorophyll *a* and POC in the East STNA gyre region (Table 3.5). The frequent correlations observed between chlorophyll *a* and POC/PON concentration was contrasting to the lack of significant correlations observed in the STNA between the parameters (see Table 3.1).

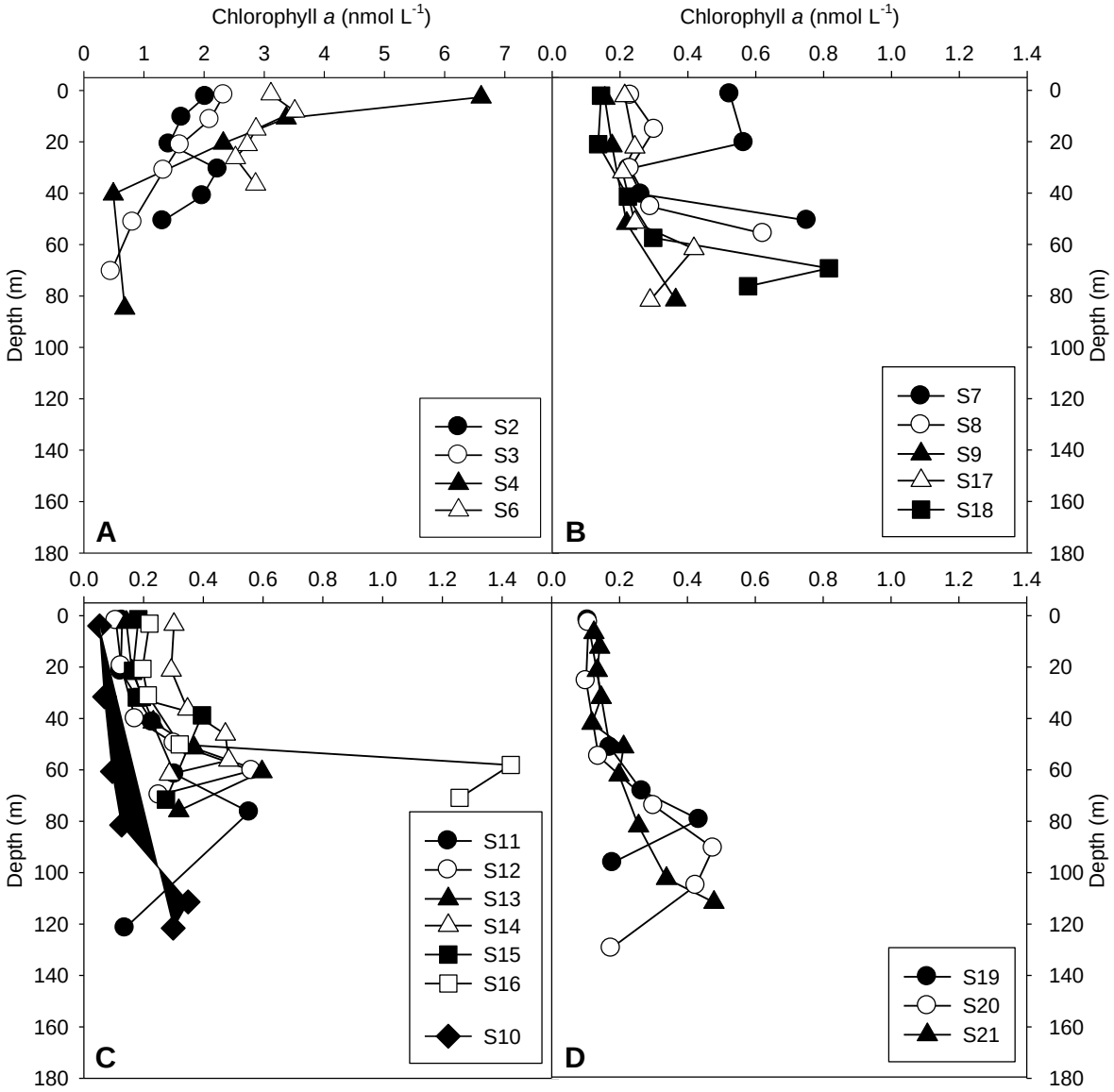

Figure 3.10. Depth profiles (<180 m depth) of chlorophyll *a* concentration (nmol L^{-1}) from (**A**) the Coastal TNA, (**B**) the Central TNA, (**C**) the TSA and EqU and (**D**) the East STNA gyre regions of the TNA (D361). Note the different *x*-axis scale of A.

The mean heme *b* concentration of the TNA was 2.18 ± 3.2 pmol L^{-1} (N = 90); higher in comparison to the STNA (D346, 1.32 ± 0.6 pmol L^{-1}). The standard deviation from the TNA was particularly high (i.e. >100% of the mean), potentially owing to the spatial variability and greater number of depths sampled per station compared to the STNA. Also, the elevated mean heme *b* concentration in the TNA was once again related to high values reported in the Coastal TNA (M = 5.70 ± 4.4 pmol L^{-1}, N = 24); analogous to increased chlorophyll *a* concentrations in the region. Mean heme *b* concentrations in the Central TNA (M = 1.22 ± 1.0 pmol L^{-1}, N = 18), TSA (M = 0.67 ± 0.1 pmol L^{-1}, N = 4) and EqU (M = 0.80 ± 0.7 pmol L^{-1}, N = 32) regions were reduced compared to the Coastal TNA, as well as the overall STNA

Variable 1	Variable 2		
	Chlorophyll *a*	POC	PON
Coastal			
Heme *b*	0.074 (23)	0.178 (24)	0.194 (24)
Chlorophyll *a*	-	0.841 (23)**	0.841 (23)**
Central TNA			
Heme *b*	0.067 (18)	0.022 (17)	-0.091 (17)
Chlorophyll *a*	-	0.456 (25)*	0.692 (25)**
Equatorial Upwelling			
Heme *b*	0.239 (32)	0.194 (32)	0.205 (32)
Chlorophyll *a*	-	0.850 (36)**	0.838 (36)**
East STNA gyre			
Heme *b*	-0.135 (12)	-0.485 (10)	-0.262 (10)
Chlorophyll *a*	-	0.208 (22)	0.673 (22)**
TNA (All)			
Heme *b*	0.553 (89)**	0.613 (86)**	0.629 (86)**
Chlorophyll *a*	-	0.934 (109)**	0.935 (109)**

Table 3.5. Results of Pearson Product Moment Correlations (*r*) for heme *b*, chlorophyll *a*, particulate organic carbon (POC) and particulate organic nitrogen (PON) concentrations from the Coastal TNA, Central TNA, Equatorial Upwelling and East STNA gyre regions, as well as all stations combined from the TNA (D361). Results from the TSA region are not presented due to lack of samples. Numbers in brackets indicate number of samples. Statistical significance represented by ** where $p < 0.01$ and * where $p < 0.05$.

(D346). The East STNA gyre region of D361 provided the closest geographical comparison to the STNA and averaged 0.78 $\pm$ 0.7 pmol L^{-1} (N = 12); notably lower than the ESNAG region of cruise D346 (M = 1.30 $\pm$ 0.4 pmol L^{-1}). Depth profiles of heme *b* concentration did not provide a clear visual comparison to chlorophyll *a*, POC or PON concentration (Fig. 3.11). This was reflected by non-significant correlations calculated between the parameters for the five different oceanographic regions (Table 3.5). However, heme *b* was significantly correlated ($p < 0.01$) to chlorophyll *a*, POC and PON concentration when considering the overall TNA cruise. Partial correlations were conducted for the overall TNA, assessing the relationship between (1) heme *b* and POC/PON concentration and (2) chlorophyll *a* and POC/PON concentration whilst controlling for chlorophyll *a* and heme *b* concentration, respectively (Table 3.6). Unlike the STNA, both chlorophyll *a* and heme *b* remained significantly correlated to POC/PON. Nevertheless, chlorophyll *a* accounted for a larger proportion of the variance (r^2) with POC and PON concentration compared to heme *b*, as well as providing strongly significant correlations within each of the oceanographic regions. Thus, it is likely that chlorophyll *a* provided a better comparison to POC and PON than heme *b* in the TNA; the opposite trend previously hypothesised and observed in the STNA (section 3.2.2.3).

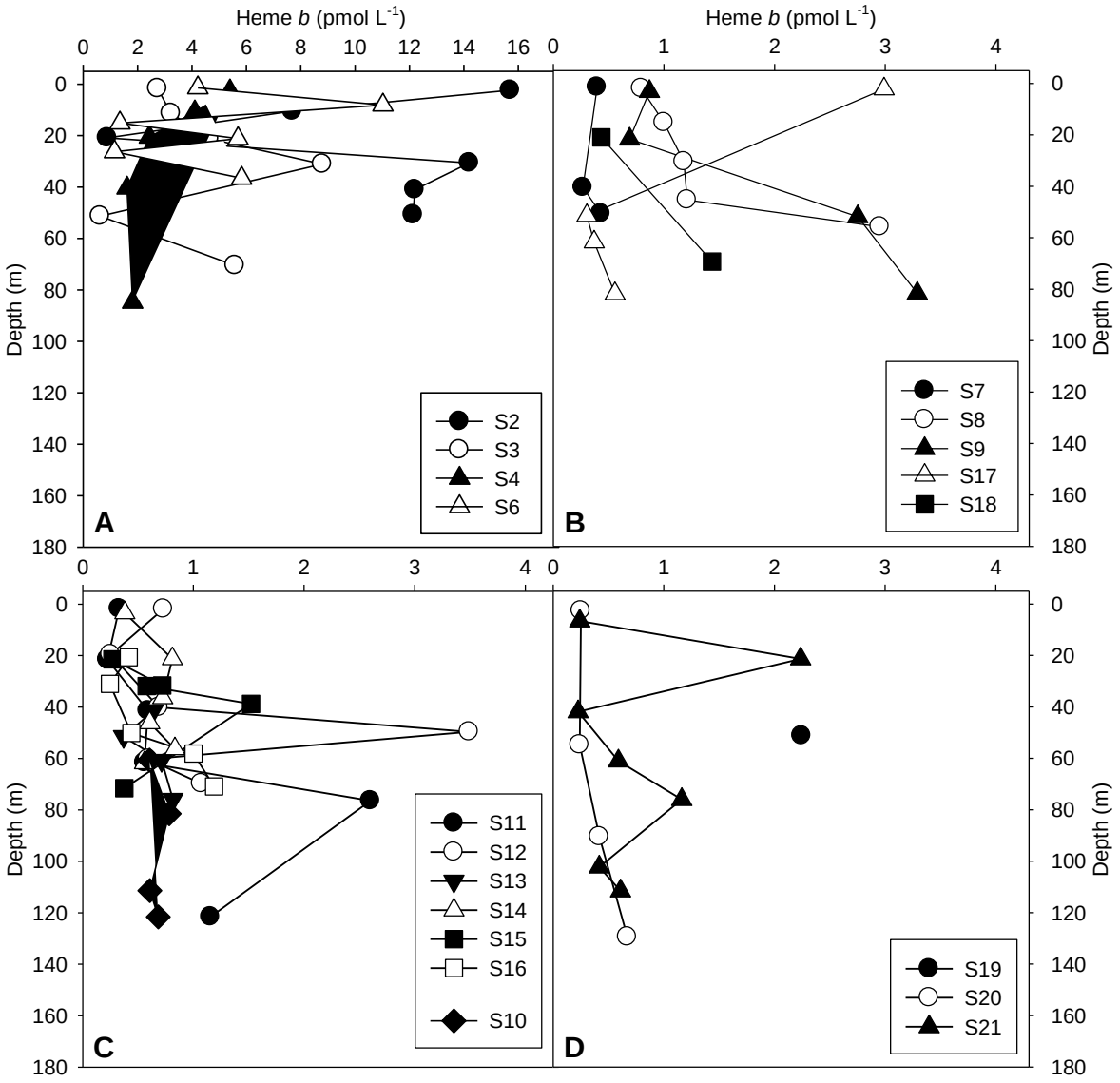

Figure 3.11. Depth profiles (<180 m depth) of heme *b* concentration (pmol L^{-1}) from (**A**) the Coastal TNA, (**B**) the Central TNA, (**C**) the TSA and EqU and (**D**) the East STNA gyre regions of the TNA (D361). Note the different *x*-axis scale of A.

Chlorophyll *a* and heme *b* concentrations were significantly correlated ($p < 0.01$) when considering all stations during cruise D361 of the TNA (Table 3.5); however, the relationship was not evident for the five separate oceanographic regions, providing a contrast to the STNA. The mean chl:heme ratio from the TNA (553 ± 446 mol mol^{-1}, N = 89) was distinctly elevated compared to the STNA (D346); especially the ESNAG region (M = 131 ± 42.1 mol mol^{-1}) which provided the closest geographical comparison. All five oceanographic regions displayed high chl:heme ratios (Fig. 3.12) with no apparent pattern regarding depth. In addition, all regions exhibited high levels of standard deviation (i.e. >50% of the mean). The highest mean chl:heme ratio was observed in the Coastal TNA region (684 ± 624 mol mol^{-1}, N = 23), with maximum ratios sampled from S6 at depths of 15 m (2119 mol mol^{-1}) and 26 m (2190 mol mol^{-1}). The lowest regional mean chl:heme

ratio was calculated for the TSA, where S10 averaged 333 ± 207 mol mol^{-1} (N = 4). However, the lowest individual chl:heme ratio was found in the East STNA gyre region at S21 (60.1 mol mol^{-1}, 21 m depth). The chl:heme ratios calculated from the East STNA gyre region during D361 were significantly different to those obtained from the ESNAG region during D346 (U = 151, n_1 = 12, n_2 = 75, p < 0.01, Mann-Whitney U test).

	Variable 2	
Variable 1	Heme *b*	Chlorophyll *a*
Controlling for heme b		
POC	-	0.906 (82)**
PON	-	0.909 (82)**
Controlling for chlorophyll a		
POC	0.434 (82)**	-
PON	0.460 (82)**	-

Table 3.6. Results of Partial Correlation Coefficient (r) tests from TNA (D361) samples for heme *b* concentration vs. POC/PON concentration and chlorophyll *a* concentration vs. POC/PON concentration, while controlling for chlorophyll *a* and heme *b* concentration, respectively. Numbers in brackets indicate degrees of freedom. Statistical significance represented by ** where p < 0.01 and * where p < 0.05.

Mean heme:C and heme:N ratios of the TNA were 0.66 ± 0.6 µmol mol^{-1} C (N = 86) and 4.95 ± 5.0 µmol mol^{-1} N (N = 86), respectively; similar to the STNA. The East STNA gyre region provided the highest mean heme:C ratio (0.95 ± 0.9 µmol mol^{-1} C, N = 10), with the lowest ratio calculated for the EqU region (0.55 ± 0.5 µmol mol^{-1} C, N = 32, Fig. 3.13A). The same trend was also apparent for heme:N ratios, where the highest mean value was calculated in the East STNA gyre (7.50 ± 8.5 µmol mol^{-1} N, N = 10) and lowest in the EqU region (3.90 ± 3.3 µmol mol^{-1} N, N = 32, Fig. 3.13B). With regards to chlorophyll *a* content, mean chl:C and chl:N ratios were increased compared to the STNA at 204 ± 86.5 µmol mol^{-1} C (N = 109) and 1505 ± 539 µmol mol^{-1} N (N = 109), respectively. The chl:C (M = 263 ± 169 µmol mol^{-1} C, N = 36) and chl:N (M = 1815 ± 1181 µmol mol^{-1} N, N = 36) ratios were highest in the TSA region (Figs. 3.13C and 3.13D). The mean chl:C and chl:N ratios from the East STNA gyre region were higher than those previously obtained during D346 in the ESNAG region. This was confirmed by statistical analysis, suggesting that chl:C and chl:N were significantly different between the ESNAG (D346) and East STNA gyre (D361) regions (both U = 0, n_1 = 22, n_2 = 60, p < 0.01). In comparison, heme:C and heme:N ratios were not significantly different between the two regions (Mann-Whitney U tests).

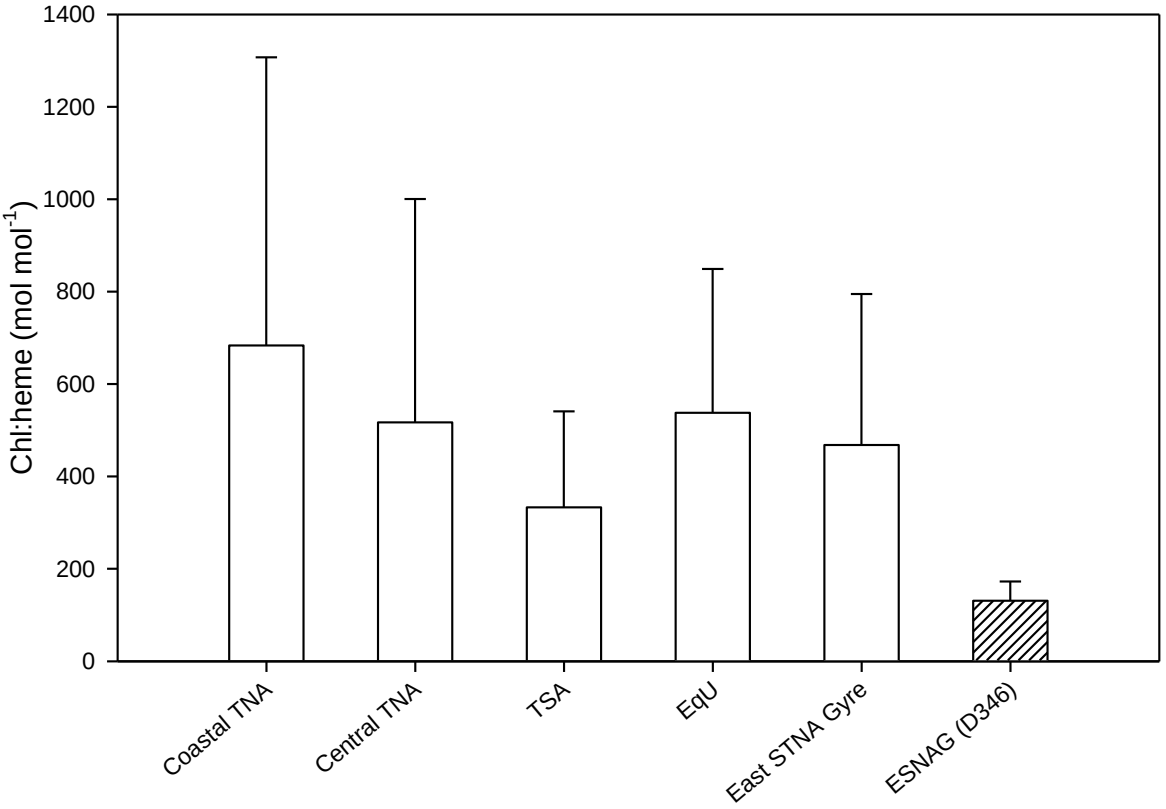

Figure 3.12. Mean chlorophyll *a* to heme *b* ratios (chl:heme, mol mol^{-1}) from five oceanographic regions of the TNA (D361, white) and the ESNAG region of the STNA (D346, striped).

In summary, the hypotheses previously outlined which were generally in agreement with results collected from the STNA (D346) were not completely supported by results from the TNA (D361). Heme *b* concentrations were significantly enhanced in the Coastal TNA as hypothesised (section 3.2.2.1). However, despite chlorophyll *a* and heme *b* concentrations providing a significant correlation for the overall TNA, relationships between chlorophyll *a* and heme *b* concentration were non-significant for each of the five oceanographic regions of the TNA (section 3.2.2.2). Also, partial correlations revealed that both heme *b* and chlorophyll *a* were significantly correlated to POC/PON concentration when controlling for chlorophyll *a* and heme *b*, respectively; a different trend to that observed in the STNA. The stronger correlations (r^2) between chlorophyll *a* and POC/PON compared to heme *b* suggest that heme *b* is not a suitable indicator of biomass in the TNA (section 3.2.2.3).

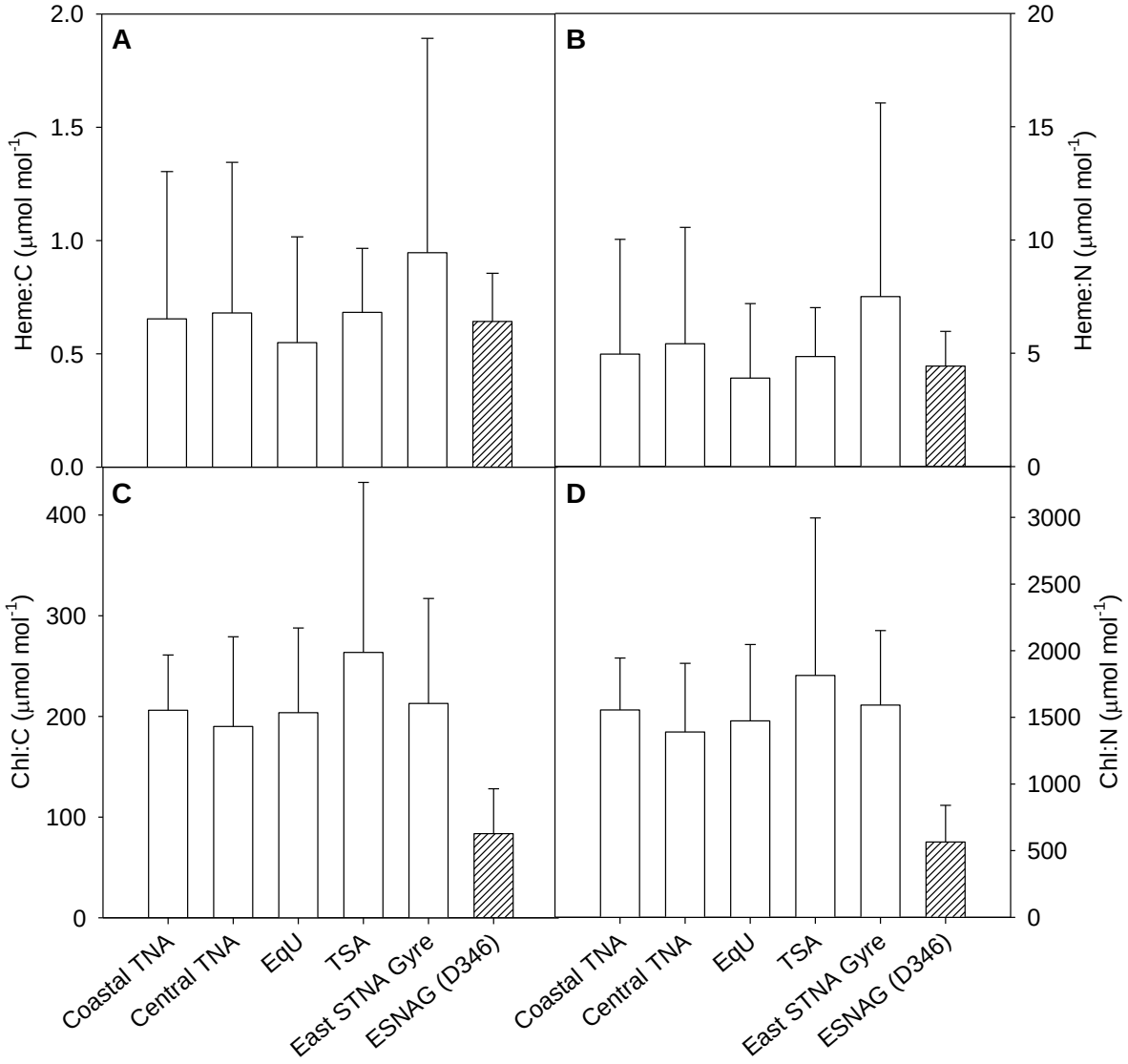

Figure 3.13. Mean (**A**) heme:C ratio (µmol mol^{-1} C), (**B**) heme:N ratio (µmol mol^{-1} N), (**C**) chl:C ratio (µmol mol^{-1} C) and (**D**) chl:N ratio (µmol mol^{-1} N) from five oceanographic regions of the TNA (D361, white) and the ESNAG region of the STNA (D346, striped).

3.5 Discussion

3.5.1 Distribution of heme b in the (sub-) tropical North Atlantic

Characteristic conditions of an oligotrophic environment were evident from the very low nitrate (Fig. 3.2C) and phosphate (Fig. 3.2D) concentrations at <100 m depth in the STNA (D346). The layer of maximum heme *b* concentration associated with the DCM was located directly above the nitracline, highlighting the influence of nutrient and physical properties on the distribution of heme *b*. Also, increased phosphate concentrations (>10 nmol L^{-1}) towards the Azores Current region of the STNA coincided with a notable increase in heme *b* abundance. Co-limitation of iron and phosphate in the marine environment has become increasingly acknowledged (e.g. Mills et al. 2004) and, given that hemoproteins are an important sink of bioavailable iron, heme abundance could address the ultimate

limiting factor in phytoplankton productivity. However, heme *b* and phosphate concentration were positively correlated throughout the STNA basin ($p < 0.01$, Table 3.1) which would suggest either heme *b* is not a suitable indicator of iron availability or that other limiting factors were involved (e.g. nitrate). The ratio of nitrate to phosphate exceeded Redfield values (Redfield 1934, 1958) which implies nitrogen fixation was prominent in the region (Capone et al. 2005, Moore et al. 2009). Hemoproteins are not associated with the iron-rich enzyme responsible for nitrogen fixation, nitrogenase, but could potentially provide a useful indication of iron utilisation in diazotrophic species (i.e. nitrogen fixing organisms) as discussed in Chapter 5.

The STNA gyre is considered a low productivity region, limited by oligotrophic conditions throughout the year (Maranon 2005). The South Atlantic receives the lowest levels of aeolian dust deposition compared to all other major oceans at only 4% of the total global input (Jickells et al. 2005, see Fig. 3.1); hence, productivity in the TSA is thought to be limited by iron and nitrogen availability (Moore et al. 2009). In contrast, the EqU and Coastal TNA regions are supplied with a rich source of upwelled nutrients that support high phytoplankton productivity. The first determinations of heme *b* concentration in the low latitude North Atlantic were reported in this chapter (Honey et al. 2013) and trends in heme *b* abundance generally reflected productivity. High heme *b* concentrations were measured in the coastal upwelling regions (i.e. Azores Current and Coastal TNA), with relatively low heme *b* concentrations observed in the Central TNA and TSA. Enhanced coastal heme *b* concentrations of the eastern (sub-) tropical North Atlantic support the hypothesis that increased iron availability in these regions influenced heme *b* abundance (section 3.2.2.1); the Coastal TNA provided the highest regional mean heme *b* concentration at 5.70 ± 4.4 pmol L^{-1}. However, moderately high heme *b* concentrations were also measured in the oligotrophic regions of the STNA (D346) and heme *b* concentrations in the EqU region were lower in comparison to the Coastal TNA, despite the nutrient-rich deep water upwelling. Therefore, the distribution of heme *b* did not provide a consistent relationship to productivity in the (sub-) tropical North Atlantic.

The mean heme *b* concentration for the STNA (D346) was 1.32 ± 0.6 pmol L^{-1}; lower than the TNA (D361; 2.18 ± 3.2 pmol L^{-1}) and the SOLAS cruise in the tropical Northeast Atlantic (D326; 2.24 ± 1.67 pmol L^{-1}, Gledhill et al. in prep, see Appendix 1). Spatial variations of the three cruises must be considered as the oligotrophic conditions within the subtropical gyre regions, where nutrient availability severely limits phytoplankton productivity, are likely to play a significant role. Heme *b* concentrations were elevated in the Azores Current region of the STNA ($M = 1.84 \pm 0.6$ pmol L^{-1}) compared to the western STNA province but, despite providing a closer geographical comparison, the average heme *b* concentrations was still lower than measurements from cruises D326 and D361 in the TNA. Spatial variability in heme *b* abundance could be the result of physiological

adaptations to differing environmental conditions between oceanographic regions, and the interannual variability in seawater iron concentrations could be significant.

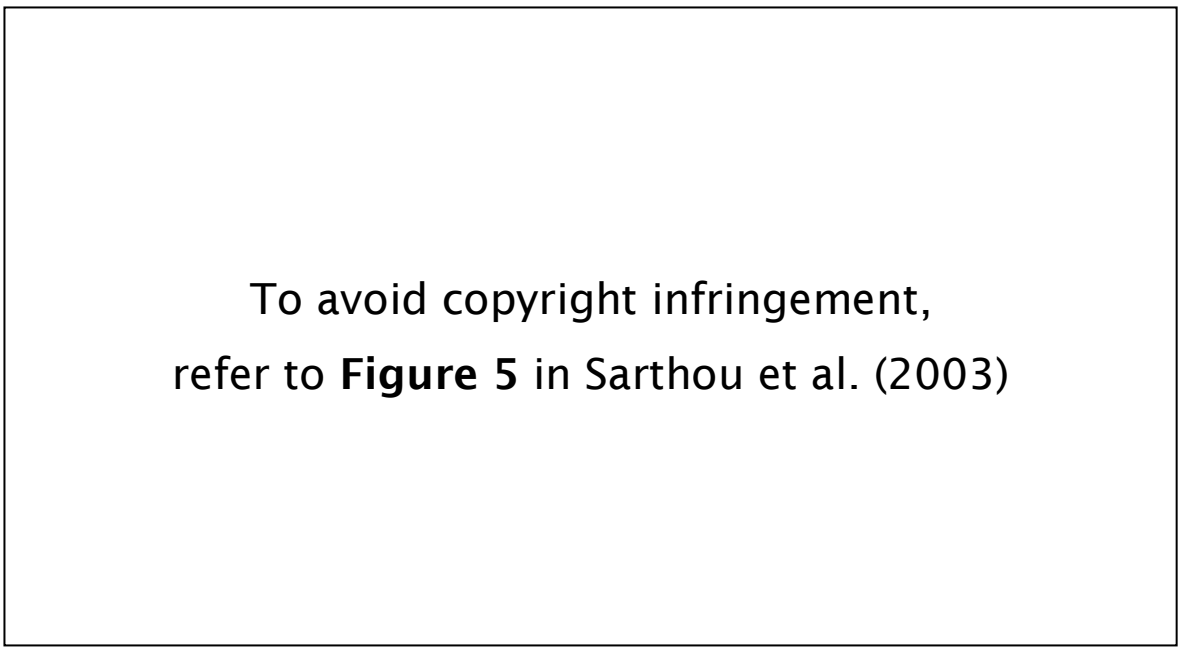

Figure 3.14. Dissolved iron concentration (nmol L^{-1}) from five regions of the eastern Atlantic Ocean measured in October 2000 during cruise ANTXVIII/1 aboard the *RV Polarstern*: North Equatorial Current and Canary Current (NEC/CC); Tropical Salinity Minimum (TSM); Equatorial Upwelling (EqUp); Guinea Gyre and South Equatorial Current (GG/SEC) and; South Tropical Gyre and Benguela Current (STG/BC). Figure from Sarthou et al. (2003).

Iron is a central component of heme complexes (Caughey 1973) and it is perhaps predictable that increased heme *b* concentrations would be reported in the ocean region impacted by dust inputs with consequent sporadic iron supply (Jickells et al. 2005). Numerous iron enrichment studies have been conducted in HNLC regions, predominantly suggesting that iron is the limiting factor that restricts phytoplankton productivity in these large parts of the global ocean (e.g. Martin et al. 1994, Coale et al. 1996, Landry et al. 2000). However, the (sub-) tropical North Atlantic is not considered a HNLC region, at least not permanently. Therefore, variations in heme *b* concentration between the STNA (D346) and the TNA (D361) may provide an indication of iron bioavailability. It could be inferred that parts of the STNA, especially the eastern STNA province, and the Coastal TNA receive the highest iron inputs as reflected by the elevated heme *b* abundance. In contrast, the Central TNA, EqU and TSA regions demonstrated reduced heme *b* concentrations, potentially indicating low iron bioavailability. Dissolved iron concentrations in surface waters of the eastern Atlantic Ocean vary spatially, providing a significant correlation to atmospheric deposition in the area (Sarthou et al. 2003). According to Sarthou et al. (2003), dissolved iron concentrations were highest south of the Canary Islands (~27 °N), moderate close to the African coast and lowest in the South Atlantic (Fig. 3.14). This highlights the potential connection between reduced iron

concentrations and low heme *b* abundance in the TSA. However, temporal variations in the collection of heme *b* (Jan - Feb 2010 and Feb - Mar 2011) and dissolved iron (Oct 2000, Sarthou et al. 2003) concentrations make it difficult to infer a definitive relationship using this previous data set.

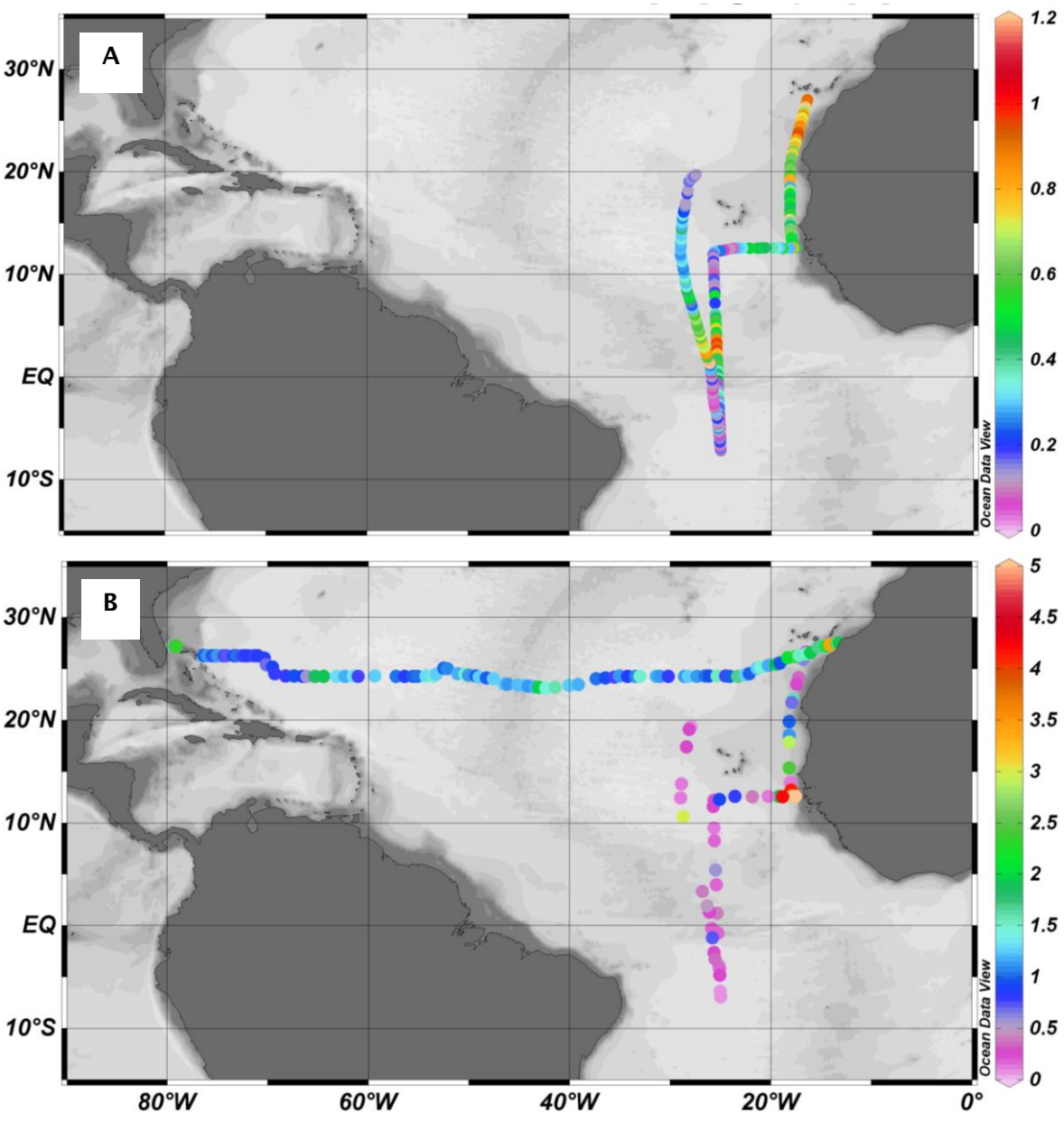

Figure 3.15. Map of surface (**A**) total dissolved iron concentration (nmol L^{-1}) and (**B**) heme *b* concentration (pmol L^{-1}) measured during D346 (STNA, Jan - Feb 2010, heme *b* only) and D346 (TNA, Feb - Mar 2011). Values represent first CTD bottle depth per station (<12 m depth) and samples acquired from the FISH supply (approximately 2 m depth). Dissolved iron concentrations courtesy of Christian Schlosser (Schlosser et al. in prep).

High dissolved iron concentrations south of the Canary Islands and coastal regions of the eastern Atlantic described by Sarthou et al. (2003) were also observed in surface dissolved

iron concentrations of cruise D361 (Fig. 3.15A). In addition, increased surface dissolved iron concentrations were measured in the EqU region; a result of wet dust deposition through rain events within the ITCZ. Surface heme *b* concentrations were consistently higher in surface samples of the STNA (>0.5 pmol L^{-1}) compared to the TNA and TSA, with the highest concentrations observed in the Azores Current and Coastal TNA regions (Fig. 3.15B). A connection between surface dissolved iron concentration and the abundance of heme *b* is feasible, given that the highest surface heme *b* concentrations were obtained at regions with high dissolved iron. Also, heme *b* concentrations from the TSA (S10 and FISH samples) were low, with minimal dissolved iron concentrations measured in surface waters within this region. However, increased dissolved iron concentrations associated with the ITCZ in the EqU region were not reflected by noticeably increased surface heme *b* concentrations.

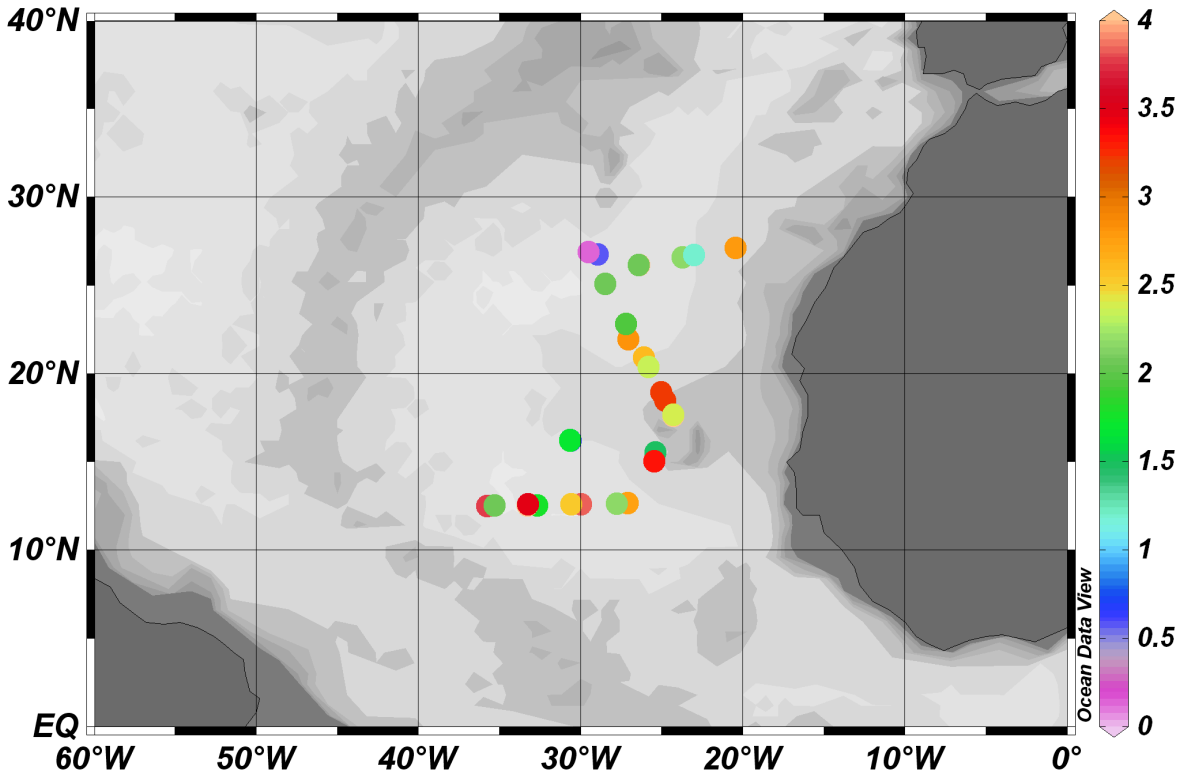

Figure 3.16. Map of surface heme *b* concentration (pmol L^{-1}) measured during the SOLAS cruise (D326) in the tropical Northeast Atlantic (Jan - Feb 2008). Values represent first bottle depth per station (<10 m depth). Data courtesy of Martha Gledhill (Gledhill et al. in prep, see Appendix 1).

Comparison of surface heme *b* concentrations from the STNA and TNA with the SOLAS cruise of the tropical Northeast Atlantic (D326, Fig. 3.16) suggested similar surface heme *b* concentrations with the eastern STNA of cruise D346 and Coastal TNA of cruise D361. Concentrations measured in the EqU and Central TNA regions were generally much lower than those reported from D326 (i.e. <0.5 pmol L^{-1}). However, it should be noted that the

SOLAS cruise encountered a major dust event (Rijkenberg and Achterberg 2008), suggesting a significant input of iron which could have influenced heme *b* abundance. Measurements from the upper 200 m of the three research cruises suggest a two-fold decrease in heme *b* concentration for the (sub-) tropical North Atlantic between 2008 and 2011.

3.5.2 Heme b, chlorophyll a, POC and PON concentration

A significant correlation was found between heme *b* and chlorophyll *a* concentration in all regions of the STNA (Fig. 3.17). The distribution of heme *b* could be associated with chlorophyll *a* due to synthesis along the same tetrappyrole pathway (Papenbrock and Grimm 2001) and a complex feedback mechanism determining the production of the two pigments (Cornah et al. 2003, Mochizuki et al. 2010). For example, increases in chlorophyll *a* will be reflected by an increase in heme *b*, perhaps to a lesser extent, as cytochrome b_6f is still required to transfer electrons. The mean chl:heme ratio for the STNA (144 ± 76 mol mol^{-1}) was similar to the integrated mixed layer depth chl:heme ratio calculated from cruise D326 (124 ± 45 mol mol^{-1}; Gledhill et al. in prep, see Appendix 1). However, the ESNAG (131 ± 42.1 mol mol^{-1}) and Azores Current (135 ± 60.1 mol mol^{-1}) regions offered even closer mean chl:heme ratios, suggesting spatial variations should be taken into account. Low chl:heme ratios from cruise D326 imply that the relative proportion of heme *b* compared to chlorophyll *a* was higher. Therefore, considering iron is essential in the structure of hemes, it could be proposed that iron availability in the D326 survey region was greater, or at least less iron limiting, compared to D346 and D361. Cruise D326 encountered a dust event (Rijkenberg and Achterberg 2008) and iron bioavailability in the region would have been increased to an extent, which could provide an explanation for the lower chl:heme ratios.

The relationship between heme *b* and chlorophyll *a* during cruise D361 in the TNA was significant ($p < 0.01$, Fig. 3.18), although the correlation was not as strong as that found in the STNA. It should also be noted that correlations were not significant when individually assessing the five oceanographic regions of the TNA. The chl:heme ratios calculated from D361 (M = 553 ± 446 mol mol^{-1}) were much greater and with a larger degree of variation compared to the STNA (D346). Increased heme *b* concentrations in the STNA would have explained the decreased chl:heme ratios to an extent as the relative chlorophyll *a* concentration would have been reduced. However, the mean heme *b* concentration was actually lower in the STNA. Seasonally elevated chlorophyll *a* concentrations have been attributed to the Mauritanian upwelling region (Pradhan et al. 2006), which would also influence the chl:heme ratio. It could be argued that heme *b* abundance would also increase in the nutrient-rich upwelling regions, but the iron requirement of hemes will also be significant. However, the SOLAS cruise (D326) surveyed a spatially similar region of the TNA, presenting chl:heme ratios in line with

D346; much lower than cruise D361. Nevertheless, even though very high chl:heme ratios are perhaps challenging to explain, they are not unprecedented. Heme *b* and chlorophyll *a* concentrations were not correlated in the Iceland Basin or Scotia Sea, and several samples with high chl:heme ratios (>500 mol mol^{-1}) were reported in these regions by Gledhill et al. (in prep, see Appendix 1).

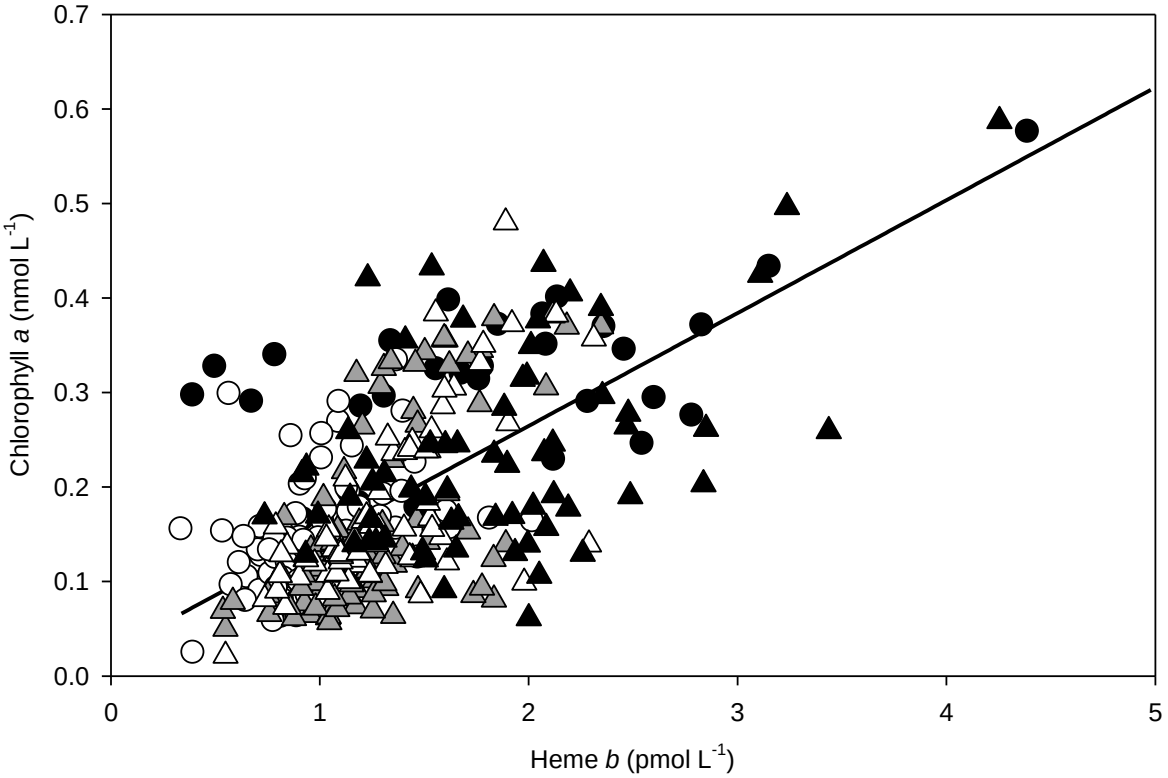

Figure 3.17. Heme *b* concentration (pmol L^{-1}) against chlorophyll *a* concentration (nmol L^{-1}) from the STNA (D346). Stations divided into five oceanographic regions: Florida Straits (black circle), Gulf Stream (white circle), WSNAG (grey triangle), ESNAG (white triangle) and Azores Current (black triangle). Solid black line represents significant correlation for the complete STNA transect. Equation: $y = 0.119x + 0.026$ ($r^2 = 0.443$).

Heme *b* and chlorophyll *a* were both significantly correlated to POC and PON when considering the entire STNA cruise transect, but the variability was better explained by heme *b* (Table 3.1). Partial correlation coefficients (e.g. de la Fuente et al. 2004) were used to determine the unique variance between (1) heme *b* and POC/PON and (2) chlorophyll *a* and POC/PON, while eliminating the variability from the other pigment. The profound significance of heme *b* and chlorophyll *a* in key metabolic functions made both pigments suitable to compare with POC and PON as estimates of biomass. Also, the feedback mechanism surrounding the production of heme and chlorophyll (Vavilin and Vermaas 2002) suggested that their abundance was interlinked, making both pigments prime candidates to control for the other. In the STNA, heme *b* remained significantly correlated to both POC and PON concentration when chlorophyll *a* was held constant

(Table 3.2). In contrast, chlorophyll *a* was no longer correlated to POC or PON when controlled by heme *b* concentration. Therefore, it could be suggested that heme *b* is more closely related to POC and PON in the STNA than chlorophyll *a*, whilst also explaining some of the relationship between chlorophyll *a* and POC/PON. However, both heme *b* and chlorophyll *a* remained significantly correlated to POC and PON in the TNA after testing with partial correlations, with chlorophyll a providing a closer comparison (r^2). This could be indicative of spatial variability, where heme *b* provides a closer comparison to phytoplankton biomass in the STNA and chlorophyll *a* provides a closer comparison to phytoplankton biomass in the TNA. Once again, it could also be related to iron as heme *b* and chlorophyll *a* may provide differing responses to the availability of iron. Either way, it does not appear that heme *b* concentration provides a definitive assessment of biomass in the marine environment.

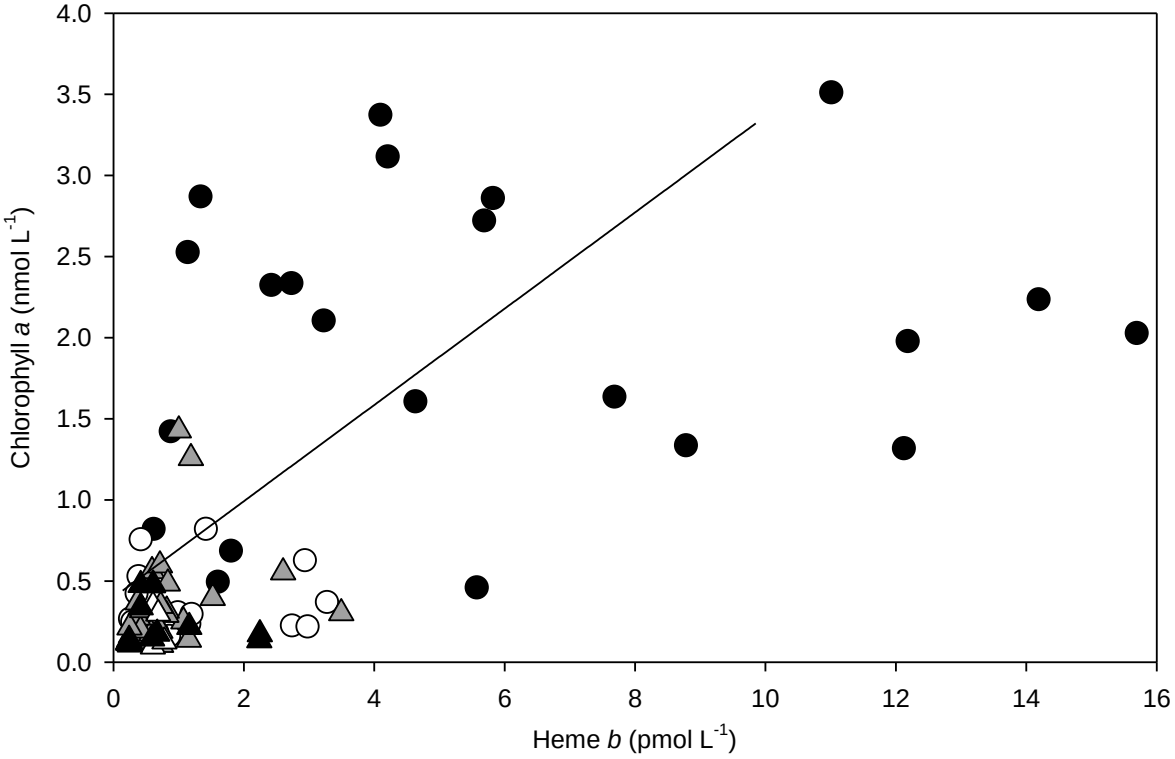

Figure 3.18. Heme *b* concentration (pmol L^{-1}) against chlorophyll *a* concentration (nmol L^{-1}) from the TNA (D361). Stations divided into five oceanographic regions: Coastal TNA (black circle), Central TNA (white circle), EqU (grey triangle), TSA (white triangle) and East STNA gyre (black triangle). Solid black line represents significant correlation for the complete TNA transect. Equation: $y = 0.296x + 0.399$ ($r^2 = 0.309$).

The thermocline and nitracline (Figs. 3.2A and 3.2C) of cruise D346 in the STNA were spatially associated to the position of the DCM; similar to previous observations in the North Atlantic (Agusti and Duarte 1999, Robinson et al. 2006). As a result of increased chlorophyll *a* relative to phytoplankton carbon content (Maranon et al. 2000), chl:heme ratios within the DCM were statistically higher compared to the SML. However, the DCM is

considered the layer of maximum pigment (i.e. increased chlorophyll *a*) and does not necessarily correspond to the depth of maximum biomass (Perez et al. 2006). Therefore, increased chl:heme ratios within the DCM do not automatically imply a reduction in cellular *b*-type hemoproteins; instead, chlorophyll *a* concentration increased disproportionately compared to heme *b* as a result of reduced light intensity. The median chl:C and chl:N ratios from the TNA (D361) were significantly different to the STNA (D346), with significantly lower chlorophyll *a* content found in the ESNAG (Figs. 3.13C and 3.13D). Also, given that heme *b* contents in the DCM of the STNA were increased to a lesser extent compared to chlorophyll *a*, this provides a further explanation as to the increased chl:heme ratios of the TNA. In terms of predicting biomass, chlorophyll *a* was better correlated to POC in the TNA; unlike the STNA where heme *b* offered the better comparison. Thus, it is unrealistic at this stage to conclude that heme *b* offered a more robust indication of phytoplankton biomass in the marine environment compared to the traditionally used chlorophyll *a* (Zbigniew et al. 1998, Suggett et al. 2001).

3.6 Conclusions

Our understanding of heme distribution in the oceans is extremely limited, despite the apparent importance of these complexes in all living organisms. This investigation has increased the database of heme *b* abundance in the marine environment by providing temporally comparable measurements from the (sub-) tropical North Atlantic. The spatial variation of heme *b* abundance suggested a physiological response in terms of environmental conditions, potentially related to iron availability. This was highlighted by high concentrations of heme *b* associated with the regions closest to the West African coast; a region known to receive high levels of atmospheric dust deposition and benthic-derived iron inputs. The abundance of heme *b* in the (sub-) tropical North Atlantic appears to have decreased between 2008 and 2011, although the sporadic nature of atmospheric iron input could be crucial. Heme *b* generally offered a good correlation with chlorophyll *a* during both research cruises, although this was not the case for the five oceanographic regions of the TNA. The relationship is most likely associated to the biosynthetic pathway along which both pigments are produced. However, significantly higher chl:C and chl:N ratios were reported from the TNA compared to the STNA which were not reflected in heme *b* contents, suggesting differing responses to environmental conditions by chlorophyll *a* and heme *b*. Conducting laboratory studies on marine phytoplankton commonly found to the (sub-) tropical North Atlantic will potentially help in our understanding of what influences heme *b* abundance in the region (see Chapters 4 and 5), albeit the phytoplankton composition from the two cruises is unknown. Furthermore, the link between heme *b* and chlorophyll *a* concentration apparent from the cruise data could be better explained through examination of phytoplankton monocultures in the laboratory.

3.7 References

Agusti, A. and C. M. Duarte. 1999. Phytoplankton chlorophyll *a* distribution and water column stability in the central Atlantic Ocean. Oceanologica Acta **22**:193-203.

Baker, A. R., T. D. Jickells, M. Witt, and K. L. Linge. 2006. Trends in the solubility of iron, aluminium, manganese and phosphorus in aerosol collected over the Atlantic Ocean. Marine Chemistry **98**:43-58.

Capone, D. G., J. A. Burns, J. P. Montoya, A. Subramaniam, C. Mahaffey, T. Gunderson, A. F. Michaels, and E. J. Carpenter. 2005. Nitrogen fixation by *Trichodesmium* spp.: An important source of new nitrogen to the tropical and subtropical North Atlantic Ocean. Global Biogeochemical Cycles **19**:GB2024.

Caughey, W. S. 1973. Iron porphyrins - hemes and hemins. Pages 797-831 *in* G. L. Eichham, editor. Inorganic biochemistry. Elsevier, Amsterdam.

Coale, K. H., K. S. Johnson, S. E. Fitzwater, R. M. Gordon, S. Tanner, F. P. Chavez, L. Feriolo, C. Sakamoto, P. Rogers, F. Millero, P. Steinberg, P. Nightingale, D. Cooper, W. P. Cochlan, M. R. Landry, J. Constantinou, G. Rollwagen, A. Trasvina, and R. Kudela. 1996. A massive phytoplankton bloom induced by ecosystem-scale iron fertilization experiment in the equatorial Pacific Ocean. Nature **383**:495-501.

Cornah, J. E., M. J. Terry, and A. G. Smith. 2003. Green or red: what stops the traffic in the tetrapyrrole pathway? TRENDS in Plant Science **8**:224-230.

de la Fuente, A., N. Bing, I. Hoeschele, and P. Mendes. 2004. Discovery of meaningful associations in genomic data using partial correlation coefficients. Bioinformatics:3565-3574.

Duce, R. A., P. S. Liss, J. T. Merrill, E. L. Atlas, P. Buat-Menard, B. B. Hicks, J. M. Miller, J. M. Prospero, R. Arimoto, T. M. Church, W. Ellis, J. N. Galloway, L. Hansen, T. D. Jickells, A. H. Knap, K. H. Reinhardt, B. Schneider, A. Soudine, J. J. Tokos, S. Tsunogai, R. Wollast, and M. Zhou. 1991. The atmospheric input of trace species to the world ocean. Global and Biogeochemical Cycles **5**:193-259.

Eglinton, T. I., G. Eglinton, L. Dupont, E. R. Sholkovitz, D. Montlucon, and C. M. Reddy. 2002. Composition, age and provenance of organic matter in NW African dust over the Atlantic Ocean. Geochemistry Geophysics Geosystems **3**:1050.

Emerson, S. P., P. Quay, D. M. Karl, C. Winn, L. Tupas, and M. R. Landry. 1997. Experimental determination of the organic carbon flux from open ocean surface waters. Nature **389**:951-954.

Geider, R. J. and J. La Roche. 1994. The role of iron in phytoplankton photosynthesis, and the potential for iron-limitation of primary productivity in the sea. Photosynthesis Research **39**:275-301.

Gledhill, M. 2007. The determination of heme b in marine phyto- and bacterioplankton. Marine Chemistry **103**:393-403.

Gledhill, M., E. P. Achterberg, D. J. Honey, M. Nielsdottir, and M. Rijkenberg. in prep. Distributions of particulate heme *b* in the Atlantic and Southern Ocean - implications for changes in phytoplankton photosystems (see Appendix 1).

Goudie, A. S. and N. J. Middleton. 2001. Saharan dust storms: nature and consequences. Earth-Science Reviews **56**:179-204.

Honey, D. J., M. Gledhill, T. S. Bibby, F-E. Legiret, N. J. Pratt, A. E. Hickman, T. Lawson, and E. P. Achterberg. 2013. Heme *b* in marine phytoplankton and particulate material from the North Atlantic Ocean. Marine Ecology Progress Series **483**: 1-17.

Jickells, T. D., Z. S. An, K. K. Andersen, A. R. Baker, G. Bergametti, N. Brooks, J. J. Cao, P. W. Boyd, R. A. Duce, K. A. Hunter, H. Kawahata, N. Kubilay, J. laRoche, P. S. Liss, N. Mahowald, J. M. Prospero, A. J. Ridgwell, I. Tegen, and R. Torres. 2005. Global iron connections between desert dust, ocean biogeochemistry, and climate. Science **308**:67-71.

Jickells, T. D. and L. J. Spokes. 2001. Atmospheric iron inputs to the oceans. Pages 85-121 *in* D. R. Turner and K. A. Hunter, editors. The biogeochemistry of iron in seawater, IUPAC. Wiley.

Kurisu, G., H. Zhang, J. L. Smith, and W. A. Cramer. 2003. Structure of the cytochrome b_6f complex of oxygenic photosynthesis: Tuning the cavity. Science **302**:1009-1014.

Landry, M. R., J. Constantinou, M. Latasa, S. L. Brown, R. R. Bidigare, and M. E. Ondrusek. 2000. Biological response to iron fertilization in the eastern equatorial Pacific (IronEx II). III. Dynamics of phytoplankton growth and microzooplankton grazing. Marine Ecology Progress Series **201**:57-72.

Maranon, E. 2005. Phytoplankton growth rates in the Atlantic subtropical gyres. Limnology and Oceanography **50**:299-310.

Maranon, E., P. M. Holligan, M. Varela, B. Mourino, and A. J. Bale. 2000. Basin-scale variability of phytoplankton biomass, production and growth in the Atlantic Ocean. Deep-Sea Research I **47**:825-857.

Martin, J. H., K. H. Coale, K. S. Johnson, S. E. Fitzwater, R. M. Gordon, S. J. Tanner, C. N. Hunter, V. A. Elrod, J. L. Nowicki, T. L. Coley, R. T. Barber, S. Lindley, A. J. Watson, K. Van Scoy, C. S. Law, M. I. Liddicoat, R. Ling, T. Stanton, J. Stockel, C. Collins, A. Anderson, R. Bidigare, M. Ondrusek, M. Latasa, F. J. Millero, K. Lee, W. Yao, J. Z. Zhang, G. Friederich, C. Sakamoto, F. Chavez, K. Buck, Z. Kolber, R. Greene, P. Falkowski, S. W. Chisholm, F. Hoge, R. Swift, J. Yungel, S. Turner, P. Nightingale, A. Hatton, P. Liss, and N. W. Tindale. 1994. Testing the iron hypothesis in ecosystems of the equatorial Pacific Ocean. Nature **371**:123-129.

Mills, M. M., C. Ridame, M. Davey, J. La Roche, and R. J. Geider. 2004. Iron and phosphorus co-limit nitrogen fixation in the eastern tropical North Atlantic. Nature **429**:292-294.

Mochizuki, N., R. Tanaka, B. Grimm, T. Masuda, M. Moulin, A. G. Smith, A. Tanaka, and M. J. Terry. 2010. The cell biology of tetrapyrroles: a life and death struggle. TRENDS in Plant Science **15**:488-498.

Moore, C. M., M. M. Mills, E. P. Achterberg, R. J. Geider, J. La Roche, M. I. Lucas, E. L. McDonagh, X. Pan, A. J. Poulton, M. J. A. Rijkenberg, D. J. Suggett, S. J. Ussher, and E. M. S. Woodward. 2009. Large-scale distribution of Atlantic nitrogen fixation controlled by iron availability. Nature Geoscience **2**:867-871.

Moore, C. M., M. M. Mills, A. Milnes, R. Langlois, E. P. Achterberg, K. Lochte, R. J. Geider, and J. La Roche. 2006. Iron limits primary productivity during spring bloom development in the central North Atlantic. Global Change Biology **12**:626-634.

Moore, G. R. 1996. Haemoproteins. Pages 189-216 *in* D. S. Bendall, editor. Protein Electron Transfer. BIOS Scientific Publishers Ltd, Oxford.

Nelson, N. and C. F. Yocum. 2006. Structure and function of photosystems I and II. Annual Review of Plant Biology **57**:521-565.

Papenbrock, J. and B. Grimm. 2001. Regulatory network of tetrapyrrole biosynthesis - studies of intracellular signalling involved in metabolic and developmental control of plastids. Planta **213**:667-681.

Patey, M. D., M. J. A. Rijkenberg, P. J. Statham, M. Mowlem, M. C. Stinchcombe, and E. P. Achterberg. 2008. Determination of nitrate and phosphate in seawater at nanomolar concentrations. Trends in Analytical Chemistry **27**:169-182.

Perez, V., E. Fernandez, E. Maranon, X. A. G. Moran, and M. V. Zubkov. 2006. Vertical distribution of phytoplankton biomass, production and growth in the Atlantic subtropical gyres. Deep-Sea Research I **53**:1616-1634.

Pradhan, Y., S. J. Lavender, N. J. Hardman-Mountford, and J. Aiken. 2006. Seasonal and inter-annual variability of chlorophyll-*a* concentration in the Mauritanian upwelling: Observation of an anomalous event during 1998-1999. Deep-Sea Research II **53**:1548-1559.

Redfield, A. C. 1934. On the proportions of organic derivations in sea water and their relation to the composition of plankton. Pages 177-192 *in* R. J. Daniel, editor. James Johnstone Memorial Volume. University Press of Liverpool

Redfield, A. C. 1958. The biological control of chemical factors in the environment. American Scientist **46**:205-221.

Ridame, C. and C. Guieu. 2002. Saharan input of phosphate to the oligotrophic water of the open western Mediterranean Sea. Limnology and Oceanography **47**:856-869.

Rijkenberg, M. and E. Achterberg. 2008. Chasing Saharan Dust Storms II: RRS *Discovery 326*, 5 January - 5 February 2008. UK SOLAS Cruise Report.

Robinson, C., A. J. Poulton, P. M. Holligan, A. R. Baker, G. Forster, N. Gist, T. D. Jickells, G. Malin, R. Upstill-Goddard, R. G. Williams, E. M. S. Woodward, and M. V. Zubkov. 2006. The Atlantic Meridional Transect (AMT) Programme: A contextual view 1995-2005. Deep-Sea Research II **53**:1485-1515.

Sarthou, G., A. R. Baker, S. Blain, E. P. Achterberg, M. Boye, A. R. Bowie, P. Croot, P. Laan, H. J. W. de Baar, T. D. Jickells, and P. J. Worsfold. 2003. Atmospheric iron deposition and sea-surface dissolved iron concentrations in the eastern Atlantic Ocean. Deep-Sea Research I **50**:1339-1352.

Schafstall, J., M. Dengler, P. Brandt, and H. Bange. 2010. Tidal-induced mixing and diapycnal nutrient fluxes in the Mauritanian upwelling region. Journal of Geophysical Research **115**:C10014.

Schutz, L. W., J. M. Prospero, P. Buat-Menard, R. A. C. Carvalho, A. Cruzado, P. Harriss, N. Z. Heidam, and R. Jaenicke. 1990. The long range transport of mineral aerosols. Pages 197-229 *in* A. H. Knap, editor. The long range atmospheric transport of natural and contaminant substances. Kluwer Academic Publisher.

Suggett, D., G. Kraay, P. Holligan, M. Davey, J. Aiken, and R. Geider. 2001. Assessment of photosynthesis in a spring cyanobacterial bloom by use of a fast repetition rate fluorometer. Limnology and Oceanography **46**:802-810.

Taylor, A. H. and J. A. Stephens. 1998. The North Atlantic Oscillation and the latitude of the Gulf Stream. Tellus **50A**:134-142.

Vavilin, D. V. and W. F. J. Vermaas. 2002. Regulation of the tetrapyrrole biosynthetic pathway leading to heme and chlorophyll in plants and cyanobacteria. Physiologia Plantarum **115**:9-24.

Vong, L., A. Laes, and S. Blain. 2007. Determination of iron-porphyrin-like complexes at nanomolar levels in seawater. Analytica Chimica Acta **588**.

Zbigniew, S., S. Kolber, O. Prasil, and P. G. Falkowski. 1998. Measurements of variable chlorophyll fluorescence using fast repetition rate techniques: defining methodology and experimental protocols. Biochimica et Biophysica Acta **1367**:88-106.

Zhang, J.-Z. 2000. Shipboard automated determination of trace concentrations of nitrite and nitrate in oligotrophic water by gas-segmented continuous flow analysis with a liquid waveguide capillary flow cell. Deep-Sea Research I: Oceanographic Research Papers **47**:1157-1171.

Zhang, J. Z. and J. Chi. 2002. Automated analysis of nanomolar concentrations of phosphate in natural waters with liquid waveguide. Environmental Science and Technology **36**:1048-1053.

Chapter 4

Heme *b* requirement of the unicellular cyanobacteria *Synechococcus* sp. WH7803

4.1 Abstract

The cyanobacterial genus *Synechococcus* is ubiquitous throughout the global ocean, whilst also significantly contributing to phytoplankton biomass in large oceanographic regions. An investigation was conducted on the physiologically well-defined strain *Synechococcus* sp. WH7803 regarding heme *b* concentrations in cultures grown under three different total iron concentrations. Growth rates and cell size were significantly reduced in low iron cultures. Results also suggested particulate organic carbon (POC), particulate organic nitrogen (PON), chlorophyll *a* and heme *b* concentrations were reduced at low iron concentrations, leading to sensitive discrepancies in chlorophyll *a* to heme *b* ratio (chl:heme) and heme *b* concentration per unit carbon (heme:C) between iron treatments. The highest chl:heme ratios were found in high iron cultures (35.9 ± 18.6 mol mol^{-1}) and lowest in low iron cultures (19.1 ± 8.8 mol mol^{-1}). Similarly, heme:C ratios were elevated in high iron cultures (1.94 ± 0.86 µmol mol^{-1} C) compared to low iron cultures (0.72 ± 0.30 µmol mol^{-1} C). A hypothesis was developed regarding the required heme *b* concentration to enable maximum growth rates of *Synechococcus* sp. WH7803, providing a conservative estimate between 1 and 1.5 µmol mol^{-1} C. *Synechococcus* sp. WH7803 was also compared to five eukaryotic phytoplankton species, all of which increased their cellular heme *b* content with increased iron availability, except *Thalassiosira weissflogii*. Ratios of chl:heme and heme:C were lower in *Synechococcus* sp. WH7803 compared to the other species grown at equivalent iron availabilities. A comparison of laboratory cultures and the (sub-) tropical North Atlantic suggested greater chl:heme ratios in the natural marine environment, although heme:C ratios were typically higher in laboratory monocultures.

4.2 Introduction

Cyanobacteria are a group of photosynthetic prokaryotes that occupy a diverse array of ecological niches (Stanier and Cohen-Bazire 1977, Ferris and Palenik 1998). The genus *Synechococcus* represents a collection of unicellular marine cyanobacteria that, along with *Prochlorococcus*, dominate the photoautotrophic picoplankton community (i.e. <2 µm, Scanlan 2001), whilst also significantly contributing towards the overall photosynthetic biomass of the (sub-) tropical North Atlantic (Maranon et al. 2000). After discovery in the 1970s (Johnson and Sieburth 1979, Waterbury et al. 1979), subsequent investigations have shown the distribution of *Synechococcus* to be ubiquitous throughout oceanographic regions (Zwirglmaier et al. 2008). However, the abundance of *Synechococcus* is greatest in nutrient-rich waters as opposed to oligotrophic regions (Partensky et al. 1999, Scanlan and West 2002). The photosynthetic apparatus of *Synechococcus* spp. is unique amongst cyanobacteria, containing the red light harvesting phycobiliprotein, phycoerythrin (Barlow and Alberte 1985). Phycoerythrin permits *Synechococcus* to utilise absorption bands from the mid-visible spectrum (blue-green light) which enables photosynthetic activity in low light intensity conditions (Rabinowitch and Govindjee 1969, Platt et al. 1983).

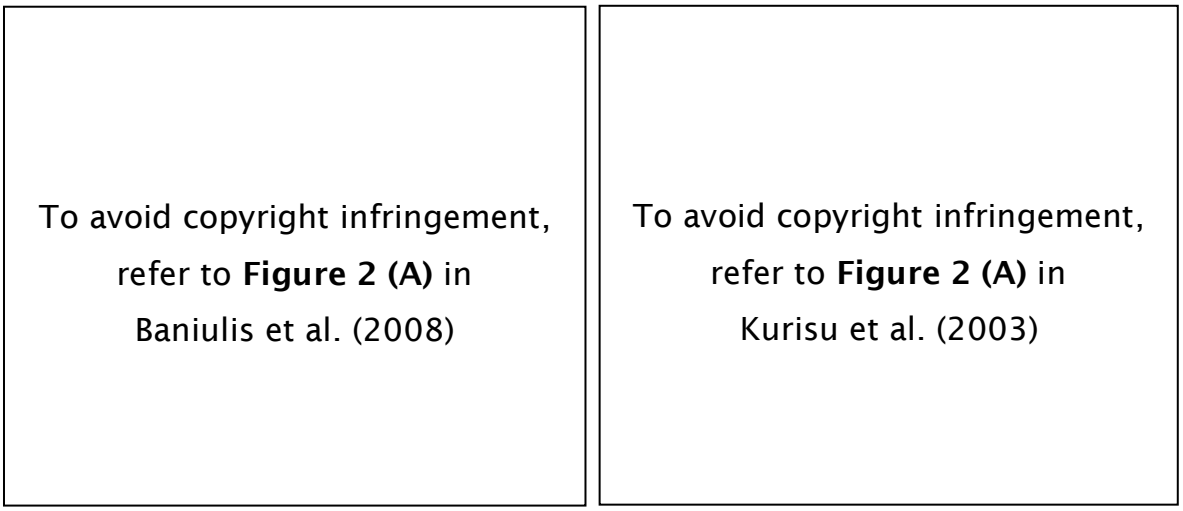

Figure 4.1 (**left**) Structure of the cytochrome b_6f complex of the cyanobacterium *Mastigocladus laminosus*, highlighting the central position of two *b*-type heme groups (red boxes) and (**right**) the electron and proton transfer pathways of the cytochrome b_6f complex, involving two *b*-type hemes groups, between the stromal (*n*) and lumen (*p*) side of the thylakoid membrane. Figures from (left) Baniulis et al. (2008) and (right) from Kurisu et al. (2003).

Cytochromes can be loosely defined as hemoproteins that function in electron transfer (Lemberg and Barrett 1973). In oxygenic photosynthesis, the *b*- and *c*-type cytochromes are of particular importance, helping to create a transmembrane electrochemical proton gradient to enable the synthesis of adenosine triphosphate (ATP). Cytochrome b_6f mediates the link between photosystem I (PSI) and photosystem II (PSII) reaction centres

by translocating protons across the thylakoid membrane (see Fig. 4.1, Cramer et al. 1996, Cramer et al. 2006). The precise function of cytochrome b_{559} remains unclear (Whitmarsh and Pakrasi 1996), although it is thought to protect PSII from photoinhibition and is essential in the assembly of functional PSII complexes (Barber and De Las Rivas 1993, Stewart and Brudvig 1998, Burda et al. 2003). Two heme *b* groups are found in the cytochromes b_6f complex and one heme *b* group is associated with cytochrome b_{559} and, consequently, PSII. Therefore, changes in cellular heme *b* content of marine organisms could be used to infer physiological responses through changes in photosynthetic apparatus.

Numerous investigations have been conducted on cyanobacteria and specifically *Synechococcus* spp. with regards to the influence of nutrient stress and light availability (Webb et al. 2001). Cellular carbon, nitrogen and chlorophyll *a* content of *Synechococcus* sp. WH7803 varied under nitrogen-limited conditions (Liu et al. 1999), with the same species not exhibiting the typical ferredoxin / flavodoxin response to iron limitation (Chadd et al. 1996). Maximum growth rates and chlorophyll *a* content of *Synechococcus* sp. PCC 7002 were also decreased under growth-limiting iron availability, whilst also showing signs of reduced iron requirement (Wilhelm et al. 1996). Molecular studies have found that coastal and open ocean strains of *Synechococcus* possess different genes in association with iron stress (Rivers et al. 2009) and *Synechococcus* sp. PCC 7942 expressed the *isiA* gene to protect PSII from excessive light under iron limiting conditions (Park et al. 1999). As part of this project, an investigation was conducted upon the most physiologically well-defined species of the *Synechococcus* genus; *Synechococcus* sp. WH7803. Batch cultures were maintained under varying iron regimes in order to measure the influence, if any, upon cellular heme *b* content. Results were compared to five eukaryotic phytoplankton species also subjected to variations in iron availability (data provided by Martha Gledhill, Honey et al. 2013), as well as data collected from research cruises in the subtropical North Atlantic (STNA, D346) and tropical North Atlantic (TNA, D361).

4.2.1 Aims and objectives

Preliminary heme *b* concentrations and chlorophyll *a* to heme *b* ratios (chl:heme) have been reported for nutrient (iron) replete conditions of several laboratory grown cultures of marine phytoplankton and bacterioplankton (Gledhill 2007). The primary aim of this chapter was to undertake an investigation of heme *b* abundance in the marine cyanobacteria *Synechococcus* sp. WH7803 to provide a detailed species-specific database upon which other species can be referred. Changes in iron availability are likely to alter cellular heme *b* content due to the central position of iron in the structure of heme complexes (see Fig. 1.2); thus examining *Synechococcus* sp. WH7803 cultures under

varying iron concentrations could provide valuable information regarding the allocation of iron to *b*-type hemoproteins in marine microorganisms. Comparison of results from *Synechococcus* sp. WH7803 with five eukaryotic phytoplankton species and data collected from the (sub-) tropical North Atlantic will determine whether discrepancies in heme *b* content between species are detectable and how they relate to the natural marine environment. Therefore, the specific objectives of this chapter were:

4.2.1.1 To determine the relationship, if any, between heme *b* concentration and iron availability for cultures of the unicellular cyanobacteria *Synechococcus* sp. WH7803.

4.2.1.2 To compare heme *b* concentrations from *Synechococcus* sp. WH7803 cultures with five marine eukaryotic phytoplankton species previously investigated (data provided by Martha Gledhill, Honey et al. 2013) and to examine differences in heme *b* content in response to iron availability.

4.2.1.3 To compare heme *b* concentrations from cultures of *Synechococcus* sp. WH7803 and five eukaryotic phytoplankton species with data collected from the (sub-) tropical North Atlantic.

4.2.2 Hypotheses

The following hypotheses were developed to test the previously described objectives:

4.2.2.1 Heme *b* concentrations in *Synechococcus* sp. WH7803 will increase as total iron concentration in the culture medium increases. Iron is an essential component in the structure of heme *b*; hence, cellular heme *b* content will increase with enhanced iron availability.

4.2.2.2 Cultures of *Synechococcus* sp. WH7803 will exhibit similar responses to five species of eukaryotic marine phytoplankton in terms heme *b* content with respect to iron availability.

4.2.2.3 The heme *b* concentration of *Synechococcus* sp. WH7803 cultures will be representative of heme *b* values collected from the (sub-) tropical North Atlantic as the strain was originally isolated from the Sargasso Sea (Waterbury et al. 1986).

4.3 Methods

4.3.1 Synechococcus sp. WH7803 culturing

The unicellular cyanobacteria *Synechococcus* sp. WH7803 was grown at three total iron concentrations (Fe_T = 1200 nmol L^{-1}, high; 120 nmol L^{-1}, medium; 12 nmol L^{-1}, low) in an artificial seawater (ASW, section 2.2.1) medium defined by Wilson et al. (1996). Cultures were monitored in respective iron concentrations for a minimum of 6 generations prior to experimentation. During experimental runs, batch cultures were grown for 8 days during three consecutive generations. Cell number, cell diameter and total cellular biovolume measured from fresh culture samples every two days (i.e. days 0, 2, 4, 6 and 8) using a Beckman Coulter counter with 30 µm aperture (section 2.2.5). Cultures were vacuum filtered (section 2.1A) onto glass microfibre filters (GF/Fs, MF300, Fisher Scientific) every two days for the determination of heme *b* (10 - 40 ml, section 2.4) and chlorophyll *a* (10 ml, section 2.5) concentration, as well as pre-ashed GF/Fs (450 °C, >12 hours) for particulate organic carbon (POC) and particulate organic nitrogen (PON) concentration (POC/N, 10 - 40 ml, section 2.6).

4.3.2 Eukaryotic phytoplankton cultures

The marine phytoplankton *Dunaliella tertiolecta*, *Emiliania huxleyi*, *Thalassiosira weissflogii*, *Thalassiosira oceanica* and *Phaeodactylum tricornutum* were previously studied for the influence of iron on heme *b* abundance by Martha Gledhill (Ocean and Earth Science, University of Southampton). Batch cultures of each phytoplankton were grown in an experimental medium prepared from 0.2 µm filtered seawater collected from the North Atlantic subtropical gyre. All cultures were maintained at 19 °C under cool white fluorescent lights at 150 µmol quanta m^{-2} s^{-1} (high light), with *E. huxleyi* and *T. oceanica* also grown at 45 µmol quanta m^{-2} s^{-1} (low light), on a 12:12 hour light:dark cycle. Refer to Honey et al. (2013) for more details regarding phytoplankton growth conditions. Samples for the determination of heme *b*, chlorophyll *a*, POC and PON concentration were collected during the exponential growth phase and analysed using the same techniques described in Chapter 2. In addition, the maximum quantum yield of PSII (F_v/F_m) and the effective absorbance cross section of PSII (σ_{PSII}) were determined using fast repetition rate fluorometry (FRRF).

4.4 Results

Data collected from experiments on *Synechococcus* sp. WH7803 are described first, followed by comparison to eukaryotic phytoplankton and field data from the (sub-) tropical North Atlantic. Values are typically described as the mean ± standard deviation and bar graphs represent the mean with standard deviation error bars, unless otherwise

stated. Plots are offset from days 0, 2, 4, 6 and 8 to improve clarity of standard deviation.

4.4.1 Synechococcus sp. WH7803 experiments

The final biovolume (day 8) of *Synechococcus* sp. WH7803 was markedly reduced for cultures grown in low iron media (i.e. Fe_T = 12 nmol L^{-1}) compared to those grown under medium (120 nmol L^{-1}) and high (1200 nmol L^{-1}) iron treatments (Fig. 4.2A). The mean final biovolume was highest for high iron cultures at 48.3 x 10^6 μm^3 ml^{-1}, and lowest for low iron cultures which averaged (mean) 10.3 x 10^6 μm^3 ml^{-1}. The final biovolume of the three iron conditions were significantly different ($H_{(2)}$ = 11.38, $p < 0.05$, Kruskal-Wallis test). The median of high and medium iron cultures were not significantly different from each other, but low iron cultures were significantly different compared to high and medium iron cultures (Mann-Whitney *U* tests, both $p < 0.01$, Table 4.1). A similar trend was observed with regards to cell number (Fig. 4.2B), although the mean final cell number was highest for medium iron cultures (31.3 x 10^6 cells ml^{-1}) and lowest in the low iron cultures (7.6 x 10^6 cells ml^{-1}). Comparison of all three iron regimes suggested a significant difference in final cell number of *Synechococcus* sp. WH7803 ($H_{(2)}$ = 10.05, $p <$ 0.05). High and medium iron cultures were not significantly different from each other, but the final cell numbers of low iron cultures were significantly different compared to both medium and high iron cultures (both $p < 0.01$, Table 4.1).

	Comparison		
Variable	High vs. Medium	High vs. Low	Medium vs. Low
Biovolume	*U* = 17	*U* = 0**	*U* = 0**
Cell Number	*U* = 13	*U* = 0**	*U* = 0**
Heme *b*	*U* = 12	*U* = 0**	*U* = 0**
Chlorophyll *a*	*U* = 11	*U* = 0**	*U* = 0**
POC	*U* = 17	*U* = 0**	*U* = 0**
PON	*U* = 14	*U* = 0**	*U* = 0**

Table 4.1. Results of Mann-Whitney *U* tests (two-tailed) for comparison of the median biovolume, cell number, heme *b* concentration, chlorophyll *a* concentration and particulate organic carbon (POC) and particulate organic nitrogen (PON) concentrations on the final day (i.e. day 8) of *Synechococcus* sp. WH7803 cultures grown under three different iron regimes: Fe_T = 1200 nmol L^{-1} (high), 120 nmol L^{-1} (medium) and 12 nmol L^{-1} (low). For all comparisons, $n_1 = n_2 = 6$. Statistical significance represented by ** where $p < 0.01$ and * where $p < 0.05$.

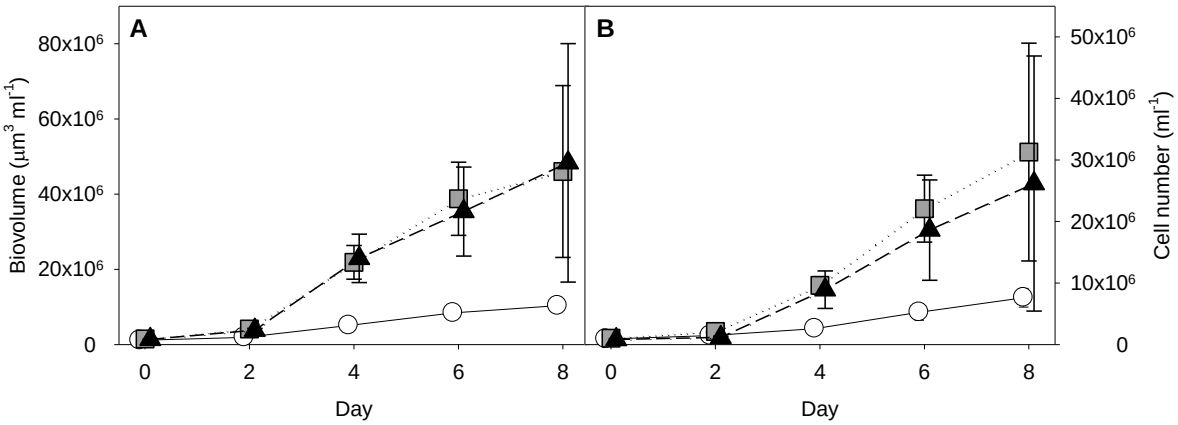

Figure 4.2. (**A**) Biovolume (µm³ ml⁻¹) and (**B**) cell number (ml⁻¹) determined for *Synechococcus* sp. WH7803 cultures grown under three different iron regimes: Fe_T = 1200 nmol L^{-1} (black triangle), 120 nmol L^{-1} (grey square) and 12 nmol L^{-1} (white circle).

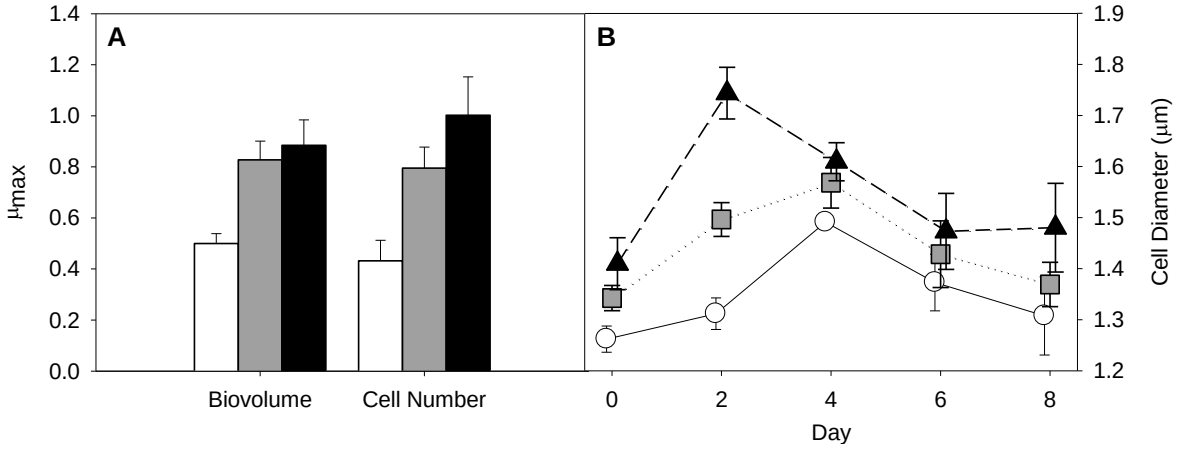

Figure 4.3. (**A**) Maximum growth rate (μ_{max}, day^{-1}) with regards to biovolume and cell number and (**B**) mean cell diameter (µm) determined for *Synechococcus* sp. WH7803 cultures grown under three different iron regimes: Fe_T = 1200 nmol L^{-1} (black triangle), 120 nmol L^{-1} (grey square) and 12 nmol L^{-1} (white circle). Note *y*-scale of B starts at 1.2 µm.

The maximum specific growth rate (μ_{max}) of *Synechococcus* sp. WH7803 cultures with regards to biovolume and cell number showed a similar trend (Fig. 4.3A). High iron cultures displayed the highest μ_{max} for both biovolume (0.88 ± 0.10) and cell number (1.00 ± 0.15); low iron cultures displayed the lowest μ_{max} for both biovolume (0.50 ± 0.04) and cell number (0.43 ± 0.08). A Kruskal-Wallis test showed that the biovolume μ_{max} was significantly different between the three iron regimes ($H_{(2)} = 11.94$, $p < 0.01$). Subsequent Mann-Whitney *U* tests found that the biovolume μ_{max} of high and medium iron cultures were not significantly different, but both were significantly different compared to low iron cultures (both $U = 0$, $n_1 = n_2 = 6$, $p < 0.01$). Statistical analysis of cell number μ_{max} also suggested a difference between the three iron concentrations ($H_{(2)} = 13.66$, $p < 0.01$). The high and medium iron cultures were not significantly different, but low iron cultures were

significantly different compared to high and medium iron cultures (both $U = 0$, $n_1 = n_2 = 6$, $p < 0.01$).

The mean cell diameter of *Synechococcus* sp. WH7803 appeared to be associated with iron concentration (Fig. 4.3B), with low iron cultures expressing a 13.8% reduction in cell size compared to high iron cultures. The maximum mean cell diameter was observed in high iron cultures at 1.80 µm, compared to 1.62 µm and 1.51 µm for medium and low iron cultures, respectively. Cell diameter typically increased to a maximum by day 2 for high iron cultures and day 4 for medium and low iron cultures, before decreasing during the exponential growth phase (i.e. days 6 and 8). Cell diameter was significantly different between the three iron treatments ($H_{(2)} = 28.57$, $p < 0.01$, Kruskal-Wallis test). However, unlike previous statistical comparisons, high iron cultures were significantly different to both medium ($U = 184$, $n_1 = n_2 = 26$, $p < 0.01$) and low ($U = 75$, $n_1 = n_2 = 26$, $p < 0.01$) iron cultures with regards to cell diameter. In addition, cell diameter of medium iron cultures were significantly different from low iron cultures ($U = 147$, $n_1 = n_2 = 26$, $p < 0.01$) of *Synechococcus* sp. WH7803.

The POC concentration of *Synechococcus* sp. WH7803 cultures increased throughout each growth cycle (Fig. 4.4A), similar to increases in biovolume and cell number. A significant difference was found between the final POC concentration of the three different iron treatments ($H_{(2)} = 11.42$, $p < 0.01$, $N = 18$, Kruskal-Wallis test), with distinctly increased mean concentrations in high and medium iron cultures compared to low iron cultures. Mann-Whitney *U* tests showed that final POC concentrations were significantly greater ($p < 0.01$) in high iron cultures ($M = 2075 \pm 119$ µmol L^{-1}) compared to low iron cultures ($M = 903 \pm 11$ µmol L^{-1}). A significant difference was also apparent between medium ($M = 2051 \pm 82$ µmol L^{-1}) and low iron cultures ($p < 0.01$), but not between high and medium iron cultures (Table 4.1). The concentration of PON offered a similar pattern to POC during the 8-day growth cycle, with noticeably increased final PON concentrations in high ($M = 447 \pm 29$ µmol L^{-1}) and medium ($M = 429 \pm 36$ µmol L^{-1}) iron cultures, compared to low iron cultures ($M = 286 \pm 60$ µmol L^{-1}, Fig. 4.4B). However, a Kruskal-Wallis test suggested that the final PON concentration of *Synechococcus* sp. WH7803 cultures were not significantly different between the three iron regimes ($H_{(2)} = 3.59$, $p = 0.166$, $N = 18$). When examining Figure 4.4B, this was most likely the result of large standard deviation in low iron cultures. For interest, this was followed up by Mann-Whitney *U* tests which showed that PON concentration of high and medium iron cultures became significantly different to low iron cultures on day 8 ($p < 0.01$, Table 4.1), as opposed to day 4 for POC. High and medium iron cultures were not considered significantly different with regards to the final PON concentration (Table 4.1).

Chlorophyll *a* concentrations were noticeably increased in high and medium iron cultures compared to low iron cultures of *Synechococcus* sp. WH7803 from day 4 onwards (Fig 4.5A). Final mean chlorophyll *a* concentrations (i.e. day 8) of the high and medium iron cultures were 118.9 ± 49.9 nmol L^{-1} and 87.6 ± 32.2 nmol L^{-1}, respectively whereas low iron cultures were much reduced at 11.6 ± 0.67 nmol L^{-1}. Statistical analysis suggested that final chlorophyll *a* concentrations were significantly different between the three iron treatments ($H_{(2)}$ = 11.94, $p < 0.01$, Kruskal-Wallis test). Further Mann-Whitney *U* tests showed that high and medium iron cultures were not significantly different, but both were significantly different to low iron cultures ($p < 0.01$, Table 4.1). Heme *b* concentration offered a similar trend to chlorophyll *a*, with low iron cultures noticeably reduced compared to both high and medium iron cultures (Fig 4.5B). Final mean heme *b* concentrations were nearly an order of magnitude greater for high (3.69 ± 1.67 nmol L^{-1}) and medium (4.26 ± 2.15 nmol L^{-1}) iron cultures compared to low iron cultures (0.59 ± 0.22 nmol L^{-1}). A significant difference was found between all three iron regimes with regards to final heme *b* concentration ($H_{(2)}$ = 11.80, $p < 0.01$, Kruskal-Wallis test) and, similar to chlorophyll *a* concentration, low iron cultures were significantly different to high and medium iron cultures ($p < 0.01$). Final heme *b* concentrations of high and medium iron cultures were not significantly different from each other (Table 4.1).

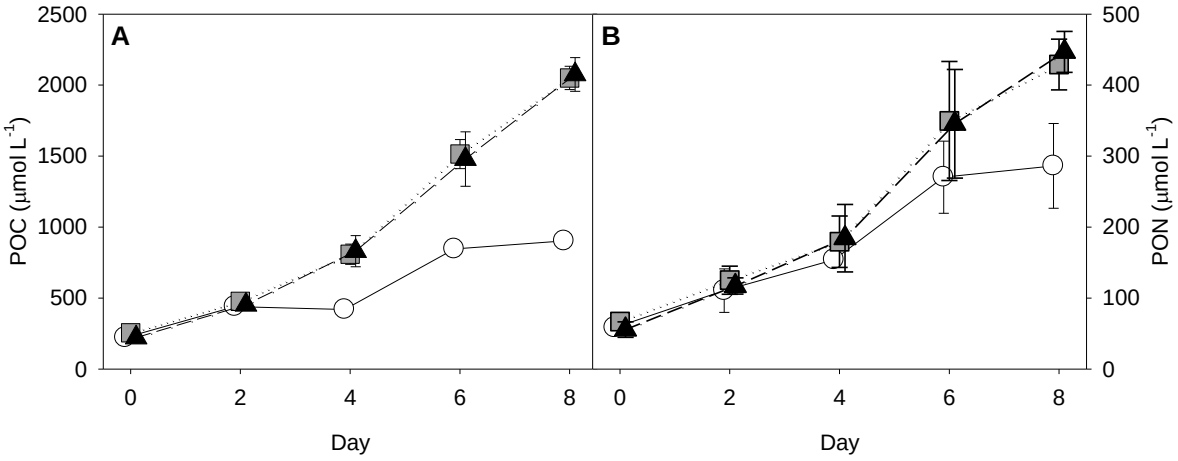

Figure 4.4. Concentration of (**A**) particulate organic carbon (POC, µmol L^{-1}) and (**B**) particulate organic nitrogen (PON, µmol L^{-1}) determined for *Synechococcus* sp. WH7803 cultures grown under three different iron regimes: Fe_T = 1200 nmol L^{-1} (black triangle), 120 nmol L^{-1} (grey square) and 12 nmol L^{-1} (white circle).

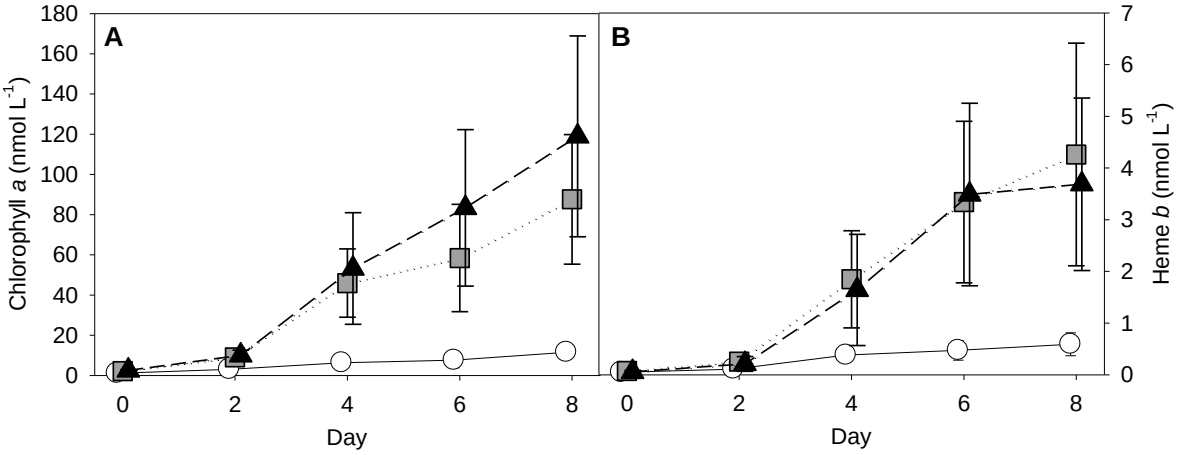

Figure 4.5. Concentration of (**A**) chlorophyll *a* (nmol L^{-1}) and (**B**) heme *b* (nmol L^{-1}) determined for *Synechococcus* sp. WH7803 cultures grown under three different iron regimes: Fe_T = 1200 nmol L^{-1} (black triangle), 120 nmol L^{-1} (grey square) and 12 nmol L^{-1} (white circle).

	Variable 2		
Variable 1	Chlorophyll *a*	POC	PON
High			
Heme *b*	0.666 (18)**	0.761 (18)**	0.577 (18)*
Chlorophyll *a*	-	0.879 (18)**	0.427 (18)
Medium			
Heme *b*	0.834 (18)**	0.816 (18)**	0.584 (18)*
Chlorophyll *a*	-	0.814 (18)**	0.469 (18)*
Low			
Heme *b*	0.636 (18)**	0.245 (18)	0.196 (18)
Chlorophyll *a*	-	0.463 (18)	0.337 (18)
All			
Heme *b*	0.817 (54)**	0.847 (54)**	0.612 (54)**
Chlorophyll *a*	-	0.863 (54)**	0.517 (54)**

Table 4.2. Results of Pearson Product Moment Correlations (*r*) for heme *b*, chlorophyll *a*, particulate organic carbon (POC) and particulate organic nitrogen (PON) concentration in *Synechococcus* sp. WH7803 cultures grown under three different iron regimes: Fe_T = 1200 nmol L^{-1} (high), 120 nmol L^{-1} (medium) and 12 nmol L^{-1} (low). Results also provided for all iron treatments combined. Correlations calculated from values measured during the exponential growth phase only (i.e. days 4, 6 and 8).

Heme *b* concentration per cell was greater in high (1.73 ± 0.72 amol $cell^{-1}$; 'atto' (a) = 1 x 10^{-18}) and medium (1.49 ± 0.58 amol $cell^{-1}$) iron cultures of *Synechococcus* sp. WH7803 compared to low iron cultures (1.09 ± 0.54 amol $cell^{-1}$) during the exponential growth phase (i.e. days 4, 6 and 8). Statistical analysis suggested a significant difference

between all three iron cultures ($H_{(2)}$ = 7.77, $p < 0.05$, Kruskal-Wallis test). Heme *b* concentration per cell of high ($p < 0.01$) and medium ($p < 0.05$) iron cultures were significantly different to low iron cultures (Mann-Whitney *U* tests). However, no significant difference was found between high and medium iron cultures. The concentration of heme *b* was significantly correlated to both POC and PON concentration in high and medium iron cultures of *Synechococcus* sp. WH7803, whereas low iron cultures did not offer a significant relationship (Table 4.2). The same trend was also evident between chlorophyll *a* and POC concentrations, with high and medium iron cultures providing a statistically significant correlation, whereas low iron cultures were not significantly correlated. However, in comparison to PON concentration, chlorophyll *a* was only significantly correlated in medium iron cultures ($p < 0.05$), with statistical analysis suggesting that high and low iron cultures offered non-significant relationships (Table 4.2). Strong significant correlations were found between both tetrapyroles and POC/PON concentration when results of all three iron concentrations were combined. Nevertheless, heme *b* concentration accounted for a larger degree of the variance (r^2) with regards to the relationship with POC and PON compared to chlorophyll *a* concentration (Table 4.2).

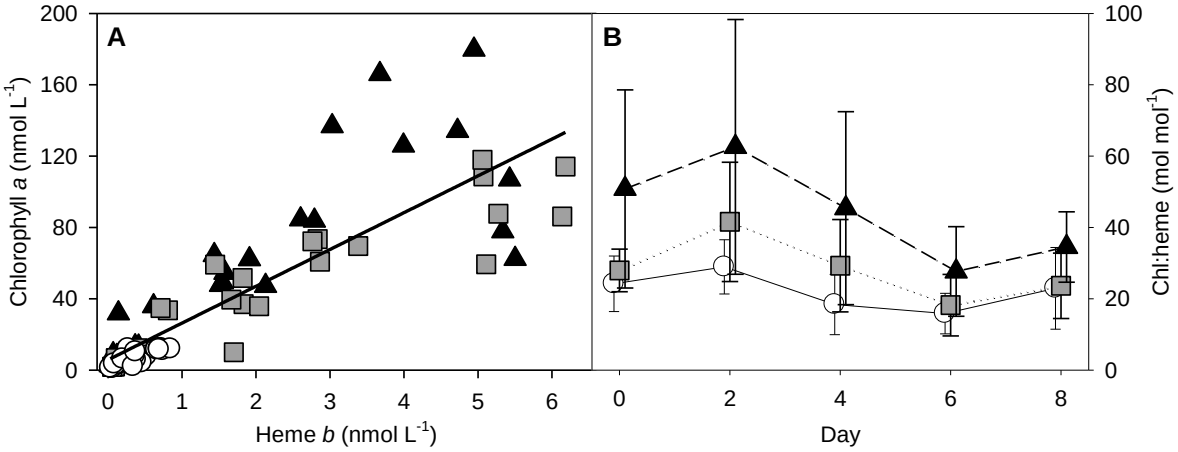

Figure 4.6. (**A**) Heme *b* concentration (nmol L^{-1}) versus chlorophyll *a* concentration (nmol L^{-1}) and (**B**) chlorophyll *a* to heme *b* ratio (chl:heme, mol mol^{-1}) determined for *Synechococcus* sp. WH7803 cultures grown under three different iron regimes: Fe_T = 1200 nmol L^{-1} (black triangle), 120 nmol L^{-1} (grey square) and 12 nmol L^{-1} (white circle). Equation for correlation (line) in A: $y = 20.641x + 5.750$ ($r^2 = 0.753$, $p < 0.01$).

A significant correlation ($p < 0.01$) was found between heme *b* and chlorophyll *a* concentration in *Synechococcus* sp. WH7803 cultures during the exponential growth phase (i.e. days 4, 6 and 8, Table 4.2). However, the slope of the correlation (Fig. 4.6A) was less steep compared to those calculated from cruises D346 and D361 (Figs. 3.17 and 3.18), indicating lower ratios of chlorophyll *a* to heme *b* (chl:heme) in *Synechococcus* sp. WH7803 compared to the overall (sub-) tropical North Atlantic. Variations in chl:heme

ratio were apparent between the three different iron regimes, with increased mean values for high iron cultures throughout the 8-day growth cycle (Fig. 4.6B). The mean chl:heme ratio during the exponential growth phase was highest for high iron cultures at 35.9 ± 18.6 mol mol^{-1}, compared to 23.7 ± 10.8 and 19.1 ± 8.8 mol mol^{-1} for medium and low iron cultures, respectively. A significant difference in chl:heme ratio from the exponential growth phase was found between the three iron regimes ($H_{(2)}$ = 13.70, p < 0.01, Kruskal-Wallis test). Low iron cultures were not significantly different to medium iron cultures with regards to chl:heme ratio (U = 111, $n_1 = n_2$ = 18, p = 0.107). However, chl:heme ratios of high iron cultures were significantly different to both medium (U = 82.5, $n_1 = n_2$ = 18, p < 0.05) and low (U = 54, $n_1 = n_2$ = 18, p < 0.01) iron cultures during the exponential growth phase.

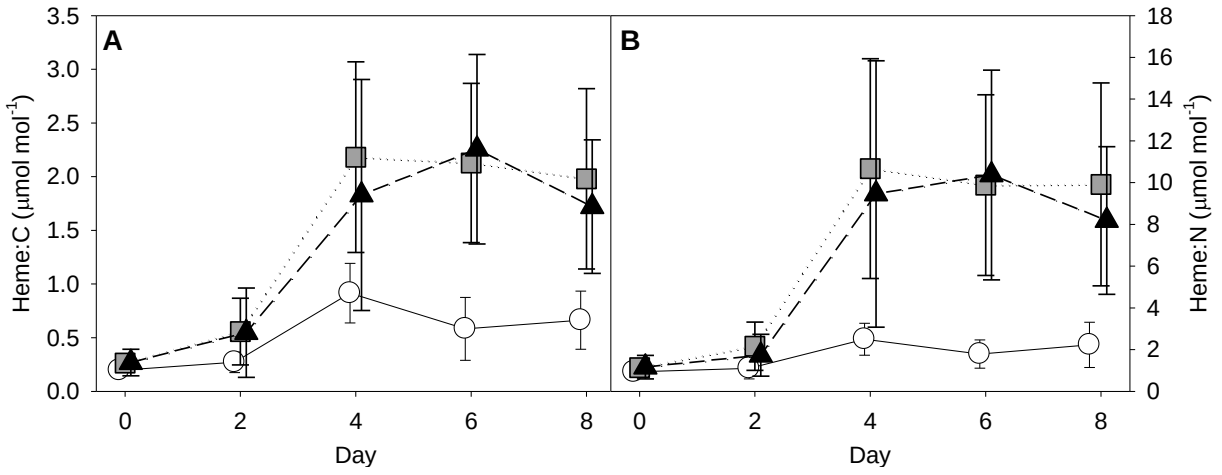

Figure 4.7. Ratio of (**A**) heme *b* per unit carbon (heme:C, µmol mol^{-1} C) and (**B**) heme *b* per unit nitrogen (heme:N, µmol mol^{-1} N) determined for *Synechococcus* sp. WH7803 cultures grown under three different iron regimes: Fe_T = 1200 nmol L^{-1} (black triangle), 120 nmol L^{-1} (grey square) and 12 nmol L^{-1} (white circle).

The ratio of heme *b* concentration per unit carbon (heme:C) and per unit nitrogen (heme:N) for *Synechococcus* sp. WH7803 cultures offered similar patterns throughout the 8-day growth cycle, with noticeably increased values on days 4, 6 and 8 (i.e. exponential phase, Figs. 4.7A and 4.7B). Mean heme:C ratios from the exponential phase were greatest in medium iron cultures (2.1 ± 0.8 µmol mol^{-1} C) and lowest in low iron cultures (0.7 ± 0.3 µmol mol^{-1} C). Statistical analysis showed that heme:C ratios of low iron cultures were significantly different to high and medium iron cultures during the exponential phase (p < 0.01), but no significant difference was apparent between high and medium iron cultures (Table 4.3). The highest mean heme:N ratio from the exponential growth phase was found in medium iron cultures (10.2 ± 4.6 µmol mol^{-1} N), with the lowest mean heme:N ratio observed in low iron cultures (2.2 ± 0.9 µmol mol^{-1} N). Both high and medium iron cultures were significantly different to low iron cultures (p <

0.01), but not each other with regards to mean heme:N ratio during the exponential growth phase (Table 4.3).

	Comparison		
Variable	High vs. Medium	High vs. Low	Medium vs. Low
Heme:C	$U = 143.5$	$U = 26^{**}$	$U = 7^{**}$
Heme:N	$U = 121.5$	$U = 22^{**}$	$U = 4^{**}$
Chl:C	$U = 99^{*}$	$U = 0^{**}$	$U = 15^{**}$
Chl:N	$U = 127$	$U = 0^{**}$	$U = 15^{**}$

Table 4.3. Results of Mann-Whitney *U* tests (two-tailed) for comparison of the median concentrations of heme *b* per unit carbon (heme:C), heme *b* per unit nitrogen (heme:N), chlorophyll *a* per unit carbon (chl:C) and chlorophyll *a* per unit nitrogen (chl:N) from the exponential growth phase (i.e. days 4, 6 and 8) of *Synechococcus* sp. WH7803 cultures grown under three different iron regimes: Fe_T = 1200 nmol L^{-1} (high), 120 nmol L^{-1} (medium) and 12 nmol L^{-1} (low). For all comparisons, $n_1 = n_2 = 18$. Statistical significance represented by ** where $p < 0.01$ and * where $p < 0.05$.

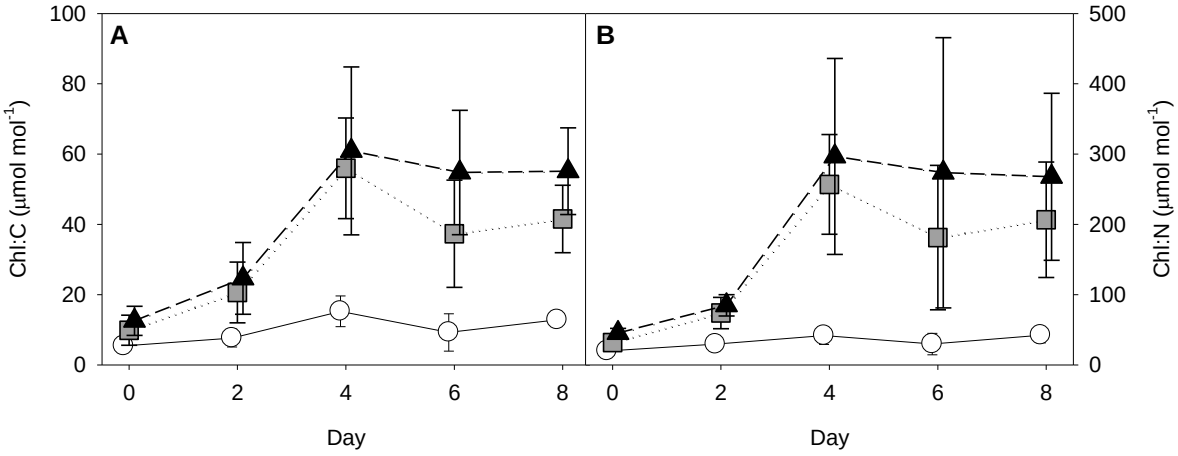

Figure 4.8. Ratio of (**A**) chlorophyll *a* per unit carbon (chl:C, µmol mol^{-1} C) and (**B**) chlorophyll *a* per unit nitrogen (chl:N, µmol mol^{-1} N) determined for *Synechococcus* sp. WH7803 cultures grown under three different iron regimes: Fe_T = 1200 nmol L^{-1} (black triangle), 120 nmol L^{-1} (grey square) and 12 nmol L^{-1} (white circle).

Chlorophyll *a* concentration per unit carbon (chl:C) and per unit nitrogen (chl:N) were similar to the corresponding heme *b* content ratios with increased values during days 4, 6 and 8 (Figs. 4.8A and 4.8B). Mean chl:C ratios were greatest in high iron cultures (56.9 ± 17.7 µmol mol^{-1} C) and lowest in low iron cultures (12.4 ± 4.6 µmol mol^{-1} C) during the exponential growth phase. Statistical analysis showed that chl:C ratios of low iron

cultures were significantly different to high and medium iron cultures during the exponential phase ($p < 0.01$). In addition, a significant difference was found between chl:C ratios of high and medium iron cultures of *Synechococcus* sp. WH7803 ($p < 0.05$, Table 4.3). The highest mean chl:N ratio from the exponential growth phase was found in high iron cultures (279 ± 145 μmol mol^{-1} N), with the lowest values in low iron cultures (37.9 ± 13.7 μmol mol^{-1} N). High and medium iron cultures were significantly different to low iron cultures ($p < 0.01$), but not between each other with regards to mean chl:N ratio during the exponential growth phase (Table 4.3).

4.4.2 Comparison with eukaryotic phytoplankton

Results from experiments on the cyanophyte *Synechococcus* sp. WH7803 were compared to laboratory grown cultures of the flagellate *D. tertiolecta* (cell diameter ~10 μm), the coccolithophore *E. huxleyi* (~4 μm) and the diatoms *T. weissflogii* (~10 μm), *T. oceanica* (~8 μm) and *P. tricornutum* (~3 μm) which were also subjected to various iron treatments. The μ_{max} (biovolume) of all six species were significantly reduced in the lowest iron treatments (Table 4.4), with the exception of *T. weissflogii* which could not be sustained beyond three subcultures in 5 nmol L^{-1} Fe_T concentrations (results not shown). Cultures of *T. oceanica* exhibited the greatest decrease in μ_{max} with a greater than two-fold reduction between 5 and 1500 nmol L^{-1} Fe_T conditions. In contrast, the lowest reduction in μ_{max} between high and low iron concentrations was found in *D. tertiolecta* and *P. tricornutum* cultures. Photosynthetic efficiency was measured in all five phytoplankton species with decreased maximum quantum yields of PSII (F_v/F_m) found at the lowest iron concentrations (Table 4.4). The functional absorption cross-section of PSII (σ_{PSII}), expressed relative to σ_{PSII} observed under iron and light replete conditions was generally increased under low iron conditions, with the exception of *E. huxleyi* (Table 4.4). Saturation of PSII reaction centres was considered incomplete for cultures of *Synechococcus sp.* WH7803; hence neither F_v/F_m nor relative σ_{PSII} values are reported.

Cell volumes (μm^3) were reduced in the lowest iron conditions of all cultures with the exception of *T. oceanica* which was greater at 5 nmol L^{-1} compared to 1500 nmol L^{-1} Fe_T concentrations (Table 4.4). The cyanobacteria *Synechococcus sp.* WH7803 exhibited the smallest cellular volumes with an average (mean) of 1.97 ± 0.60 μm^3 for all iron regimes, compared to *T. weissflogii* cells which were nearly three orders of magnitude larger (M = 1071 ± 120 μm^3). However, despite having the lowest cellular volume, *Synechococcus* sp. WH7803 displayed relatively high cellular carbon and nitrogen contents per unit biovolume compared to the five marine phytoplankton species (Table 4.4). Low iron cultures of *Synechococcus* sp. WH7803 were elevated in carbon and nitrogen content compared to high iron cultures. This trend was also observed in the other phytoplankton species, apart from *T. weissflogii* which instead exhibited reduced carbon and nitrogen

Species	Treatment (Fe_T)	pFe'	Growth rate (day^{-1})	F_v/F_m	Relative σ_{PSII}	Cell volume (μm^3)	Carbon (mol C L^{-1})	Nitrogen (mol N L^{-1})	Chl:heme (mol mol^{-1})
D. tertiolecta	5 nmol L^{-1}	11.7	0.61 ± 0.11	0.37 ± 0.02	1.34	113 ± 6.74	14.6 ± 4.51	2.58 ± 0.96	188 ± 21.9
	45 nmol L^{-1}	10.8	1.06 ± 0.05	0.52 ± 0.01	1.04	213 ± 1.98	13.3 ± 0.61	2.25 ± 0.10	88.3 ± 16.7
	1500 nmol L^{-1}	9.2	0.94 ± 0.03	0.55 ± 0.01	1	276 ± 2.70	13.3 ± 0.77	2.17 ± 0.12	84.4 ± 20.0
E. huxleyi	0.5 nmol L^{-1}	12.7	0.67 ± 0.05	0.34 ± 0.02	0.76	21.6 ± 0.18	15.6 ± 1.06	2.17 ± 0.07	262 ± 49.3
	5 nmol L^{-1}	11.7	0.99 ± 0.04	0.36 ± 0.01	1.04	27.7 ± 0.54	15.6 ± 1.84	1.98 ± 0.17	144 ± 4.85
	45 nmol L^{-1}	10.8	1.35 ± 0.03	0.40 ± 0.02	1.01	28.2 ± 0.01	15.3 ± 0.54	2.13 ± 0.07	88.7 ± 16.5
	1500 nmol L^{-1}	9.2	1.26 ± 0.05	0.39 ± 0.02	1	29.0 ± 4.41	15.1 ± 0.29	2.02 ± 0.02	82.0 ± 9.24
T. weissflogii	45 nmol L^{-1}	10.8	0.97 ± 0.07	0.46 ± 0.02	1.08	923 ± 24.1	9.98 ± 1.72	1.07 ± 0.16	73.0 ± 23.1
	188 nmol L^{-1}	10.1	1.06 ± 0.14	0.50 ± 0.01	0.98	1101 ± 38.0	11.8 ± 4.25	1.33 ± 0.45	44.7 ± 10.8
	1500 nmol L^{-1}	9.2	1.23 ± 0.14	0.49 ± 0.01	1	1191 ± 7.18	12.0 ± 2.64	1.43 ± 0.32	64.2 ± 9.50
T. oceanica	5 nmol L^{-1}	11.7	0.36 ± 0.07	0.38 ± 0.02	1.2	87.2 ± 1.54	32.0 ± 4.97	4.95 ± 0.53	23.5 ± 4.16
	45 nmol L^{-1}	10.8	0.75 ± 0.06	0.48 ± 0.01	0.93	87.4 ± 0.79	18.4 ± 1.37	2.78 ± 0.12	52.8 ± 4.92
	188 nmol L^{-1}	10.1	0.91 ± 0.05	0.49 ± 0.01	1.01	89.3 ± 0.78	15.4 ± 0.39	2.19 ± 0.08	60.2 ± 25.0
	1500 nmol L^{-1}	9.2	0.84 ± 0.02	0.50 ± 0.01	1	82.2 ± 0.68	21.6 ± 1.90	2.93 ± 0.23	38.3 ± 5.05
P. tricornutum	0.5 nmol L^{-1}	12.7	0.63 ± 0.11	0.31 ± 0.02	1.5	55.0 ± 2.10	11.4 ± 1.76	1.84 ± 0.38	23.2 ± 6.26
	5 nmol L^{-1}	11.7	1.03 ± 0.03	0.45 ± 0.02	1.15	80.4 ± 4.00	13.6 ± 0.40	1.86 ± 0.08	13.5 ± 3.17
	45 nmol L^{-1}	10.8	1.04 ± 0.04	0.48 ± 0.01	1.04	83.4 ± 1.55	15.8 ± 0.20	1.84 ± 0.10	36.1 ± 8.93
	1500 nmol L^{-1}	9.2	0.92 ± 0.09	0.49 ± 0.02	1	84.7 ± 1.34	14.5 ± 0.70	1.76 ± 0.10	38.1 ± 10.6
Synechococcus sp. WH7803	12 nmol L^{-1}	10	0.49 ± 0.04	-	-	1.54 ± 0.30	90.3 ± 9.15	30.1 ± 2.19	19.1 ± 8.83
	120 nmol L^{-1}	9	0.83 ± 0.06	-	-	1.83 ± 0.34	40.2 ± 3.92	8.85 ± 0.58	23.7 ± 10.8
	1200 nmol L^{-1}	8	0.89 ± 0.09	-	-	2.44 ± 0.65	40.3 ± 3.61	9.02 ± 0.89	35.9 ± 18.6

Table 4.4. Specific growth rate (μmax, day^{-1}), maximum quantum yield of PSII (F_v/F_m), effective absorbance cross section of PSII relative to iron replete conditions (relative σ_{PSII}), cellular volume (μm^3), cellular carbon and nitrogen content per unit biovolume (mol L^{-1}) and chlorophyll *a* to heme *b* ratio (chl:heme, mol mol^{-1}) determined for *Dunaliella tertiolecta*, *Emiliania huxleyi*, *Thalassiosira weissflogii*, *Thalassiosira oceanica*, *Phaeodactylum tricornutum* and *Synechococcus* sp. WH7803 grown under varying iron concentrations and high light conditions. pFe' represents -log[inorganic Fe]. Values are expressed ± standard deviation.

concentrations per unit biovolume under the lowest sustainable iron concentration (Fe_T = 45 nmol L^{-1}).

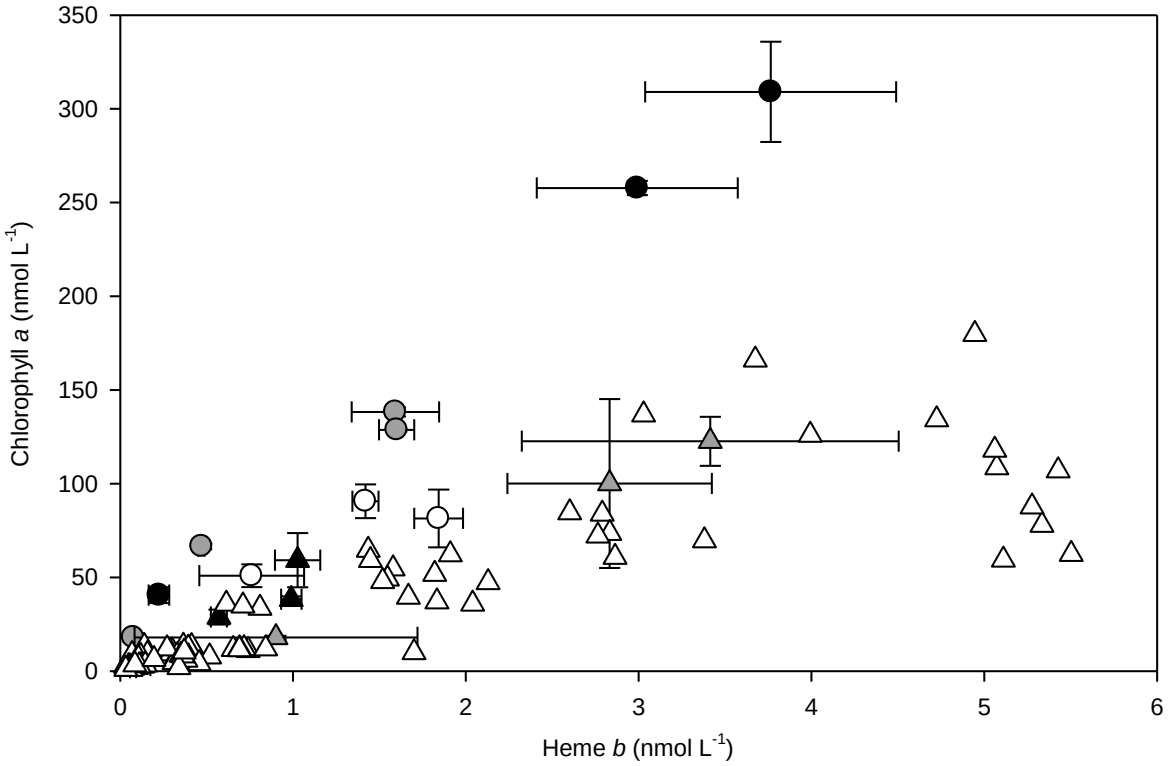

Figure 4.9. Heme *b* concentration (nmol L^{-1}) versus chlorophyll *a* concentration (nmol L^{-1}) determined for cultures of *Dunaliella tertiolecta* (black circle), *Emiliana huxleyi* (grey circle), *Thalassiosira weissflogii* (white circle), *Thalassiosira oceanica* (black triangle), *Phaeodactylum tricornutum* (grey triangle) and *Synechococcus* sp. WH7803 (white triangle) grown under varying iron concentrations and high light conditions; sampled during the exponential growth phase.

The positive correlation between heme *b* and chlorophyll *a* concentration observed in *Synechococcus* sp. WH7803 (Fig. 4.5A) was also evident in the five eukaryotic phytoplankton species (Fig. 4.9). The highest heme *b* concentration was found in *Synechococcus* sp. WH7803 (6.18 nmol L^{-1}, Fe_T = 120 nmol L^{-1}), whereas *D. tertiolecta* demonstrated the most elevated mean chlorophyll *a* concentration (309 ± 26.8 nmol L^{-1}, Fe_T = 1500 nmol L^{-1}). This was reflected in chl:heme ratios under high iron conditions (Fig. 4.10A), with the highest values calculated for *D. tertiolecta* (84.4 ± 20.0 mol mol^{-1}) and lowest for *Synechococcus* sp. WH7803 (35.9 ± 18.6 mol mol^{-1}). Chl:heme ratios were also high for *E. huxleyi* (82.0 ± 9.24 mol mol^{-1}), moderate for *T. weissflogii* (64.2 ± 9.50 mol mol^{-1}) and low for *T. oceanica* and *P. tricornutum* (38.3 ± 5.05 and 38.1 ± 10.6 mol mol^{-1}, respectively) when grown under high iron conditions. The three phytoplankton species with the highest chl:heme ratios when grown under high iron conditions exhibited a further increase in chl:heme ratio when grown under the lowest iron treatments (Fig.

4.10B). The most prominent difference was found for *E. huxleyi* cultures where a three-fold increase in chl:heme ratio was observed for low iron cultures (262 ± 49.3 mol mol^{-1}). A notable increase in chl:heme ratio was also apparent for *D. tertiolecta* when grown under low iron conditions (188 ± 21.9 mol mol^{-1}), as well as a slight elevation for *T. weissflogii* (73.0 ± 23.1 mol mol^{-1}). In contrast, *T. oceanica* (23.5 ± 4.16 mol mol^{-1}), *P. tricornutum* (23.2 ± 6.26 mol mol^{-1}) and *Synechococcus* sp. WH7803 (19.1 ± 8.83 mol mol^{-1}) all displayed a reduction in chl:heme ratios when cultured under the lowest total iron concentrations.

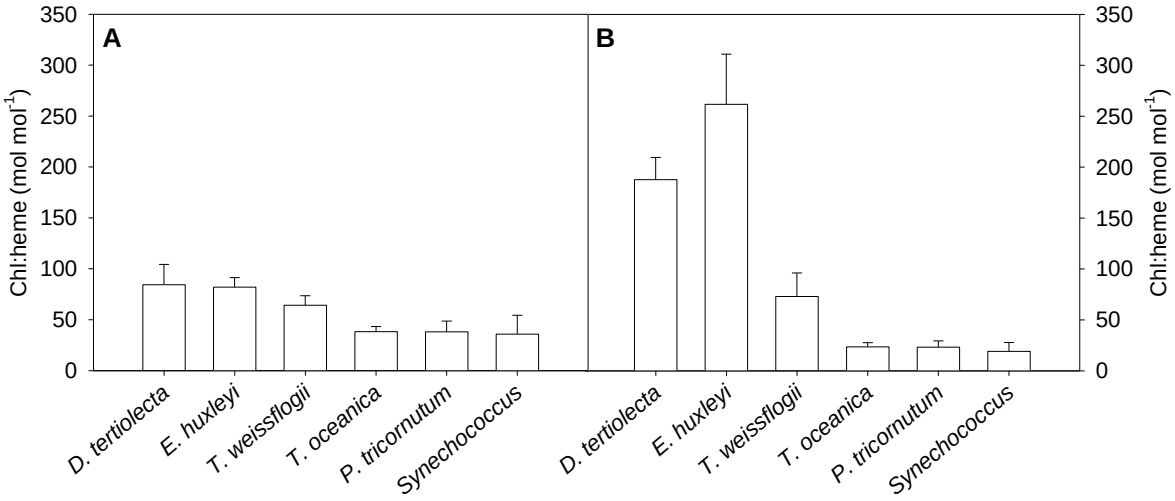

Figure 4.10. Mean chl:heme (mol mol^{-1}) ratios determined for cultures of *Dunaliella tertiolecta*, *Emiliana huxleyi*, *Thalassiosira weissflogii*, *Thalassiosira oceanica*, *Phaeodactylum tricornutum* and *Synechococcus* sp. WH7803 grown under (**A**) high iron (Fe_T = 1500 nmol L^{-1} for *D. tertiolecta*, *E. huxleyi*, *T. weissflogii*, *T. oceanica* and *P. tricornutum*; 1200 nmol L^{-1} for *Synechococcus* sp. WH7803) and (**B**) low iron (Fe_T = 0.5 nmol L^{-1} for *E. huxleyi*; 5 nmol L^{-1} for *D. tertiolecta*, *P. tricornutum* and *T. oceanica*; 12 nmol L^{-1} for *Synechococcus* sp. WH7803; 45 nmol L^{-1} for *T. weissflogii*) conditions (all light replete). All cultures were sampled during the exponential growth phase.

Comparison of heme *b* content per unit carbon (heme:C, Fig. 4.11A) and per unit nitrogen (heme:N, Fig. 4.11B) suggested a relatively similar pattern between the six cultures. High iron cultures showed elevated heme *b* contents compared to low iron cultures in all species, with the exception of *T. weissflogii* which demonstrated higher ratios when grown under low iron conditions. When considering high iron cultures, heme:C and heme:N ratios were highest in cultures of *D. tertiolecta* (5.60 ± 1.02 µmol mol^{-1} C and 34.4 ± 6.26 µmol mol^{-1} N) and lowest for *Synechococcus* sp. WH7803 (1.94 ± 0.86 µmol mol^{-1} C and 9.34 ± 4.89 µmol mol^{-1} N). In contrast, *T. weissflogii* offered the highest heme:C (3.29 ± 1.24 µmol mol^{-1} C) and heme:N (30.9 ± 12.5 µmol mol^{-1} N) ratios for low iron cultures. Cultures of *E. huxleyi* and *Synechococcus* sp. WH7803 provided the lowest heme:C (0.38 ± 0.07 µmol mol^{-1} C) and heme:N (2.17 ± 0.86 µmol mol^{-1} N) ratios for low

Species	Treatment (Fe_T)	Heme *b* (μ mol L^{-1} bio)	Heme *b* (amol $cell^{-1}$)	Heme:C (μ mol mol^{-1})	Heme:N (μ mol mol^{-1})	Chl:C (μ mol mol^{-1})	Chl:N (μ mol mol^{-1})	C:N (mol mol^{-1})
D. tertiolecta	5 nmol L^{-1}	26.9 ± 11.0	2.64 ± 0.97	1.81 ± 0.31	10.3 ± 1.69	336 ± 35.3	1912 ± 111	5.72 ± 0.33
	45 nmol L^{-1}	66.0 ± 13.6	12.9 ± 2.71	4.94 ± 0.92	29.4 ± 5.67	426 ± 5.42	2535 ± 30.0	5.94 ± 0.04
	1500 nmol L^{-1}	75.1 ± 17.2	18.2 ± 4.13	5.60 ± 1.02	34.4 ± 6.26	460 ± 22.1	2826 ± 157	6.15 ± 0.05
E. huxleyi	0.5 nmol L^{-1}	5.79 ± 1.21	0.14 ± 0.02	0.38 ± 0.07	2.67 ± 0.64	95.2 ± 8.47	683 ± 36.5	7.19 ± 0.26
	5 nmol L^{-1}	13.9 ± 1.64	0.31 ± 0.03	0.91 ± 0.04	7.00 ± 0.21	128 ± 4.24	1007 ± 3.49	7.87 ± 0.23
	45 nmol L^{-1}	37.8 ± 8.30	0.75 ± 0.16	2.56 ± 0.37	17.7 ± 3.30	214 ± 0.25	1544 ± 0.05	7.21 ± 0.01
	1500 nmol L^{-1}	40.4 ± 4.15	0.93 ± 0.03	2.70 ± 0.23	20.0 ± 2.30	218 ± 1.99	1631 ± 3.79	7.49 ± 0.05
T. weissflogii	45 nmol L^{-1}	34.1 ± 18.3	29.0 ± 16.0	3.29 ± 1.24	30.9 ± 12.5	222 ± 20.3	2063 ± 269	9.29 ± 0.40
	188 nmol L^{-1}	54.6 ± 21.9	56.3 ± 23.4	4.59 ± 0.29	40.4 ± 3.16	204 ± 44.8	1788 ± 357	8.80 ± 0.22
	1500 nmol L^{-1}	34.3 ± 9.86	38.0 ± 8.07	2.82 ± 0.18	23.8 ± 1.38	180 ± 17.5	1519 ± 149	8.44 ± 0.07
T. oceanica	5 nmol L^{-1}	82.7 ± 13.9	7.14 ± 1.55	2.51 ± 0.71	16.9 ± 4.61	60.5 ± 8.90	388 ± 37.9	6.44 ± 0.32
	45 nmol L^{-1}	60.2 ± 0.32	5.69 ± 0.40	3.43 ± 0.22	21.7 ± 0.81	173 ± 4.15	1142 ± 63.7	6.61 ± 0.21
	188 nmol L^{-1}	56.2 ± 21.9	5.75 ± 2.00	3.65 ± 1.02	25.4 ± 9.09	202 ± 10.6	1419 ± 88.7	7.01 ± 0.07
	1500 nmol L^{-1}	100.2 ± 19.8	9.10 ± 1.63	4.53 ± 0.34	34.1 ± 4.08	175 ± 3.71	1293 ± 15.8	7.38 ± 0.07
P. tricornutum	0.5 nmol L^{-1}	11.0 ± 1.32	0.49 ± 0.12	0.99 ± 0.25	6.19 ± 1.70	22.0 ± 1.68	137 ± 6.24	6.22 ± 0.38
	5 nmol L^{-1}	19.8 ± 5.12	0.86 ± 1.19	1.45 ± 0.42	10.8 ± 3.41	19.5 ± 1.24	142 ± 9.24	7.31 ± 0.22
	45 nmol L^{-1}	41.9 ± 8.98	3.00 ± 0.66	2.65 ± 0.60	22.8 ± 4.55	92.5 ± 6.90	603 ± 371	8.64 ± 0.48
	1500 nmol L^{-1}	50.1 ± 17.0	3.78 ± 1.16	3.42 ± 1.06	28.4 ± 9.48	123 ± 11.2	1018 ± 130	8.26 ± 0.33
Synechococcus sp. WH7803	12 nmol L^{-1}	61.5 ± 24.8	0.10 ± 0.04	0.72 ± 0.30	2.17 ± 0.86	12.4 ± 4.55	37.9 ± 13.7	5.36 ± 2.23
	120 nmol L^{-1}	77.2 ± 21.6	0.14 ± 0.04	2.10 ± 0.78	10.2 ± 4.56	44.9 ± 15.0	215 ± 87.3	6.43 ± 0.54
	1200 nmol L^{-1}	77.9 ± 32.9	0.17 ± 0.08	1.94 ± 0.86	9.34 ± 4.89	56.9 ± 17.7	279 ± 145	6.55 ± 0.48

Table 4.5. Heme *b* per unit biovolume (μmol L^{-1} biovolume), heme *b* per cell (amol $cell^{-1}$, 1 amol = 1 x 10^{-18} moles), heme *b* per unit carbon (heme:C, μmol mol^{-1} C) and per unit nitrogen (heme:N, μmol mol^{-1} N), chlorophyll *a* per unit carbon (chl:C, μmol mol^{-1} C) and per unit nitrogen (chl:N, μmol mol^{-1} N) and carbon to nitrogen ratio (C:N, mol mol^{-1}) determined for *Dunaliella tertiolecta*, *Emiliania huxleyi*, *Thalassiosira weissflogii*, *Thalassiosira oceanica*, *Phaeodactylum tricornutum* and *Synechococcus* sp. WH7803 cultures grown under varying iron concentrations and high light conditions. Values are expressed ± standard deviation.

iron cultures, respectively. Chlorophyll *a* content of high iron cultures was elevated compared to low iron cultures (Figs. 4.11C and 4.11D), again with the exception of *T. weissflogii* similar to heme *b* content. High iron cultures of *D. tertiolecta* offered the highest chl:C (459 ± 22.1 μmol mol^{-1} C) and chl:N (2826 ± 157 μmol mol^{-1} N) ratios, with *Synechococcus* sp. WH7803 providing the lowest ratios (56.9 ± 17.7 μmol mol^{-1} C and 279 ± 145 μmol mol^{-1} N). When considering low iron cultures, *D. tertiolecta* and *T. weissflogii* offered the highest chl:C (336 ± 35.3 μmol mol^{-1} C) and chl:N (2063 ± 269 μmol mol^{-1} N) ratios, respectively. *Synechococcus* sp. WH7803 provided the lowest chl:C (12.1 ± 4.55 μmol mol^{-1} C) and chl:N (37.9 ± 13.7 μmol mol^{-1} N) ratios under low iron conditions.

Comparison of heme *b* content per unit carbon (heme:C, Fig. 4.11A) and per unit nitrogen (heme:N, Fig. 4.11B) suggested a relatively similar pattern between the six cultures. High iron cultures showed elevated heme *b* contents compared to low iron cultures in all species, with the exception of *T. weissflogii* which demonstrated higher ratios when grown under low iron conditions. When considering high iron cultures, heme:C and heme:N ratios were highest in cultures of *D. tertiolecta* (5.60 ± 1.02 μmol mol^{-1} C and 34.4 ± 6.26 μmol mol^{-1} N) and lowest for *Synechococcus* sp. WH7803 (1.94 ± 0.86 μmol mol^{-1} C and 9.34 ± 4.89 μmol mol^{-1} N). In contrast, *T. weissflogii* offered the highest heme:C (3.29 ± 1.24 μmol mol^{-1} C) and heme:N (30.9 ± 12.5 μmol mol^{-1} N) ratios for low iron cultures. Cultures of *E. huxleyi* and *Synechococcus* sp. WH7803 provided the lowest heme:C (0.38 ± 0.07 μmol mol^{-1} C) and heme:N (2.17 ± 0.86 μmol mol^{-1} N) ratios for low iron cultures, respectively. Chlorophyll *a* content of high iron cultures was elevated compared to low iron cultures (Figs. 4.11C and 4.11D), again with the exception of *T. weissflogii* similar to heme *b* content. High iron cultures of *D. tertiolecta* offered the highest chl:C (459 ± 22.1 μmol mol^{-1} C) and chl:N (2826 ± 157 μmol mol^{-1} N) ratios, with *Synechococcus* sp. WH7803 providing the lowest ratios (56.9 ± 17.7 μmol mol^{-1} C and 279 ± 145 μmol mol^{-1} N). When considering low iron cultures, *D. tertiolecta* and *T. weissflogii* offered the highest chl:C (336 ± 35.3 μmol mol^{-1} C) and chl:N (2063 ± 269 μmol mol^{-1} N) ratios, respectively. *Synechococcus* sp. WH7803 provided the lowest chl:C (12.1 ± 4.55 μmol mol^{-1} C) and chl:N (37.9 ± 13.7 μmol mol^{-1} N) ratios under low iron conditions.

A comparison of heme *b* and chlorophyll *a* content was made for the six species to assess which pigment varied the most between the highest and lowest iron concentrations (Fig. 4.12). Heme *b* and chlorophyll *a* content relative to carbon (Fig. 4.12A) and nitrogen (Fig. 4.12B) suggested a similar pattern, with three distinct outcomes amongst the various cultures. Firstly, the decrease in heme *b* content of low iron *D. tertiolecta* and *E. huxleyi* cultures was greater than the decrease in chlorophyll *a* content. Secondly, cultures of *T. oceanica*, *P. tricornutum* and *Synechococcus* sp. WH7803 presented the opposite trend, with chlorophyll *a* contents decreasing proportionately more compared to heme *b*

contents in low iron conditions. Finally, heme *b* and chlorophyll *a* contents relative to both carbon and nitrogen were increased in low iron cultures of *T. weissflogii*; a different response compared to the other five species. Therefore, it can be inferred that heme *b* and chlorophyll *a* content were influenced by iron concentration, but differing responses were observed among the species investigated.

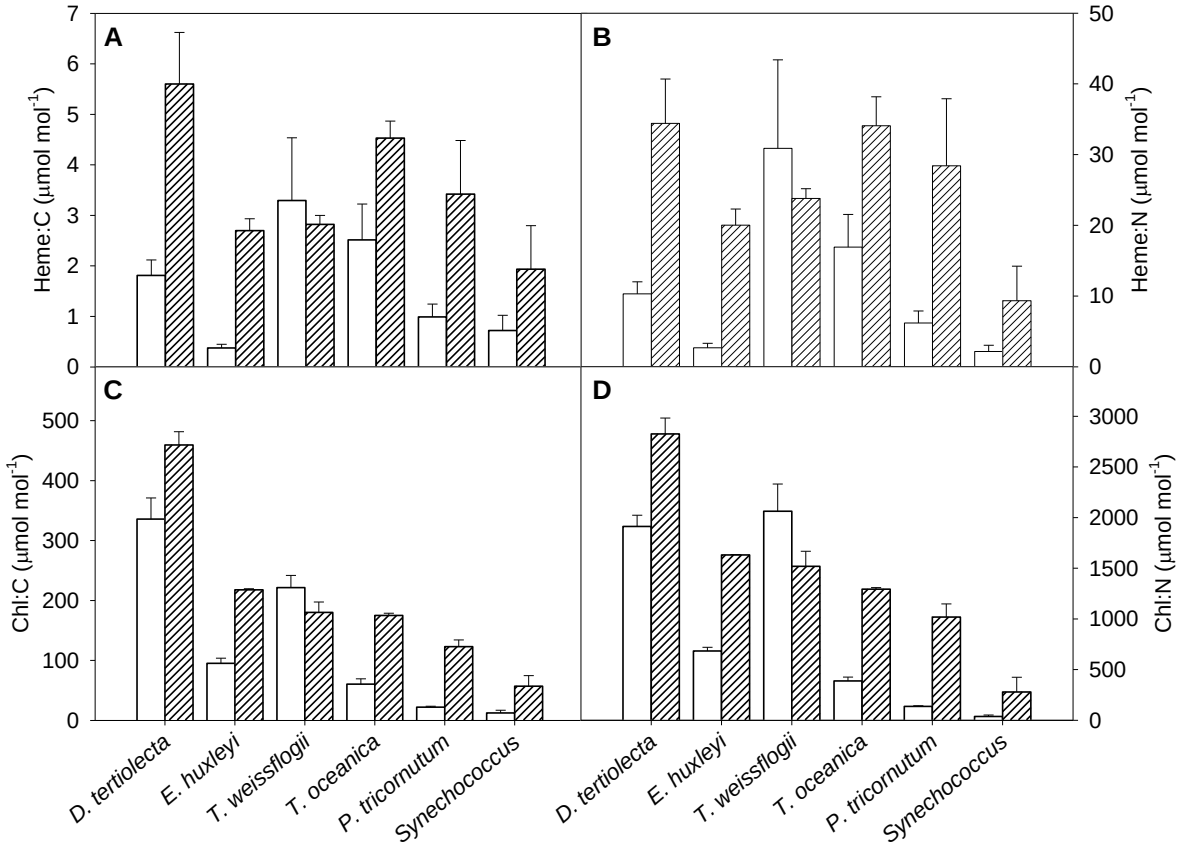

Figure 4.11. (**A**) Heme *b* concentration per unit carbon (heme:C, µmol mol^{-1} C), (**B**) heme *b* concentration per unit nitrogen (heme:N, µmol mol^{-1} N), (**C**) chlorophyll *a* concentration per unit carbon (chl:C, µmol mol^{-1} C) and (**D**) chlorophyll *a* concentration per unit nitrogen (chl:N, µmol mol^{-1} N) determined for cultures of *Dunaliella tertiolecta*, *Emiliana huxleyi*, *Thalassiosira weissflogii*, *Thalassiosira oceanica*, *Phaeodactylum tricornutum* and *Synechococcus* sp. WH7803 grown under high iron (striped, Fe_T = 1500 nmol L^{-1} for *D. tertiolecta*, *E. huxleyi*, *T. weissflogii*, *T. oceanica* and *P. tricornutum*; 1200 nmol L^{-1} for *Synechococcus* sp. WH7803) and low iron (white, Fe_T = 0.5 nmol L^{-1} for *E. huxleyi*; 5 nmol L^{-1} for *D. tertiolecta*, *P. tricornutum* and *T. oceanica*; 12 nmol L^{-1} for *Synechococcus* sp. WH7803; 45 nmol L^{-1} for *T. weissflogii*) conditions (all light replete).

Data previously described from five phytoplankton species were obtained whilst cultures were grown under high light conditions (150 µmol quanta m^{-2} s^{-1}, 12:12 hour light:dark cycle). Experiments were also conducted on *E. huxleyi* and *T. oceanica* grown under low light conditions (45 µmol quanta m^{-2} s^{-1}, 12:12 hour light:dark cycle) and, given that

Synechococcus sp. WH7803 was grown at only 30 µmol quanta m^{-2} s^{-1}, it is reasonable to compare results. Growth rates of *E. huxleyi* and *T. oceanica* were reduced under low light conditions, with the exception of *T. oceanica* cultures grown at 5 nmol L^{-1} (Fe_T) which instead displayed an increased growth rate (Table 4.6). Mean growth rates of *T. oceanica* grown under low light conditions offered a closer comparison to *Synechococcus* sp. WH7803 compared to *E. huxleyi* cultures. Cell volumes were not distinctly altered for *T. oceanica* cultures grown in high and low light conditions, although the mean cell volume of *E. huxleyi* was slightly reduced in all four iron concentrations under low light (data not shown).

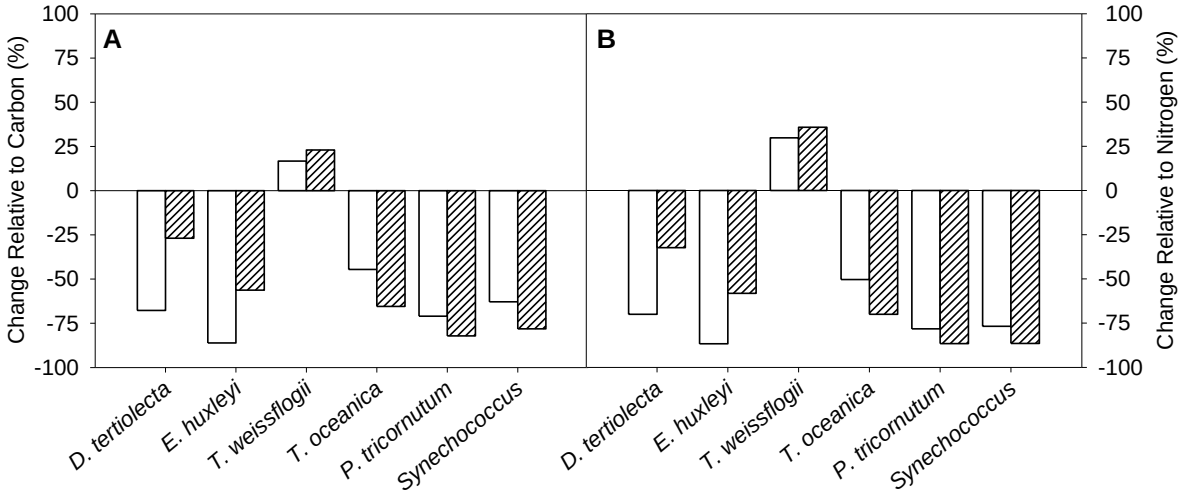

Figure 4.12. Change (% increase or decrease) in heme *b* concentration (white) and chlorophyll *a* concentration (striped) per unit (**A**) carbon and (**B**) nitrogen of low iron cultures relative to high iron cultures of *Dunaliella tertiolecta*, *Emiliana huxleyi*, *Thalassiosira weissflogii*, *Thalassiosira oceanica*, *Phaeodactylum tricornutum* and *Synechococcus* sp. WH7803.

Mean chl:heme ratios were elevated in *E. huxleyi* cultures grown in low light conditions (>1.5-fold increase), whereas the response of *T. oceanica* was more varied when comparing the two different light conditions (Table 4.6). Similar to high light cultures, *E. huxleyi* provided an inverse relationship between chl:heme ratio and iron concentration, with a maximum value (mean) of 430 ± 4.53 mol mol^{-1} at 0.5 nmol L^{-1} Fe_T. In contrast, low light chl:heme ratios of *T. oceanica* increased with increasing total iron concentration, with the highest ratio (M = 61.6 ± 5.51 mol mol^{-1}) calculated for cultures grown at 1500 nmol L^{-1} Fe_T. Heme *b* contents (i.e. heme:C and heme:N ratios) of *E. huxleyi* cultures were reduced under low light compared to high light conditions for all iron regimes, although most notably in the highest iron cultures (i.e. Fe_T = 1500 nmol L^{-1}, Table 4.6). In contrast, heme *b* contents of *T. oceanica* cultures were relatively similar under both low and high light conditions. At low light, chlorophyll *a* contents (i.e. chl:C and chl:N) were increased for *E. huxleyi* at all iron concentrations, while chlorophyll *a* contents of *T. oceanica*

Species	Treatment (Fe_T)	pFe'	Growth rate (day^{-1})	Chl:heme (mol mol^{-1})	Heme:C (µ mol mol^{-1})	Heme:N (µ mol mol^{-1})	Chl:C (µ mol mol^{-1})	Chl:N (µ mol mol^{-1})
E. huxleyi	0.5 nmol L^{-1}	13	0.49 ± 0.06	431 ± 4.53	0.39 ± 0.04	2.37 ± 0.04	158 ± 5.21	1022 ± 26.4
	5 nmol L^{-1}	12	0.84 ± 0.09	229 ± 63.1	0.73 ± 0.13	5.86 ± 1.47	165 ± 4.80	1298 ± 33.1
	45 nmol L^{-1}	11.1	1.15 ± 0.05	155 ± 17.9	1.90 ± 0.12	14.1 ± 0.34	283 ± 31.3	2181 ± 199
	1500 nmol L^{-1}	9.6	1.12 ± 0.01	127 ± 3.73	1.97 ± 0.05	15.7	250	2028
E. huxleyi *	0.5 nmol L^{-1}	-	0.73	1.65	0.98	0.89	1.66	1.5
	5 nmol L^{-1}	-	0.85	1.59	0.81	0.84	1.29	1.29
	45 nmol L^{-1}	-	0.85	1.75	0.77	0.8	1.32	1.41
	1500 nmol L^{-1}	-	0.89	1.55	0.73	0.79	1.15	1.24
T. oceanica	5 nmol L^{-1}	12	0.47 ± 0.08	25.0 ± 2.68	2.92 ± 0.28	18.8 ± 1.10	72.7 ± 0.78	467 ± 22.8
	45 nmol L^{-1}	11.1	0.44 ± 0.06	23.4 ± 1.06	3.99 ± 0.20	20.5 ± 0.69	93.6 ± 8.95	481 ± 38.1
	188 nmol L^{-1}	10.5	0.85 ± 0.24	37.5 ± 1.00	3.88 ± 0.20	27.9 ± 1.92	146 ± 11.3	1047 ± 100
	1500 nmol L^{-1}	9.6	0.83 ± 0.01	61.6 ± 5.51	3.98 ± 0.31	26.3 ± 2.38	246 ± 41.3	1625 ± 291
T. oceanica *	5 nmol L^{-1}	-	1.31	1.06	1.16	1.11	1.2	1.2
	45 nmol L^{-1}	-	0.59	0.44	1.16	0.94	0.54	0.42
	188 nmol L^{-1}	-	0.93	0.62	1.06	1.1	0.72	0.74
	1500 nmol L^{-1}	-	0.99	1.63	0.88	0.77	1.41	1.26

Table 4.6. Specific growth rate (μ_{max}, day^{-1}), chlorophyll *a* to heme *b* ratio (chl:heme, mol mol^{-1}), heme *b* per unit biovolume (µmol L^{-1} biovolume), heme *b* per cell (amol $cell^{-1}$, 1 amol = 1 x 10^{-18} moles), heme *b* per unit carbon (heme:C, µmol mol^{-1} C) and per unit nitrogen (heme:N, µmol mol^{-1} N) and chlorophyll *a* per unit carbon (chl:C, µmol mol^{-1} C) and per unit nitrogen (chl:N, µmol mol^{-1} N) determined for *Emiliania huxleyi* and *Thalassiosira oceanica* cultures grown under varying iron concentrations and low light conditions. pFe' represents -log[inorganic Fe]. Values are expressed ± standard deviation. The * symbol indicates the mean of low light values relative to the mean of corresponding high light values.

cultures only increased in the highest and lowest iron concentrations examined (Table 4.6).

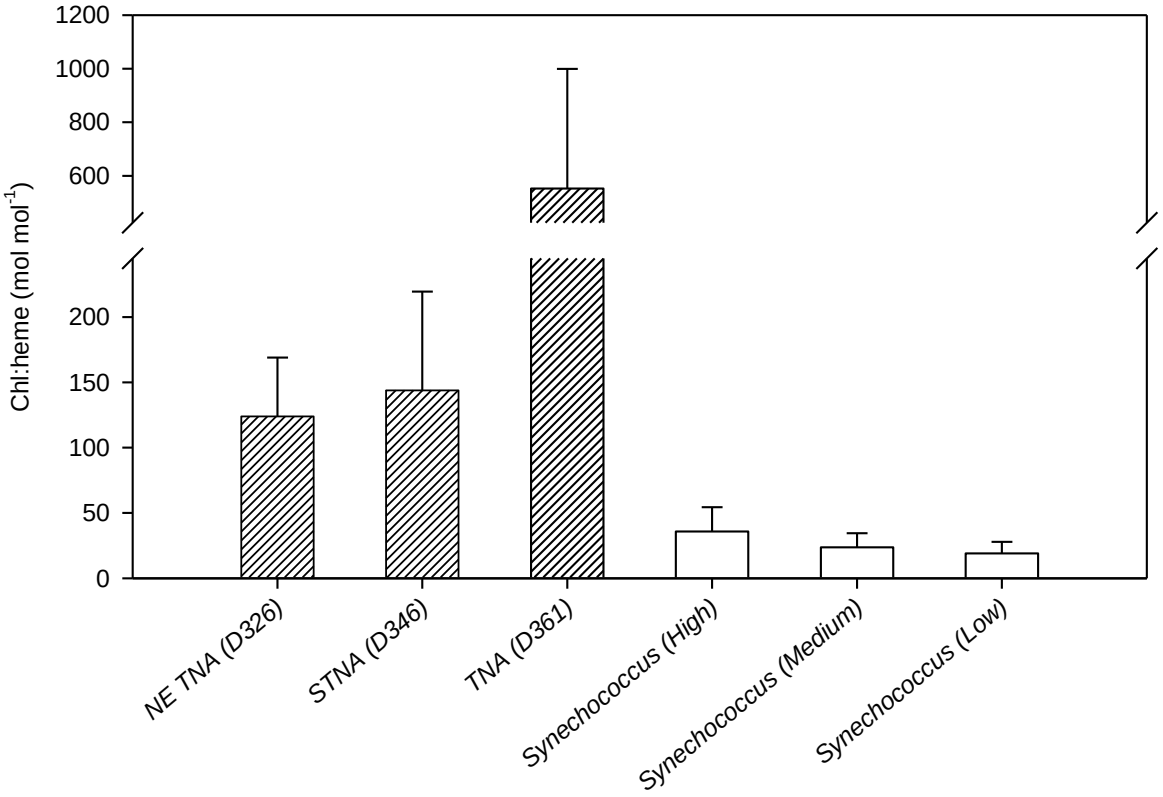

Figure 4.13. Chlorophyll *a* to heme *b* ratios (chl:heme, mol mol^{-1}) determined from research cruises (striped) in the northeast Tropical North Atlantic (NE TNA, D326), the subtropical North Atlantic (STNA, D346), the TNA (D361) and *Synechococcus* sp. WH7803 cultures (white) grown under three different iron regimes: Fe_T = 1200 nmol L^{-1} (high), 120 nmol L^{-1} (medium) and 12 nmol L^{-1} (low).

4.4.3 Comparison to (sub-) tropical North Atlantic

Three research cruises in the (sub-) tropical North Atlantic (D326, D346 and D361) have provided a baseline of heme *b* abundance and distribution in the marine environment (see Chapter 3). Visual comparison of chl:heme ratios from these three cruises and laboratory cultures of *Synechococcus* sp. WH7803 suggest a degree of natural variation, with much higher values reported in natural seawaters of the low latitude North Atlantic (Fig. 4.13). The mean chl:heme ratio from cruise D361 in the TNA (M = 553 ± 446 mol mol^{-1}) was an order of magnitude greater than *Synechococcus* sp. WH7803 cultures, with even the lowest regional value calculated from the Tropical South Atlantic (TSA) distinctly greater in comparison (M = 333 ± 207 mol mol^{-1}, see Fig. 3.12). In addition, cultures of *D. tertiolecta*, *E. huxleyi*, *T. weissflogii*, *T. oceanica* and *P. tricornutum* grown under high iron and high light conditions also provided lower chl:heme ratios compared to the cruises (Fig. 4.10A). However, chl:heme ratios of high light, low iron cultures of *D.*

tertiolecta (M = 188 ± 21.9 mol mol^{-1}) and *E. huxleyi* (M = 262 ± 49.3 mol mol^{-1}) as well as low light *E. huxleyi* cultures grown under all iron concentrations examined, were more comparable with the cruise values, particularly the Northeast TNA (D326) and the STNA (D346).

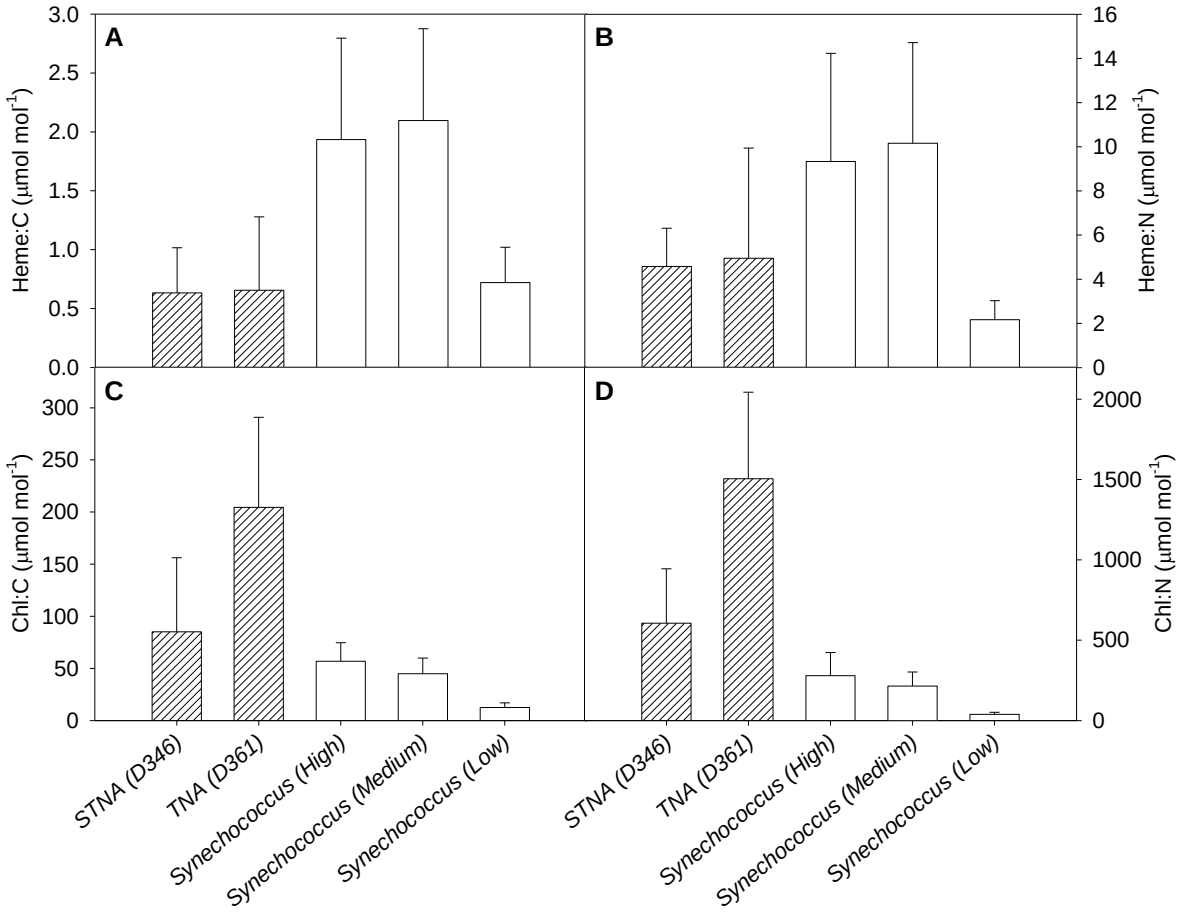

Figure 4.14. (**A**) Heme *b* concentration per unit carbon (heme:C, µmol mol^{-1} C), (**B**) heme *b* concentration per unit nitrogen (heme:N, µmol mol^{-1} N), (**C**) chlorophyll *a* concentration per unit carbon (chl:C, µmol mol^{-1} C) and (**D**) chlorophyll *a* concentration per unit nitrogen (chl:N, µmol mol^{-1} N) determined from the subtropical North Atlantic (STNA, D346), the tropical North Atlantic (TNA, D361) and cultures of *Synechococcus* sp. WH7803 grown under three different iron regimes: Fe_T = 1200 nmol L^{-1} (high), 120 nmol L^{-1} (medium) and 12 nmol L^{-1} (low). Heme *b* and chlorophyll *a* contents calculated from values measured during the exponential growth phase (i.e. days 4, 6 and 8).

Heme *b* concentrations per unit carbon (heme:C) of *Synechococcus* sp. WH7803 cultures were elevated in high and medium iron concentrations when compared to low iron cultures and values from the (sub-) tropical North Atlantic. The heme *b* contents of low iron cultures were relatively similar to ratios calculated from the natural marine environment. Mean heme:C (Fig. 4.14A) and heme:N (Fig. 4.14B) ratios from the (sub-) tropical North Atlantic and low iron cultures of *Synechococcus* sp. WH7803 were <1 µmol

mol^{-1} C and <5 µmol mol^{-1} N; whereas high and medium iron cultures were >1.9 µmol mol^{-1} C and >9 µmol mol^{-1} N, respectively. Chlorophyll *a* contents of *Synechococcus* sp. WH7803 were lower in all three iron regimes compared to the (sub-) tropical North Atlantic, with particularly high ratios calculated from the TNA during cruise D361. High iron cultures of *Synechococcus* sp. WH7803 offered the closest comparison with the (sub-) tropical North Atlantic in terms of mean chl:C (Fig. 4.14C) and chl:N (Fig. 4.14D) ratio, but were still reduced compared to values from both cruises.

4.5 Discussion

4.5.1 Heme b requirement of Synechococcus sp. WH7803

Heme *b* containing proteins are functionally diverse (Caughey 1973, Chapman et al. 1997, Mochizuki et al. 2010) and a decreased intracellular heme *b* concentration is likely to compromise an organism's ability to undertake a range of fundamental processes. It could be proposed that cells have a set minimum heme *b* requirement that facilitates basal respiratory and/or photosynthetic functioning, which ultimately enables the organism to survive. As iron is a central component in the structure of hemes, iron availability almost certainly plays a key role in the regulation of heme *b*. This was demonstrated by the increased cellular heme *b* content of *Synechococcus* sp. WH7803 cultures grown under high and medium iron concentrations (Fig. 4.5A), as was initially hypothesised (section 4.2.2.1). Therefore, the availability of iron is critical in determining whether an organism is able to alleviate the metabolic pressures to achieve the minimum heme *b* requirement. Low iron concentrations led to reduced growth and cell size in *Synechococcus* sp. WH7803 (i.e. Figs. 4.2 and 4.3) which was brought about, at least in part, by an inability to produce sufficient *b*-type hemoproteins. Increases in iron availability beyond the point needed to achieve the minimum heme *b* requirement do not necessarily lead to further increases in cellular heme *b* content. However, other iron dependent structures such as chlorophyll *a* may continue to increase, demonstrated by the elevated chl:heme ratios of high iron cultures of *Synechococcus* sp. WH7803.

Mean chl:heme ratios of high iron cultures of *Synechococcus* sp. WH7803 were significantly greater compared to medium and low iron cultures during the exponential growth phase, suggesting a proportionately elevated chlorophyll *a* concentration in relation to heme *b*. A schematic representing a possible hypothesis for this data is presented in Figure 4.15. Crucially, low and medium iron cultures were not significantly different with regards to mean chl:heme ratio, which suggests heme *b* and chlorophyll *a* were produced in relatively similar proportions (Fig. 4.15, grey area), even though the absolute quantities were greater in medium iron cultures (Fig. 4.5). Consequently, it could be suggested that the heme *b* requirement for basal metabolic functioning was not

met in either low or medium iron cultures of *Synechococcus* sp. WH7803. In contrast, chl:heme ratios were significantly increased in high iron cultures, indicating the heme *b* requirement had been surpassed; additional iron availability beyond the required quantity of heme *b* did not lead to proportional increases in heme *b* in relation to chlorophyll *a* (Fig. 4.15, e.g. dashed line). Therefore, this hypothesis could also be developed to infer that increased iron availability, or iron-replete conditions, will be reflected by elevated chl:heme ratios. However, the chl:heme ratio did not consistently increase with iron concentration for the five species of eukaryotic phytoplankton examined.

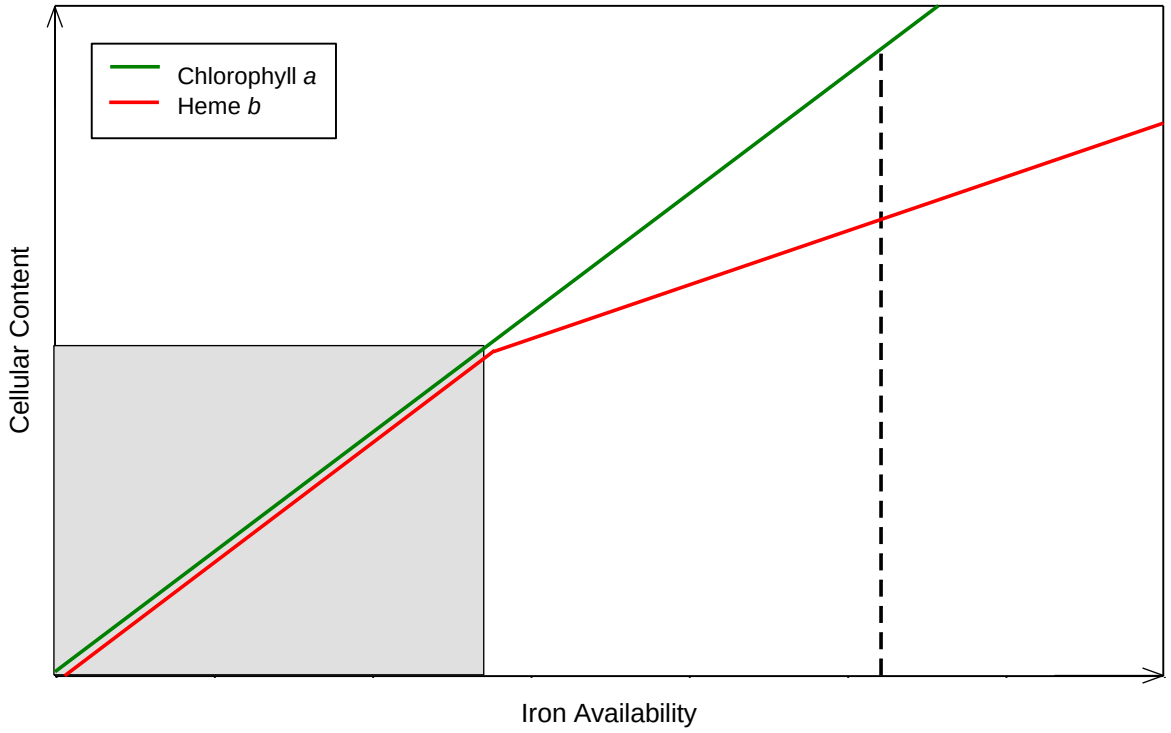

Figure 4.15. Iron availability against cellular contents of heme *b* (red line) and chlorophyll *a* (green line) providing a simplified representation of the heme *b* requirement of *Synechococcus* sp. WH7803 using chl:heme ratios. Graph is a visual representation and does not directly correspond to recorded data. Grey area represents iron availability whereby the basal heme *b* requirement has not been met; hence heme *b* and chlorophyll *a* content increase proportionately with iron. Within the white area (i.e. further increases in iron availability), heme *b* cellular content does not continue to increase in a similar proportion compared to chlorophyll *a* as the minimum heme *b* requirement has been achieved. Dashed line used to highlight divergence in heme *b* and chlorophyll *a* cellular contents at high iron availability.

Heme *b* content (i.e. heme:C and heme:N ratios) increased with iron concentration in all cultures investigated, with the exception of *T. weissflogii* (Table 4.5, Fig. 4.16A and B), but the response in terms of chl:heme ratio differed between the five species. The diatoms *T. oceanica* (high and low light) and *P. tricornutum* offered a similar pattern to

Synechococcus sp. WH7803 by exhibiting decreased chl:heme ratios under iron deplete conditions (Fig. 4.17A). In contrast, increased chl:heme ratios were observed in low iron cultures of *E. huxleyi* (high and low light) and *D. tertiolecta*; the opposite trend expected by the heme *b* requirement hypothesis (Fig. 4.17B). Finally, cultures of *T. weissflogii* did not increase or decrease their chl:heme ratio under varying iron concentrations, once again dissimilar to the trend found in *Synechococcus* sp. WH7803. Therefore, even though the idea of a minimum heme *b* requirement is not necessarily rejected at this stage, it is certainly not a suitable model for all marine phytoplankton. In addition, the comparison of chlorophyll *a* to heme *b* (chl:heme ratio) is likely to complicate the issue further as iron availability also influences chlorophyll *a* concentrations, perhaps in different ways (Fig. 4.16C and D); thus, chl:heme ratios are not suitable for estimating the minimum heme *b* requirement.

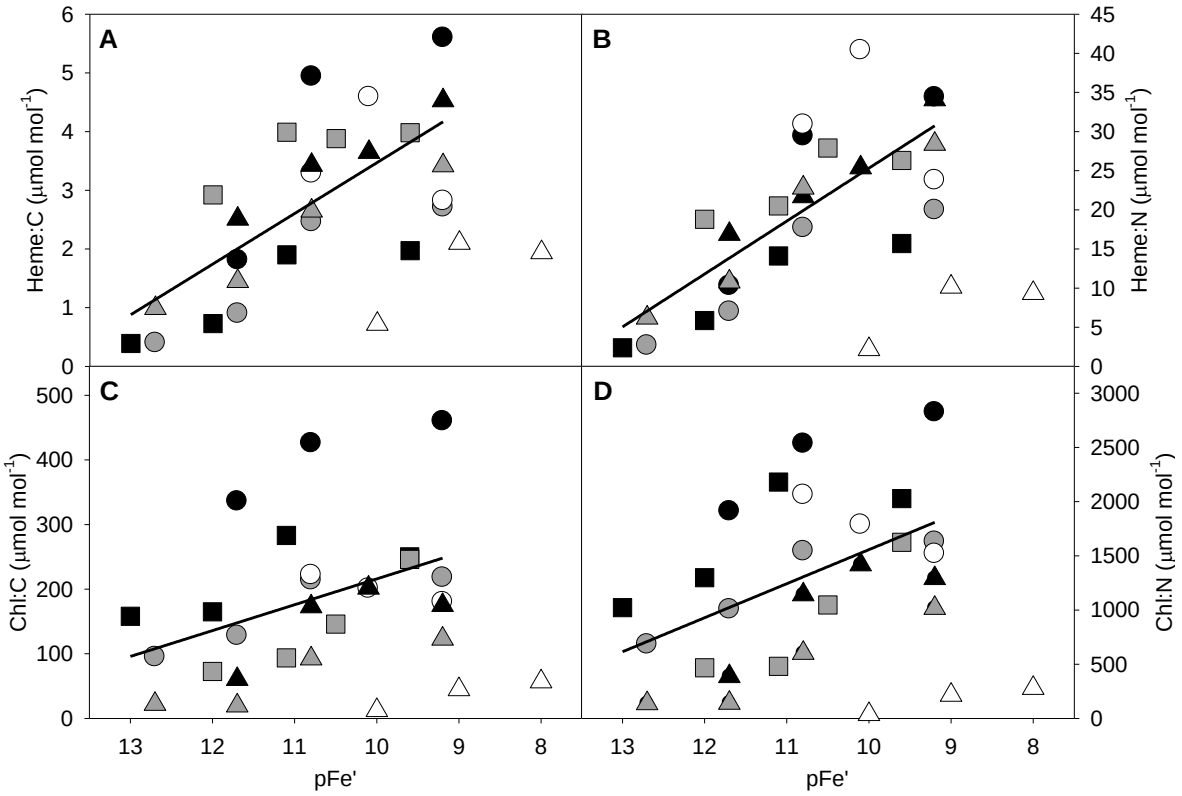

Figure 4.16. Mean (**A**) heme *b* concentration per unit carbon (heme:C, µmol mol^{-1} C), (**B**) heme *b* concentration per unit nitrogen (heme:N, µmol mol^{-1} N), (**C**) chlorophyll *a* concentration per unit carbon (chl:C, µmol mol^{-1} C) and (**D**) chlorophyll *a* concentration per unit nitrogen (chl:N, µmol mol^{-1} N) determined for cultures of *Dunialella tertiolecta* (black circle), *Emiliania huxleyi* (grey circle), *Thalassiosira weissflogii* (white circle), *Thalassiosira oceanica* (black triangle), *Phaeodactylum tricornutum* (grey triangle) and *Synechococcus* sp. WH7803 (white triangle) grown under varying iron concentrations and high light conditions, and *E. huxleyi* (black square) and *T. oceanica* (grey square) grown under varying iron concentrations and low light conditions. pFe' represents -log[inorganic Fe]. Black lines represent best fit for eukaryotic phytoplankton only.

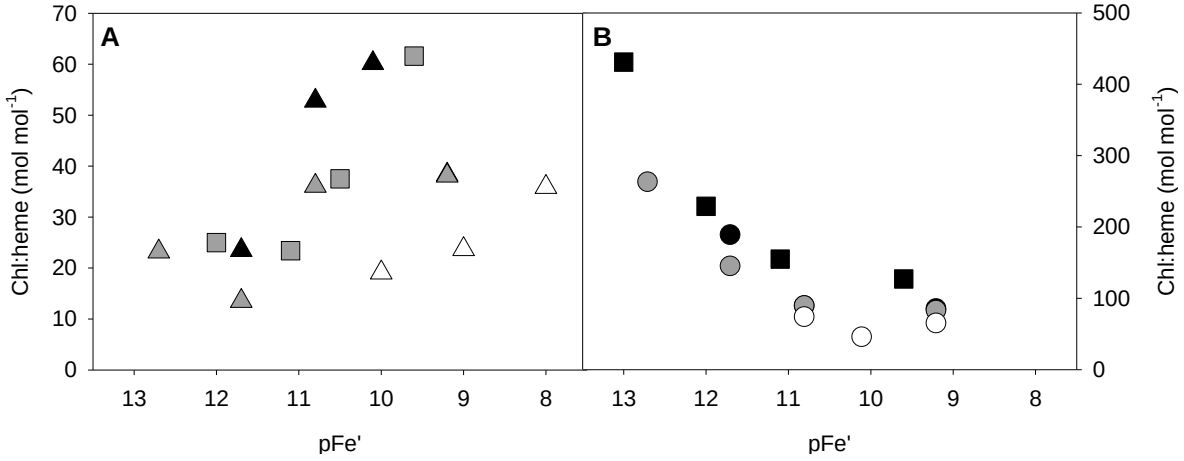

Figure 4.17. Mean chlorophyll *a* to heme *b* ratios (chl:heme, mol mol^{-1}) determined for cultures of (**A**) *Thalassiosira oceanica* (black triangle), *Phaeodactylum tricornutum* (grey triangle) and *Synechococcus* sp. WH7803 (white triangle) grown high light conditions and *T. oceanica* (grey square) grown under low light conditions, and (**B**) *Dunialella tertiolecta* (black circle), *Emiliania huxleyi* (grey circle) and *Thalassiosira weissflogii* (white circle) grown under high light conditions and *E. huxleyi* (black square) grown under low light conditions. pFe' represents -log[inorganic Fe]. Note different scales on *y*-axis of A and B.

A key factor in whether an organism is stressed could be attributed to their ability to achieve maximum growth rates (μ_{max}). The comparison of μ_{max} (biovolume) and concurrent heme:C ratios for *Synechococcus* sp. WH7803 cultures provided a 'Michaelis-Menten-type' curve (Fig. 4.18), with the high and medium iron cultures demonstrating greater μ_{max} and possessing more heme *b* per unit carbon compared to low iron cultures. Maximum growth rates were significantly reduced in low iron cultures (Fig. 4.3), suggesting a physiological response to iron stress. In contrast, high and medium iron cultures were not significantly different with regards to heme *b* content suggesting both regimes were relatively iron-replete, at least compared to low iron cultures. The 'lowest' heme:C ratios of high and medium iron cultures in conjunction with μ_{max} were approximately 1 µmol mol^{-1} C. In turn, it could be proposed that heme:C ratios lower than 1 µmol mol^{-1} C would restrict the organisms' ability to facilitate maximal growth rates (red striped area). However, two low iron cultures exhibited heme:C ratios greater than 1 µmol mol^{-1} C whilst still demonstrating notably reduced μ_{max} (<0.5 d^{-1}). Therefore, a conservative lower limit between 1.0 and 1.5 µmol mol^{-1} C (blue striped area) provides a more realistic estimate of the minimum heme *b* requirement of *Synechococcus* sp. WH7803. A few other issues need to be considered when determining the minimum heme *b* requirement, most importantly the recognition that other factors are likely to be influential upon the growth rates of *Synechococcus* sp. WH7803. These factors are potentially crucial in our understanding of physiological responses to low iron availability with several low iron cultures demonstrating heme:C ratios 'sufficient' to achieve high growth rates, but showing reduced μ_{max} compared to high and medium iron cultures.

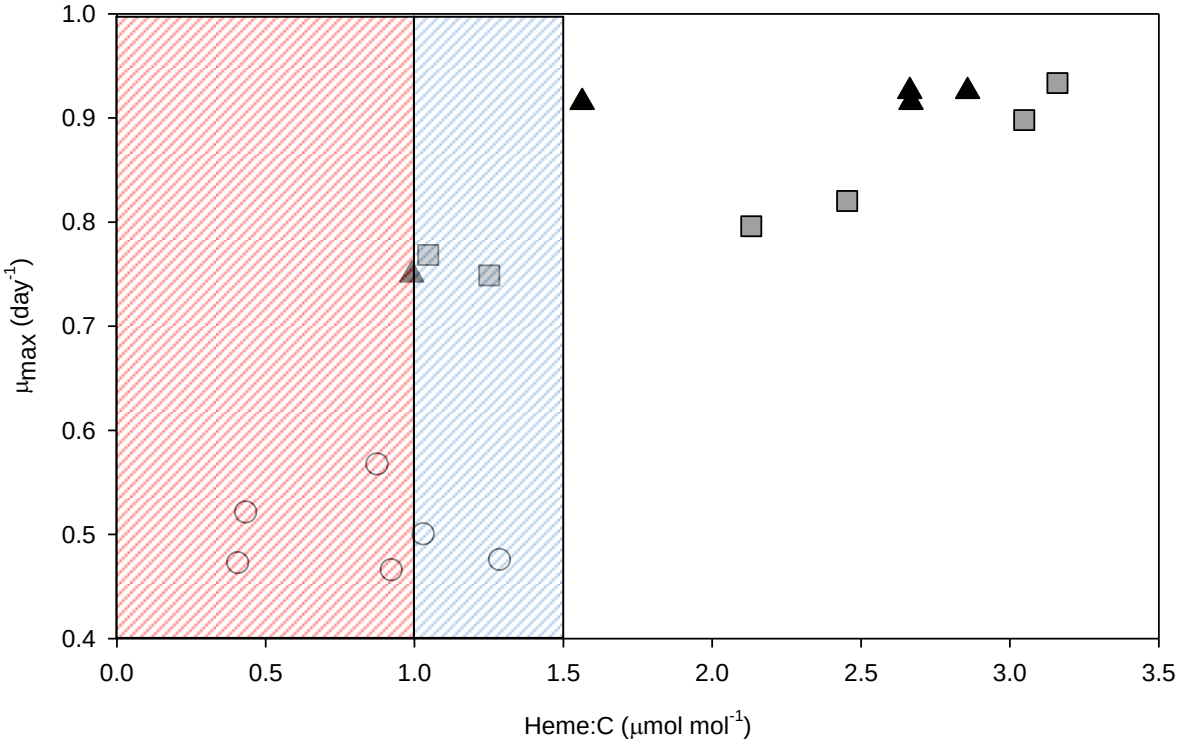

Figure 4.18. Heme *b* concentration per unit carbon (heme:C, μmol mol^{-1} C) versus the maximum growth rate (biovolume μ_{max}) determined for *Synechococcus* sp. WH7803 cultures grown under three different iron regimes: Fe_T = 1200 nmol L^{-1} (black triangle), 120 nmol L^{-1} (grey square) and 12 nmol L^{-1} (white circle). Red striped area represents heme:C ratios below 1.0 μmol mol^{-1} C, with the blue striped area representing the estimated heme *b* requirement of *Synechococcus* sp. WH7803 between 1.0 and 1.5 μmol mol^{-1} C.

The heme *b* requirement of *Synechococcus* sp. WH7803 to achieve maximum growth rates (1 - 1.5 μmol mol^{-1} C) provided a testable hypothesis upon which the eukaryotic phytoplankton cultures could be compared (Fig. 4.19). A similar pattern to that displayed by *Synechococcus* sp. WH7803 was demonstrated by the eukaryotes, with the exception of *T. weisflogii* which decreased heme:C ratios at high iron concentrations (data not included). In particular, *E. huxleyi* and *P. tricornutum* suggested similar minimum heme *b* concentrations were required for maximal growth in relation to *Synechococcus* sp. WH7803. The heme *b* requirements of *D. tertiolecta* and *T. oceanica* were higher, potentially around 5 and 3.5 μmol mol^{-1} C, respectively. However, heme *b* and POC concentrations of the eukaryotes were only measured at the end of the experiments during the exponential growth phase, which did not necessarily associate with the μ_{max}. Therefore, it is assumed that the heme:C ratio did not alter during the exponential growth phase when μ_{max} occurred; a realistic assumption given the three different *Synechococcus* sp. WH7803 iron cultures did not differ in heme:C ratio during the exponential growth phase (i.e. days 4, 6 and 8, Fig. 4.7). It also appears that cellular volume (Table 4.4) influences heme:C ratios. A non-linear pattern of carbon per unit cell volume was

previously reported for marine phytoplankton, suggesting relatively elevated carbon densities for smaller cells (Verity et al. 1992). The smaller *E. huxleyi*, *P. tricornutum* and *Synechococcus* sp. WH7803 exhibited lower minimum heme *b* requirements, potentially owing to increased carbon content. Similarly, the relatively high cellular volumes of *D. tertiolecta* and *T. oceanica*, as well as *T. weissflogii*, could explain the elevated heme:C ratios and subsequently high heme *b* requirements.

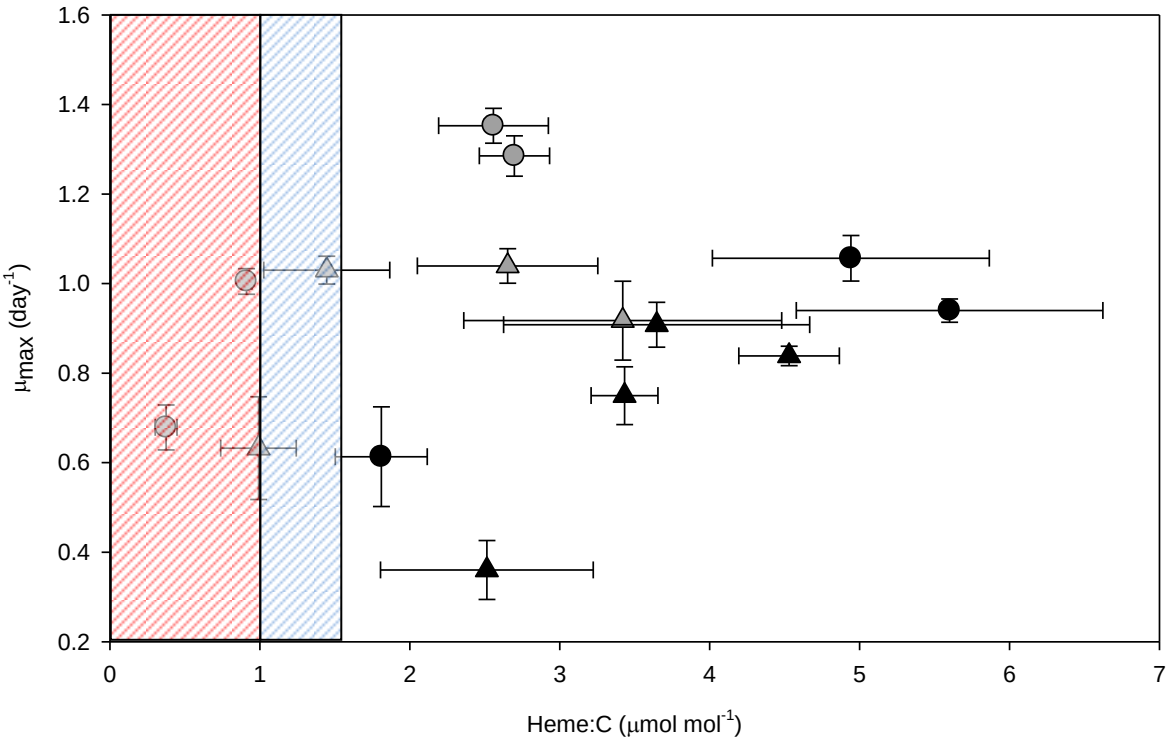

Figure 4.19. Heme *b* concentration per unit carbon (μmol mol^{-1} C) versus the maximum growth rate (biovolume μ_{max}) determined for cultures of *Dunialella tertiolecta* (black circle), *Emiliania huxleyi* (grey circle), *Thalassiosira oceanica* (black triangle) and *Phaeodactylum tricornutum* (grey triangle) grown under various different iron regimes and high light conditions. See Fig. 4.18 and in text for explanation of red and blue striped areas.

Variation in chl:heme ratio relative to alterations in iron availability suggest a divergence in physiological response between different species with regards to heme *b* and/or chlorophyll *a* abundance. This study has previously focussed upon the relieving of iron stress in high iron cultures and how iron-replete cultures respond in terms of chl:heme ratio. However, as iron is considered a limiting nutrient in large parts of the global ocean (Martin and Fitzwater 1988, Martin et al. 1991, Boyd and Ellwood 2010), it is pertinent to assess the response from an iron limitation viewpoint. The decreasing of chl:heme ratios in low iron *T. oceanica*, *P. tricornutum* and *Synechococcus* sp. WH7803 cultures infers a strategy which increases cellular heme *b* content relative to chlorophyll *a* when iron stressed (Fig. 4.17A). This approach implies the contribution of *b*-type hemoproteins are

predominantly maintained compared to chlorophyll *a* content when iron concentrations are low. Reduced iron availability will inevitably result in the decline of cellular heme *b* content (as shown in Table 4.5); however, this is exceeded by chlorophyll *a* reduction in order to 'buffer' the iron stress and facilitate continued *b*-type hemoprotein functioning at the expense of chlorophyll *a* proteins and light harvesting capacity. An alternative strategy appears to be employed by *D. tertiolecta* and *E. huxleyi* cultures, with chl:heme ratios inversely related to iron availability (Fig. 4.17B). The increased chl:heme ratio observed in low iron cultures is presumably the result of a greater reduction in heme *b* with respect to chlorophyll *a*-associated complexes. As iron availability increased, both *D. tertiolecta* and *E. huxleyi* increased their pool of *b*-type hemoproteins which consequently reduced the chl:heme ratio. The chl:heme ratio of *T. weissflogii* neither increased nor decreased with varying iron concentration implying both heme *b* and chlorophyll *a* proteins were proportionately maintained throughout (Fig. 4.17B), or at least increased/decreased at the same rate. However, cultures could not be sustained at the lowest iron regimes (i.e. <45 nmol L^{-1} Fe_T) and, consequently, it is not feasible to conclude the physiological response of *T. weissflogii* in terms of *b*-type hemoproteins when iron stressed.

Low light conditions noticeably increased chl:heme ratios of *E. huxleyi* cultures grown under all iron concentration investigated (Table 4.6). Nevertheless, low light did not alter the strategy employed by either *E. huxleyi* or *T. oceanica* with regards to heme *b* production due to iron availability. Cultures of *T. oceanica* continued to conserve cellular heme *b* content at low iron concentrations, whereas *b*-type hemoproteins for *E. huxleyi* were proportionately 'lost' compared to chlorophyll *a* when iron stressed. The red light-harvesting phycobiliprotein phycoerythrin is highly abundant in *Synechococcus* spp. and despite chlorophyll *a* remaining the primary photosynthetic pigment, accessory chlorophyll is not present (Waterbury et al. 1979, Morel et al. 1993). Also, it has previously been suggested that measuring chlorophyll *a* is unreliable in assessing the physiological state of *Synechococcus* spp. as a result of phycoerythrin dominating the light harvesting process (Barlow and Alberte 1985). This would help to explain the low chlorophyll *a* contents of *Synechococcus* sp. WH7803 compared to other phytoplankton species (Chl:C and chl:N, Table 4.5) and, subsequently, the relatively low chl:heme ratios calculated despite the low minimum heme *b* requirement previously described.

4.5.2 Implications of photosynthetic apparatus

Hemes are highly toxic if not associated with proteins when present in cells; thus, it can be assumed that measurements of heme *b* in marine organisms are predominantly associated within hemoprotein complexes (Tanaka and Tanaka 2007). As previously discussed (Chapter 1), heme and chlorophyll porphyrins are produced along the same biosynthetic pathway (Papenbrock and Grimm 2001, Cornah et al. 2003) and their production is regulated by ferrochelatase and magnesium chelatase, respectively (Vavilin and Vermaas 2002). Heme *b* is incorporated into cytochrome b_6f and PSII which forms the main pool of *b*-type hemoproteins connected with photosynthesis (see Table 4.7; Cramer et al. 2006, Nelson and Yocum 2006, Pospisil 2012) as well as cytochrome bc_1 and succinate dehydrogenase in respiration (Zhang et al. 1998, Cecchini et al. 2002, Yankovskaya et al. 2003). On the other hand, PSI and to a lesser extent PSII and cytochrome b_6f are linked with chlorophyll *a* (Nelson and Yocum 2006, Baniulis et al. 2008, Amunts et al. 2010). Changes in the abundance of heme *b* and the ratio of chl:heme will depend, to an extent, on *b*-type hemoprotein regulation within cells. The predominant function of chlorophyll *a* is harvesting light, as opposed to heme *b* which is typically prevalent in electron transport, exchange and catalysis. Therefore, comparison of cellular heme *b* and chlorophyll *a* contents (i.e. chl:heme ratios) could enable an estimation of photosynthetic components in specific marine organisms and, perhaps most importantly, provide subtle clues to physiological responses as a result of environmental change. However, further studies directly assessing the abundance of specific hemoproteins (e.g. cytochrome b_6f and PSII) is necessary in order to fully comprehend the impact of variations in intracellular heme *b* concentration.

	Photosynthetic Apparatus		
Complex	PSI	PSII	Cyt b_6f
Heme *b*	-	1[a]	2[b,c]
Chlorophyll *a*	96[d]	36[e]	1[b,c]
Ratio	n/a	36	0.5

Table 4.7. Number of heme *b* and chlorophyll *a* complexes in photosystem I (PSI), photosystem II (PSII) and cytochrome b_6f (Cyt b_6f) according to Pospisil (2012)[a], Baniulis et al. (2008)[b], Cramer et al. (2006)[c], Amunts et al. (2010)[d] and Nelson and Yocum (2006)[e]. Ratio of chlorophyll *a* to heme *b* complexes associated with PSII and cytochrome b_6f provided.

The relatively low chl:heme ratio observed in *Synechococcus* sp. WH7803 cultures compared to the eukaryotic phytoplankton suggests a tight regulation and maintenance of heme *b* content relative to chlorophyll *a*. It can also be assumed that this would be reflected in the ratio of heme *b* containing proteins (e.g. cytochromes b_6f and bc_1, PSII,

succinate dehdrogenase, catalase, nitrate reductase) to those associated primarily with chlorophyll *a* (PSI, PSII, light harvesting antenna). The relative proportions of PSI, PSII and cytochrome b_6f in different marine organisms are known to vary considerably. For example, oceanic and coastal diatoms manipulate iron requirements by altering their photosynthetic architecture (Strzepek and Harrison 2004), two strains of *E. huxleyi* employ photoacclimation strategies through alterations to their photosynthetic unit (Suggett et al. 2007) and changes in PSI/PSII stoichiometry in response to light intensity have been detected in *Synechocystis* PCC 6803 (Aizawa et al. 1992). Also, the quantity of trimeric PSI was significantly reduced in iron-deficient cells of *Synechococcus* sp. PCC 7942, which also promoted a protein 'supercomplex' linked to numerous chlorophyll molecules (Boekema et al. 2001, Bibby et al. 2001). Therefore, it is highly feasible that changes in chl:heme ratio are the result of physiological modification to an organism's photosynthetic apparatus related to sub-optimal growth conditions. It must also be considered that heme *b* is associated with respiratory processes, such as succinate dehydrogenase (1 heme *b* group) and cytochrome bc_1 (2 heme *b* groups), which do not incorporate chlorophyll *a* complexes.

4.5.3 Comparison of laboratory and field work

In general, the relationship between heme *b* and chlorophyll *a* concentration in laboratory cultures offered a good resemblance to field data (Fig. 4.20). The diatoms *T. oceanica* and *P. tricornutum* were analogous to *Synechococcus* sp. WH7803 in terms of chl:heme ratio and offered a similar contrast to the (sub-) tropical North Atlantic cruise data. Chlorophyll *a* content of *T. oceanica* and *P. tricornutum* cultures was reduced compared to the relatively conserved *b*-type hemoproteins; hence low chl:heme ratios were observed. However, the coccolithophorid *E. huxleyi* and the flagellate *D. tertiolecta* offered closer comparisons to the STNA (D346), particularly when grown under low iron concentrations. This would imply that the natural population decrease their heme *b* content in response to decreased iron and light availability, whilst subsequently increasing the chl:heme ratio; contradicting the strategy proposed by *Synechococcus* sp. WH7803 (as well as *T. oceanica* and *P. tricornutum*). The relatively high chl:heme ratios found in STNA were contrasting to laboratory cultures, but could imply the strategies employed by *E. huxleyi* and *D. tertiolecta* were most similar to the (sub-) tropical North Atlantic population. However, as the microbial community composition from the two cruises is unknown and, crucially, field samples measured all particles instead of a single monoculture, it is unreasonable to confirm such a conclusion at this time.

The cyanobacterial genera *Synechococcus* and *Prochlorococcus* are thought to dominate phytoplankton carbon biomass in the (sub-) tropical North Atlantic (70 - 90% along with small flagellates, Maranon et al. 2000). *Synechococcus* sp. WH7803 was originally

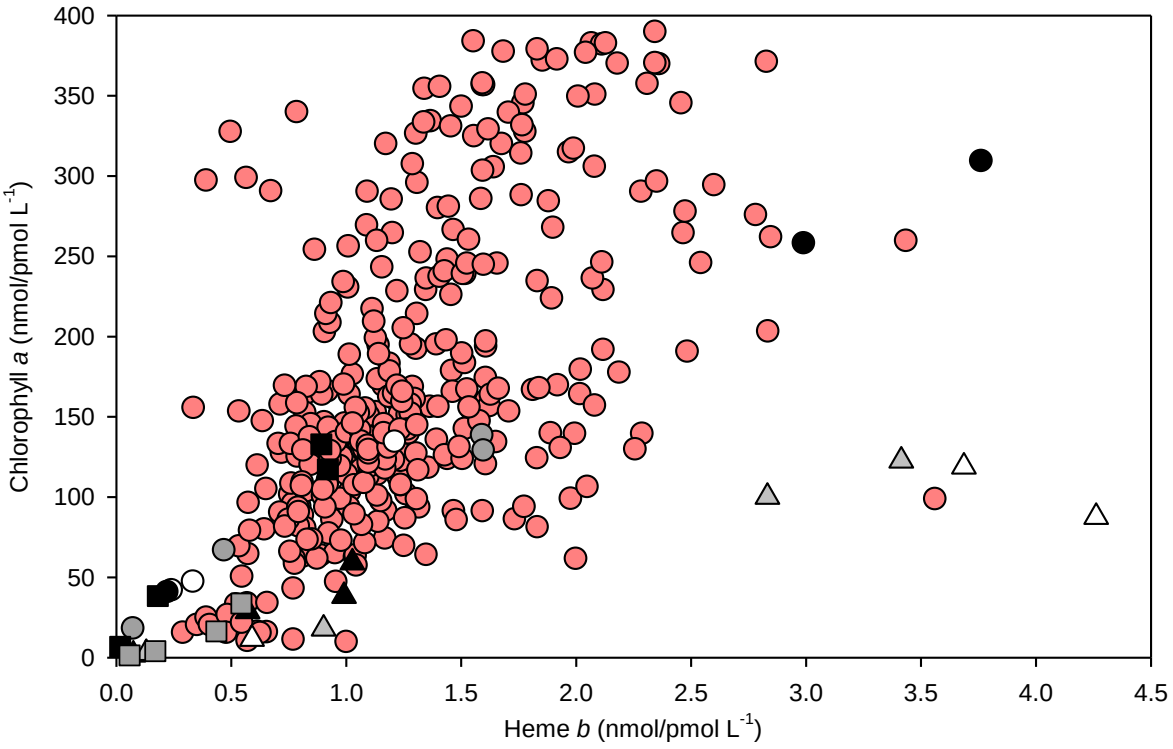

Figure 4.20. Heme *b* concentration (nmol L^{-1}) versus chlorophyll *a* concentration (nmol L^{-1}) determined for cultures of *Dunialella tertiolecta* (black circle), *Emiliania huxleyi* (grey circle), *Thalassiosira weissflogii* (white circle), *Thalassiosira oceanica* (black triangle), *Phaeodactylum tricornutum* (grey triangle) and *Synechococcus* sp. WH7803 (white triangle) grown under varying iron concentrations and high light conditions, and *E. huxleyi* (black square) and *T. oceanica* (grey square) grown under varying iron concentrations and low light conditions. Heme *b* and chlorophyll *a* concentrations (pmol L^{-1}) measured in the STNA (D346) are also presented (red circle).

isolated from the Sargasso Sea (approx 33.4 °N, 67.3 °W, Waterbury et al. 1986), slightly North of the D346 cruise transect (Fig. 2.3). However, chl:heme ratios of *Synechococcus* sp. WH7803 in the three iron concentrations investigated were lower compared to the five oceanographic regions of the STNA. In addition, the mean chl:heme ratio observed in the TNA (D361) was an order of magnitude greater than *Synechococcus* sp. WH7803 cultures. If the strategy for the production and/or maintenance of heme *b* content as previously described for low iron concentrations of *Synechococcus* sp. WH7803 was employed by organisms in the (sub-) tropical North Atlantic, it would imply that iron availability was very high in the region; certainly not iron limited. This was also supported by the low mean heme:C ratios of the two cruises (Fig. 4.14A) compared to iron-replete cultures of *Synechococcus* sp. WH7803. Mean heme:C ratios from the STNA (0.63 ± 0.38 µmol mol^{-1} C) and TNA (0.66 ± 0.62 µmol mol^{-1} C) were both less than the heme *b* requirement of *Synechococcus* sp. WH7803 and potentially five eukaryotic phytoplankton as well. Nevertheless, the apparent variation in heme *b* requirement between different species

should be taken into account. Organisms occupying the (sub-) tropical North Atlantic may exhibit very low heme *b* requirements and the species examined in the laboratory may not be completely representative, in particular *Synechococus* sp. WH7803 as was initially considered/hypothesised (section 4.2.2.3).

Variations in chl:heme ratio were high between different regions of the (sub-) tropical North Atlantic (see Chapter 3). In particular, the Coastal TNA offered a mean chl:heme ratio (M = 684 ± 624 mol mol^{-1}) far greater than the STNA (D346), as well as all six species investigated in the laboratory described here. The TNA exhibited similar heme *b* content and increased chlorophyll *a* content compared to the STNA; a similar trend behind the variation in chl:heme ratio of laboratory cultures. Despite the obvious discrepancy with *Synechococcus* sp. WH7803 cultures, the high chl:heme ratios of the TNA highlight the potential variability in cellular contents of heme *b* and chlorophyll *a*. Low light cultures of *E. huxleyi* displayed notably elevated chl:heme ratios compared to high light conditions, reaching a maximum ratio of 431 ± 4.53 mol mol^{-1} at the lowest iron concentration. Therefore, environmental conditions including iron and light availability (MacIntyre et al. 2002), as well as the phytoplankton community composition are likely to play a significant role in controlling heme *b* concentration in the marine environment.

4.6 Conclusions

Hemoproteins are fundamental components of PSII, cytochrome b_6f, cytochrome bc_1 and succinate dehydrogenase (Stewart and Brudvig 1998, Cecchini et al. 2002, Yankovskaya et al. 2003, Baniulis et al. 2008). Therefore, they are incorporated into numerous key metabolic processes including photosynthetic and respiratory electron transfer. This chapter investigated the influence of iron availability on the abundance of heme *b* in the unicellular cyanobacteria *Synechococcus* sp. WH7803, whilst making comparisons to five eukaryotic phytoplankton species and measurements from the (sub-) tropical North Atlantic. Low iron cultures of *Synechococcus* sp. WH7803 were iron stressed, as reflected by reduced growth rates and cell sizes. Cellular contents of both chlorophyll *a* and heme *b* were decreased when iron availability was low, with the mean chl:heme ratio also reduced. This would infer that *Synechococcus* sp. WH7803 employs a strategy to maintain heme *b* complexes and, therefore, *b*-type hemoproteins under iron limiting conditions relative to chlorophyll *a*. A heme *b* requirement of 1 - 1.5 µmol mol^{-1} C was established to facilitate maximum growth rates. Heme *b* concentrations below this threshold led to reduced maximum growth rates, as demonstrated by low iron cultures falling below this requisite and displaying reduced optimum growth rates. The development of a heme *b* requirement hypothesis provides a basic framework for which other organisms can compare, helping to determine physiological adaptations to iron availability in terms of photosynthetic apparatus.

Comparison of *Synechococcus* sp. WH7803 with *D. tertiolecta*, *E. huxleyi*, *T. weissflogii*, *T. oceanica* and *P. tricornutum* showed that, with the exception of *T. weissflogii,* phytoplankton cultures increased their cellular heme *b* content with increased iron availability. *Synechococcus* sp. WH7803 offered the lowest chl:heme ratio (35.9 ± 18.6 mol mol^{-1}) and *D. tertiolecta* the highest chl:heme ratio (84.4 ± 20.0 mol mol^{-1}) under iron replete conditions, although low light did lead to much elevated ratios in high iron *E. huxleyi* cultures (127 ± 3.73 mol mol^{-1}). Cultures of *T. oceanica* and *P. tricornutum* displayed a similar strategy to *Synechococcus* sp. WH7803 with regards to chl:heme ratio in iron limiting cultures, suggesting a maintenance of *b*-type hemoproteins at low iron concentrations. In contrast, *D. tertiolecta* and *E. huxleyi* cultures increased their chl:heme ratio in low iron conditions, suggesting *b*-type hemoproteins were less favourable or down regulated when iron stressed. The heme *b* requirement of *Synechococcus* sp. WH7803 was relatively low compared to the five eukaryotes, suggesting it does not provide a suitable match for all phytoplankton cultures. The (sub-) tropical North Atlantic provided increased chl:heme ratios compared to laboratory cultures. Low iron cultures of *E. huxleyi* (high and low light conditions) and *D. tertiolecta* showed the closest comparison to the STNA (D346) with regards to chl:heme ratio, but were still much reduced compared to the TNA (D361). Low heme:C ratios of the (sub-) tropical North Atlantic could imply that the population was iron stressed, despite the North Atlantic being considered a relatively iron-replete environment.

4.7 References

Aizawa, K., T. Shimizu, T. Hiyama, K. Satoh, Y. Nakamura, and Y. Fujita. 1992. Changes in composition of membrane proteins accompanying the regulation of PSI/PSII stoichiometry observed with *Synechocystis* PCC 6803. Photosynthesis Research **32**:131-138.

Amunts, A., H. Toporik, A. Borovikova, and N. Nelson. 2010. Structure determination and improved model of plant photosystem I. Journal of Biological Chemistry **285**:3478-3486.

Baniulis, D. E., E. Yamashita, Y. H. Zhang, S. S. Hasan, and W. A. Cramer. 2008. Structure-function of the cytochrome b_6f complex. Photochemistry and Photobiology:1349-1358.

Barber, J. and J. De Las Rivas. 1993. A functional model for the role of cytochrome b_{559} in the protection against donor and acceptor side photoinhibition. Proceedings of the National Academy of Sciences **90**:10942-10946.

Barlow, R. G. and R. S. Alberte. 1985. Photosynthetic characteristics of phycoerythrin-containing marine *Synechococcus* spp. Marine Biology **86**:63-74.

Bibby, T. S., J. Nield, and J. Barber. 2001. Iron deficiency induces the formation of an antenna ring around trimeric photosystem I in cyanobacteria. Nature 412: 743-745.

Boekema, E. J., A. Hifney, A. E. Yakushevska, M. Piotrowski, W. Keegstra, S. Berry, K.-P. Michel, E. K. Pistorius, and J. Kruip. 2001. A giant chlorophyll-protein complex induced by iron deficiency in cyanobacteria. Nature **412**:745-748.

Boyd, P. W. and M. J. Ellwood. 2010. The biogeochemical cycle of iron in the ocean. Nature Geoscience **3**:675-682.

Burda, K., J. Kruk, R. Borgstadt, J. Stanek, K. Strzalka, G. H. Schmid, and O. Kruse. 2003. Mossbauer studies of the non-heme iron and cytochrome b_{559} in a *Chlamydomonas reinhardtii* PSI^- mutant and their interactions with α-tocopherol quinone. Federation of European Biochemical Societies **535**:159-165.

Caughey, W. S. 1973. Iron porphyrins - hemes and hemins. Pages 797-831 *in* G. L. Eichham, editor. Inorganic biochemistry. Elsevier, Amsterdam.

Cecchini, G., I. Schroder, R. P. Gunsalus, and E. Maklashina. 2002. Succinate dehydrogenase and fumarate reductase from *Escherichia coli*. Biochimica et Biophysica Acta **1553**:140-157.

Chadd, H. E., I. R. Joint, N. H. Mann, and N. G. Carr. 1996. The marine picoplankter *Synechococcus* sp. WH7803 exhibits an adaptive response to restricted iron availability. FEMS Microbiology Ecology **21**:69-76.

Chapman, S. K., S. Daff, and A. W. Munro. 1997. Heme: The most versatile redox centre in biology? Metal Sites in Proteins and Models. Structure and Bonding **88**:39-70.

Cornah, J. E., M. J. Terry, and A. G. Smith. 2003. Green or red: what stops the traffic in the tetrapyrrole pathway? TRENDS in Plant Science **8**:224-230.

Cramer, W. A., G. M. Soriano, M. Ponomarev, D. Huang, H. Zhang, S. E. Martinez, and J. L. Smith. 1996. Some new structural aspects and old controversies concerning the cytochrome b_6f complex of oxygenic photosynthesis. Annual Review of Plant Physiology and Plant Molecular Biology **47**:477-508.

Cramer, W. A., H. Zhang, J. Yan, G. Kurisu, and J. L. Smith. 2006. Transmembrane traffic in the cytochrome b_6f complex. Annual Review of Biochemistry **75**:769-790.

Ferris, M. J. and B. Palenik. 1998. Niche adaptation in ocean cyanobacteria. Nature **396**:226-228.

Gledhill, M. 2007. The determination of heme b in marine phyto- and bacterioplankton. Marine Chemistry **103**:393-403.

Honey, D. J., M. Gledhill, T. S. Bibby, F-E. Legiret, N. J. Pratt, A. E. Hickman, T. Lawson, and E. P. Achterberg. 2013. Heme *b* in marine phytoplankton and particulate material from the North Atlantic Ocean. Marine Ecology Progress Series **483**: 1-17.

Johnson, P. W. and J. M. Sieburth. 1979. Chroococcoid cyanobacteria in the sea: a ubiquitous and diverse phototrophic biomass. Limnology and Oceanography **24**:928-935.

Kurisu, G., H. Zhang, J. L. Smith, and W. A. Cramer. 2003. Structure of the cytochrome b_6f complex of oxygenic photosynthesis: Tuning the cavity. Science **302**:1009-1014.

Lemberg, R. and J. Barrett. 1973. Cytochromes. Academic Press Inc. Ltd, London.

Liu, H., R. R. Bidigare, E. Laws, M. R. Landry, and L. Campbell. 1999. Cell cycle and physiological characteristics of *Synechococcus* (WH7803) in chemostat culture. Marine Ecology Progress Series **189**:17-25.

MacIntyre, H. L., T. M. Kana, T. Anning, and R. J. Geider. 2002. Photoacclimation of photosynthesis irradiance response curves and photosynthetic pigments in microalgae and cyanobacteria. Journal of Phycology **38**:17-38.

Maranon, E., P. M. Holligan, M. Varela, B. Mourino, and A. J. Bale. 2000. Basin-scale variability of phytoplankton biomass, production and growth in the Atlantic Ocean. Deep-Sea Research I **47**:825-857.

Martin, J. H. and S. E. Fitzwater. 1988. Iron deficiency limits phytoplankton growth in the North-east Pacific Subarctic. Nature **331**:341-343.

Martin, J. H., R. M. Gordon, and S. E. Fitzwater. 1991. The case for iron. Limnology and Oceanography **36**:1793-1802.

Mochizuki, N., R. Tanaka, B. Grimm, T. Masuda, M. Moulin, A. G. Smith, A. Tanaka, and M. J. Terry. 2010. The cell biology of tetrapyrroles: a life and death struggle. TRENDS in Plant Science **15**:488-498.

Morel, A., Y.-H. Ahn, F. Partensky, D. Vaulot, and H. Claustre. 1993. *Prochlorococcus* and *Synechococcus*: A comparative study of their optical properties in relation to their size and pigmentation. Journal of Marine Research **51**:617-649.

Nelson, N. and C. F. Yocum. 2006. Structure and function of photosystems I and II. Annual Review of Plant Biology **57**:521-565.

Papenbrock, J. and B. Grimm. 2001. Regulatory network of tetrapyrrole biosynthesis - studies of intracellular signalling involved in metabolic and developmental control of plastids. Planta **213**:667-681.

Park, Y.-I., S. Sandstrom, P. Gustafsson, and G. Oquist. 1999. Expression of the *isiA* gene is essential for the survival of the cyanobacterium *Synechococcus* sp. PCC 7942 by protecting photosystem II from excess light under iron limitation. Molecular Microbiology **32**:123-129.

Partensky, F., J. Blanchot, and D. Vaulot. 1999. Differential distribution and ecology of Prochlorococcus and Synechococcus in oceanic waters: a review. Pages 457-475 *in* L. Charpy and A. W. D. Larkum, editors. Marine cyanobacteria. Bulletin de l'Institut oceanographique, Monaco.

Platt, T., D. V. S. Rao, and B. Irwin. 1983. Photosynthesis of picoplankton in the oligotrophic ocean. Nature **301**:702-704.

Pospisil, P. 2012. Enzymatic function of cytochrome b_{559} in photosystem II. Journal of Photochemistry and Photobiology B: Biology **104**:341-347.

Rabinowitch, E. and Govindjee. 1969. Photosynthesis. Wiley, New York.

Rivers, A. R., R. W. Jakuba, and E. A. Webb. 2009. Iron stress genes in marine *Synechococcus* and the development of a flow cytometric iron stress assay. Environmental Microbiology **11**:382-396.

Scanlan, D. 2001. Cyanobacteria: ecology, niche adaptation and genomics. Microbiology Today **28**:128-130.

Scanlan, D. J. and N. J. West. 2002. Molecular ecology of the marine cyanobacterial genera *Prochlorococcus* and *Synechococcus*. FEMS Microbiology Ecology **40**:1-12.

Stanier, R. Y. and G. Cohen-Bazire. 1977. Phototrophic prokaryotes: the cyanobacteria. Annual Review of Microbiology **31**:225-274.

Stewart, D. H. and G. W. Brudvig. 1998. Cytochrome b_{559} of photosystem II. Biochimica et Biophysica Acta **1367**:63-87.

Strzepek, R. F. and P. J. Harrison. 2004. Photosynthetic architecture differs in coastal and oceanic diatoms. Nature **431**:689-692.

Suggett, D. J., E. Le Floc'H, G. N. Harris, N. Leonardos, and R. J. Geider. 2007. Different strategies of photoacclimation by two strains of *Emiliania huxleyi* (Haptophyta). Journal of Phycology **43**:1209-1222.

Tanaka, R. and A. Tanaka. 2007. Tetrapyrrole biosynthesis in higher plants. Annual Review of Plant Biology **58**:321-346.

Vavilin, D. V. and W. F. J. Vermaas. 2002. Regulation of the tetrapyrrole biosynthetic pathway leading to heme and chlorophyll in plants and cyanobacteria. Physiologia Plantarum **115**:9-24.

Verity, P. G., R. C. Y., C. R. Tronzo, M. G. Andrews, J. R. Nelson, and M. E. Sieracki. 1992. Relationships between cell volume and the carbon and nitrogen content of marine photosynthetic nanoplankton. Limnology and Oceanography **37**:1434-1446.

Waterbury, J. B., S. W. Watson, R. R. Guillard, and L. E. Brand. 1979. Widespread occurence of a unicellular, marine, planktonic, cyanobacterium. Nature **277**:293-294.

Waterbury, J. B., S. W. Watson, F. W. Valois, and D. G. Franks. 1986. Biological and ecological characterization of the marine unicellular cyanobacterium *Synechococcus*. Canadian Bulletin of Fisheries and Aquatic Sciences **214**:71-120.

Webb, E. A., J. W. Moffett, and J. B. Waterbury. 2001. Iron stress in open-ocean cyanobacteria (*Synechococcus*, *Trichodesmium*, and *Crocosphaera* spp.): Idenitification of the IdiA protein. Applied and Environmental Microbiology **67**:5444-5452.

Whitmarsh, J. and H. B. Pakrasi. 1996. Form and function of cytochrome *b*-559. Pages 249-264 *in* D. R. Ort, C. F. Yocum, and I. F. Heichel, editors. Oxygenic Photosynthesis: The Light Reactions. Kluwer Academic Publishers.

Wilhelm, S. W., D. P. Maxwell, and C. G. Trick. 1996. Growth, iron requirements, and siderophore production in iron-limited *Synechococcus* PCC 7002. Limnology and Oceanography **41**:89-97.

Wilson, W. H., N. G. Carr, and N. H. Mann. 1996. The effect of phosphate status on the kinetics of cyanophage infection in the oceanic cyanobacterium *Synechococcus* sp. WH7803. Journal of Phycology **32**:506-516.

Yankovskaya, V., R. Horsefield, S. Tornroth, C. Luna-Chavez, H. Miyoshi, C. Leger, B. Byrne, G. Cecchini, and S. Iwata. 2003. Architecture of succinate dehydrogenase and reactive oxygen species generation. Science **299**:700-704.

Zhang, Z., L. Huang, V. M. Shulmeister, Y.-I. Chi, K. K. Kim, L.-W. Hung, A. R. Crofts, E. A. Berry, and S.-H. Kim. 1998. Electron transfer by domain movement in cytochrome *bc*1. Nature **392**:677-684.

Zwirglmaier, K., L. Jardillier, M. Ostrowski, S. Mazard, L. Garczarek, D. Vaulot, F. Not, R. Massana, O. Ulloa, and D. J. Scanlan. 2008. Global phylogeography of marine *Synechococcus* and *Prochlorococcus* reveals a distinct partitioning of lineages among oceanic biomes. Environmental Microbiology **10**:147-161.

Chapter 5

Heme *b* and nitrogen fixation rates in laboratory marine diazotroph cultures and the (sub-) tropical North Atlantic

5.1 Abstract

Diazotrophs are a specialised group of organisms capable of undertaking nitrogen fixation to produce biologically accessible forms of nitrogen from atmospheric dinitrogen (N_2). The enzyme responsible for nitrogen fixation, nitrogenase, is comprised of iron-rich proteins which do not include heme complexes. This chapter investigates the abundance of heme *b* and rates of nitrogen fixation in two marine diazotrophs; *Crocosphaera watsonii* (WH8501) and *Trichodesmium erythraeum* (IMS101). Batch cultures of *Crocosphaera* and *Trichodesmium* were subjected to variations in iron concentration between 0 and 120 nmol L^{-1} total iron (Fe_T) and sampled for heme *b*, chlorophyll *a*, particulate organic carbon (POC) and particulate organic nitrogen (PON) concentration, as well as biophysical measurements (F_v/F_m) and nitrogen fixation rates. Growth rates and F_v/F_m decreased with decreasing iron concentration for both species, although μ_{max} was only significantly reduced in *Crocosphaera* cultures with no added iron. Heme *b* contents of *Crocosphaera* cultures were similar to the previously studied non-diazotrophic unicellular cyanobacteria *Synechococcus* sp. WH7803, whereas *Trichodesmium* showed very low heme *b* content throughout the different iron treatments (<0.2 μmol mol^{-1} C). Chlorophyll *a* to heme *b* ratios (chl:heme) of the two diazotrophs were elevated compared to *Synechococcus* sp. WH7803 and five eukaryotic phytoplankton. Nitrogen fixation of *Crocosphaera* and *Trichodesmium* increased with iron availability, with the latter demonstrating higher rates. *Crocosphaera* are considered to employ a strategy to reduce their iron requirement by degrading photosynthetic (night) and nitrogen fixation (day) proteins when not in use. In contrast, it was proposed that *Trichodesmium* possess a relatively low quantity of *b*-type hemoproteins as available iron was primarily allocated to nitrogenase and photosystem I. Nitrogen fixation rates and heme *b* abundance were also reported from the (sub-) tropical North Atlantic; a region known to exhibit high rates of nitrogen fixation. Evidence is presented suggesting heme *b* concentrations were reduced in areas of high nitrogen fixation and *Trichodesmium* abundance, and vice versa.

5.2 Introduction

Nitrogen fixation is an important component of the nitrogen cycle, creating biogeochemically fixed forms of nitrogen which are available for incorporation into living organisms, including those in the marine community (Carpenter and Capone 2008). A great deal of progress has been made since the late 1970s (e.g. Wada and Hattori 1976, Delwiche et al. 1979) with regards to the marine nitrogen cycle and the potential global influences of marine nitrogen fixation (see review by Mahaffey et al. 2005). The term diazotroph refers to an exclusive group of organisms that are able to fix gaseous dinitrogen (N_2) into biologically available forms of nitrogen (i.e. ammonia). Importantly, this means that diazotrophs are able to grow without an external source of fixed nitrogen, whilst also providing additional nitrogen to the surrounding biological community. Consequently, the production of new nitrogen by marine diazotrophs has become increasingly important as nitrogen is the proximal limiting nutrient in many open ocean oligotrophic regions (Capone et al. 2005, La Roche and Breitbarth 2005, Montoya et al. 2007, Landrum et al. 2011). In comparison to non-nitrogen fixers, a high iron demand is thought to accompany an organism's ability to fix nitrogen due to the enzyme responsible for the process, nitrogenase, which requires 19 iron atoms per monomer (Falkowski 1997, Schindelin et al. 1997, Berman-Frank et al. 2001a, Shi et al. 2007). This has led to speculation that iron exerts a further limiting stress on the productivity of diazotrophs compared to non-diazotrophic organisms (Kustka et al. 2003a, Tuit et al. 2004). Heme complexes are not directly incorporated into the nitrogenase apparatus; instead the nitrogenase complex consists of iron-sulphur (nitrogenase reductase) and iron-molybdenum (dinitrogen reductase) proteins (Berges and Mulholland 2008). The nitrogenase enzyme complex requires both proteins to function, catalysing the energetically costly reaction to break the strong triple bond between the two nitrogen atoms of N_2 (Karl et al. 2002).

The filamentous cyanobacteria *Trichodesmium* is the most commonly studied genus of marine diazotroph and can form large blooms when conditions are favourable (Capone et al. 1997). *Trichodesmium* blooms are often ephemeral in nature, but developments in remote sensing techniques have enabled scientists to view these expansive formations from space (Subramaniam et al. 2002, Capone and Subramaniam 2005). As well as long individual strands of cells (trichomes), *Trichodesmium* can also form radial (spherical clumps) or fusiform (aligned trichome tufts) colonies (Capone et al. 1997). The causal factors for colony formation are unknown, although it has been suggested to result from an oxidation defence method to protect the nitrogenase enzyme (Mulholland and Capone 2000). It has also been found that diazotrophic diatom associations (Poulton et al. 2009) and unicellular bacterioplankton (Falcón et al. 2004), including those from the genus *Crocosphaera*, contribute towards the pool of biologically accessible nitrogen via marine

nitrogen fixation. Furthermore, despite previous reservations, these unicellular diazotrophs are potentially of equal importance to the well-documented *Trichodesmium* genus (Zehr et al. 2001, Montoya et al. 2004). The distribution of *Trichodesmium* is thought to be reasonably ubiquitous in the oligotrophic (sub-) tropics, characterised by low nutrients and very clear waters with deep light penetration (Capone et al. 1997; see Fig. 5.1). They play a critical role in the cycling of carbon and nitrogen in the tropical North Atlantic and could be even more influential than the picoplanktonic community (<2 µm), including *Synechococcus*, regarding productivity and carbon fixation in these regions (Carpenter and Romans 1991). A large degree of phylogenetic diversity has been reported from the tropical Atlantic Ocean using the *nifH* gene which encodes for the iron protein of the nitrogenase enzyme (Goebel et al. 2010). Langlois et al. (2005) described the distribution of filamentous (e.g. *Trichodesmium*) and non-filamentous (e.g. *Crocosphaera*) species in the subtropical and tropical Atlantic Ocean using gene expression techniques, whilst highlighting possible physiological influences upon their range such as water temperature; filamentous *nifH* sequences were typically present in warmer waters (>26 °C), whereas non-filamentous *nifH* sequences were found throughout a wider range of temperatures, but predominantly in relatively cooler waters (<26 °C).

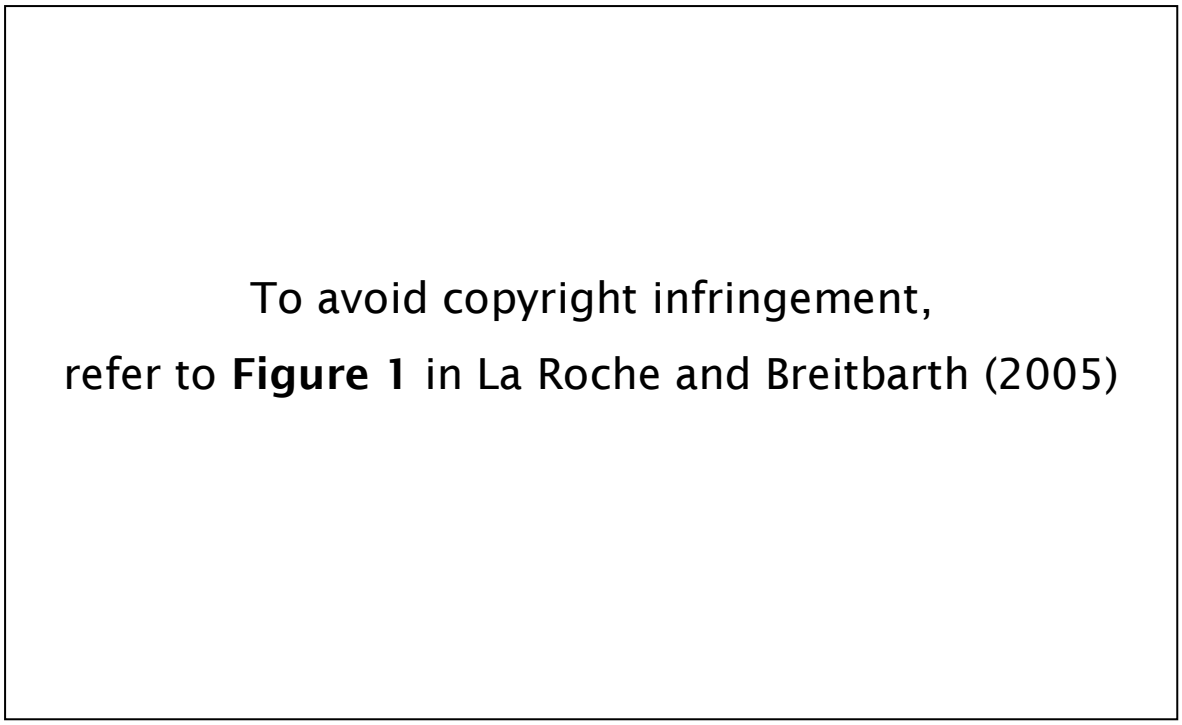

Figure 5.1. Distribution (not abundance) of *Trichodesmium* in the global ocean compiled by La Roche and Breitbarth (2005). Red dots indicate locations whereby nitrogen fixation by *Trichodesmium* is likely to occur. Pink dotted lines indicate the annual mean 20 °C surface seawater temperature isotherm. Blue dots indicate locations of *Trichodesmium* that are unlikely to fix nitrogen. Note the plot only signifies sampling locations and does not represent the complete distribution of *Trichodesmium*.

Diazotrophs respire and photosynthesise similar to other cyanobacterial organisms, whilst also fulfilling their niche role of fixing nitrogen (Fig. 5.2). Despite receiving a lot of attention surrounding their nitrogen fixation abilities, diazotrophs still possess *b*-type hemoproteins such as those incorporated into photosystem II (PSII) and cytochrome b_6f of the photosynthetic apparatus (Cramer et al. 2006, Baniulis et al. 2008, Pospisil 2012, Richier et al. 2012). It should be noted that cytochrome b_6f also functions in the respiratory electron transport chain of cyanophytes (Vermaas 2001). Therefore, diazotrophs are likely to impose strict regulations upon iron usage to enable nitrogen fixation (nitrogenase) and other key metabolic functions (i.e. hemoproteins amongst other iron uses) to co-occur, especially when iron is limited (Küpper et al. 2008). Using laboratory cultures of *Crocosphaera* and *Trichodesmium*, this chapter investigates the influence of iron availability on the abundance of heme *b* and nitrogen fixation rates in marine diazotrophs. With iron concentrations present at low levels even when not considered limiting in the natural marine environment, it is likely that diazotrophic organisms will demonstrate physiological responses to iron availability through measurements closely linked to iron (e.g. *b*-type hemoproteins and nitrogen fixation).

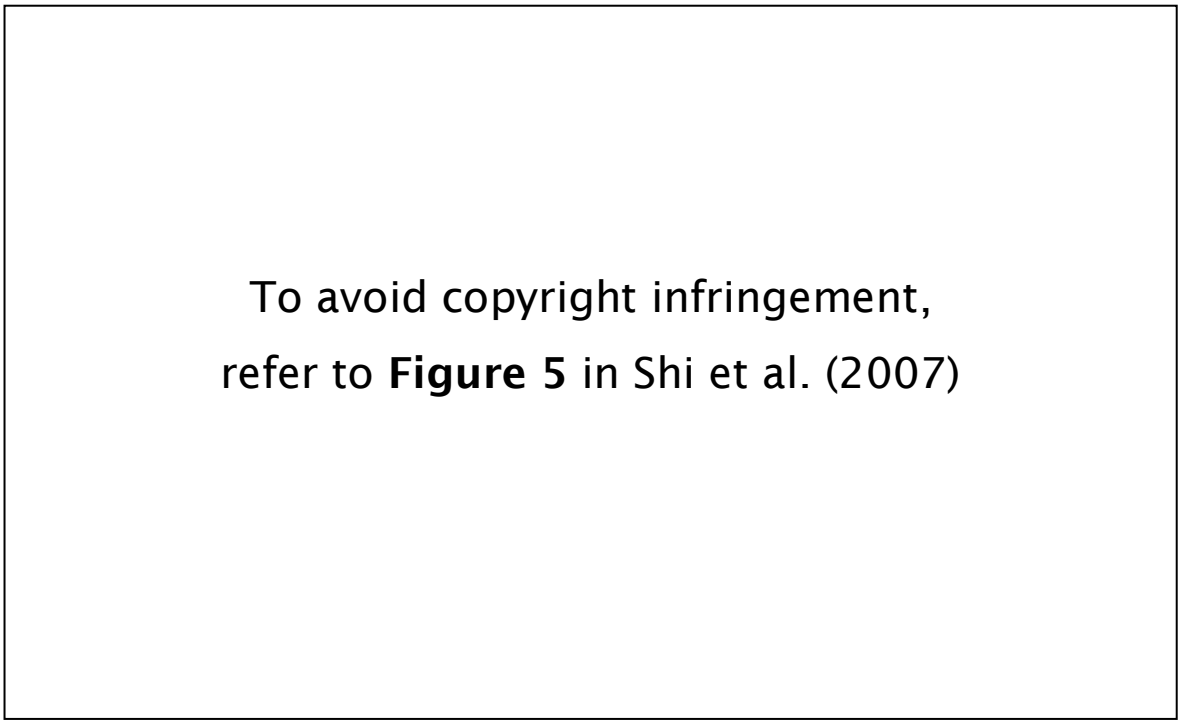

Figure 5.2. Schematic diagram of the effects of iron limitation in *Trichodesmium erythraeum* (IMS101) incorporating electron transport along photosynthetic, respiratory, nitrogen and carbon fixation and Mehler reaction pathways, whereby red and blue arrows indicate electron and proton transport, respectively. Block arrows indicate increased cyclic electron transfer around PSI and decreased linear electron transport (PSII → Cyt b_6f → PSI) and nitrogen fixation. Annotation of the Mehler reaction includes superoxide dismutase (SOD) and ascorbate peroxidase (APX). Figure from Shi et al. (2007).

A relatively high nitrate to phosphate ratio in surface waters of the (sub-) tropical North Atlantic (Michaels et al. 1996, Gruber and Sarmiento 1997) suggests an excess of nitrate (>16:1) with respect to Redfield's ratio (Redfield 1934). This characteristic is often deemed to signify nitrogen fixation activity, whereby increased levels of new reactive (fixed) nitrogen have been generated (Karl et al. 1997, Hansell and Follows 2008). Consequently, the (sub-) tropical North Atlantic provides the ideal location to investigate nitrogen fixation rates (Mahaffey et al. 2003, Sohm et al. 2011), which is further enhanced given that populations of *Trichodesmium* are known to thrive in the region (Carpenter and Romans 1991, Capone et al. 1997, Capone et al. 2005). Nitrogen fixation rates and heme *b* abundances measured during the research cruises D346 (Jan - Feb 2010) and D361 (Feb - Mar 2011) in the (sub-) tropical North Atlantic (see Chapter 3) were used as a comparison to laboratory cultures of *Crocosphaera watsonii* (WH8501) and *Trichodesmium erythraeum* (IMS101). Furthermore, studies upon the unicellular cyanobacteria *Synechococcus* sp. WH7803 provided a non-diazotrophic comparison (see Chapter 4).

5.2.1 Aims and objectives

Adaptations to iron limitation in marine diazotrophs typically focus upon nitrogen fixation rates and the iron-rich non-heme nitrogenase enzyme complex. The aim of this project was to assess the effect of iron limitation on heme *b* abundance as hemes represent a further important iron protein pool in diazotrophs. Furthermore, the potential relationship between heme *b* concentration and nitrogen fixation in marine diazotrophs were investigated through investigations of laboratory grown cultures of *Crocosphaera watsonii* and *Trichodesmium erythraeum* and comparison to measurements collected in the field and non-diazotrophic cultures. Therefore, the specific objectives of this chapter were:

5.2.1.1 To provide the first assessment of heme *b* abundance in laboratory cultures of the marine diazotrophs *Crocosphaera watsonii* and *Trichodesmium erythraeum*.

5.2.1.2 To determine the influence of iron availability on the abundance of heme *b* and the rates of nitrogen fixation in laboratory cultures of marine diazotrophs.

5.2.1.3 To determine the relationship between heme *b* abundance and nitrogen fixation rates in laboratory cultures of marine diazotrophs.

5.2.1.4 To establish whether any relationships between heme *b* abundance and nitrogen fixation rates in laboratory cultures are reflected in the marine environment, specifically the (sub-) tropical North Atlantic.

5.2.2 Hypotheses

The following hypotheses were developed to test the previously described objectives:

5.2.2.1 The concentration of heme *b* per cell or per unit biovolume will be lower in laboratory cultures of *Crocosphaera watsonii* and *Trichodesmium erythraeum* compared to *Synechococcus* sp. WH7803 and other eukaryotic phytoplankton as marine diazotrophs possess a relatively greater iron requirement for their nitrogen fixation apparatus, which is not associated with heme *b*.

5.2.2.2 Heme *b* content will decrease with decreasing iron availability in laboratory cultures of marine diazotrophs, similar to previously studied cultures of *Synechococcus* sp. WH7803 and eukaryotic phytoplankton. Nitrogen fixation rates will also decrease with decreasing iron concentration as previously reported (e.g. Paerl et al. 1987, Berman-Frank et al. 2001a, Fu and Bell 2003, Richier et al. 2012).

5.2.2.3 A positive correlation will be found between heme *b* content (*b*-type hemoproteins) and nitrogen fixation rates in cultures of *Crocosphaera* and *Trichodesmium* as both will change proportionately with iron availability.

5.2.2.4 Decreased nitrogen fixation rates will be reflected by decreased heme *b* concentrations in the (sub-) tropical North Atlantic, providing an indication of low iron availability.

5.3 Methods

The marine diazotrophs *Crocosphaera watsonii* (WH8501) and *Trichodesmium erythraeum* (IMS101) were grown at six different total iron concentrations (Fe_T = 0, 4, 10, 20, 40 and 120 nmol L^{-1}) in YBC-II medium (section 2.2.2, Chen et al. 1996). Batch cultures were vacuum filtered (section 2.2.4) onto glass microfibre filters (GF/Fs, MF300, Fisher Scientific, 0.7 µm) for the determination of heme *b* concentration (10 – 40 ml, section 2.4) on day 8 of the growth cycle (during the exponential phase). Concurrent samples for the determination of chlorophyll *a* (10 ml, section 2.5), particulate organic carbon (POC) and particulate organic nitrogen (PON, 10 – 40 ml, section 2.6) were also vacuum filtered onto GF/Fs, although POC/N filters were ashed (450 °C, 12 hours) prior to use. Cell number, cell diameter and total biovolume of *Crocosphaera* cultures were determined using a Beckman Coulter counter with 70 µm aperture, whereas trichome number and length were determined using light microscopy for *Trichodesmium* cultures (section 2.2.5). *Trichodesmium* biovolume was calculated under the assumption that trichomes form an elongated cylindrical morphology ($0.25\pi W^2 L$; where W = width (µm) and L = length (µm), Suzuki et al. 2007). The maximum quantum yield of PSII (F_v/F_m) and

the effective absorbance cross-section of PSII (σ_{PSII}) were determined using fast repetition rate fluorometry (FRRF, section 2.8). Nitrogen fixation rates from laboratory cultures of *Crocosphaera* and *Trichodesmium* grown under all six iron concentrations were measured during the exponential growth phase (section 2.7.2). In addition, nitrogen fixation rates from the (sub-) tropical North Atlantic were obtained during research cruises D346 and D361 (section 2.7.1).

5.4 Results

Data collected from experiments on *Crocosphaera* and *Trichodesmium* are described first, followed by field data from the (sub-) tropical North Atlantic. Values are typically described as the mean ± standard deviation and line graphs represent the mean with standard deviation error bars, unless otherwise stated. Plots are offset from days 0, 2, 4, 6 and 8 to improve clarity of standard deviation.

5.4.1 Growth, carbon, nitrogen and photosynthetic efficiency

The number of *Crocosphaera* cells and the number of trichomes (filaments) in *Trichodesmium* cultures increased throughout each 8-day growth cycle at all iron concentrations (Fig. 5.3). The highest final number of cells for *Crocosphaera* cultures was measured at 40 nmol L^{-1} Fe_T (i.e. day 8, $M = 1.33 \times 10^6$ ml^{-1}, Fig. 5.3A). Statistical analysis suggested there was a significant difference in final cell number between the six different iron concentrations examined ($H_{(5)} = 24.631$, $N = 36$, $p < 0.01$) and specifically between cultures with no added iron and the highest iron treatment (120 nmol L^{-1} Fe_T, Table 5.1). Similar to the trend in *Crocosphaera*, the highest final number of trichomes was observed in 40 nmol L^{-1} Fe_T cultures of *Trichodesmium* (1828 ± 244 ml^{-1}); more than three-times greater in comparison to cultures with no added iron (501 ± 183 ml^{-1}, Fig. 5.3B). A Kruskal-Wallis test suggested there were significant differences in the final number of trichomes between the different iron regimes ($H_{(5)} = 25.808$, $N = 36$, $p < 0.01$) and Mann-Whitney *U* tests found the number of trichomes in 120 nmol L^{-1} Fe_T cultures were significantly different to cultures with no added iron at the end of each experimental growth cycle (Table 5.1).

Species / Treatment	Diameter / Length (µm)	Biovolume (µm^3 ml^{-1})	Growth Rate (µ d^{-1})	μ_{max} (d^{-1})	Carbon (mol C L^{-1})	Nitrogen (mol N L^{-1})	F_v/F_m	σ_{PSII}
Crocosphaera watsonii								
0 nmol L^{-1} Fe_T	3.40 ± 0.10**	1.0x10^7 ± 1.6x10^6**	0.29 ± 0.10**	0.39 ± 0.05*	19.6 ± 3.5	3.07 ± 0.4	0.37 ± 0.02**	1.05 ± 0.06*
4 nmol L^{-1} Fe_T	3.38 ± 0.09**	1.9x10^7 ± 0.5x10^6	0.35 ± 0.17	0.51 ± 0.08	19.2 ± 2.6	2.51 ± 0.4	0.41 ± 0.02**	1.01 ± 0.03**
10 nmol L^{-1} Fe_T	3.26 ± 0.09	2.1x10^7 ± 3.0x10^6	0.36 ± 0.11	0.50 ± 0.08	18.6 ± 2.5	2.76 ± 0.4	0.46 ± 0.01**	1.03 ± 0.03**
20 nmol L^{-1} Fe_T	3.29 ± 0.09	2.3x10^7 ± 6.4x10^6	0.37 ± 0.10	0.46 ± 0.03	21.0 ± 5.2	2.77 ± 0.4	0.50 ± 0.02**	1.08 ± 0.01
40 nmol L^{-1} Fe_T	3.25 ± 0.11	2.6x10^7 ± 4.2x10^6	0.39 ± 0.10	0.48 ± 0.03	19.5 ± 1.6	2.53 ± 0.3	0.51 ± 0.01**	1.07 ± 0.01*
120 nmol L^{-1} Fe_T	3.22 ± 0.15	2.2x10^7 ± 4.1x10^6	0.36 ± 0.10	0.46 ± 0.04	21.3 ± 3.8	2.77 ± 0.3	0.52 ± 0.01	1.10 ± 0.02
Trichodesmium erythraeum								
0 nmol L^{-1} Fe_T	619 ± 113**	2.5x10^7 ± 6.1x10^6	0.28 ± 0.06*	0.59 ± 0.07	8.63 ± 2.0**	1.37 ± 0.2**	0.43 ± 0.05*	0.44 ± 0.02
4 nmol L^{-1} Fe_T	496 ± 88.9**	3.5x10^7 ± 7.8x10^6	0.33 ± 0.04*	0.56 ± 0.11	10.3 ± 3.3	1.51 ± 0.4*	0.44 ± 0.04**	0.42 ± 0.02*
10 nmol L^{-1} Fe_T	388 ± 66.3	3.1x10^7 ± 1.1x10^7	0.35 ± 0.04	0.58 ± 0.09	10.7 ± 2.4	1.76 ± 0.4	0.50 ± 0.02	0.43 ± 0.02
20 nmol L^{-1} Fe_T	313 ± 49.4	3.2x10^7 ± 1.3x10^7	0.42 ± 0.04	0.65 ± 0.10	10.4 ± 2.0*	1.70 ± 0.4	0.53 ± 0.02	0.45 ± 0.01
40 nmol L^{-1} Fe_T	339 ± 50.3	5.2x10^7 ± 8.9x10^6	0.40 ± 0.03	0.65 ± 0.11	10.3 ± 1.5*	1.59 ± 0.2**	0.54 ± 0.01*	0.44 ± 0.01
120 nmol L^{-1} Fe_T	335 ± 32.7	3.4x10^7 ± 9.9x10^6	0.39 ± 0.06	0.56 ± 0.07	13.0 ± 0.9	2.06 ± 0.2	0.51 ± 0.01	0.45 ± 0.01

Table 5.1. Cell diameter / trichome length (µm), total biovolume (µm^3 ml^{-1}), growth rate (biovolume d^{-1}), maximum growth rate (μ_{max}), particulate organic carbon (POC) and particulate organic nitrogen (PON) content per unit biovolume (mol L^{-1}), maximum quantum yield of PSII (F_v/F_m) and the effective absorbance cross-section of PSII (σ_{PSII}) determined for *Crocosphaera watsonii* (WH8501) and *Trichodesmium erythraeum* (IMS101) cultures grown under varying total iron concentration (nmol L^{-1} Fe_T). Cell diameter / trichome length and growth rate measurements averaged (mean) from the complete 8-day growth cycle. Total biovolume, carbon and nitrogen contents and fluorometry measurements averaged (mean) from day 8 only. Significant differences relative to the highest iron concentration (120 nmol L^{-1} Fe_T) represented by ** where $p < 0.01$ and * where $p < 0.05$ (Mann-Whitney *U* test).

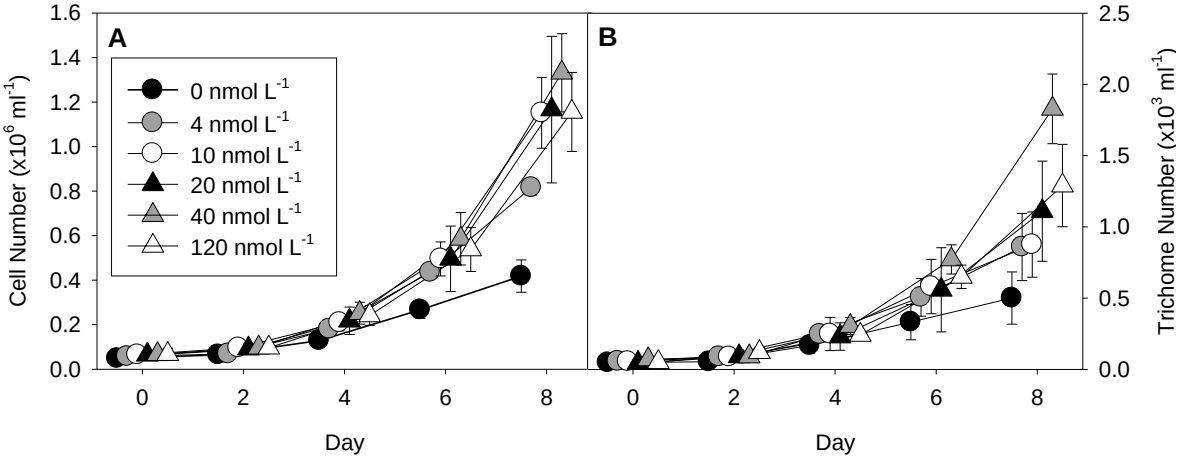

Figure 5.3. (**A**) Cell number (ml^{-1}) of *Crocosphaera watsonii* cultures and (**B**) trichome number (ml^{-1}) of *Trichodesmium erythraeum* cultures grown under varying total iron concentration: 0 nmol L^{-1} Fe$_T$ (black circle), 4 nmol L^{-1} Fe$_T$ (grey circle), 10 nmol L^{-1} Fe$_T$ (white circle), 20 nmol L^{-1} Fe$_T$ (black triangle), 40 nmol L^{-1} Fe$_T$ (grey triangle) and 120 nmol L^{-1} Fe$_T$ (white triangle).

The mean diameter of *Crocosphaera* cells increased with decreasing iron concentration (Fig. 5.4A) and a significant difference was observed between the highest and the lowest iron treatments (Table 5.1). A similar trend was observed with regards to the length of *Trichodesmium* trichomes, which also increased as the total iron concentration decreased (Fig. 5.4B). *Trichodesmium* cultures grown with no added iron exhibited the longest mean trichome length at 619 ± 113 µm; twice the length of trichomes measured in 20 nmol L^{-1} Fe$_T$ (313 ± 49.4 µm). The two lowest iron concentrations (0 and 4 nmol L^{-1} Fe$_T$) were significantly different in trichome length compared to the highest iron concentration (Table 5.1). However, no distinct pattern in cell diameter or trichome length was observed during the 8-day growth cycle for either *Crocosphaera* or *Trichodesmium* cultures, unlike *Synechococcus* sp. WH7803 which displayed an increase in cell diameter post-subculture (see Fig. 4.3). Nevertheless, *Trichodesmium* cultures typically displayed a higher mean trichome length on days 0 and 8, which could be indicative of cells not dividing during these periods.

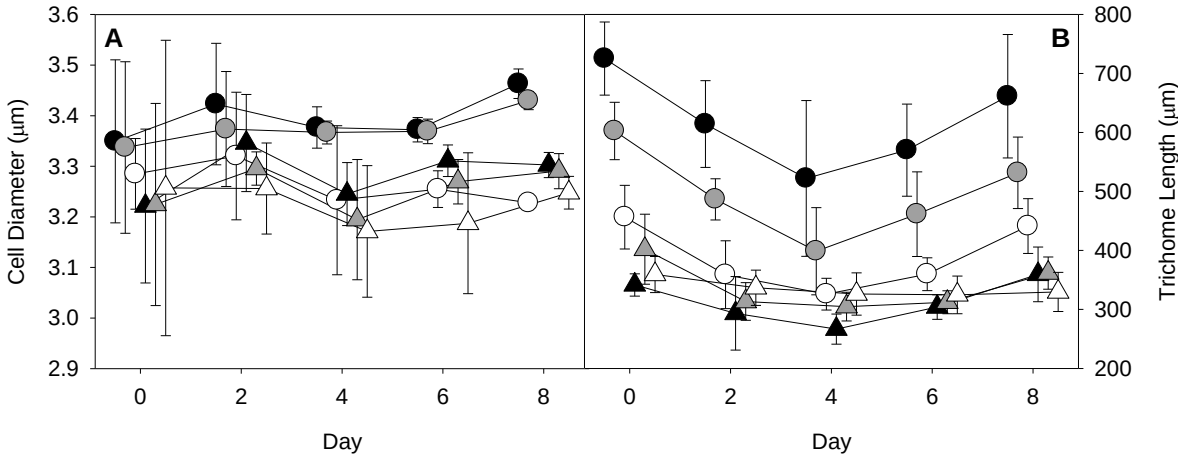

Figure 5.4. (**A**) Cell diameter (µm) of *Crocosphaera watsonii* cultures and (**B**) trichome length (µm) of *Trichodesmium erythraeum* cultures grown under varying total iron concentration: 0 nmol L^{-1} Fe_T (black circle), 4 nmol L^{-1} Fe_T (grey circle), 10 nmol L^{-1} Fe_T (white circle), 20 nmol L^{-1} Fe_T (black triangle), 40 nmol L^{-1} Fe_T (grey triangle) and 120 nmol L^{-1} Fe_T (white triangle). Note *y*-axis scales of A and B do not start at zero.

The total cellular biovolume (µm³ ml^{-1}) of *Crocosphaera* and *Trichodesmium* cultures increased in a similar pattern to cell and trichome number, respectively (Fig. 5.5). *Crocosphaera* cultures were markedly reduced in terms of final biovolume at the lowest iron concentration compared to high iron cultures, in particular 40 nmol L^{-1} Fe_T (Fig. 5.5A). Post-subculture biovolumes of *Crocosphaera* were approximately 1.0×10^6 µm³ ml^{-1}, measured using a coulter counter. Cultures with no added iron showed a 10-fold increase in biovolume by day 8 ($M = 1.0 \times 10^7$ µm³ ml^{-1}) compared to a greater than 20-fold increase by 40 nmol L^{-1} Fe_T cultures ($M = 2.6 \times 10^7$ µm³ ml^{-1}). A significant difference in final *Crocosphaera* biovolume was found between the six different iron concentrations ($H_{(5)} = 20.538$, $N = 36$, $p < 0.01$). Subsequent Mann-Whitney *U* tests confirmed that *Crocosphaera* cultures with no added iron were significantly different in terms of final biovolume compared to the highest iron treatment (Table 5.1). The increase in total biovolume throughout the growth cycle was analogous to *Crocosphaera* cultures, although *Trichodesmium* cultures with no added iron were not as noticeably reduced in relation to the other iron concentrations (Fig. 5.5B). A Kruskal-Wallis test suggested there was a significant difference in the final biovolume of *Trichodesmium* cultures between the different iron concentrations ($H_{(5)} = 15.718$, $N = 36$, $p < 0.01$). However, only 40 nmol L^{-1} Fe_T cultures were found to be significantly different in terms of biovolume compared to cultures with no added iron (statistical summary).

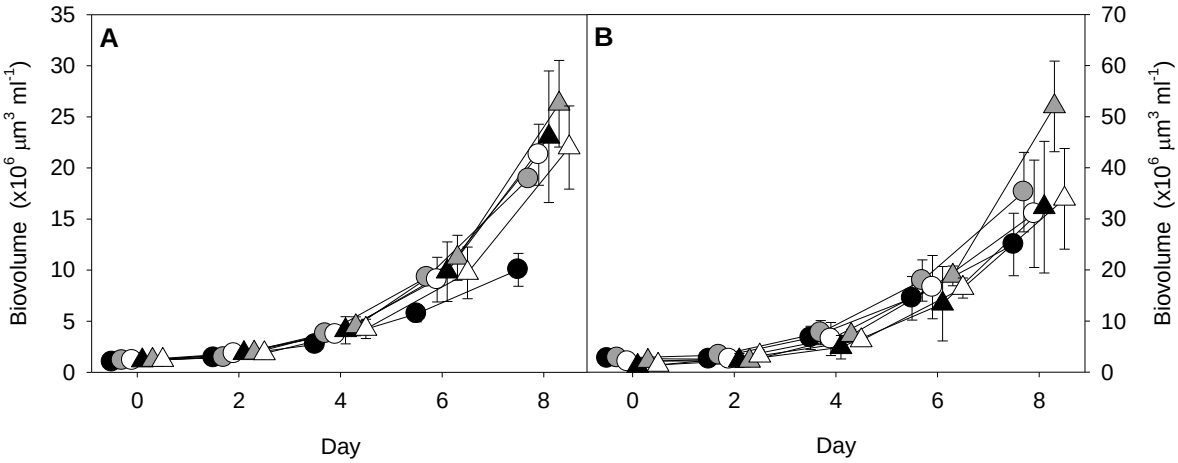

Figure 5.5. Total cellular biovolume (µm^3 ml^{-1}) determined for cultures of (**A**) *Crocosphaera watsonii* and (**B**) *Trichodesmium erythraeum* grown under varying total iron concentration: 0 nmol L^{-1} Fe$_T$ (black circle), 4 nmol L^{-1} Fe$_T$ (grey circle), 10 nmol L^{-1} Fe$_T$ (white circle), 20 nmol L^{-1} Fe$_T$ (black triangle), 40 nmol L^{-1} Fe$_T$ (grey triangle) and 120 nmol L^{-1} Fe$_T$ (white triangle).

Growth rates of *Crocosphaera* and *Trichodesmium* cultures were calculated using the change in total biovolume throughout each growth cycle (Fig. 5.6). The average growth rate was similar between the two species with a significantly reduced value calculated in cultures with no added iron in relation to 120 nmol L^{-1} Fe$_T$ cultures (Table 5.1). The maximum growth rate (μ_{max}) of *Crocosphaera* was significantly reduced ($p < 0.05$) in low iron cultures ($M = 0.29 \pm 0.02$ day^{-1}) compared to high iron cultures ($M = 0.36 \pm 0.01$ day^{-1}). In contrast, the mean μ_{max} of *Trichodesmium* cultures with no added iron was greater than high iron cultures, although a significant difference was not observed (Table 5.1). Nevertheless, μ_{max} was generally lower in both diazotrophs when compared to the non-diazotrophic cyanobacteria *Synechococcus* sp. WH7803, which averaged (mean) 0.88 ± 0.10 and 0.83 ± 0.07 day^{-1} in the two highest iron cultures (1200 and 120 nmol L^{-1} Fe$_T$, respectively; see Fig. 4.3).

The concentration of POC (Fig. 5.7A) and PON (Fig. 5.7B) in cultures of *Crocosphaera* and *Trichodesmium* were relatively similar between the corresponding total iron concentrations. A significant difference was observed between the POC and PON concentration in cultures with no added iron (0 nmol L^{-1} Fe$_T$) in comparison to all other iron treatments for both species (statistical summary). The carbon to nitrogen (C:N) ratio ranged between 5.74 and 8.99 ($M = 7.29 \pm 0.83$, $N = 35$) for *Crocosphaera* and 5.46 and 7.46 ($M = 6.34 \pm 0.44$, $N = 36$) for *Trichodesmium*, with no obvious pattern relating to iron treatment (Table 5.2). Mean carbon and nitrogen contents expressed as biovolume for *Crocosphaera* cultures increased and decreased respectively, with increasing iron concentration, but no significant difference was found between the highest and lowest iron concentrations. *Trichodesmium* carbon content increased at higher iron

concentrations, with a significant difference found between the highest and lowest iron regimes ($p < 0.01$). Nitrogen content of *Trichodesmium* cultures also increased with increasing iron, with a significantly higher value measured in the 120 nmol L^{-1} Fe_T iron cultures compared to cultures with no added iron ($p < 0.01$, Table 5.1).

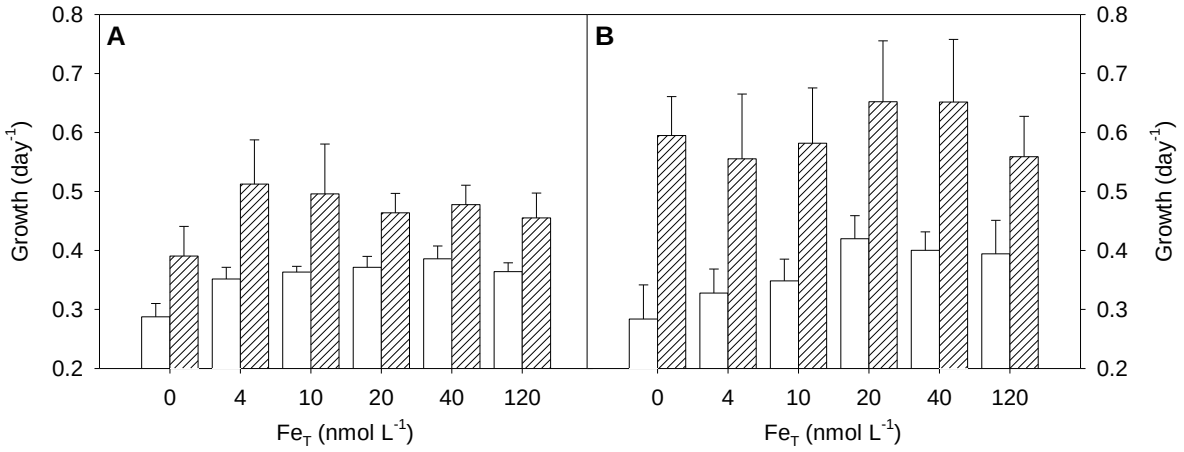

Figure 5.6. Average growth rate (white) and maximum growth rate (μ_{max}, striped) determined for cultures of (**A**) *Crocosphaera watsonii* and (**B**) *Trichodesmium erythraeum* grown under varying total iron concentration (nmol L^{-1} Fe_T). Note *y*-axis scales start at 0.2 for A and B.

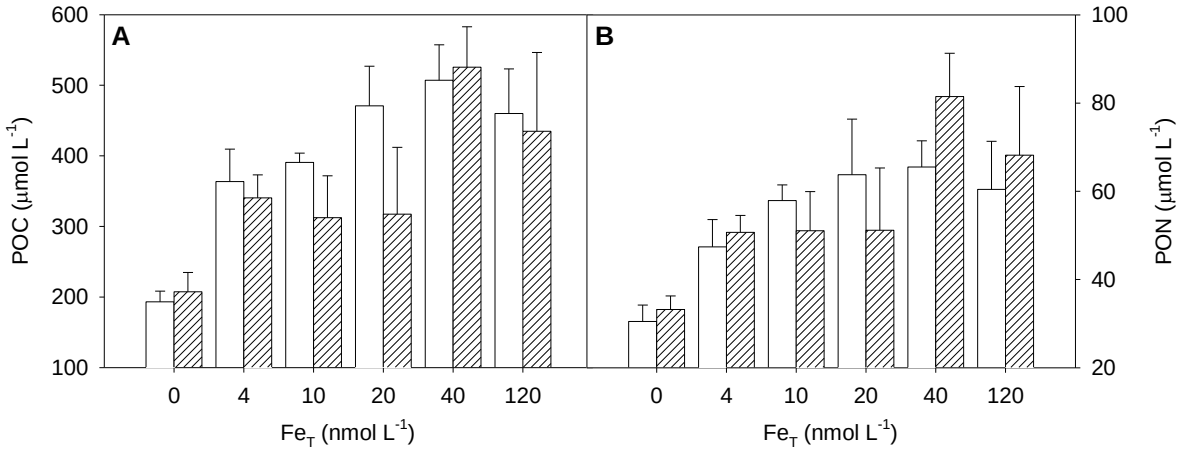

Figure 5.7. Concentration of (**A**) particulate organic carbon (POC, µmol L^{-1}) and (**B**) particulate organic nitrogen (PON, µmol L^{-1}) determined for cultures of *Crocosphaera watsonii* (white) and *Trichodesmium erythraeum* (striped) grown under varying total iron concentration (nmol L^{-1} Fe_T). Note *y*-axis scales of A and B do not start at zero.

	Carbon:nitrogen ratio (C:N)	
Treatment	*Crocosphaera*	*Trichodesmium*
0 nmol L^{-1} Fe_T	6.38 ± 0.46	6.27 ± 0.78
4 nmol L^{-1} Fe_T	7.70 ± 0.68	6.72 ± 0.47
10 nmol L^{-1} Fe_T	6.77 ± 0.51	6.10 ± 0.16
20 nmol L^{-1} Fe_T	7.51 ± 1.07	6.16 ± 0.26
40 nmol L^{-1} Fe_T	7.75 ± 0.48	6.46 ± 0.20
120 nmol L^{-1} Fe_T	7.69 ± 0.79	6.34 ± 0.34

Table 5.2. Carbon to nitrogen ratio (C:N) determined for cultures of *Crocosphaera watsonii* and *Trichodesmium erythraeum* grown under varying total iron concentration (nmol L^{-1} Fe_T).

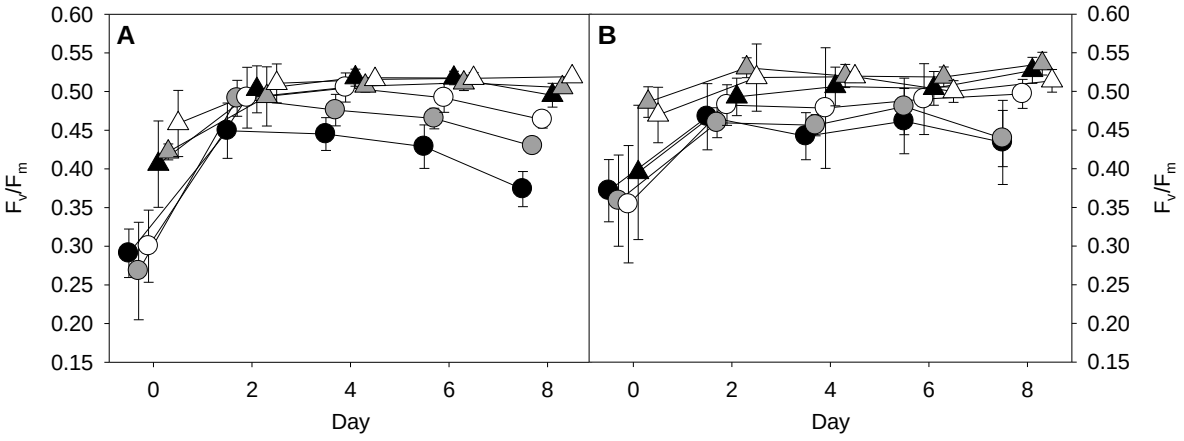

Figure 5.8. Maximum quantum yield of PSII (F_v/F_m) determined for cultures of (**A**) *Crocosphaera watsonii* and (**B**) *Trichodesmium erythraeum* grown under varying total iron concentration: 0 nmol L^{-1} Fe_T (black circle), 4 nmol L^{-1} Fe_T (grey circle), 10 nmol L^{-1} Fe_T (white circle), 20 nmol L^{-1} Fe_T (black triangle), 40 nmol L^{-1} Fe_T (grey triangle) and 120 nmol L^{-1} Fe_T (white triangle). Note *y*-axis scales start at 0.15 for A and B.

The maximum quantum yield of PSII (F_v/F_m) for both *Crocosphaera* and *Trichodesmium* decreased as iron concentration decreased (Fig. 5.8). The mean F_v/F_m for the highest iron concentration of *Crocosphaera* cultures (120 nmol L^{-1} Fe_T, 0.52 ± 0.01) was significantly greater than all other iron treatments ($p < 0.01$, Table 5.1). A significant difference in F_v/F_m was found between the highest and lowest iron cultures of *Trichodesmium* ($p < 0.05$, Table 5.1), although the highest mean F_v/F_m was calculated for 40 nmol L^{-1} Fe_T cultures (0.54 ± 0.01). Post-subculture F_v/F_m measurements (i.e. day 0) were noticeably reduced, particularly in the 0, 4 and 10 nmol L^{-1} Fe_T cultures, compared to the fairly consistent values reported throughout the rest of the growth cycle (Fig. 5.8). The effective absorbance cross-section of PSII (σ_{PSII}) was significantly reduced in *Crocosphaera* cultures

with no added iron relative to the highest iron treatment ($p < 0.05$, Table 5.1). However, cultures grown under 4 nmol L^{-1} Fe_T offered the lowest σ_{PSII} compared to 120 nmol L^{-1} Fe_T cultures for both *Crocosphaera* and *Trichodesmium*.

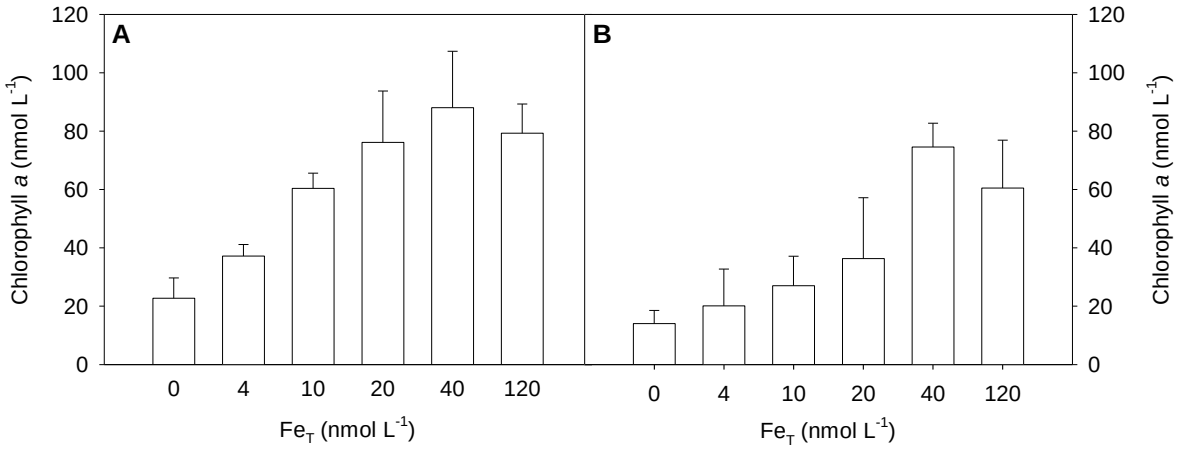

Figure 5.9. Chlorophyll *a* concentration (nmol L^{-1}) determined for cultures of (**A**) *Crocosphaera watsonii* and (**B**) *Trichodesmium erythraeum* grown under varying total iron concentration (nmol L^{-1} Fe_T).

5.4.2 Chlorophyll a and heme b

Mean chlorophyll *a* concentrations of *Crocosphaera* and *Trichodesmium* cultures were relatively similar at corresponding iron concentrations (Fig. 5.9), with both species showing increased chlorophyll *a* with increasing iron concentration. However, the increase in chlorophyll *a* concentration of *Trichodesmium* cultures was more pronounced between 20 and 40 nmol L^{-1} Fe_T (Fig. 5.9B) compared to *Crocosphaera* cultures (Fig. 5.9A). The highest mean chlorophyll *a* concentration was measured at 40 nmol L^{-1} Fe_T for both *Crocosphaera* (88.0 ± 19.3 nmol L^{-1}) and *Trichodesmium* (74.6 ± 8.11 nmol L^{-1}) cultures (Table 5.3). Kruskal Wallis tests showed that there was a significant difference in the median chlorophyll *a* concentration between the six different iron concentrations for both *Crocosphaera* ($H_{(5)} = 28.130$, $N = 36$, $p < 0.01$) and *Trichodesmium* ($H_{(5)} = 25.135$, $N = 36$, $p < 0.01$). Furthermore, Mann-Whitney *U* tests showed that a significant difference was apparent between the highest (120 nmol L^{-1} Fe_T) and the three lowest (0, 4 and 10 nmol L^{-1} Fe_T) iron conditions (Table 5.3). The chlorophyll *a* concentrations of *Crocosphaera* and *Trichodesmium* cultures were comparable to previously described results of *Synechococcus* sp. WH7803, which provided mean values of 11.6 ± 0.67 and 87.6 ± 32.2 nmol L^{-1} for 12 and 120 nmol L^{-1} Fe_T cultures, respectively (see Chapter 4).

Chlorophyll *a* concentration was significantly correlated to POC and PON for both *Crocosphaera* and *Trichodesmium* (Table 5.4). Mean chlorophyll *a* contents per unit carbon (chl:C, Fig. 5.10A) and per unit nitrogen (chl:N, Fig. 5.10B) increased with

increasing iron concentration for both species. The highest mean chl:C (173 ± 10.4 µmol mol^{-1}) and chl:N (1328 ± 146 µmol mol^{-1}) ratios for *Crocosphaera* were found in 120 and 40 nmol L^{-1} Fe_T cultures, respectively. Statistical analysis (Kruskal Wallis test) showed that a significant different was apparent between the different iron concentrations with regards to chl:C ($H_{(5)}$ = 18.749, N = 36, p < 0.01) and chl:N ($H_{(5)}$ = 25.938, N = 36, p < 0.01) ratio. In both cases, 0, 4 and 10 nmol L^{-1} Fe_T cultures were significantly reduced compared to the highest iron cultures of *Crocosphaera* (Table 5.3). Ratios of chl:C (142 ± 11.0 µmol mol^{-1}) and chl:N (921 ± 96.2 µmol mol^{-1}) in *Trichodesmium* cultures were both highest at 40 nmol L^{-1} Fe_T. A significant difference in the median of chl:C ($H_{(5)}$ = 19.556, N = 36, p < 0.01) and chl:N ($H_{(5)}$ = 20.204, N = 36, p < 0.01) ratio was found between the six different iron regimes and, similar to *Crocosphaera*, the three lowest iron concentrations were significantly reduced compared to the highest iron cultures of *Trichodesmium* (Table 5.3).

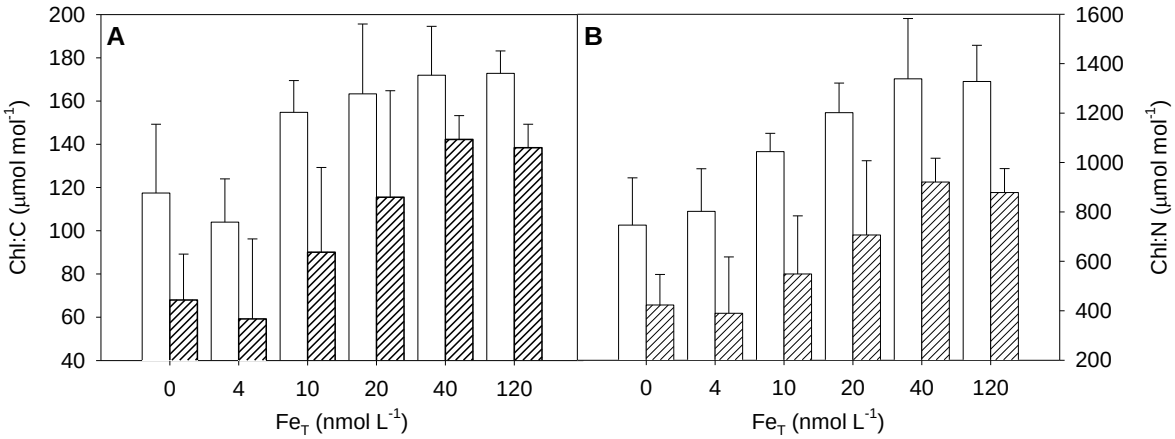

Figure 5.10. (**A**) Chlorophyll *a* concentration per unit carbon (µmol mol^{-1} C) and (**B**) chlorophyll *a* concentration per unit nitrogen (µmol mol^{-1} N) determined for cultures of *Crocosphaera watsonii* (white) and *Trichodesmium erythraeum* (striped) grown under varying iron concentration (nmol L^{-1} Fe_T). Note *y*-axis scales of A and B do not start at zero.

The determination of heme *b* concentration in *Crocosphaera* and *Trichodesmium* cultures was achieved using both spectrophotometry and mass spectrometry; similar to the analysis of samples from the tropical North Atlantic (TNA) previously described (D361, see Chapters 2 and 3). The heme *b* concentration of *Crocosphaera* cultures ranged between 0.12 and 1.43 nmol L^{-1} (N = 36), with 20 nmol L^{-1} Fe_T cultures providing the highest mean heme *b* concentration (0.90 ± 0.40 nmol L^{-1}, Fig. 5.11A). The lowest mean heme *b* concentration of *Crocosphaera* was calculated from cultures grown with no added iron (M = 0.32 ± 0.11 nmol L^{-1}). A Kruskal Wallis test suggested a significant difference in heme *b* concentration between the six iron conditions ($H_{(5)}$ = 14.249, N = 36, p < 0.05), although only cultures grown with no added iron were significantly different to those grown at 120 nmol L^{-1} Fe_T (Table 5.3). In contrast, the heme *b* concentration of *Trichodesmium* cultures

Species / Treatment	pFe'	Chlorophyll *a* (nmol L^{-1})	Heme *b* (nmol L^{-1})	Chl:heme (mol mol^{-1})	Heme:C (µmol mol^{-1})	Heme:N (µmol mol^{-1})	Chl:C (µmol mol^{-1})	Chl:N (µmol mol^{-1})
Crocosphaera watsonii								
0 nmol L^{-1} Fe_T	10.6	22.7 ± 7.0**	0.32 ± 0.11*	80.1 ± 33.4	1.64 ± 0.57	10.6 ± 4.0	117 ± 31.8*	747 ± 192**
4 nmol L^{-1} Fe_T	9.7	37.2 ± 3.9**	0.56 ± 0.35	84.1 ± 38.4	1.47 ± 0.72	11.4 ± 6.2	104 ± 20.0**	802 ± 172**
10 nmol L^{-1} Fe_T	9.3	60.4 ± 5.2*	0.67 ± 0.24	102 ± 39.7	1.72 ± 0.64	11.5 ± 4.0	155 ± 14.7*	1044 ± 74.2*
20 nmol L^{-1} Fe_T	9	76.1 ± 17.6	0.90 ± 0.40	97.4 ± 39.2	1.93 ± 0.80	14.5 ± 6.9	163 ± 32.3	1202 ± 120
40 nmol L^{-1} Fe_T	8.7	88.0 ± 19.3	0.81 ± 0.12	112 ± 37.0	1.63 ± 0.37	12.6 ± 2.6	172 ± 22.6	1339 ± 244
120 nmol L^{-1} Fe_T	8.2	79.3 ± 10.0	0.80 ± 0.39	119 ± 51.5	1.70 ± 0.73	13.1 ± 5.8	173 ± 10.4	1328 ± 146
Trichodesmium erythraeum								
0 nmol L^{-1} Fe_T	10.6	14.1 ± 4.48**	0.06 ± 0.03	226 ± 141	0.31 ± 0.16	1.70 ± 0.88	68.0 ± 21.2**	423 ± 124**
4 nmol L^{-1} Fe_T	9.7	20.1 ± 12.6**	0.07	267	0.23	1.5	59.2 ± 37.1**	390 ± 228**
10 nmol L^{-1} Fe_T	9.3	27.0 ± 10.1*	0.08 ± 0.05	426 ± 281	0.30 ± 0.19	1.81 ± 1.19	90.1 ± 39.2*	549 ± 235*
20 nmol L^{-1} Fe_T	9	36.3 ± 20.9*	0.11 ± 0.08	387 ± 369	0.57 ± 0.47	3.36 ± 2.73	115 ± 49.3	707 ± 300
40 nmol L^{-1} Fe_T	8.7	74.6 ± 8.11	<d.l.	n/a	n/a	n/a	142 ± 11.0	921 ± 96.2
120 nmol L^{-1} Fe_T	8.2	60.5 ± 16.4	<d.l.	n/a	n/a	n/a	138 ± 10.9	878 ± 97.3

Table 5.3. Chlorophyll *a* concentration (nmol L^{-1}), heme *b* concentration (nmol L^{-1}), chlorophyll *a* to heme *b* ratio (chl:heme), heme *b* concentration per unit carbon (heme:C, µmol mol^{-1} C), heme *b* concentration per unit nitrogen (heme:N, µmol mol^{-1} N), chlorophyll *a* concentration per unit carbon (chl:C, µmol mol^{-1} C) and chlorophyll *a* concentration per unit nitrogen (chl:N, µmol mol^{-1} N) determined for *Crocosphaera watsonii* and *Trichodesmium erythraeum* cultures grown under varying total iron concentration (nmol L^{-1} Fe_T). Values are expressed ± standard deviation, with the exception of *Trichodesmium* heme *b* concentrations and subsequent derivatives whereby values are expressed ± the range. pFe' represents -log[inorganic Fe]. Significant differences relative to the highest iron concentration (120 nmol L^{-1} Fe_T) represented by ** where $p < 0.01$ and * where $p < 0.05$ (Mann-Whitney *U* test). <d.l. indicates samples were below the detection limit.

was markedly lower (M = 80.0 ± 46.4 pmol L^{-1}, N = 8, Fig. 5.11B) compared to *Crocosphaera*, ranging from below the detection limit (18 pmol L^{-1}) to 170 pmol L^{-1}. The mean heme *b* concentration appeared to increase with iron concentration up to 20 nmol L^{-1} Fe_T (Table 5.3); however, due to the lack of *Trichodesmium* samples above the detection limit as well as no valid measurements from 40 or 120 nmol L^{-1} Fe_T cultures, statistical analysis was not feasible.

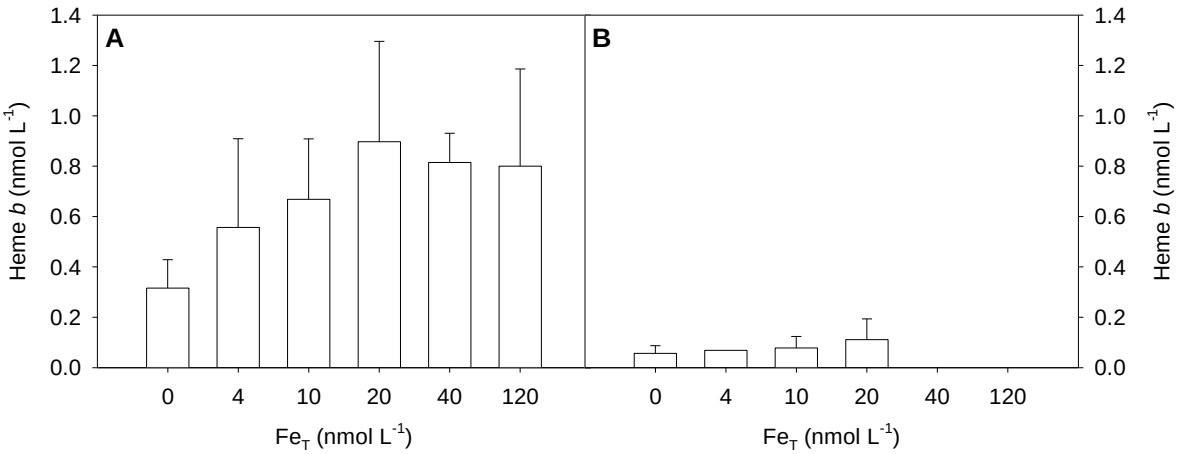

Figure 5.11. Heme *b* concentration (nmol L^{-1}) determined for cultures of (**A**) *Crocosphaera watsonii* and (**B**) *Trichodesmium erythraeum* grown under varying total iron concentration (nmol L^{-1} Fe_T). Note heme *b* concentrations of *Trichodesmium* cultures grown at 40 and 120 nmol L^{-1} Fe_T were below the detection limit; hence no data is plotted.

A significant correlation was observed between chlorophyll *a* and heme *b* concentration for cultures of *Crocosphaera* (p < 0.01), but not *Trichodesmium* (Table 5.4). However, it should be considered that the limited heme *b* data obtained from *Trichodesmium* cultures restricted the comparisons with chlorophyll *a*. Variations in mean chlorophyll *a* to heme *b* ratio (chl:heme) were apparent between the different iron treatments of *Crocosphaera* cultures (Fig. 5.12A). The highest mean chl:heme ratio was observed in 120 nmol L^{-1} Fe_T cultures at 119 ± 51.5, compared to 80.1 ± 33.4 calculated from cultures with no added iron. However, no significant differences in chl:heme ratio were detected between the six iron concentrations (Table 5.3). Chl:heme ratios from *Trichodesmium* cultures (Fig. 5.12B) were generally much higher than *Crocosphaera*, ranging between 126 and 750 (N = 8). Also, mean chl:heme ratios appeared to increase with increasing total iron concentration, but once again the limited number of heme *b* measurements restricted interpretation.

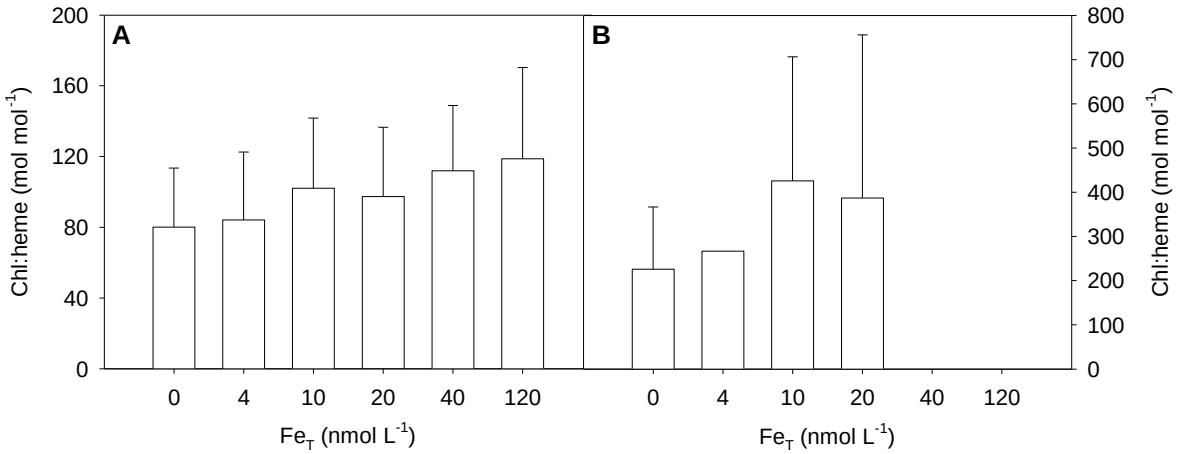

Figure 5.12. Chlorophyll *a* to heme *b* ratio (chl:heme) determined for cultures of (**A**) *Crocosphaera watsonii* and (**B**) *Trichodesmium erythraeum* grown under varying total iron concentration (nmol L^{-1} Fe_T). Note different *y*-axis scales for A and B.

Significant correlations were found between heme *b* and POC/PON concentration for cultures of *Crocosphaera*, but not *Trichodesmium* (Table 5.4). Mean heme *b* contents per unit carbon (heme:C, Fig. 5.13A) and per unit nitrogen (heme:N, Fig. 5.13B) did not appear to change with iron concentration in either *Crocosphaera* or *Trichodesmium* cultures. The highest mean heme:C (1.93 ± 0.80 μmol mol^{-1}) and heme:N (14.5 ± 6.9 μmol mol^{-1}) ratios for *Crocosphaera* were found in 20 nmol L^{-1} Fe_T cultures (Table 5.3), but Kruskal Wallis tests suggested there was no significant difference between the different iron concentrations. Mean heme:C and heme:N ratios of *Trichodesmium* cultures (Fig. 5.13) were much lower than *Crocosphaera* cultures. The highest mean heme:C (0.57 ± 0.47 μmol mol^{-1}) and heme:N (3.36 ± 2.73 μmol mol^{-1}) ratios for *Trichodesmium* were also found in 20 nmol L^{-1} Fe_T cultures (Table 5.3). A slight increase in mean heme *b* contents with increasing iron concentration could be observed for *Trichodesmium*, but the limited number of samples prevented statistical analysis.

	Crocosphaera			*Trichodesmium*		
Tetrapyrrole	Chl *a*	POC	PON	Chl *a*	POC	PON
Chlorophyll *a*	-	0.900** (35)	0.879** (35)	-	0.840** (36)	0.861**(36)
Heme *b*	0.598** (36)	0.675** (35)	0.640** (35)	0.155 (8)	-0.130 (8)	-0.205 (8)

Table 5.4. Results of Pearson Product Moment Correlations (*r*) for chlorophyll *a* (chl *a*), heme *b*, particulate organic carbon (POC) and particulate organic nitrogen (PON) concentration determined for cultures of *Crocosphaera watsonii* and *Trichodesmium erythraeum*. Numbers in brackets indicate number of samples. Significant differences represented by ** where $p < 0.01$ and * where $p < 0.05$.

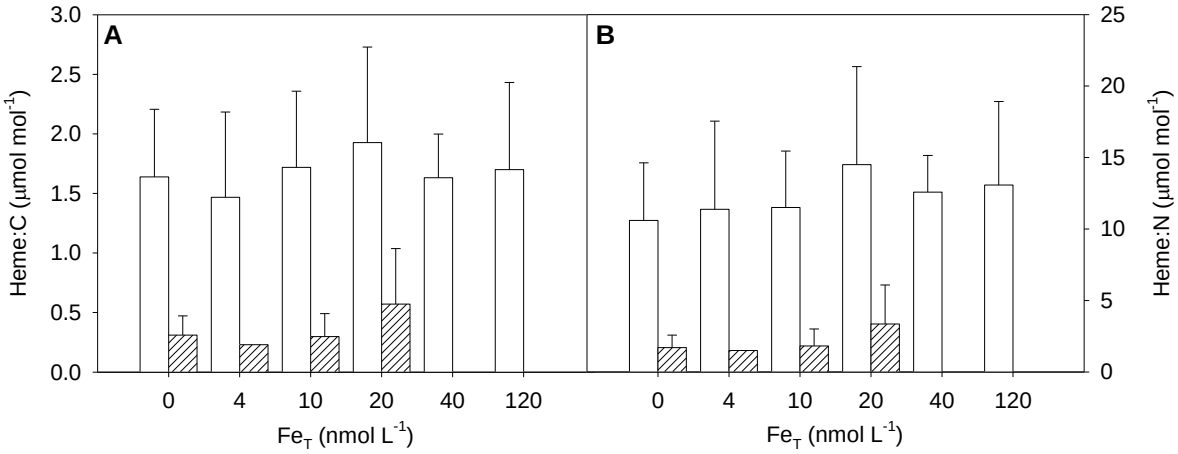

Figure 5.13. (**A**) Heme *b* concentration per unit carbon (µmol mol^{-1} C) and (**B**) heme *b* concentration per unit nitrogen (µmol mol^{-1} N) determined for cultures of *Crocosphaera watsonii* (white) and *Trichodesmium erythraeum* (striped) grown under varying total iron concentration (nmol L^{-1} Fe_T).

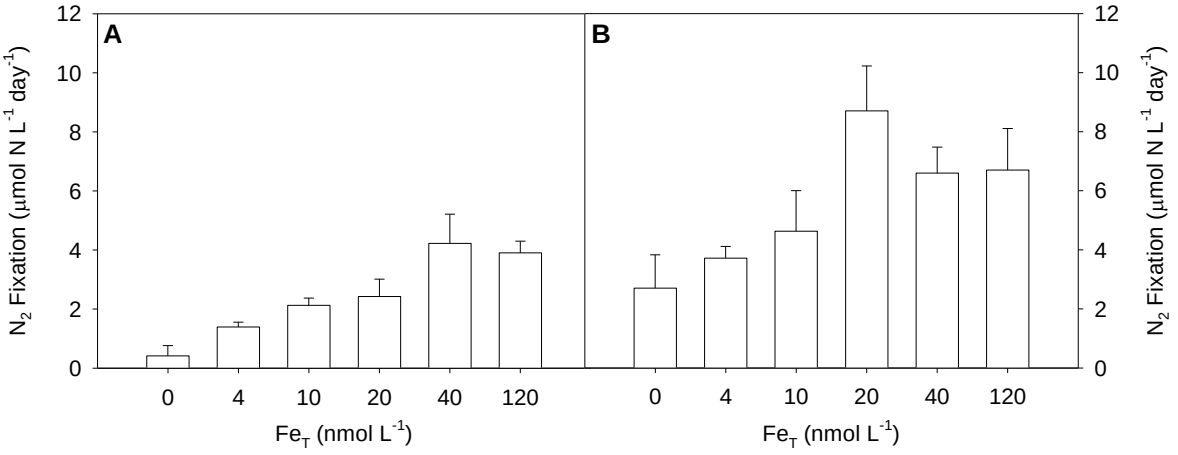

Figure 5.14. Nitrogen fixation rate (µmol N L^{-1} day^{-1}) determined for cultures of (**A**) *Crocosphaera watsonii* and (**B**) *Trichodesmium erythraeum* grown under varying total iron concentration (nmol L^{-1} Fe_T).

5.4.3 Nitrogen fixation in diazotroph cultures

Nitrogen fixation rates for *Crocosphaera* and *Trichodesmium* cultures were investigated at all six total iron concentrations between 0 and 120 nmol L^{-1} Fe_T. The nitrogen fixation rate of *Crocosphaera* cultures ranged between 0.06 and 5.80 µmol N L^{-1} day^{-1}, with the mean nitrogen fixation rate increasing with increasing iron concentration (Fig. 5.14A). The lowest (M = 0.41 ± 0.35 µmol N L^{-1} day^{-1}) and highest (M = 4.23 ± 0.99 µmol N L^{-1} day^{-1}) mean nitrogen fixation rates for *Crocosphaera* were measured in 0 and 40 nmol L^{-1} Fe_T cultures, respectively. An overall significant difference was found between the different iron concentrations, with 0, 4, 10 and 20 nmol L^{-1} Fe_T cultures significantly different to the highest iron cultures (Table 5.5). Nitrogen fixation rates for *Trichodesmium* cultures were

greater than *Crocosphaera* at the corresponding iron concentrations (Fig. 5.14B). An increase in nitrogen fixation rates appeared to coincide with increasing total iron concentration, although the highest mean nitrogen fixation rate was measured in 20 nmol L^{-1} Fe_T cultures (M = 8.71 ± 1.52 µmol N L^{-1} day^{-1}). Cultures of *Trichodesmium* grown at 0, 4 and 10 nmol L^{-1} Fe_T were significantly different to the highest iron cultures (Table 5.5).

	Crocosphaera		*Trichodesmium*	
Analysis / Treatment	N_2 Fixation (µmol N L^{-1} day^{-1})	Vnfix (day^{-1})	N_2 Fixation (µmol N L^{-1} day^{-1})	Vnfix (day^{-1})
Kruskal Wallis	42.78 (5)**	36.45 (5)**	34.24 (5)**	29.08 (5)**
Mann-Whitney *U* test				
0 nmol L^{-1} Fe_T	0.41 ± 0.35**	0.02 ± 0.01**	2.70 ± 1.13**	0.12 ± 0.01**
4 nmol L^{-1} Fe_T	1.40 ± 0.16**	0.04 ± 0.01**	3.72 ± 0.39**	0.13 ± 0.01**
10 nmol L^{-1} Fe_T	2.12 ± 0.25**	0.04 ± 0.01**	4.63 ± 1.38*	0.15 ± 0.05*
20 nmol L^{-1} Fe_T	2.43 ± 0.59**	0.04 ± 0.01**	8.71 ± 1.52*	0.20 ± 0.02
40 nmol L^{-1} Fe_T	4.23 ± 0.99	0.05 ± 0.01	6.60 ± 0.88	0.20 ± 0.02
120 nmol L^{-1} Fe_T	3.90 ± 0.40	0.06 ± 0.01	6.70 ± 1.41	0.21 ± 0.02

Table 5.5. Nitrogen fixation rate (µmol N L^{-1} day^{-1}) and nitrogen-specific growth rate via nitrogen fixation (Vnfix, day^{-1}) determined for cultures of *Crocosphaera watsonii* and *Trichodesmium erythraeum* grown under varying total iron concentration (nmol L^{-1} Fe_T). Numbers in brackets indicate degrees of freedom. Mann-Whitney *U* tests compared to the highest iron concentration (120 nmol L^{-1} Fe_T). Significant differences represented by ** where $p < 0.01$ and * where $p < 0.05$. n = 8 for each iron concentration, with the exception of *Trichodesmium* cultures with no added iron where n = 5.

Despite subculturing to similar biovolumes (*Crocosphaera*) or trichome numbers (*Trichodesmium*), biomass at the start of the nitrogen fixation incubations would have varied between the six different iron treatments. It could be expected that cultures with a greater biomass would exhibit greater nitrogen fixation rates in comparison to those with a lower biomass. Therefore, the nitrogen-specific growth due to nitrogen fixation (Vnfix, equivalent to a growth rate) offered a better comparison between the different iron concentrations as it determined the change in nitrogen content specifically attributed to nitrogen fixation. Essentially, this measure standardises the rate of nitrogen fixation against the quantity of PON in the cultures before and after incubations which negates the effect of varying biomass. *Crocosphaera* and *Trichodesmium* cultures displayed increasing Vnfix with increasing iron concentration; however, Vnfix rates for *Trichodesmium* cultures (Fig. 5.15B) were approximately 4 times greater than

Crocosphaera cultures (Fig. 5.15A) at each corresponding iron concentration. Significant differences in Vnfix were found between the highest iron cultures and 0, 4 and 10 nmol L^{-1} Fe_T cultures for both *Crocosphaera* and *Trichodesmium* (Table 5.5).

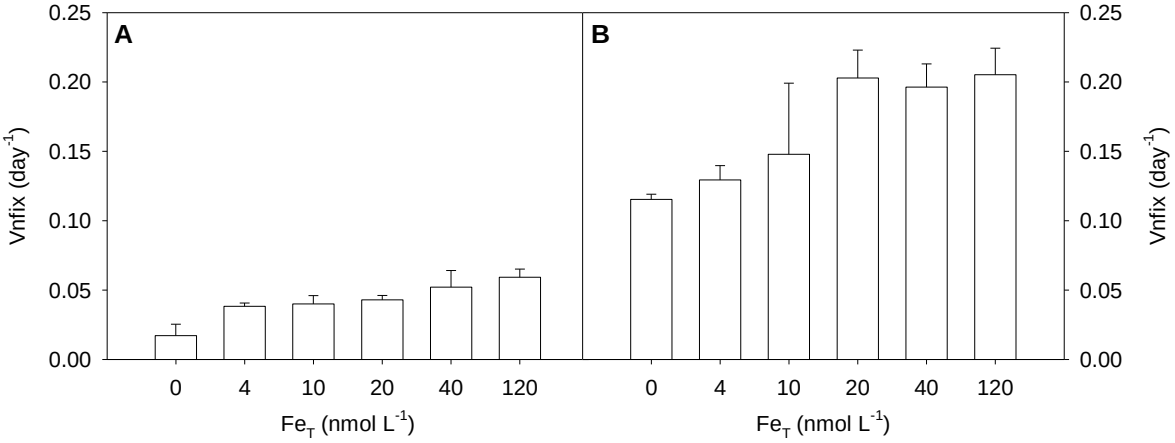

Figure 5.15. Nitrogen-specific growth rate via nitrogen fixation (Vnfix, day^{-1}) determined for cultures of (**A**) *Crocosphaera watsonii* and (**B**) *Trichodesmium erythraeum* grown under varying total iron concentration (nmol L^{-1} Fe_T).

5.4.3 Nitrogen fixation in the (sub-) tropical North Atlantic

Nitrogen fixation incubations were conducted during two research cruises in the (sub-) tropical North Atlantic in 2010 (D346) and 2011 (D361). Nitrogen fixation rates ranged from <0.20 to 4.92 nmol N L^{-1} day^{-1} (N = 75) during the first cruise across the subtropical North Atlantic (STNA, Fig. 5.16). The vertical resolution was limited as only two depths were sampled (surface and chlorophyll max) from one station per day. When the occurrence of nitrogen fixation was detected, the majority was observed in surface waters (<12 m depth). Significant increases in nitrogen fixation were measured at two separate regions of the cross-sectional transect: between 65 and 55 °W in the Western Subtropical North Atlantic Gyre (WSNAG) and towards the eastern margin (Azores Current region, Fig. 5.16). Nitrogen fixation rates on the second cruise in the TNA ranged between <0.20 and 10.9 nmol N L^{-1} day^{-1} (N = 82). A higher degree of vertical resolution was achieved with up to five depths sampled per station in the upper 100 m of the water column. Surface nitrogen fixation rates were highest at S9 (3.2 m, 6.17 nmol N L^{-1} day^{-1}) and S11 (1.8 m, 6.11 nmol N L^{-1} day^{-1}) of the Central TNA and Equatorial Upwelling (EqU) regions, respectively. In contrast, very low rates (<0.20 nmol N L^{-1} day^{-1}) were calculated in the Coastal TNA and Tropical South Atlantic (TSA).

Cruise D361 provided an opportunity to assess the vertical distribution of nitrogen fixation in more detail compared to D346; in particular the South-North (SN) transect (S10 - S21, see Fig. 3.3) from the TSA to the Eastern STNA gyre (Fig. 5.17). Nitrogen fixation

rates were very low in the TSA (S10) with values typically <0.20 nmol N L^{-1} day^{-1} throughout the water column. A notable increase in nitrogen fixation rate up to >2 nmol N L^{-1} day^{-1} was observed in the upper 50 m of the EqU and Central TNA regions. The highest nitrogen fixation rate was measured at 51.4 m depth from S17 of the Central TNA region (10.9 nmol N L^{-1} day^{-1}). Nitrogen fixation rates decreased as the SN transect progressed into the East STNA gyre region of D361, ranging from <0.20 up to 3.65 nmol N L^{-1} day^{-1} (N = 15). Values from the East STNA gyre of D361 were comparable with nitrogen fixation rates calculated from surface waters of the similar oceanographic region of the STNA measured during D346.

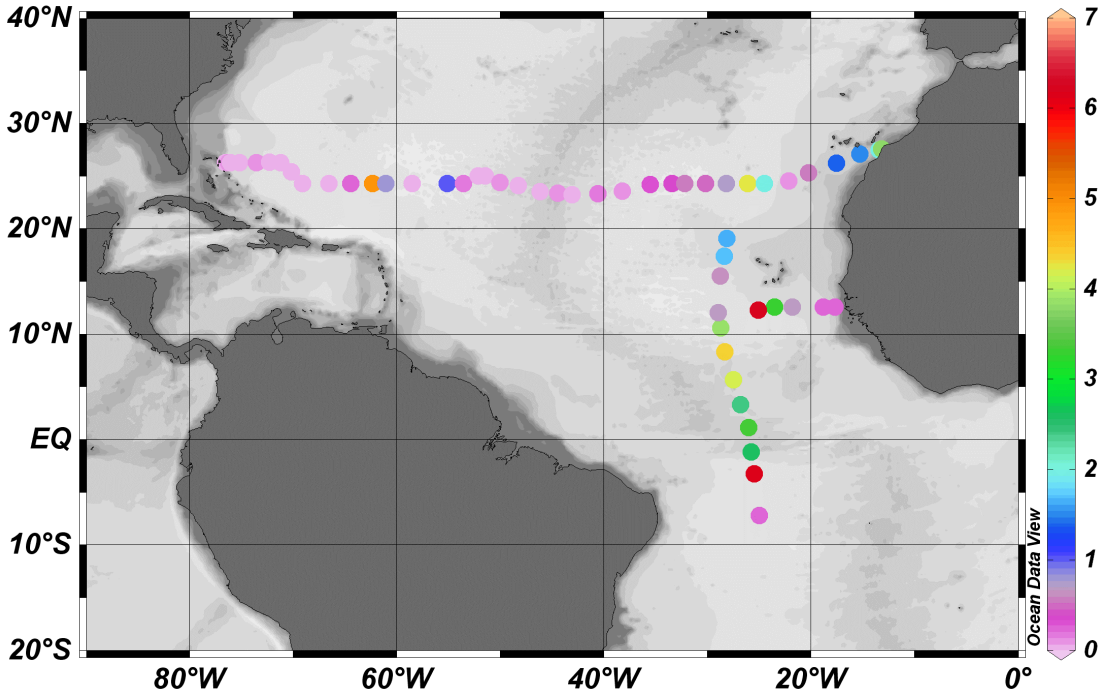

Figure 5.16. Surface nitrogen fixation rates (nmol N L^{-1} day^{-1}) in the (sub-) tropical North Atlantic. Dots above 20 °N collected from cruise D346 (STNA, Jan - Feb 2010) and dots below 20 °N collected from D361 (TNA, Feb - Mar 2011). Values represent first bottle depth per station (<12 m depth).

Nitrogen fixation rates were integrated between the upper most surface sample and the chlorophyll maximum to assess overall nitrogen fixation within the water column and to compare between oceanographic regions of the TNA. The highest integrated nitrogen fixation rate was calculated from S17 of the Central TNA region at 317 µmol N m^{-2} day^{-1}. In addition, all stations combined from the Central TNA provided the highest mean integrated nitrogen fixation rate compared to the other four oceanographic regions (M = 189 ± 115 µmol N m^{-2} day^{-1}, Fig. 5.18). The EqU and East STNA gyre regions also suggested relatively high rates of nitrogen fixation. A notable reduction in integrated nitrogen fixation rate was observed in the Coastal TNA and TSA oceanographic regions.

This pattern was also reflected in surface seawater samples (Fig. 5.16) in the Coastal TNA and TSA regions which demonstrated nitrogen fixation rates <1 nmol N L^{-1} day^{-1}. The lowest mean integrated nitrogen fixation rate was calculated from the Coastal TNA region at 8.2 ± 6.0 µmol N m^{-2} day^{-1} (Fig. 5.18).

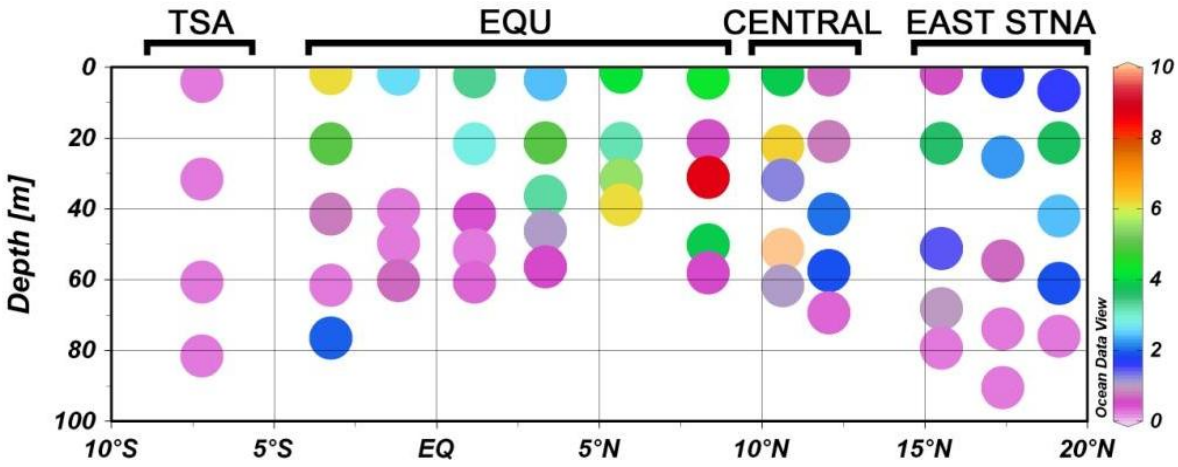

Figure 5.17. Cross-sectional profile (<100 m depth) of nitrogen fixation (nmol N L^{-1} day^{-1}) from the South-North (SN) transect of cruise D361 in the TNA (Feb - Mar 2011). Stations designated to four oceanographic groups: Tropical South Atlantic (TSA), Equatorial Upwelling Region (EqU), Central Tropical North Atlantic (Central TNA) and Eastern STNA gyre (STNA East).

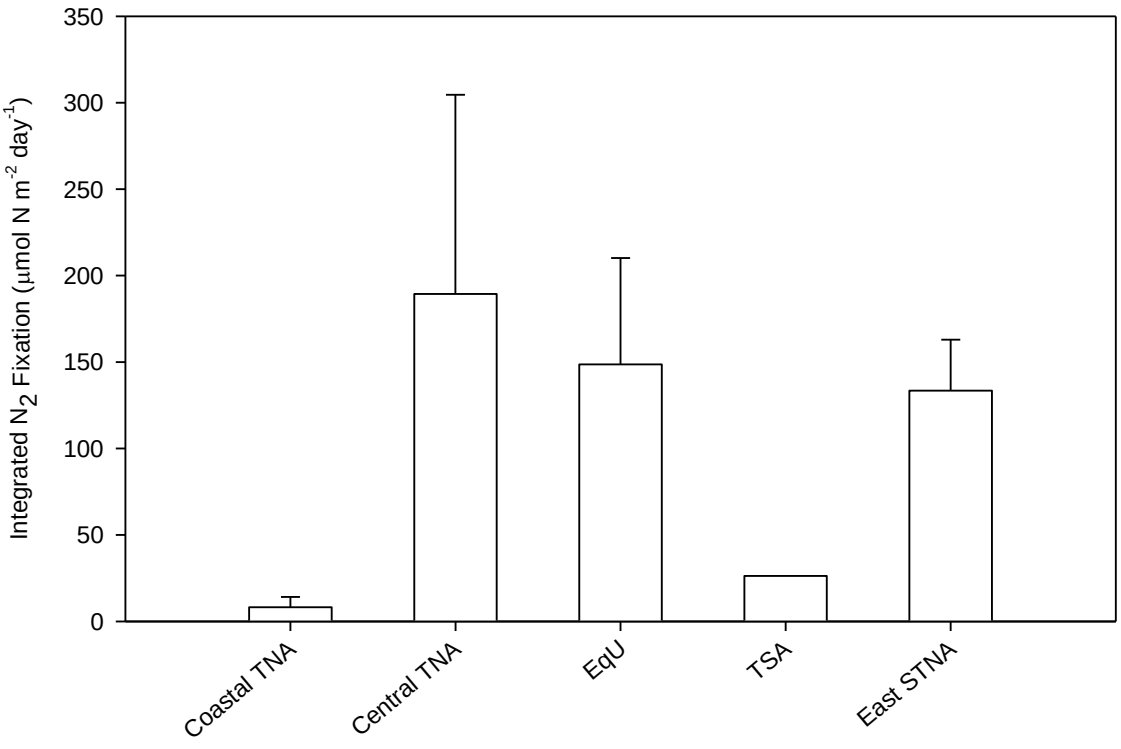

Figure 5.18. Mean integrated nitrogen fixation rate (µmol N m^{-2} day^{-1}) from five oceanographic regions sampled from the TNA during cruise D361 (see Fig. 2.4).

5.5 Discussion

5.5.1 Influence of iron availability on Crocosphaera and Trichodesmium

The availability of iron is known to significantly influence growth of marine cyanobacteria, with particular attention often focussed upon *Trichodesmium* spp. (e.g. Paerl et al. 1994, Kustka et al. 2002, Fu and Bell 2003). Growth rate, cell/trichome number and cellular biovolume of *Crocosphaera* and *Trichodesmium* cultures were significantly reduced in conditions with no added iron compared to those grown under 120 nmol L^{-1} Fe_T. The increased trichome length of iron stressed *Trichodesmium* cultures was a strategy employed to increase the surface to volume ratio, potentially increasing the organisms' chances of survival through enhanced nutrient uptake (Küpper et al. 2008). In turn, it could be assumed that the increased cell size of iron stressed *Crocosphaera* cultures was a similar survival response to increase the uptake of nutrients, including scarcely available iron, although this was the opposite trend observed in the unicellular cyanobacteria *Synechococcus* sp. WH7803 (see Chapter 4). Reduced growth rates of *Crocosphaera* have been previously reported for iron-limiting conditions (Fu et al. 2008), although the study primarily assessed the influence of changing CO_2 partial pressure (pCO_2) along with iron availability. The reduced μ_{max} at low iron concentrations for *Crocosphaera* was similar to *Synechococcus* sp. WH7803 and several eukaryotic phytoplankton, but the reduction was only significant in cultures with no added iron and did not present an apparent linear decline as iron availability decreased. Maximum growth rates of *Trichodesmium* were comparable with a previous study on the same strain grown at 26 °C (approximately 0.6 day^{-1}, Chappell and Webb 2010). However, μ_{max} of *Trichodesmium* cultures from the present study did not vary with iron concentration as was previously seen in *Synechococcus* sp. WH7803. Therefore, it is possible that μ_{max} in diazotrophs is typically maintained under conditions of iron stress, whereas other physiological responses could be more clearly demonstrated.

The influence of iron was reflected by decreased photosynthetic efficiencies (F_v/F_m) under low iron concentrations for both *Crocosphaera* and *Trichodesmium*, suggesting a decline in the photochemical quantum yield of PSII (see review by Suggett et al. 2009). Photophysiology measurements were obtained using FRRF, although the timing of data collection was different between the two species. *Crocosphaera* cultures were sampled six hours into the photoperiod as previous studies have shown that F_v/F_m rapidly increases upon the onset of light and markedly decreases during the hours of darkness (Fig. 5.19 left, Wilson et al. 2010). Furthermore, a two-fold reduction in cytochrome b_6 was reported during the dark phase for *Crocosphaera watsonii* (Fig. 5.19 *right*, Saito et al. 2011); hence why F_v/F_m measurements as well as filtered heme *b*, chlorophyll *a*, POC and PON samples were collected during the light for *Crocosphaera* cultures in this study. *Crocosphaera*

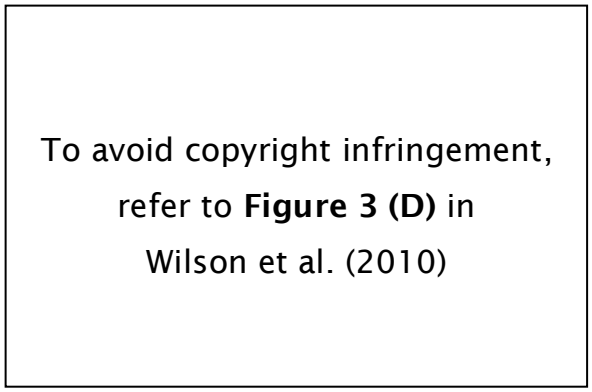

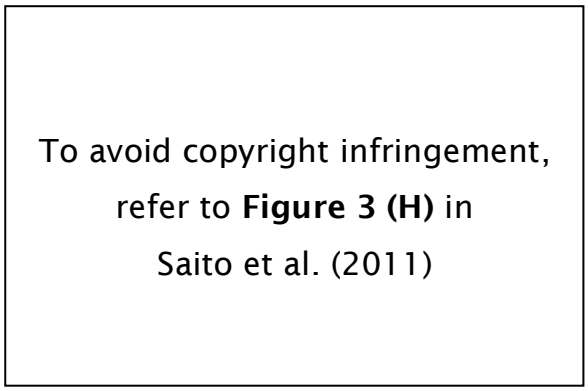

Figure 5.19. Diel cycle of (***left***) photosynthetic quantum yield of PSII measured via fast repetition rate fluorometry (FRRF) and (***right***) cytochrome b_6 content (fmol ug^{-1} total protein) for laboratory cultures of *Crocosphaera watsonii*. Dark periods are indicated by solid black lines along the *x*-axis. Figures from Wilson et al. (2010) and Saito et al. (2011), respectively.

photosynthesise during the light period and perform nitrogen fixation during darkness (Mohr et al. 2010). This temporal separation of the two processes helps to avoid oxygen-evolution in the presence of nitrogenase which leads to permanent deactivation of the complex (Gallon 1992, Milligan et al. 2007). The temporal photophysiology of *Trichodesmium* is considered more complex and less well understood compared to *Crocosphaera*. *Trichodesmium* do not temporally separate photosynthetic and diazotrophic processes; instead they photosynthesise and fix nitrogen during daylight hours (Capone et al. 1997, Berman-Frank et al. 2003). A study of natural surface populations of *Trichodesmium thiebautii* showed a decline in their photosynthetic activity (^{14}C uptake) in the middle of the light photoperiod when nitrogen fixation rates peaked (Berman-Frank et al. 2001b). Therefore, *Trichodesmium* cultures in this study were sampled prior to the onset of light (-2 hours) to coincide with the period of elevated F_v/F_m. Photophysiology measurements were collected on one occasion during the light period where cultures showed reduced and inconsistent F_v/F_m (e.g. <0.3 for 10 and 20 nmol L^{-1} Fe_T, data not shown). In order to measure sufficient quantities of *b*-type hemoproteins associated with the photosynthetic electron transport chain, the timing of *Trichodesmium* sampling was set during the period when photosynthetic efficiency (F_v/F_m) was highest and it could be hypothesised that PSII (1 heme *b* group) and cytochrome b_6f (2 heme *b* groups) would be most abundant.

Decreased chl:C ratios in iron stressed *Trichodesmium* cultures have previously been reported (Kustka et al. 2003b), with a similar trend also apparent from this investigation under matching light levels. However, chl:C ratios presented here were lower (68 - 138 µmol mol^{-1} across the six iron concentrations) in comparison to the aforementioned study, which ranged from 175 up to 350 µmol mol^{-1} (Kustka et al. 2003b). Chlorophyll *a* is primarily associated with PSI in cyanobacteria (Suggett et al. 2009, Amunts et al. 2010)

and chlorophyll *a* concentrations decreased with decreasing F_v/F_m for both *Crocosphaera* and *Trichodesmium* (Fig. 5.20); thus it could be inferred that both species reduced their PSI pool as iron concentration decreased. Richier et al. (2012) showed that the PSI to PSII ratio (PSI:PSII) in *Trichodesmium*, estimated from the ratio of the photosystem proteins PsaC and PsbA respectively, decreased as cultures became iron stressed; a trend previously reported by Berman-Frank et al. (2001a). Furthermore, it has also been shown that iron deficiency leads to a marked decrease in PSI reaction centres in *Trichodesmium* (Shi et al. 2007). Evidence from this study supports the idea that PSI abundance declines as *Crocosphaera* and *Trichodesmium* cultures become iron stressed; a result of the high iron demand attributed to this component of the photosynthetic apparatus. Nevertheless, without concurrent PSI (PsaC) and PSII (PsbA) data from the current study, it is necessary to consider the potential reduction in PSI with caution.

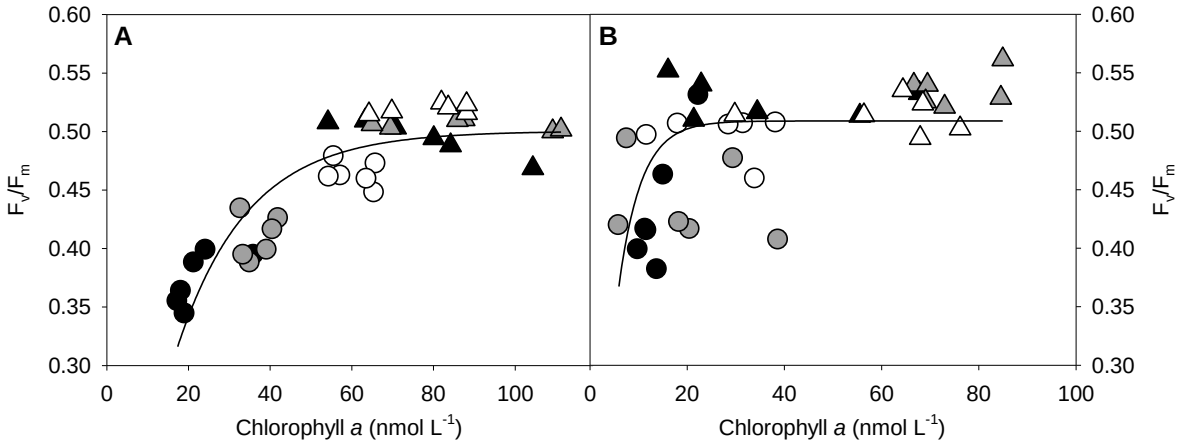

Figure 5.20. Chlorophyll *a* concentration (nmol L^{-1}) against the maximum photochemical quantum yield of PSII (F_v/F_m) determined for cultures of (**A**) *Crocosphaera watsonii* and (**B**) *Trichodesmium erythraeum* grown under varying iron concentration: 0 nmol L^{-1} Fe_T (black circle), 4 nmol L^{-1} Fe_T (grey circle), 10 nmol L^{-1} Fe_T (white circle), 20 nmol L^{-1} Fe_T (black triangle), 40 nmol L^{-1} Fe_T (grey triangle) and 120 nmol L^{-1} Fe_T (white triangle). Exponential rise to maximum (single, 2 parameter) lines fitted to each plot. Equations: (A) $y = 0.500 * (1 - \exp^{(-0.058 * x)})$, ($r^2 = 0.766$); (B) $y = 0.508 * (1 - \exp^{(-0.217 * x)})$, ($r^2 = 0.199$).

5.5.2 Heme b in marine diazotrophs

Heme *b* concentrations of the two marine diazotroph cultures, in particular *Trichodesmium* (Table 5.3), were generally lower compared to *Synechococcus* sp. WH7803 and five eukaryotic phytoplankton species, as previously hypothesised (section 5.2.2.1). Decreased mean heme *b* concentrations, although not significant, were reflected by decreased F_v/F_m in *Crocosphaera* cultures (Fig. 5.21A), similar to the response by eukaryotic phytoplankton (Fig. 5.21B). However, the abundance of heme *b* in *Trichodesmium* cultures did not provide an obvious reduction with decreasing F_v/F_m (Fig. 5.21A). Given the majority of iron is associated with photosynthesis in marine

phytoplankton (Strzepek and Harrison 2004), it could be expected that a large proportion of *b*-type hemoproteins are located in the photosynthetic architecture. Heme *b* is incorporated into PSII via cytochrome b_{559} (Pospisil 2012) as well as the cytochrome b_6f complex (Kurisu et al. 2003, Cramer et al. 2006, Baniulis et al. 2008) of the membrane bound photosynthetic apparatus (see Table 4.7, Chapter 4); hence quantification of heme *b* could be closely related to the abundance of *b*-type hemoproteins within these key complexes. F_v/F_m represents the probability that photons will be converted to electrons and is thus likely to be linked to the presence of functional PSII and subsequent transport of electrons downstream to other proteins, presumably via cytochrome b_6f. However, consistently low heme *b* concentrations of *Trichodesmium* cultures did not correspond to the biophysical measurements. A possible explanation for reduced heme *b* concentrations in both diazotrophs could be related to the allocation of iron towards nitrogen fixation, especially given that heme *b* is not incorporated into the nitrogenase complex. As previously mentioned, the primary use of iron is associated with photosynthesis, whereas nitrogen fixation represents an additional iron sink for diazotrophs; therefore, it is reasonable to assume that iron that would 'typically' be incorporated within *b*-type hemoproteins (i.e. non-nitrogen fixers) will instead be allocated to nitrogenase, which subsequently reduces the overall heme *b* pool.

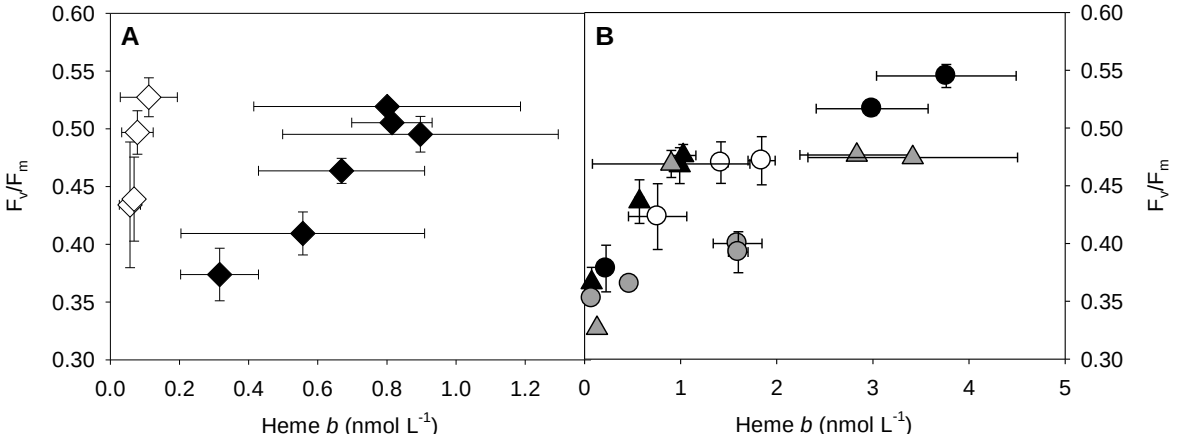

Figure 5.21. Mean heme *b* concentration (nmol L^{-1}) versus maximum photochemical quantum yield of PSII (F_v/F_m) determined for cultures of (**A**) the diazotrophs *Crocosphaera watsonii* (black diamond) and *Trichodesmium erythraeum* (white diamond) and (**B**) the eukaryotic phytoplankton *Dunialella tertiolecta* (black circle), *Emiliania huxleyi* (grey circle), *Thalassiosira weissflogii* (white circle), *Thalassiosira oceanica* (black triangle) and *Phaeodactylum tricornutum* (grey triangle) grown under varying iron concentration and high light conditions (Honey et al. 2013). Note different scales on *x*-axis of A and B.

An alternative explanation for low heme *b* concentrations in *Trichodesmium* cultures could be linked to nitrogen fixation once again, but specifically a mechanism by which the organism protects the nitrogenase enzyme from oxidation by PSII-derived oxygen

molecules. The Mehler reaction (see Fig 5.2, Mehler 1957) involves the catalysed reduction (and subsequent 're-oxidation') of oxygen to water by superoxide dismutase (SOD) and ascorbate peroxidase (APX) (Falkowski and Raven 1997, Asada 1999). Electron transport via the Mehler reaction can be prominent in cyanobacterial organisms (Lewitus and Kana 1995) and Milligan et al. (2007) showed that *Trichodesmium* demonstrate high levels of cellular oxygen consumption by Mehler activity. Furthermore, it has been suggested that as much as 70% of photosynthetic electrons in *Trichodesmium* are transferred to oxygen through Mehler reactions (Kana 1992). Both SOD and APX incorporate iron cofactors within their structure, with one heme *b* group associated with APX (Sharp et al. 2004, Zamocky and Obinger 2010). This could represent a 'low heme *b* pathway' upon which oxygen consumption occurs whilst still facilitating the process of nitrogen fixation; creating a pseudocyclic electron transfer flow in conjunction with ATP production via PSI. Kana (1993) speculated the possibility that Mehler activity enables the production of additional ATP required by nitrogen fixation on top of photosynthetic carbon fixation. In which case, the occurrence of Mehler reactions could have an influence upon the abundance of photosynthetic structures, including the cytochrome b_6f complex (2 heme *b* groups); although this would be dependent upon the efficiency and quantity of APX required to remove hydrogen peroxide (H_2O_2), an intermediate product of the Mehler reaction, compared to electron transfer through cytochrome b_6f. On a similar note, H_2O_2 and other reactive oxygen species (ROS) produced as intermediate components of the Mehler reaction are known to lead to the degradation of hemes (Ryter and Tyrrell 2000). If substantial quantities of these intermediates were present at the time of sampling or were continued to be produced post-filtration, an unknown fraction of heme *b* could have been lost prior to analysis; hence reduced heme *b* concentrations. It could be argued that heme *b* concentrations of *Crocosphaera* cultures were not reduced to the same extent, but nitrogen fixation levels were greater in *Trichodesmium* cultures. Either way, this scenario (Mehler activity) provides a potential mechanism by which *Trichodesmium* protects nitrogenase from oxygen-induced inhibition, as well as assisting nitrogen fixation with minimal cellular heme *b* content.

Heme *b* was positively correlated to POC and PON concentration in cultures of *Crocosphaera*, but not *Trichodesmium* (Table 5.4). The ratio of heme *b* to carbon (heme:C) was relatively low for both diazotrophs throughout the different iron treatments (Fig. 5.22A); comparable to the lowest iron concentrations of five eukaryotic phytoplankton (Fig. 5.22B). Despite the heme *b* concentration of *Crocosphaera* cultures decreasing with lowering total iron concentration, which also resulted in decreased F_v/F_m (Fig. 5.21A), heme *b* contents were not significantly different between the six different iron concentrations examined. This suggested that the abundance of heme *b* in *Crocosphaera* cultures was maintained irrespective of iron concentration, as opposed to

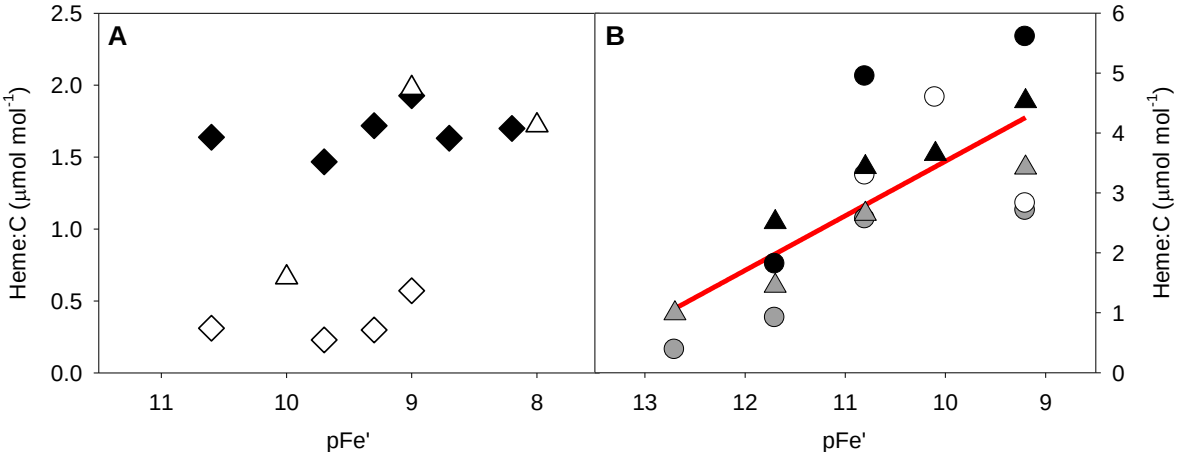

Figure 5.22. Mean heme *b* concentration per unit carbon (heme:C, µmol mol^{-1} C) determined for cultures of (**A**) the cyanobacteria *Synechococcus* sp. WH7803 (white triangle), *Crocosphaera watsonii* (black diamond) and *Trichodesmium erythraeum* (white diamond) and (**B**) the eukaryotic phytoplankton *Dunialella tertiolecta* (black circle), *Emiliania huxleyi* (grey circle), *Thalassiosira weissflogii* (white circle), *Thalassiosira oceanica* (black triangle) and *Phaeodactylum tricornutum* (grey triangle) grown under varying iron concentration and high light conditions. pFe' represents -log[inorganic Fe]. Note different scales on *x*- and *y*-axis of A and B. Red line (B) indicates linear regression for all eukaryotic phytoplankton ($y = 0.910x - 12.631$, $r^2 = 0.555$, $p < 0.01$).

being dependent on iron availability as displayed by *Synechococcus* sp. WH7803 and various eukaryotic species (Fig. 5.22B). This trend was also evident in *Trichodesmium* cultures, although heme:C ratios were much lower than *Crocosphaera* (<0.6 compared to <2.0 µmol mol^{-1} C). The non-diazotrophic unicellular cyanobacteria *Synechococcus* sp. WH7803 provided similar mean heme:C ratios when compared to the two diazotrophs, but a significant increase was observed between the lowest and highest iron regimes. *Crocosphaera* cultures were relatively comparable to *Synechococcus* sp. WH7803 cultures grown at 120 nmol L^{-1} Fe_T with regards to heme:C (2.10 ± 0.78 µmol mol^{-1} C) and heme:N (10.2 ± 4.6 µmol mol^{-1} N) ratios. However, 12 nmol L^{-1} Fe_T cultures (lowest iron regime) of *Synechococcus* sp. WH7803 provided a closer comparison to *Trichodesmium* in terms of heme:C (0.72 ± 0.30 µmol mol^{-1} C) and heme:N (2.17 ± 0.86 µmol mol^{-1} N) ratio. Therefore, the strict regulation of heme *b* content in *Crocosphaera* and *Trichodesmium* cultures could be a specific response of marine diazotroph to regulate iron usage. Furthermore, it appears that *Trichodesmium* require less heme *b* compared to both *Crocosphaera* and *Synechococcus* sp. WH7803 to function. A minimum heme *b* requirement as described in Chapter 4 for *Synechococcus* sp. WH7803 is not possible for either diazotroph, as heme:C ratios were not modified at lower iron concentrations; thus it is more appropriate to suggest *Crocosphaera* and *Trichodesmium* maintain their heme *b* content at roughly 1.5 and 0.5 µmol mol^{-1} C, respectively. If this is the case, *Crocosphaera* actually enforces a greater, or at least equal, heme *b* requirement

compared to the non-diazotrophic cyanobacteria *Synechococcus* sp. WH7803 (1 - 1.5 µmol mol^{-1} C). Nevertheless, heme:C ratios of the two diazotrophs were generally lower than eukaryotic phytoplankton, potentially the result of the high non-heme iron requirement of nitrogenase or a phylogenetic trait of cyanobacteria (i.e. low heme *b* content in cyanophytes), including *Synechococcus* sp. WH7803.

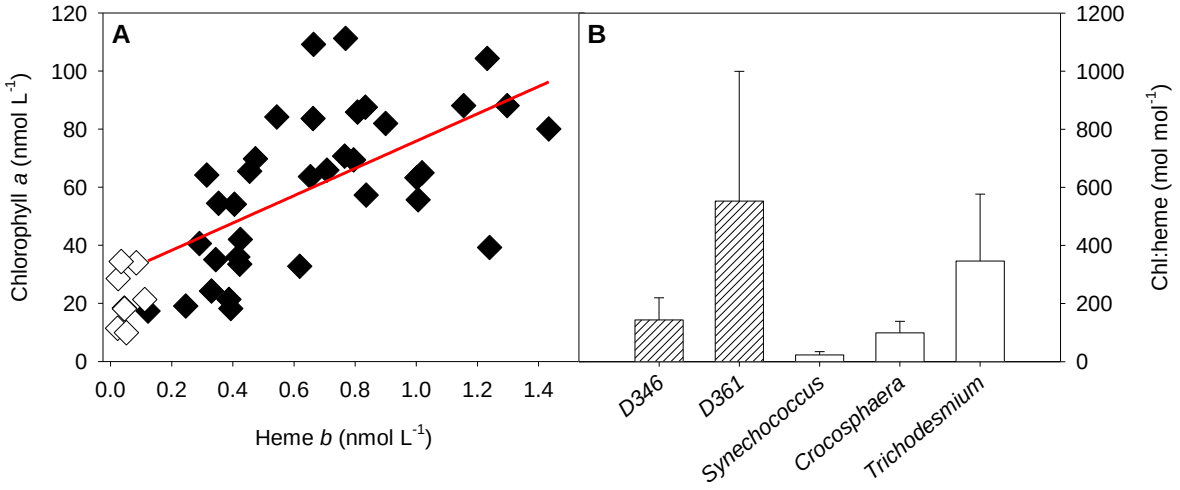

Figure 5.23. (**A**) Heme *b* concentration (nmol L^{-1}) against chlorophyll *a* concentration (nmol L^{-1}) determined for cultures of *Crocosphaera watsonii* (black diamond) and *Trichodesmium erythraeum* (white diamond) grown under varying iron concentrations and (**B**) the mean chlorophyll *a* to heme *b* ratio (chl:heme, mol mol^{-1}) from the (sub-) tropical North Atlantic (striped, cruises D346 and D361) and laboratory cultures of the cyanobacteria *Synechococcus* sp. WH7803, *Crocosphaera* and *Trichodesmium* (white, iron concentrations combined). Red line (A) indicates linear regression for *Crocosphaera* data only ($y = 46.993x + 28.881$, $r^2 = 0.358$, $p < 0.01$).

Heme *b* and chlorophyll *a* concentrations were significantly correlated in *Crocosphaera* cultures (Fig. 5.23A). However, the same trend was not observed in *Trichodesmium*, although the number of heme *b* samples was limited. Changes in chl:heme ratios for both diazotrophic species were comparable to *Synechococcus* sp. WH7803 (Fig. 4.5) as mean chl:heme ratios increased with increasing iron availability, but were not significantly different (Fig 5.12). Similar chlorophyll *a* contents for the two diazotrophs suggested that the increased chl:heme ratios in *Trichodesmium* cultures were the result of reduced heme *b* content. Given that chlorophyll *a* concentrations were elevated and the heme *b* concentration was below the detection limit for *Trichodesmium* cultures grown at 40 or 120 nmol L^{-1} Fe_T, chl:heme ratios would most likely have increased further at these iron concentrations (Fig. 5.12). Compared to field data (Fig. 5.23B), the overall mean chl:heme ratio of *Crocosphaera* cultures ($M = 99.1 \pm 39.8$ mol mol^{-1}) offered a closer relationship to cruise D346 of the STNA ($M = 144 \pm 75.7$ mol mol^{-1}) as opposed to cruise D361 of the TNA ($M = 553 \pm 446$ mol mol^{-1}). On the other hand, the elevated chl:heme ratios of

Trichodesmium cultures (M = 346 ± 230 mol mol^{-1}) were more akin to cruise D361 than *Crocosphaera*. Therefore, variability in chl:heme ratios could indicate spatial distributions of marine diazotrophs in the (sub-) tropical North Atlantic.

The distribution of the nitrogenase iron protein gene, *nifH*, in the (sub-) tropical North Atlantic was used to indicate diazotroph temperature ranges via the detection of filamentous and non-filamentous *nifH* sequences (Langlois et al. 2005). Filamentous diazotrophs, such as *Trichodesmium*, were predominantly found to occupy waters of temperature between 26.5 and 30 °C; whereas non-filamentous nitrogen fixers, such as *Crocosphaera*, occupied a greater temperature range between 15 and 30 °C, but more frequently in waters <26 °C (Langlois et al. 2005). It is possible that the slightly lower temperatures measured during the cross-sectional transect of the STNA during D346 (Fig. 3.2A) were more suited to *Crocosphaera* spp., compared to the warmer region surveyed in the TNA during D361 (Figs. 3.6A and 3.7A). Furthermore, *Trichodesmium* spp. could have been proportionately more abundant compared to non-filamentous diazotrophs during D361 as a result of the warmer waters in the TNA. Therefore, the link between seawater temperature and diazotroph diversity explains, to some extent, the variation in chl:heme ratios between the two research cruises. Nevertheless, the entire phytoplankton community contributes to the heme *b* pool in field samples including non-diazotrophic organisms, and it is unreasonable to suggest chl:heme ratios are reflective of one particular group of organisms.

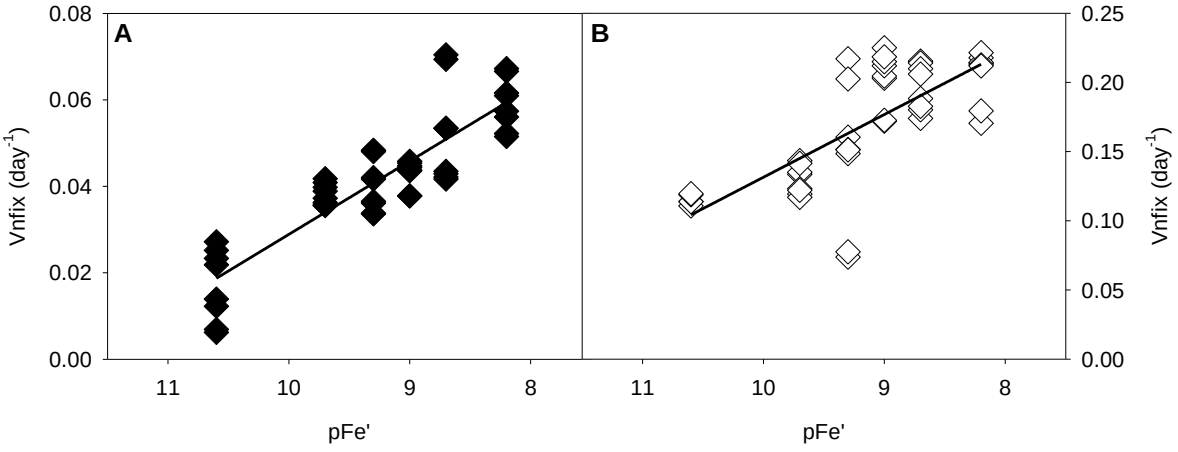

Figure 5.24. Nitrogen-specific growth rate via nitrogen fixation (Vnfix, day^{-1}) determined for cultures of (**A**) *Crocosphaera watsonii* and (**B**) *Trichodesmium erythraeum* grown under varying iron concentration. pFe' represents -log[inorganic Fe]. Lines indicate linear regression: (A) $y = 0.017x - 0.198$ ($r^2 = 0.773$, $p < 0.01$); (B) $y = 0.045x - 0.585$ ($r^2 = 0.550$, $p < 0.01$). Note different scales on y-axis of A and B.

5.5.3 Nitrogen fixation and heme b in laboratory cultures and the field

Numerous studies on nitrogen fixation rates in marine diazotrophs have shown a marked decrease when grown under iron stressed conditions, often with particular reference to *Trichodesmium* spp. (Paerl et al. 1994, Fu and Bell 2003, Küpper et al. 2008, Richier et al. 2012). *Crocosphaera* and *Trichodesmium* expressed significantly reduced nitrogen fixation rates in cultures with no added iron compared to those grown at the highest iron concentrations during this study (Table 5.5). This was also reflected in the nitrogen-specific growth rate (Vnfix) which decreased as iron availability was reduced in cultures of *Crocosphaera* (Fig. 5.24A) and *Trichodesmium* (Fig. 5.24B). The iron requirement of marine diazotrophs is elevated compared to non-diazotrophs, given the added necessity for iron to accommodate the iron-rich nitrogenase complex (Kustka et al. 2003a, Kustka et al. 2003b). Therefore, the impact of reduced iron availability on diazotrophs effectively leads to a reduction in the production of nitrogenase, as demonstrated by a down-regulation of *nifH* in iron stressed *Trichodesmium* cultures (Shi et al. 2007, Richier et al. 2012).

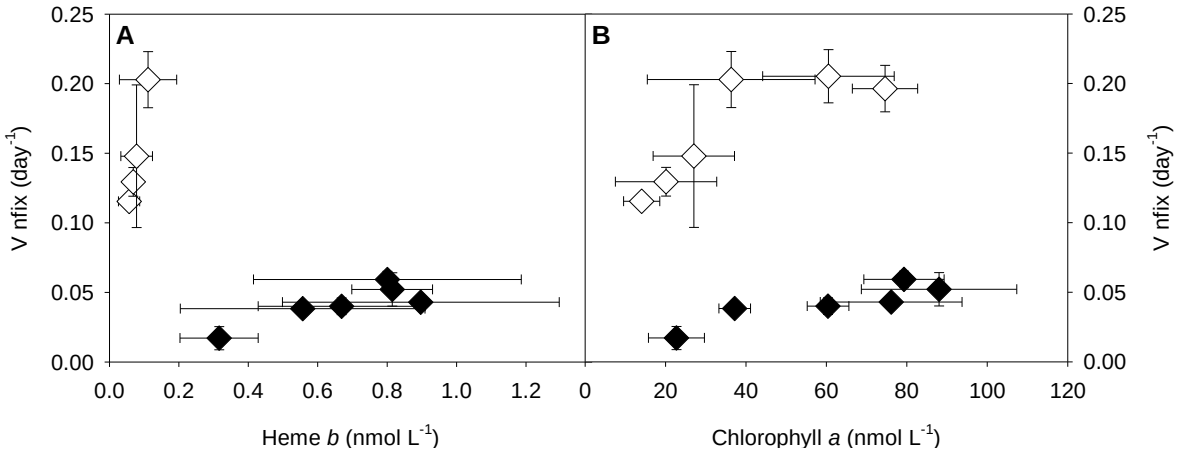

Figure 5.25. Nitrogen-specific growth rate via nitrogen fixation (Vnfix, day^{-1}) versus (**A**) heme *b* concentration (nmol L^{-1}) and (**B**) chlorophyll *a* concentration (nmol L^{-1}) determined for cultures of *Crocosphaera watsonii* (black diamond) and *Trichodesmium erythraeum* (white diamond) grown under varying iron concentration (nmol L^{-1} Fe_T).

Iron availability influences the ability of diazotrophs to fix nitrogen, but iron stress also presents a further impact on fundamental metabolic processes (i.e. photosynthesis and respiration) similar to non-diazotrophic organisms; as shown by the cyanobacteria *Synechococcus* sp. WH7803 and eukaryotic phytoplankton (see Chapter 4). Heme *b*, associated with PSII and cytochrome b_6f proteins, increased in concentration with increasing Vnfix rates (and iron) for *Crocosphaera* cultures, but not for *Trichodesmium* (Fig. 5.25A); whereas chlorophyll *a*, primarily linked to PSI, increased for both species (Fig. 5.25B). This could provide evidence to suggest the physiological response of

Trichodesmium differs from other organisms with regards to iron availability. In maintaining a low heme *b* content, *Trichodesmium* could allocate a greater proportion of iron to the production of nitrogenase in order to maximise nitrogen fixation output. Higher nitrogen-specific growth via nitrogen fixation was observed in *Trichodesmium* cultures compared to *Crocosphaera* (Fig. 5.24), supporting the idea that *Trichodesmium* are the primary nitrogen fixers of the oceans (Letelier and Karl 1996, Capone et al. 1997), particularly in the (sub-) tropical North Atlantic (Carpenter and Romans 1991, Capone et al. 2005). Nevertheless, increasing evidence is suggesting that the smaller, but potentially more abundant, unicellular diazotroph population play a similarly important role in global nitrogen production (Zehr et al. 2000, Zehr et al. 2001, Montoya et al. 2004, Moisander et al. 2010).

High iron content is associated with PSI, PSII and cytochrome b_6f of the photosynthetic apparatus (Raven et al. 1999, Kurisu et al. 2003), as well as the nitrogenase complex involved in nitrogen fixation (Rubio and Ludden 2008). To incorporate these different components simultaneously in diazotrophic organisms requires a large inventory of iron; this could be considered unfavourable due to the low iron conditions in the marine environment (Falkowski 1997, Mills et al. 2004). A previous study on cultures of *Crocosphaera watsonii* has proposed a method by which these organisms conserve iron by temporally (diel cycle) changing their metalloproteins / metalloenzymes associated with photosynthesis (day) and nitrogen fixation (night) (Saito et al. 2011). This daily alteration has been referred to as "*hotbunking*" in that *Crocosphaera* up-regulates photosynthetic metalloproteins (e.g. PsaA, PsaB and cytochrome b_6) during the light photoperiod, which are then down-regulated and degraded at night. In contrast, the nitrogenase enzyme is primarily synthesised during darkness and broken down during the day. Despite the energetic cost attributed to this strategy, cultures exhibited a reduced iron requirement by as much as 40% (Fig. 5.26; Saito et al. 2011). Heme *b* contents of *Crocosphaera* cultures measured in the present study were lower compared to eukaryotic phytoplankton, presumably due to the allocation of iron towards nitrogen fixation. However, the relatively increased heme *b* contents of *Crocosphaera* cultures compared to *Trichodesmium* could be attributed to the iron "*hotbunking*" strategy.

Cultures of *Trichodesmium* are unlikely to modify cellular metalloproteins in order to achieve the requisite iron requirements akin to the strategy employed by *Crocosphaera*, as they fix nitrogen and photosynthesise simultaneously during the day (Saito et al. 2011). Richier et al. (2012) showed that the PSI:PSII ratio is reduced in iron stressed cultures of *Trichodesmium* (0.6) when compared to iron-replete conditions (1.1), highlighting the down-regulation of iron-rich PSI proteins when iron availability is low. Relatively high nitrogen fixation rates compared to *Crocosphaera* also imply a large

allocation of iron towards nitrogenase in *Trichodesmium*. In order to protect nitrogenase from oxygen evolved from PSII (Compaore and Stal 2010), electron transport via PSI may be utilised to consume cellular oxygen (Milligan et al. 2007) as previously described. Also, the increased accumulation of the *IsiA* protein in iron stressed *Trichodesmium* cultures (Richier et al. 2012), which acts as a light harvesting antennae for PSI (Ryan-Keogh et al. 2012), suggests that electron transport via PSI is maintained in low iron conditions. However, the down-regulation of genes encoding for proteins with the highest iron requirements (nitrogenase and PSI) is greater compared to the lower iron-requiring proteins (PSII and cytochrome b_6f) when iron becomes limiting (Shi et al. 2007). Therefore, the heme *b* containing proteins may be low in total abundance, but are less influenced by iron stress than nitrogenase and PSI. Compared to *Crocosphaera*, *Trichodesmium* may allocate more available iron towards nitrogenase and PSI, whilst maintaining a minimum PSII content; hence the low heme *b* contents of *Trichodesmium* cultures measured in this study.

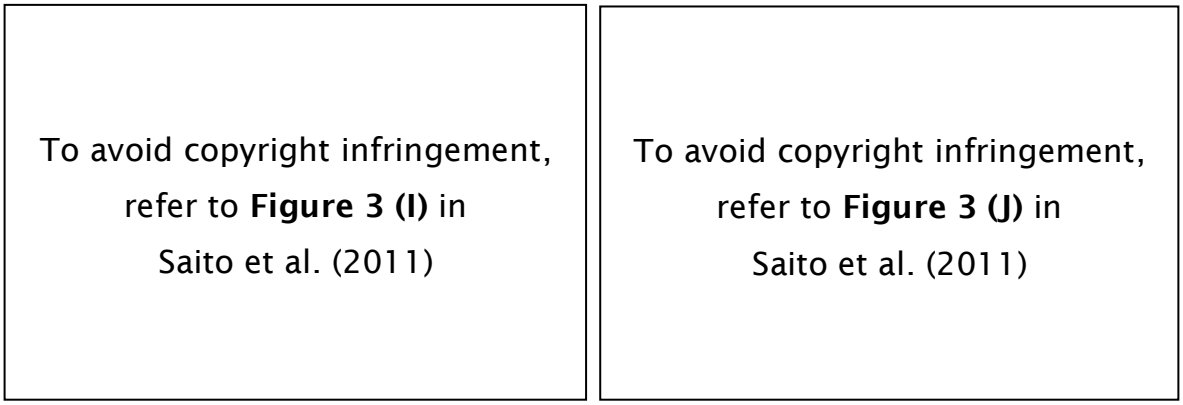

Figure 5.26. Theoretical iron usage of laboratory cultures of *Crocosphaera watsonii* showing (***left***) daily iron demand per cell associated with photosynthesis (black) and nitrogen fixation (red) and (***right***) the sum of photosynthetic and nitrogen fixation iron demand per cell under the "*hotbunking*" scenario (black circles with lines) and "*no hotbunking*" scenario (black dashed line). The *x*-axis indicates hours (darkness, thick black line). Figures from Saito et al. (2011).

Nitrogen fixation rates (Moore et al. 2009, Sohm et al. 2011) and *Trichodesmium* abundance (Tyrrell et al. 2003) are known to be relatively high in the (sub-) tropical North Atlantic compared to the rest of the global ocean. The number of *Trichodesmium* colonies recorded during the SN transect of D361 coincided with increased nitrogen fixation rates (Fig. 5.27), suggesting *Trichodesmium* were most likely the primary nitrogen fixers in the region. Interestingly, the integrated heme *b* concentration did not reflect surface iron concentrations, but did appear to inversely relate to nitrogen fixation rates. Given that *Trichodesmium* spp. were prominent in the region, it is possible that the majority of available iron was incorporated into nitrogenase and PSI; hence low heme *b*

concentrations which are associated with PSII and cytochrome b_6f. Comparison between surface heme *b* (Fig. 3.19) and surface nitrogen fixation (Fig. 5.16) also provided trends between these two parameters; for instance, particularly high heme *b* concentrations were demonstrated in the Coastal TNA, whereas nitrogen fixation rates were minimal and *Trichodesmium* colonies were absent. This suggested the opposite trend to that predicted in hypothesis 5.2.2.4, where heme *b* concentrations were expected to positively correlated to nitrogen fixation rates. Therefore, *Trichodesmium* distribution may strongly influence heme *b* abundance in the TNA, although high *Trichodesmium* abundance and heme:C ratios south of the equator highlight the necessity to consider the impact of other microorganisms upon the distribution of heme *b* in the marine environment.

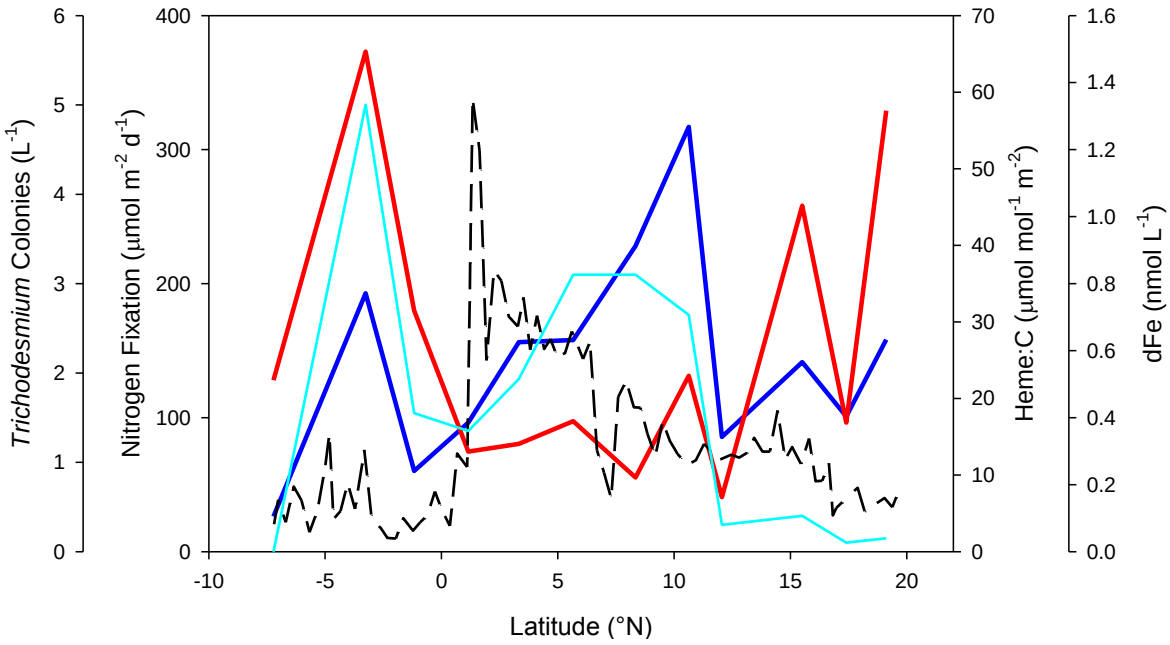

Figure 5.27. Integrated nitrogen fixation rate (dark blue, µmol m^{-2} d^{-1}), *Trichodesmium* colony abundance (light blue, L^{-1}), integrated heme *b* concentration per unit carbon (heme:C, red, µmol mol^{-1} m^{-2}) and surface dissolved iron (dFe) concentration (black dashed, nmol L^{-1}) from the South-North (SN) transect of cruise D361 in the (sub-) tropical North Atlantic (see Fig. 2.4 and Chapter 3). Nitrogen fixation and heme *b* values measured using samples collected from the CTD; dFe concentrations sampled from the continuous trace-metal clean FISH supply. Data for dissolved iron (dFe) concentrations and *Trichodesmium* colony number courtesy of Christian Schlosser (Schlosser et al. in prep) and Joe Snow, respectively (School of Ocean and Earth Science, University of Southampton).

5.6 Conclusions

A laboratory-based investigation of two marine diazotroph species has provided an insight into the allocation of iron between the iron-rich non-heme nitrogenase complex and the *b*-type hemoproteins associated with PSII and cytochrome b_6f (i.e. photosynthesis and respiration). Heme *b* content did not vary as a result of iron availability in laboratory

cultures of *Crocosphaera watsonii* and *Trichodesmium erythraeum*, with abundance in the latter much lower in comparison. In contrast, nitrogen fixation increased with increasing iron concentration, with *Trichodesmium* cultures demonstrating much higher rates than *Crocosphaera* at corresponding iron concentrations. Heme *b* content of *Crocosphaera* cultures were consistent with results obtained for other (non-nitrogen fixing) cyanobacteria and previous work on the abundance of *b*-type hemoproteins (~1.5 μmol mol^{-1} C). It is feasible that the elevated heme *b* abundance of *Crocosphaera* compared to *Trichodesmium* is the result of a diel allocation of cellular iron between *b*-type hemoproteins and nitrogenase. On the other hand, heme *b* contents of *Trichodesmium* cultures remained low in all iron regimes (~0.5 μmol mol^{-1} C), possibly reflecting the different mechanism by which *Trichodesmium* fixes nitrogen in the presence of oxygen (Mehler activity). Two research cruises in the (sub-) tropical North Atlantic demonstrated high nitrogen fixation rates, particularly towards the eastern margin. Evidence to suggest that heme *b* concentrations were reduced in regions of *Trichodesmium* abundance has been proposed, but further investigation is required to provide a stronger conclusion.

5.7 References

Amunts, A., H. Toporik, A. Borovikova, and N. Nelson. 2010. Structure determination and improved model of plant photosystem I. Journal of Biological Chemistry **285**:3478-3486.

Asada, K. 1999. The water-water cycle in chloroplasts: Scavenging of active oxygens and dissipation of excess photos. Annual Review of Plant Physiology and Plant Molecular Biology **50**:601.639.

Baniulis, D. E., E. Yamashita, Y. H. Zhang, S. S. Hasan, and W. A. Cramer. 2008. Structure-function of the cytochrome b_6f complex. Photochemistry and Photobiology:1349-1358.

Berges, J. A. and M. R. Mulholland. 2008. Enzymes and nitrogen cycling. Pages 1385-1444 *in* D. G. Capone, D. A. Bronk, M. R. Mulholland, and E. J. Carpenter, editors. Nitrogen in the Marine Environment. Elsevier Inc.

Berman-Frank, I., J. T. Cullen, Y. Shaked, R. M. Sherrell, and P. G. Falkowski. 2001a. Iron availability, cellular iron quotas, and nitrogen fixation in *Trichodesmium*. Limnology and Oceanography **46**:1249-1260.

Berman-Frank, I., P. Lundgren, Y.-B. Chen, H. Kupper, Z. Kolber, B. Bergman, and P. Falkowski. 2001b. Segregation of nitrogen fixation and oxygenic photosynthesis in the marine cyanobacterium *Trichodesmium*. Science **294**:1534-1537.

Berman-Frank, I., P. Lundgren, and P. Falkowski. 2003. Nitrogen fixation and photosynthetic oxygen evolution in cyanobacteria. Research in Microbiology **154**:157-164.

Capone, D. G., J. A. Burns, J. P. Montoya, A. Subramaniam, C. Mahaffey, T. Gunderson, A. F. Michaels, and E. J. Carpenter. 2005. Nitrogen fixation by *Trichodesmium* spp.: An important source of new nitrogen to the tropical and subtropical North Atlantic Ocean. Global Biogeochemical Cycles **19**:GB2024.

Capone, D. G. and A. Subramaniam. 2005. Seeing microbes from space. ASM News **71**:179-186.

Capone, D. G., J. P. Zehr, H. W. Paerl, B. Bergman, and E. J. Carpenter. 1997. *Trichodesmium*, a globally significant marine cyanobacterium. Science **276**:1221-1229.

Carpenter, E. J. and D. G. Capone. 2008. Nitrogen fixation in the marine environment. Pages 141-198 *in* D. G. Capone, D. A. Bronk, M. R. Mulholland, and E. J. Carpenter, editors. Nitrogen in the marine environment. Elsevier Inc.

Carpenter, E. J. and K. Romans. 1991. Major role of the cyanobacterium *Trichodesmium* in nutrient cycling in the North Altantic Ocean. Science **254**:1356-1358.

Chappell, P. D. and E. A. Webb. 2010. A molecular assessment of the iron stress response in the two phylogenetic clades of *Trichodesmium*. Environmental Microbiology **12**:13-27.

Chen, Y.-B., J. P. Zehr, and M. Mellon. 1996. Growth and nitrogen fixation of the diazotrophic filamentous nonheterocystous cyanobacterium *Trichodesmium* sp. IMS 101 in defined media: evidence for a circadian rhythm. Journal of Phycology **32**:916-923.

Compaore, J. and L. J. Stal. 2010. Oxygen and the light-dark cycle of nitrogenase activity in two unicellular cyanobacteria. Environmental Microbiology **12**:54-62.

Cramer, W. A., H. Zhang, J. Yan, G. Kurisu, and J. L. Smith. 2006. Transmembrane traffic in the cytochrome b_6f complex. Annual Review of Biochemistry **75**:769-790.

Delwiche, C. C., P. J. Zinke, C. M. Johnson, and R. A. Virginia. 1979. Nitrogen isotope distribution as a presumptive indicator of nitrogen fixation. Botanical Gazette **140**:S65-S69.

Falcón, L. I., E. J. Carpenter, F. Cipriano, B. Bergman, and D. G. Capone. 2004. N_2 fixation by unicellular bacterioplankton from the Atlantic and Pacific Oceans: Phylogeny and in situ rates. Applied and Environmental Microbiology **70**:765-770.

Falkowski, P. G. 1997. Evolution of the nitrogen cycle and its influence on the biological sequestration of CO_2 in the ocean. Nature **387**:272-275.

Falkowski, P. G. and J. A. Raven. 1997. Aquatic Photosynthesis. Second edition. Princeton University Press, Oxford.

Fu, F.-X., M. R. Mulholland, N. S. Garcia, A. Beck, P. W. Bernhardt, M. E. Warner, S. A. Sanudo-Wilhelmy, and D. A. Hutchins. 2008. Interactions between changing pCO_2, N_2 fixation, and Fe limitation in the marine unicellular cyanobacterium *Crocosphaera*. Limnology and Oceanography **53**:2472-2484.

Fu, F. and P. R. F. Bell. 2003. Growth, N_2 fixation and photosynthesis in cyanobacterium, *Trichodesmium* sp., under Fe stress. Biotechnology Letters **25**:645-649.

Gallon, J. R. 1992. Reconciling the incompatible: N_2 fixation and O_2. New Phytologist **122**:571-609.

Goebel, N. L., K. A. Turk, K. M. Achilles, R. Paerl, I. Hewson, A. E. Morrison, J. P. Montoya, C. A. Edwards, and J. P. Zehr. 2010. Abundance and distribution of major groups of diazotrophic cyanobacteria and their potential contribution to N_2 fixation in the tropical Atlantic Ocean. Environmental Microbiology **12**:3272-3289.

Gruber, N. and J. L. Sarmiento. 1997. Global patterns of marine nitrogen fixation and denitrification. Global Biogeochemical Cycles **11**:235-266.

Hansell, D. A. and M. J. Follows. 2008. Nitrogen in the Atlantic Ocean. Pages 597-630 *in* D. G. Capone, D. A. Bronk, M. R. Mulholland, and E. J. Carpenter, editors. Nitrogen in the Marine Environment. Elsevier Inc.

Honey, D. J., M. Gledhill, T. S. Bibby, F-E. Legiret, N. J. Pratt, A. E. Hickman, T. Lawson, and E. P. Achterberg. 2013. Heme *b* in marine phytoplankton and particulate material from the North Atlantic Ocean. Marine Ecology Progress Series **483**: 1-17.

Kana, T. M. 1992. Oxygen cycling in cyanobacteria, with specific reference to oxygen protection in *Trichodesmium* spp. Pages 29-41 *in* E. J. Carpenter, D. G. Capone, and J. G. Rueter, editors. Marine Pelagic Cyanobacteria: *Trichodesmium* and Other Diazotrophs. Kluwer Academic Publishers, Dordrecht, Netherlands.

Kana, T. M. 1993. Rapid oxygen cycling in *Trichodesmium thiebautii*. Limnology and Oceanography **38**:18-24.

Karl, D., R. Letelier, L. Tupas, J. Dore, J. Christian, and D. Hebel. 1997. The role of nitrogen fixation in the biogeochemical cycling in the subtropical North Pacific Ocean. Nature **388**:533-538.

Karl, D., A. Michaels, B. Bergman, D. Capone, E. Carpenter, R. Letelier, F. Lipschultz, H. Paerl, D. Sigman, and L. Stal. 2002. Dinitrogen fixation in the world's oceans. Biogeochemistry **57/58**:47-98.

Küpper, H., I. Šetlík, S. Seibert, O. Prášil, E. Šetlikova, M. Strittmatter, O. Levitan, J. Lohscheider, I. Adamska, and I. Berman-Frank. 2008. Iron limitation in the marine cyanobacterium *Trichodesmium* reveals new insight into regulation of photosynthesis and nitrogen fixation. New Phytologist **179**:784-798.

Kurisu, G., H. Zhang, J. L. Smith, and W. A. Cramer. 2003. Structure of the cytochrome b_6f complex of oxygenic photosynthesis: Tuning the cavity. Science **302**:1009-1014.

Kustka, A., E. J. Carpenter, and S. A. Sanudo-Wilhelmy. 2002. Iron and marine nitrogen fixation: progress and future directions. Research in Microbiology **153**:255-262.

Kustka, A., S. Sanudo-Wilhelmy, E. J. Carpenter, D. G. Capone, and J. A. Raven. 2003a. A revised estimate of the iron use efficiency of nitrogen fixation, with special reference to the marine cyanobacterium *Trichodesmium* spp. (Cyanophyta). Journal of Phycology **39**:12-25.

Kustka, A. B., S. A. Sanudo-Wilhelmy, and E. J. Carpenter. 2003b. Iron requirements for dinitrogen- and ammonium-supported growth in cultures of *Trichodesmium* (IMS 101): Comparison with nitrogen fixation rates and iron:carbon ratios of field populations. Limnology and Oceanography **48**:1869-1884.

La Roche, J. and E. Breitbarth. 2005. Importance of the diazotrophs as a source of new nitrogen in the ocean. Journal of Sea Research **53**:67-91.

Landrum, J. P., M. A. Altabet, and J. P. Montoya. 2011. Basin-scale distributions of stable nitrogen isotopes in the subtropical North Atlantic Ocean: Contributions of diazotroph nitrogen to particulate organic matter and mesozooplankton. Deep Sea Research I **58**:615-625.

Langlois, R. J., J. La Roche, and P. A. Raab. 2005. Diazotrophic diversity and distribution in the tropical and subtropical Atlantic Ocean. Applied and Environmental Microbiology **71**:7910-7919.

Letelier, R. M. and D. M. Karl. 1996. Role of *Trichodesmium* spp. in the productivity of the subtropical North Pacific Ocean. Marine Ecology Progress Series **133**:263-273.

Lewitus, A. J. and T. M. Kana. 1995. Light respiration in six estuarine phytoplankton species: contrasts under photoautotrophic and mixotrophic growth conditions. Journal of Phycology **31**:754-761.

Mahaffey, C., A. F. Michaels, and D. G. Capone. 2005. The conundrum of marine N_2 fixation. American Journal of Science **305**:546-595.

Mahaffey, C., R. G. Williams, G. A. Wolff, N. Mahowald, W. Anderson, and M. Woodward. 2003. Biogeochemical signatures of nitrogen fixation in the eastern North Atlantic. Geophysical Research Letters **30**:1300.

Mehler, A. H. 1957. Studies on reactions of illuminated chloroplasts. I. Mechanism of the reduction of oxygen and other Hill reagents. Archives of Biochemistry and Biophysics **33**:65-77.

Michaels, A. F., D. Olson, J. L. Sarmiento, J. W. Ammerman, K. Fanning, R. Jahnke, A. H. Knap, F. Lipschultz, and J. M. Prospero. 1996. Inputs, losses and transformations of nitrogen and phosphorus in the pelagic North Atlantic Ocean. Biogeochemistry **35**:181-226.

Milligan, A. J., I. Berman-Frank, Y. Gerchman, G. C. Dismukes, and P. G. Falkowski. 2007. Light-dependent oxygen consumption in nitrogen-fixing cyanobacteria plays a key role in nitrogenase protection. Journal of Phycology **43**:845-852.

Mills, M. M., C. Ridame, M. Davey, J. La Roche, and R. J. Geider. 2004. Iron and phosphorus co-limit nitrogen fixation in the eastern tropical North Atlantic. Nature **429**:292-294.

Mohr, W., M. P. Intermaggio, and J. La Roche. 2010. Diel rhythm of nitrogen and carbon metabolism in the unicellular, diazotrophic cyanobacterium *Crocosphaera watsonii* WH8501. Environmental Microbiology **12**:412-421.

Moisander, P. H., R. A. Beinart, I. Hewson, A. E. White, K. S. Johnson, C. A. Carlson, J. P. Montoya, and J. P. Zehr. 2010. Unicellular cyanobacterial distributions broaden the oceanic N_2 fixation domain. Science **327**:1512-1514.

Montoya, J. P., C. M. Holl, J. P. Zehr, A. Hansen, T. A. Villareal, and D. G. Capone. 2004. High rates of N_2 fixation by unicellular diazotrophs in the oligotrophic Pacific Ocean. Nature **430**:1027-1031.

Montoya, J. P., M. Voss, and D. G. Capone. 2007. Spatial variations in N_2-fixation rate and diazotroph activity in the Tropical Atlantic. Biogeosciences **4**:369-376.

Moore, C. M., M. M. Mills, E. P. Achterberg, R. J. Geider, J. La Roche, M. I. Lucas, E. L. McDonagh, X. Pan, A. J. Poulton, M. J. A. Rijkenberg, D. J. Suggett, S. J. Ussher, and

E. M. S. Woodward. 2009. Large-scale distribution of Atlantic nitrogen fixation controlled by iron availability. Nature Geoscience **2**:867-871.

Mulholland, M. R. and D. G. Capone. 2000. The nitrogen physiology of the marine N2-fixing cyanobacteria Trichodesmium spp. TRENDS in Plant Science **5**:148-153.

Paerl, H. W., K. M. Crocker, and L. E. Prufert. 1987. Limitation of N_2 fixation in coastal marine waters: Relative importance of molybdenum, iron, phosphorus, and organic matter availability. Limnology and Oceanography **32**:525-536.

Paerl, H. W., L. E. Prufert-Bebout, and C. Guo. 1994. Iron-stimulated N_2 fixation and growth in natural and cultured populations of the planktonic marine cyanobacteria *Trichodesmium* spp. Applied and Environmental Microbiology **60**:1044-1047.

Pospisil, P. 2012. Enzymatic function of cytochrome b_{559} in photosystem II. Journal of Photochemistry and Photobiology B: Biology **104**:341-347.

Poulton, A. J., M. C. Stinchcombe, and G. D. Quartly. 2009. High numbers of *Trichodesmium* and diazotrophic diatoms in the southwest Indian Ocean. Geophysical Research Letters **36**:L15610.

Raven, J. A., M. C. W. Evans, and R. E. Korb. 1999. The role of trace metals in photosynthetic electron transport on O_2-evolving organisms. Photosynthesis Research **60**:111-149.

Redfield, A. C. 1934. On the proportions of organic derivations in sea water and their relation to the composition of plankton. Pages 177-192 *in* R. J. Daniel, editor. James Johnstone Memorial Volume. University Press of Liverpool

Richier, S., A. I. Macey, N. J. Pratt, D. J. Honey, C. M. Moore, and T. S. Bibby. 2012. Abundances of iron-binding photosynthetic and nitrogen-fixing proteins of *Trichodesmium* both in culture and *in situ* from the North Atlantic. PLoS ONE **7**:e35571.

Rubio, L. M. and P. W. Ludden. 2008. Biosynthesis of the iron molybdenum cofactor of nitrogenase. Annual Review of Microbiology **62**:93-111.

Ryan-Keogh, T. J., A. I. Macey, A. M. Cockshutt, M. C. Moore, and T. S. Bibby. 2012. The cyanobacterial chlorophyll-binding-protein IsiA acts to increase the in vivo effective absorption cross-section of photosystem I under iron limitation. Journal of Phycology **48**:145-154.

Ryter, S. W. and R. M. Tyrrell. 2000. The heme synthesis and degradation pathways: Role in oxidant sensitivity. Free Radical Biology and Medicine **28**:289-309.

Saito, M. A., E. M. Bertrand, S. Dutkiewicz, V. V. Bulygin, D. M. Moran, F. M. Monteiro, M. J. Follows, F. W. Valois, and J. B. Waterbury. 2011. Iron conservation by reduction of metalloenzyme inventories in the marine diazotroph *Crocosphaera watsonii*. PNAS **106**:2184-2189.

Schindelin, H., C. Kisker, J. L. Schlessman, J. B. Howard, and D. C. Rees. 1997. Structure of $ADP{\cdot}AlF_4^-$-stabilized nitrogenase complex and its implications for signal transduction. Nature **387**:370-376.

Sharp, K. H., P. C. E. Moody, K. A. Brown, and E. L. Raven. 2004. Crystal structure of the ascorbate peroxidase-salicylhydroxamic acid complex. Biochemistry **43**:8644-8651.

Shi, T., Y. I. Sun, and P. G. Falkowski. 2007. Effects of iron limitation on the expression of metabolic genes in the marine cyanobacterium *Trichodesmium erythraeum* IMS101. Environmental Microbiology **9**:2945-2956.

Sohm, J. A., E. A. Webb, and D. G. Capone. 2011. Emerging patterns of marine nitrogen fixation. Nature Reviews Microbiology **9**:499-508.

Strzepek, R. F. and P. J. Harrison. 2004. Photosynthetic architecture differs in coastal and oceanic diatoms. Nature **431**:689-692.

Subramaniam, A., C. W. Brown, R. R. Hood, E. J. Carpenter, and D. G. Capone. 2002. Detecting *Trichodesmium* blooms in SeaWiFS imagery. Deep-Sea Research II **49**:107-121.

Suggett, D. J., M. C. Moore, A. E. Hickman, and R. J. Geider. 2009. Interpretation of fast repetition rate (FRR) fluorescence: signatures of phytoplankton community structure versus physiological state. Marine Ecology Progress Series **376**:1-19.

Suzuki, T., H. Mori, J. Ishizaka, and K. Katayama. 2007. Biomass and distribution of filamentous cyanobacteria, *Trichodesmium* spp., in spring in the East China Sea. Plankton and Benthos Research **2**:175-183.

Tuit, C., J. Waterbury, and G. Ravizza. 2004. Diel variation of molybdenum and iron in marine diazotrophic cyanobacteria. Limnology and Oceanography **49**:978-990.

Tyrrell, T., E. Maranon, A. J. Poulton, A. R. Bowie, D. S. Harbour, and M. S. E. Woodward. 2003. Large-scale latitudinal distribution of *Trichodesmium* spp. in the Atlantic Ocean. Journal of Plankton Research **25**:405-416.

Vermaas, W. F. J. 2001. Photosynthesis and respiration in cyanobacteria. Encyclopedia of Life Sciences:1-7.

Wada, E. and A. Hattori. 1976. Natural abundance of ^{15}N in particulate organic matter in the North Pacific Ocean. Geochimica et Cosmochimica Acta **40**:249-251.

Wilson, S. T., S. Tozzi, R. A. Foster, I. Ilikchyan, Z. S. Kolber, J. P. Zehr, and D. M. Karl. 2010. Hydrogen cycling by the unicellular marine diazotroph *Crocosphaera watsonii* strain WH8501. Applied and Environmental Microbiology **76**:6797-6803.

Zamocky, M. and C. Obinger. 2010. Molecular phylogeny of heme peroxidases.*in* E. Torres and M. Ayala, editors. Biocatalysis Based on Heme Peroxidases. Springer-Verlag, Berlin.

Zehr, J. P., E. J. Carpenter, and T. A. Villareal. 2000. New perspectives on nitrogen-fixing microorganisms in tropical and subtropical oceans. Trends in Microbiology **8**:68-73.

Zehr, J. P., J. B. Waterbury, P. J. Turner, J. P. Montoya, E. Omoregie, G. F. Steward, A. Hansen, and D. M. Karl. 2001. Unicellular cyanobacteria fix N_2 in the subtropical North Pacific Ocean. Nature **412**:635-638.

Chapter 6

Conclusions and future work

6.1 Conclusions

Hemoproteins are essential components of numerous fundamental biological processes, including photosynthetic and respiratory electron transfer (Moore 1996, Chapman et al. 1997). Nevertheless, data regarding the abundance of hemoproteins in the marine environment is limited, restricting our understanding of this important iron protein pool. The issue was initially addressed by Gledhill (2007) who outlined a chromatographic technique to quantify the most abundant prosthetic group associated with hemoproteins, heme *b*, in marine phytoplankton and bacterioplankton. Subsequently, this project has provided the first detailed species-specific studies of heme *b* abundance in three marine cyanobacterial cultures under the influence of varying iron concentration. Furthermore, a large data set has been obtained from two research cruises regarding the distribution of heme *b* in the (sub-) tropical North Atlantic. At the beginning of the project, it was tentatively considered that heme *b* could provide a better indication of biomass than the well-documented chlorophyll *a*. The extent to which heme *b* is required by organisms, given the crucial roles attributed to hemoproteins, could be such that it would not decrease or change with respect to carbon as a result of environmental conditions. Concentrations of chlorophyll *a* in the deep chlorophyll maximum (DCM) are thought to be indicative of a pigment maximum and not necessarily increased biomass (Perez et al. 2006). Alternatively, the concentration of heme *b* could be highly affected by nutrient availability or show marked variation between species. Either way, the information gained by investigating heme b in marine organisms and the marine environment will help our understanding of productivity in the oceans.

6.1.1 Heme b in the (sub-) tropical North Atlantic

Atmospheric dust presents the predominant source of iron to large parts of the marine environment (Jickells and Spokes 2001) and, given the element's central position in the structure of hemes, the (sub-) tropical North Atlantic presented an ideal location to investigate heme *b* distribution; more than a third of the global atmospheric dust flux into the oceans enters via the North Atlantic (Jickells et al. 2005). During cruise D346 in early 2010 (Jan - Feb), the subtropical North Atlantic (STNA) was characterised by a

distinct thermocline at approximately 100 m depth and low surface nutrient concentrations in the central gyre regions consistent with an oligotrophic environment. Increased phosphate concentrations were measured towards the African coast, where the depth of the thermocline and nitracline decreased as a result of the cold nutrient-rich deep water upwelling associated with the region. A second cruise (D361, Feb - Mar 2011) in the tropical North Atlantic (TNA) suggested similar physical and chemical properties, with enhanced nutrient concentrations and cooler waters towards the coast. The Intertropical Convergence Zone (ITCZ) and equatorial upwelling regions were evident in the TNA, leading to decreased salinities (rainfall) and a shoaling of the thermocline north of the equator.

Chlorophyll *a* concentrations were approximately three times greater in the TNA (M = 0.67 ± 1.0 nmol L^{-1}) compared to the STNA (M = 0.19 ± 0.1 nmol L^{-1}); although this was primarily attributed to distinctly high chlorophyll *a* concentrations in the Coastal TNA region (M = 2.18 ± 1.3 nmol L^{-1}) as a result of high nutrient availability. A similar pattern was evident for heme *b* with higher concentrations in the TNA (M = 2.18 ± 3.2 pmol L^{-1}) compared to the STNA (M = 1.32 ± 0.6 pmol L^{-1}); once again influenced by increased heme *b* concentrations in the Coastal TNA (M = 5.70 ± 4.4 pmol L^{-1}). The ratio of heme *b* to carbon (heme:C) showed very similar values for the STNA (M = 0.64 ± 0.4 µmol mol^{-1} C) and TNA (M = 0.66 ± 0.6 µmol mol^{-1} C). In contrast, chlorophyll *a* concentrations per unit carbon (chl:C) were noticeably reduced in the STNA (M = 89.0 ± 71.5 µmol mol^{-1} C) compared to the TNA (M = 204 ± 86.5 µmol mol^{-1} C). This was also reflected by elevated chlorophyll *a* to heme *b* ratios (chl:heme) in the TNA (M = 553 ± 446 mol mol^{-1}) compared to the STNA (M = 144 ± 76 mol mol^{-1}). Heme *b* provided a better relationship to particulate organic carbon (POC) and particulate organic nitrogen (PON) in the STNA than chlorophyll *a*, but heme *b* was not significantly correlated to POC or PON in five oceanographic regions of the TNA where chlorophyll *a* was instead more comparable. Differences in the abundance of heme *b* between regions of the (sub-) tropical North Atlantic indicate physiological responses to environmental conditions, including interannual variability such as iron concentration and spatial differences in seawater temperature (Langlois et al. 2005).

6.1.2 Heme b requirement of Synechococcus sp. WH7803

The *Synechococcus* genus is generally considered to have a ubiquitous distribution throughout the global ocean, whilst also dominating phytoplankton carbon biomass in the (sub-) tropical North Atlantic along with *Prochlorococcus* (Maranon et al. 2000). An investigation was conducted using laboratory cultures of the physiologically well-defined *Synechococcus* sp. WH7803 under three different total iron concentrations. The final biovolume of cultures grown under low iron concentrations (12 nmol L^{-1} Fe_T) were

significantly reduced compared to medium (120 nmol L^{-1} Fe_T) and high (1200 nmol L^{-1} Fe_T) iron cultures. Growth rates and cell size (diameter) were also significantly reduced under low iron conditions, suggesting these cultures were stressed by the reduced availability of iron. Chlorophyll *a* concentration was an order of magnitude lower in low iron cultures (*M* = 11.6 ± 0.7 nmol L^{-1}) on the final day of each growth cycle compared to high iron cultures (*M* = 119 ± 50 nmol L^{-1}). Heme *b* concentrations were also significantly reduced in low iron cultures (*M* = 0.6 ± 0.2 nmol L^{-1}) compared to high (*M* = 3.7 ± 1.7 nmol L^{-1}) and medium (*M* = 4.3 ± 2.2 nmol L^{-1}) iron cultures, with heme *b* contents (heme:C) also notably reduced in low iron cultures (*M* = 0.7 ± 0.3 µmol mol^{-1} C) compared to high iron cultures (*M* = 1.9 ± 0.9 µmol mol^{-1} C). Mean chl:heme ratios decreased with decreasing iron concentration, ranging from 35.9 ± 18.6 mol mol^{-1} (high iron) to 19.1 ± 8.83 mol mol^{-1} (low iron). Consequently, it was inferred that *Synechococcus* sp. WH7803 maintains *b*-type hemoproteins under iron limiting conditions relative to chlorophyll *a*, exhibiting a heme *b* requirement of 1.0 - 1.5 µmol mol^{-1} C to enable maximal growth rates.

Cultures of *Synechococcus* sp. WH7803 were compared to five eukaryotic phytoplankton species previously investigated by Martha Gledhill (Honey et al. 2013). Mean chl:heme ratios of *Synechococcus* sp. WH7803 were low compared to the eukaryotes, with the diatoms *Thalassiosira oceanica* (23.5 ± 4.16 mol mol^{-1}) and *Phaeodactylum tricornutum* (23.2 ± 6.26 mol mol^{-1}) showing the closest similarities in terms of chl:heme ratio under iron-deplete conditions. However, a different strategy in response to low iron availability was shown by the green algae *Dunaliella tertiolecta* (188 ± 21.9 mol mol^{-1}) and the coccolithophorid *Emiliania huxleyi* (262 ± 49.3 mol mol^{-1}) which instead increased their chl:heme ratio when iron-stressed. The heme *b* requirement of the eukaryotic phytoplankton was typically higher than *Synechococcus* sp. WH7803, potentially related to variations in cellular volume. Data obtained from the (sub-) tropical North Atlantic was also compared to *Synechococcus* sp. WH7803, with chl:heme ratios distinctly elevated in the natural marine environment. Heme *b* concentrations per unit carbon were most comparable between low iron cultures of *Synechococcus* sp. WH7803 and the (sub-) tropical North Atlantic (~0.7 µmol mol^{-1} C). Thus, the low heme:C ratios of the (sub-) tropical North Atlantic could imply that the microbial community in the region was iron limited.

6.1.3 Heme b and nitrogen fixation

Biological nitrogen fixation is catalysed by the iron-rich oxygen-sensitive enzyme complex nitrogenase, converting gaseous dinitrogen into ammonium (Mahaffey et al. 2005, Sohm et al. 2011). Hemoproteins are not involved with the nitrogenase complex and thus represent an alternative iron sink in diazotrophic organisms (i.e. nitrogen fixers). The marine diazotrophs *Crocosphaera watsonii* (WH8501) and *Trichodesmium erythraeum*

(IMS101) were investigated to determine the influence of iron availability upon cellular heme *b* concentrations and nitrogen fixation rates. Cultures were grown at six different iron treatments ranging between 0 and 120 nmol L^{-1} Fe_T. Cellular biovolume at the end of each growth cycle was significantly reduced in cultures with no added iron compared to those grown with 120 nmol L^{-1} Fe_T, which was also evident from significantly lower growth rates in the cultures with no added iron. However, μ_{max} was only significantly reduced in cultures with no added iron for *Crocosphaera*, with *Trichodesmium* cultures showing similar μ_{max} between the six different iron concentrations. Photosynthetic efficiency was closely associated with iron availability, with decreasing F_v/F_m observed with decreasing iron concentration. F_v/F_m represents the probability that photons will be converted to electrons through photosystem II (PSII, 1 heme *b* group, Pospisil 2012) and subsequently transported through the electron transfer pathway, presumably via cytochrome b_6f (2 heme *b* groups, Baniulis et al. 2008); therefore, relatively low F_v/F_m could be used to predict a reduced cellular heme *b* concentration. Nevertheless, heme *b* content was maintained in both *Crocosphaera* and *Trichodesmium* cultures under the six different iron treatments, with *Trichodesmium* showing lower heme:C ratios (~0.5 µmol mol^{-1} C) compared to *Crocosphaera* (~1.5 µmol mol^{-1} C). Heme *b* content of *Crocosphaera* cultures were more comparable to *Synechococcus* sp. WH7803 than *Trichodesmium*, although heme:C ratios of both diazotrophs were reduced compared to the eukaryotic phytoplankton.

Nitrogen fixation rates were significantly reduced in cultures with no added iron compared to 120 nmol L^{-1} Fe_T cultures for both *Crocosphaera* and *Trichodesmium*, with a similar trend also apparent for nitrogen-specific growth via nitrogen fixation (Vnfix). However, nitrogen fixation by *Trichodesmium* was approximately four-fold greater at comparative iron concentrations compared to *Crocosphaera*. This potentially provides an explanation for reduced heme *b* content in *Trichodesmium* cultures as iron was predominantly directed towards the nitrogen fixation apparatus (non-heme) as opposed to photosynthetic activity (PSII and cytochrome b_6f). Additionally, use of the Mehler reaction to consume PSII-derived oxygen and reduce the possibility of nitrogenase inactivation could be related to temporally low heme *b* contents despite increased F_v/F_m. In contrast, proportionately lower nitrogen fixation activity by *Crocosphaera* cultures resulted in increased heme:C ratios compared to *Trichodesmium*, but still lower heme *b* contents than eukaryotic phytoplankton due to the ability to fix nitrogen. Also, *Crocosphaera* cultures have previously demonstrated the ability to "*hotbunk*" iron to reduce their iron requirement (Saito et al. 2011), which in turn could have led to their increased heme *b* content at the time of sampling compared to *Trichodesmium* cultures.

Nitrogen fixation rates and heme *b* contents from the two cruises in the (sub-) tropical North Atlantic (see section 6.1.1) were also compared to *Crocosphaera* and *Trichodesmium* cultures. The (sub-) tropical North Atlantic is known to exhibit high levels of nitrogen fixation (Capone et al. 2005, Moore et al. 2009). Reduced heme:C ratios were observed in the Equatorial Upwelling (EqU) region of the TNA where high *Trichodesmium* abundance and nitrogen fixation rates were also reported. Thus, dependent upon the contribution of *Trichodesmium* spp. to the overall community composition, the low heme:C ratios could have resulted from the large *Trichodesmium* population in the region. Furthermore, low heme:C ratios observed in the (sub-) tropical North Atlantic indicate the region is dominated by cyanobacteria, including non-diazotrophic cyanobacteria such as those from the genus *Synechoccoccus*.

6.2 Summary

The key findings of this investigation were as follows:

1. The intracellular concentration of heme *b* in *Synechococcus* sp. WH7803 required to facilitate maximum growth rates was estimated between 1.0 and 1.5 μmol mol^{-1} C; decreased growth rates were associated with a decrease in heme *b* concentration per unit carbon. In contrast, the heme *b* contents of *Crocosphaera watsonii* (WH8501) and *Trichodesmium erythraeum* (IMS101) cultures were maintained at approximately 1.5 and 0.5 μmol mol^{-1} C respectively, despite variations in iron availability.

2. Nitrogen fixation rates were positively correlated to iron availability, with *Trichodesmium* cultures demonstrating higher rates than *Crocosphaera*. The low heme *b* content of *Trichodesmium* cultures (see above) is potentially related to increased (non-heme) nitrogen fixation activity.

3. Heme *b* concentrations per unit carbon in the (sub-) tropical North Atlantic were comparable to laboratory cultures of the marine cyanobacteria *Synechococcus* sp. WH7803, *Crocosphaera watsonii* (WH8501) and *Trichodesmium erythraeum* (IMS101) and low iron cultures of five eukaryotic phytoplankton species. Therefore, it could be tentatively inferred that the region was iron stressed and/or dominated by cyanobacteria.

4. Evidence has indicated that regions of high nitrogen fixation in the (sub-) tropical North Atlantic were associated with low heme *b* to carbon ratios (heme:C) and this could be attributed to high *Trichodesmium* abundance.

The significant contributions of this project to the marine biogeochemical field includes the presentation of heme *b* concentrations from the subtropical and tropical North Atlantic; enhancing the sparse data set previously available for this important iron protein pool in the marine environment. This, coupled with detailed culture studies of three prominent marine cyanobacterial genera (*Synechococcus*, *Crocosphaera* and *Trichodesmium*) provides a strong basis for further exploration in the field and laboratory. In addition, the determination of heme *b* requirements in the three aforementioned species advances our understanding regarding the physiological responses of marine microorganisms to the availability of iron and, subsequently, changes in environmental conditions in the oceans.

6.3 Future work

This study has highlighted the importance of heme *b* in marine organisms and provided a detailed account of heme *b* abundance in specific laboratory grown cyanobacteria cultures. Developing and publishing the method to quantify heme *b* concentration via high performance liquid chromatography-diode array detection-electrospray ionisation-mass spectrometry (HPLC/DAD/ESI-MS) is necessary. This technique has enhanced our ability to categorically identify heme *b* in cultures and field samples through collision-induced dissociation (CID) ms^2 of *m/z* 616 (i.e. Fe(III) protoheme IX). The method could be dramatically improved by increasing the sample loop (e.g. increased to 100 µl) to enable a greater quantity of heme *b* to be analysed which would improve peak resolution and lower the limit of detection. Another application of the HPLC/DAD/ESI-MS method that should be developed involves the investigation of alternative peaks visible in sample chromatograms (e.g. see Fig. 2.7A), most likely associated with an assortment of pigments. If these peaks can be identified and quantified in tandem with heme *b* analysis, the comprehensive data set generated could be used to determine physiological responses in monocultures or the community composition of field samples. Heme *b* is considered the most versatile natural heme group found in organisms, but alternative heme compounds are also essential, particularly hemes *a* and *c* (Caughey 1973). Therefore, developing the technique to quantify heme *b* whilst investigating alternative heme complexes could further our understanding of hemoproteins in the marine environment. A short study was conducted at the start of this project in an attempt to quantify heme *c* in bovine heart cytochrome *c* (Sigma-Aldrich). Sand bath heating and weak acid additions were employed, with preliminary results suggesting the techniques could provide the basis for future investigation (data not included).

The next suggestion of future work involves the assessment of PSI, PSII and cytochrome b_6f in conjunction with heme *b* analysis. Research to this end has been initiated through quantification of the photosynthetic proteins PsbA and PsaC of PSI and PSII, respectively in

cultures of *E. huxleyi* and *T. oceanica* (Honey et al. 2013). However, in order to determine the efficiency of heme *b* extraction and the proportion of heme *b* incorporated into the photosynthetic apparatus, further investigation is necessary. This could also be achieved through concurrent assessment of the genes encoding for the aforementioned photosynthetic complexes (Shi et al. 2007) and measurements of the absolute quantities of proteins involved in photosynthesis (Richier et al. 2012). Furthermore, this could also be used in conjunction with marine diazotrophs to improve our understanding regarding the allocation of iron between the *b*-type hemoproteins of the photosynthetic apparatus and the non-heme nitrogenase complex.

Diel variations in heme *b* containing proteins are known to occur (Saito et al. 2011); thus the collection of samples at different times of the day and night would provide a valuable insight into the allocation of iron towards hemoproteins dependent on the activity of diazotrophs (i.e. photosynthesis and/or nitrogen fixation). This could also involve the use of a chemostat in order to control the growth rate of organisms and maintain cultures in the exponential growth phase, whilst still varying the concentration of iron. This could also progress to 'iron-shock' investigations whereby heme *b* concentrations are determined in iron-replete cultures after transferal to iron stressed conditions, as well as the subsequent 'recovery' via iron additions.

Variations in heme *b* content were apparent between the three cyanobacteria examined in this project, in addition to differences observed in five eukaryotic phytoplankton. Therefore, it would be beneficial to investigate further key marine species to determine the range of variation in heme *b* content, particularly *Prochlorococcus* and other strains of *Synechococcus* given the dominant role of these genera in the (sub-) tropical North Atlantic. However, field work should not be restricted to this region, with data soon to be available regarding the Iceland Basin and Scotia Sea of the high latitude North Atlantic and Southern Ocean, respectively (Gledhill et al. in prep, see Appendix 1). Cruise D346 in the STNA provided the first cross-sectional profile of heme *b* in the marine environment, and further comprehensive surveys will enable stronger comparisons between the field and laboratory cultures.

6.4 References

Baniulis, D. E., E. Yamashita, Y. H. Zhang, S. S. Hasan, and W. A. Cramer. 2008. Structure-Function of the Cytochrome b_6f Complex. Photochemistry and Photobiology:1349-1358.

Capone, D. G., J. A. Burns, J. P. Montoya, A. Subramaniam, C. Mahaffey, T. Gunderson, A. F. Michaels, and E. J. Carpenter. 2005. Nitrogen fixation by *Trichodesmium* spp.: An important source of new nitrogen to the tropical and subtropical North Atlantic Ocean. Global Biogeochemical Cycles **19**:GB2024.

Caughey, W. S. 1973. Iron porphyrins - hemes and hemins. Pages 797-831 *in* G. L. Eichham, editor. Inorganic biochemistry. Elsevier, Amsterdam.

Chapman, S. K., S. Daff, and A. W. Munro. 1997. Heme: The most versatile redox centre in biology? Metal Sites in Proteins and Models. Structure and Bonding **88**:39-70.

Gledhill, M. 2007. The determination of heme b in marine phyto- and bacterioplankton. Marine Chemistry **103**:393-403.

Gledhill, M., E. P. Achterberg, D. J. Honey, M. Nielsdottir, and M. Rijkenberg. in prep. Distributions of particulate heme *b* in the Atlantic and Southern Ocean - implications for changes in phytoplankton photosystems (see Appendix 1).

Honey, D. J., M. Gledhill, T. S. Bibby, F-E. Legiret, N. J. Pratt, A. E. Hickman, T. Lawson, and E. P. Achterberg. 2013. Heme *b* in marine phytoplankton and particulate material from the North Atlantic Ocean. Marine Ecology Progress Series **483**: 1-17.

Jickells, T. D., Z. S. An, K. K. Andersen, A. R. Baker, G. Bergametti, N. Brooks, J. J. Cao, P. W. Boyd, R. A. Duce, K. A. Hunter, H. Kawahata, N. Kubilay, J. laRoche, P. S. Liss, N. Mahowald, J. M. Prospero, A. J. Ridgwell, I. Tegen, and R. Torres. 2005. Global iron connections between desert dust, ocean biogeochemistry, and climate. Science **308**:67-71.

Jickells, T. D. and L. J. Spokes. 2001. Atmospheric iron inputs to the oceans. Pages 85-121 *in* D. R. Turner and K. A. Hunter, editors. The biogeochemistry of iron in seawater, IUPAC. Wiley.

Langlois, R. J., J. La Roche, and P. A. Raab. 2005. Diazotrophic diversity and distribution in the tropical and subtropical Atlantic Ocean. Applied and Environmental Microbiology **71**:7910-7919.

Mahaffey, C., A. F. Michaels, and D. G. Capone. 2005. The conundrum of marine N_2 fixation. American Journal of Science **305**:546-595.

Maranon, E., P. M. Holligan, M. Varela, B. Mourino, and A. J. Bale. 2000. Basin-scale variability of phytoplankton biomass, production and growth in the Atlantic Ocean. Deep-Sea Research I **47**:825-857.

Moore, C. M., M. M. Mills, E. P. Achterberg, R. J. Geider, J. La Roche, M. I. Lucas, E. L. McDonagh, X. Pan, A. J. Poulton, M. J. A. Rijkenberg, D. J. Suggett, S. J. Ussher, and

E. M. S. Woodward. 2009. Large-scale distribution of Atlantic nitrogen fixation controlled by iron availability. Nature Geoscience **2**:867-871.

Moore, G. R. 1996. Haemoproteins. Pages 189-216 *in* D. S. Bendall, editor. Protein Electron Transfer. BIOS Scientific Publishers Ltd, Oxford.

Perez, V., E. Fernandez, E. Maranon, X. A. G. Moran, and M. V. Zubkov. 2006. Vertical distribution of phytoplankton biomass, production and growth in the Atlantic subtropical gyres. Deep-Sea Research I **53**:1616-1634.

Pospisil, P. 2012. Enzymatic function of cytochrome b_{559} in photosystem II. Journal of Photochemistry and Photobiology B: Biology **104**:341-347.

Richier, S., A. I. Macey, N. J. Pratt, D. J. Honey, C. M. Moore, and T. S. Bibby. 2012. Abundances of iron-binding photosynthetic and nitrogen-fixing proteins of *Trichodesmium* both in culture and *in situ* from the North Atlantic. PLoS ONE **7**:e35571.

Saito, M. A., E. M. Bertrand, S. Dutkiewicz, V. V. Bulygin, D. M. Moran, F. M. Monteiro, M. J. Follows, F. W. Valois, and J. B. Waterbury. 2011. Iron conservation by reduction of metalloenzyme inventories in the marine diazotroph *Crocosphaera watsonii*. PNAS **106**:2184-2189.

Shi, T., Y. I. Sun, and P. G. Falkowski. 2007. Effects of iron limitation on the expression of metabolic genes in the marine cyanobacterium *Trichodesmium erythraeum* IMS101. Environmental Microbiology **9**:2945-2956.

Sohm, J. A., E. A. Webb, and D. G. Capone. 2011. Emerging patterns of marine nitrogen fixation. Nature Reviews Microbiology **9**:499-508.

Appendix 1

Gledhill et al. (in prep)

Distributions of particulate heme *b* in the Atlantic and Southern Ocean - implications for changes in phytoplankton photosystems

Martha Gledhill[1]*, Eric P. Achterberg[1], David J. Honey[1], Maria Nielsdottir[1] and Micha Rijkenberg[1,2].

1. Ocean and Earth Science, University of Southampton, National Oceanography Centre, Southampton, Southampton, SO14 3ZH, UK
2. Royal Netherlands Institute for Sea Research, Den Burg, The Netherlands

* Corresponding author

1. Abstract

Concentrations of heme *b,* the iron containing component of heme *b* proteins, ranged from < 0.4 to 5.3 pM with an average of 1.18 ± 0.8 (± 1 σ; n = 86) in the Iceland Basin (IB), from < 0.4 to 19.1 pM with an average of 2.24 ± 1.67 pM (n = 269) in the Tropical Northeast Atlantic (TNA) and from 0.6 to 21 pM with an average of 5.1 ± 4.8 pM (n = 34) in the Scotia Sea (SS). Heme *b* concentrations were enhanced in the photic zone and decreased with depth. Heme *b* concentrations correlated positively with chlorophyll *a* (chl *a*) in the TNA ($r = 0.41$, $p < 0.01$, n = 269). Integrated mixed layer depth chl *a*: heme *b* ratios in the TNA averaged 124 ± 45. Heme *b* did not correlate with chl *a* in the IB or SS. In the IB and SS, stations characterized by high chlorophyll and low nutrient (Fe and/or Si) concentrations exhibited low heme *b* concentrations relative to POC (< 0.1 μmol mol^{-1}), and high (> 500) chl *a*: heme *b* ratios. We suggest that the high chl *a*: heme *b* ratios result from increases in light harvesting antenna coupled with decreases in heme *b* containing proteins such as cytochrome b_6f and the core complex of photosystem II. Chlorophyll *a*: heme *b* ratios are thus potential indicators of a physiological response of the phytoplankton community to the prevailing growth conditions.

2. Introduction

2.1 Heme b

Oceanic phytoplankton are known to change the abundance of iron containing proteins when nutrient concentrations or incident light levels change (Pankowski and McMinn 2009, Peers and Price 2006, Saito et al. 2011, Strzepek and Harrison 2004, Wolfe-Simon et al. 2006). The cellular abundance of such proteins influences the efficiency of photosynthesis (Bailey et al. 2008, Cardol et al. 2008, Peers and Price 2006) and so links nutrient abundance and light to ocean productivity. Ferrodoxin (Mckay et al. 1999, Pankowski and McMinn 2009), photosystem I (PSI), cytochrome b_6f ($cytb_6f$) (Eberhard et al. 2008, Saito et al. 2011, Strzepek and Harrison 2004), cytochrome c_{550} (Saito et al. 2011), soluble cytochrome c (Eberhard et al. 2008, Peers and Price 2006) and Fe superoxide dismutase (Wolfe-Simon et al. 2006) have all been shown to be reduced in abundance or replaced by non-iron containing proteins when oceanic phytoplankton are grown under low iron or nutrient conditions in the laboratory. Furthermore recent work has shown diurnal cycling of iron protein pools in order to conserve iron use (Saito et al. 2011). However, few studies have investigated the abundance of iron containing proteins in the field or how their distributions are influenced by the prevailing nutrient and light regimes (Erdner and Anderson 1999, Pankowski and McMinn 2009). Heme *b* is an iron containing porphyrin which functions as a prosthetic group for proteins involved in electron transfer and the scavenging of reactive oxygen species (Chapman et al. 1997). Heme *b* is highly toxic to cells if not incorporated into proteins and the stoichiometry of heme *b* within proteins is fixed (Shekhawat and Verma 2010, Tanaka and Tanaka 2007), so that changes

heme *b* abundance will reflect changes in the cellular abundance of heme *b* containing proteins. In marine phytoplankton, heme *b* is incorporated into proteins involved in photosynthesis and respiration, with the major fraction likely to be contained within photosystem II (PSII, 1 heme *b* per complex) and cytochrome b_6f (cytb_6f, 2 heme *b* per complex) (Honey et al. in press). The cellular heme *b* content is thus linked to the photosynthetic cytochrome content. Reduction of the photosynthetic cytochrome content can result in a reduction in the quantum yield of photosystem II (F_v/F_m), a parameter frequently used for assessing nutrient or light stress e.g. (Behrenfeld et al. 2006), although large scale changes in F_v/F_m are also influenced by community structure (Suggett et al. 2009). Heme *b* contrasts with chlorophyll *a* (chl *a*) as this pigment is predominantly (ca. 70%) associated with PSI (Eberhard et al. 2008). Changes in the chl *a*: heme *b* ratio will thus reflect changes in the ratios of PSII, cytb_6f and PSI, and the quantity of chl *a* associated with the photosynthetic proteins. Laboratory studies of marine phytoplankton have shown that heme *b* concentrations in phytoplankton average 3.7 ± 0.9 μmol mol^{-1} C in nutrient replete conditions, and that the cellular concentrations of heme *b* are reduced under nutrient deplete conditions. Chlorophyll *a*: heme *b* ratios were also found to vary when phytoplankton were grown under low iron conditions. Increases in chl *a*: heme *b* were associated with decreases in the abundance of the cytb_6f relative to the abundance of either PSI and/ or PSII (Honey et al. in press). Determination of the concentration of heme *b* in particulate material and comparison with phytoplankton biomass, particulate organic carbon and chl *a* in the ocean could thus provide information on the variation in heme *b* protein abundance within the phytoplankton population and the response of the photosystem to prevailing nutrient and light conditions.

In this study we determined heme *b* in particulate material in three contrasting regions of the Atlantic Ocean and Southern Ocean: the Iceland Basin (IB), the Tropical Northeast Atlantic (TNA) and the Scotia Sea (SS). The IB is situated in the high latitude North Atlantic and is characterized by pronounced diatom dominated spring blooms (Leblanc et al. 2009), which nevertheless do not result in the complete drawdown of nitrate and phosphate. Residual nutrients stocks are thus subsequently exploited by more mixed phytoplankton assemblages (Leblanc et al. 2009, Poulton et al. 2010). The post spring bloom period is iron limited (Nielsdottir et al. 2009), a result of both low atmospheric iron inputs (Jickells et al. 2005) and suboptimal iron: nitrate ratios in winter overturned deep waters (Nielsdottir et al. 2009).

The region of the TNA examined in this study is influenced in the east by the highly productive upwelling system off the Northwest African Coast, in the south by the oxygen minimum zone off the Cape Verde Islands and in the northwest by the permanently stratified oligotrophic sub-tropical North Atlantic Gyre (Stramma et al. 2008). Atmospheric iron inputs in this region are relatively high due to the influx of Saharan and Sahel dust

(Jickells et al. 2005, Mulitza et al. 2010, Stuut et al. 2005) with maximum dust inputs in this region occurring in winter (January to March period) (Chiapello et al. 1995). The phytoplankton community in the TNA is dominated by picoplankton comprising *Prochlorococcus* sp., *Synechococcus* sp. and picoeukaryotes (Hill et al. 2010), although nitrogen fixing *Trichodesmium* sp. are also observed in this region (Moore et al. 2009).

The SS lies within the Atlantic sector of the Southern Ocean. The SS contrasts with much of the high nutrient low chlorophyll (HNLC) regions of the Southern Ocean as it supports extensive phytoplankton blooms, with the South Orkney Islands, the South Sandwich Islands and South Georgia acting as potential sources of iron via the "island mass effect" (Doty and Oguri 1956, Korb et al. 2005, Hinz et al. 2011). The waters around South Georgia are particularly productive, and can support Antarctic diatom dominated blooms of up to 12 mg m^{-3} chl *a* for periods of up to 5 months (Korb et al. 2005). However productivity in the area is patchy, and regions to the south of South Georgia have HNLC characteristics (Hinz et al. 2011, Korb et al. 2010).

We compare the distribution of heme *b* to chlorophyll *a*, phytoplankton biomass, particulate organic carbon (POC) and particulate organic nitrogen (PON) and interpret our findings within the context of the prevailing nutrient (dissolved iron (dFe), nitrate, phosphate and silicate) and light environments. We assess how the relative abundance of heme *b* containing proteins varies in the ocean, where chl *a*: heme *b* ratios increase and thus how changes in the relative abundance of photosynthetic and light harvesting complexes relate to nutrient distributions.

3. Methods

3.1 General

Samples were obtained during three cruises in 2007 and 2008 (Fig. 1, Table 1). The IB cruise took place from 25 July to 19 August, 2007. The cruise consisted of three repeat surveys of a 90 × 90 km grid in the North Atlantic sub-polar gyre. The TNA cruise took place from 06 January to 03 February, 2008. Samples were collected in the vicinity of the Canary Islands, the sub-tropical North Atlantic Gyre, the vicinity of the Cape Verde Islands and on a latitudinal transect along 12°N. The SS cruise took place from 01 January to the 11 February, 2008. Samples were collected in the vicinity of the South Orkney Islands, within the Antarctic Circumpolar Current (ACC) and in the bloom associated with South Georgia. Hydrographic data were collected with a Seabird 9/11+ CTD on the IB and TNA cruises, and with a Seabird SBE9+ CTD on the SS cruise.

3.2 Sample Collection

Samples for heme *b*, chlorophyll *a*, POC/N and major nutrients were collected from depths < 250 m using a stainless steel CTD rosette equipped with 20 L Niskin (General Oceanics) bottles. Samples for dFe were collected using a trace metal clean titanium CTD rosette equipped with 12 L trace metal clean Teflon coated OTE bottles, or using a trace metal clean fish towed at approximately 5 m depth while the ship was steaming at 10 knots (Nielsdottir et al. 2009).

3.3 Particulate Heme b

Between 1 and 4 L of seawater was filtered over 0.7 µm glass fibre filters (MF300, Fisher) and frozen (< -80 ˚C) for analysis in the laboratory. Heme *b* was extracted into 1 mL of 0.02 M NH_4OH containing the zwitterionic detergent Empigen (2.5% v/v, Sigma). Extracts were centrifuged, filtered (0.2 µm, Minisart, Sartorius) and determined spectrophotometrically after separation from other pigments by high performance liquid chromatography (HPLC) (Gledhill 2007). Separations were performed using a polystyrene divinyl benzene stationary phase (PLRP-S, 50 x 2.1 mm, 5 µm, Varian Inc.). High performance liquid chromatography was carried out using binary gradient high pressure pumps (Shimadzu, LC-10ADVPµ) and a diode array spectrophotometer equipped with a micro cell (Shimadzu, SPD-M10AVP). 100 µL of sample was injected onto the column using an autosampler (Shimadzu, SIL-10ADVP). The system was computer operated (LCsolution software) via a controller (Shimadzu, SCL-10AVP). Mobile phases consisted of (A) 20:20:40:0.1 % (v:v:v:v) isopropanol (IPA): acetonitrile (ACN): water: nonafluoropentanoic acid (NFPA) and (B) 1:1:0.1 (v:v:v) IPA:ACN:NFPA. A standard gradient of 60 % A to 100 % B over 15 min, followed by 5 min isocratic elution with 100 % B was used. The flow rate was 200 µL min^{-1}. Elution of heme *b* (retention time 5.5 min) was monitored by absorbance at 400 nm after applying a background absorbance correction using 450 nm in order to remove baseline fluctuations caused by Empigen. Heme *b* was quantified by comparison with standard solutions of iron (III) protoporphyrin IX chloride (Frontier Scientific). The detection limit for the technique was 1.6 nM.

3.4 Chlorophyll, F_v/F_m POC/PON and Nutrients

Water samples (100 – 200 mL) for chl *a* analysis were filtered over glass fibre filters (MF300, Fisher). Chlorophyll *a* was extracted into 10 mL of 90 % (v/v) acetone over a 20-24 h period in the dark (4ºC). Chlorophyll *a* was determined by fluorimetry (Turner Design TD-700) and calibrated using a pure chl *a* standard (spinach, Sigma). The maximum quantum yield (F_v/F_m) is reported here for dawn stations in the Irminger Basin (IB222, IB226, IB260 and IB285) and Scotia Sea. F_v/F_m was determined via chlorophyll fluorescence measurements obtained using fast repetition rate fluorometer (FRRF, Chelsea Scientific Instruments) and Fluorescence Induction and Relaxation (FIRe, Satlantic) (Bibby et al. 2008, Kolber et al. 1998). Particulate organic carbon and PON were determined on the IB

cruise following filtration of 1-2 L seawater onto pre combusted GFF (0.7 µm; Whatman) filters (Poulton et al. 2006). On the TNA cruise, POC and PON was determined at selected stations by mass spectrometry after filtration of up to 4 L seawater (Moore et al. 2006). Macronutrients (nitrate + nitrite, hereafter termed nitrate, phosphate and orthosilicic acid) were determined on board using an autoanalyzer and standard colorimetric techniques (Sanders and Jickells 2000, Whitehouse 1997) or in the TNA, with a nanomolar nutrient system following the method of (Patey et al. 2008).

3.5 Dissolved iron

Dissolved iron was analyzed after gentle pressure filtration (0.2 µm) by an automated flow injection chemiluminescence method as described in (Nielsdottir et al. 2009, Obata et al. 1993).

4. Results and Discussion

4.1 Surface Heme b, chlorophyll a, POC and PON in the Iceland Basin

Particulate heme *b* concentrations in the IB ranged from < 0.4 to 5.3 pM, averaging 1.18 ± 0.8 (± 1 standard deviation; n = 86). Depth profiles showed some enhanced concentrations in surface waters, but trends were not as strong as for chl *a* (Fig. 2). Integrated mixed layer depth values for chl *a*, heme *b*, POC and PON calculated for the IB are given in Table 1. Heme *b* concentrations in the IB were found to correlate weakly with POC and PON, however, no significant correlation was observed with chl *a* (Table 2). Comparison of mixed layer depth integrated heme *b* concentrations with phytoplankton carbon (phyC, (Poulton et al. 2010)) indicated that heme *b*: phyC ratios were between 0.07 µmol mol^{-1} and 0.78 µmol mol^{-1}, considerably lower than ratios observed in phytoplankton grown under nutrient replete conditions in the laboratory (average 3.7 ± 0.9 µmol mol^{-1}; see Honey et al. in press). The low concentration of heme *b* in this region was also reflected in the heme *b*: POC and PON ratios (Table 2). The low concentrations of heme *b* with respect to carbon indicate that the abundance of *b* type cytochromes was also low and is compatible with the low F_v/F_m values (Table 3) observed in the mixed layer in this region at the time of sampling. Phytoplankton have been found to decrease their heme *b*: POC ratios in response to nutrient limitation (Honey et al. in press). At stations IB285, situated in the centre of a cyclonic eddy, low heme *b*: POC ratios (0.06 ± 0.01 µmol mol^{-1}) coincided with high (~ 90 µmol mol^{-1}) observed chl *a*: POC ratios. The combination of low heme *b*: POC and high chl *a*: POC lead to an integrated mixed layer chl *a*: heme *b* ratio of 1260 at this station. Integrated chl *a*: heme *b* ratios > 500, were also observed at stations IB260 and IB274, and again coincided with low heme *b*: POC ratios (0.07 ± 0.01 and 0.09 ± 0.03 µmol mol^{-1} respectively). Coccolithophores, dominated by *Emiliania huxleyi* made up between 10 and 25 % of the phytoplankton carbon at the time of this study (Poulton et al. 2010). Chl *a*: heme *b* ratios in *E. huxleyi* are known to increase under

low iron and/or light conditions in the laboratory (Honey et al. in press). Average daily irradiances in the IB during the cruise ranged between 9 and 39 mol PAR m^{-2} day^{-1} and were not thought to be limiting phytoplankton growth in the mixed layer (Poulton et al. 2010). The concentrations of nitrate and phosphate at stations 260, 274 and within the cyclonic eddy were also not fully depleted (average mixed layer depth concentrations at these stations: 3.6 ± 2.1 µM nitrate, 0.29 ± 0.1 µM phosphate, 0.5 ± 0.4 µM silicate). Mixed layer depth dFe concentrations averaged 0.016 ± 0.01 nM at the cyclonic eddy station and 0.05 ± 0.01 nM at station IB260 (no dFe determined at station IB274), constituting the lowest dFe concentrations detected during the IB study. The high chl *a*: heme *b* ratios observed in the IB are therefore most likely a response of the phytoplankton population to the low dFe concentrations observed at stations IB260, IB274 and in the cyclonic eddy.

4.2 Surface heme b, chlorophyll a, POC and PON in the Tropical North Atlantic

Particulate heme b in the TNA averaged 2.24 ± 1.67 pM (n = 275). Minimum concentrations were below the detection limit (< 0.4 pM) while the maximum concentration observed in this region was 19.4 pM. Depth profiles were similar to those of chl *a,* with enhanced concentrations in the photic zone (Fig. 3). In the TNA, there was a weak correlation between heme *b* and PON, but no significant relationship between heme *b* and POC (Table 2). Integrated mixed layer depth values for chl *a*, heme *b*, POC and PON calculated for the TNA are given in Table 1. Mixed layer heme *b*: POC and heme *b*: PON ratios were higher (1.0 ± 0.5 and 7.6 ± 2.9 µmol mol^{-1} respectively) than values observed for the IB, although still lower than heme *b*: POC ratios observed for nutrient replete phytoplankton in the laboratory (Honey et al. in press). There was no overall change in heme *b*: POC with depth (data not shown), indicating that light was unlikely to be influencing the level of heme *b* in this region, despite the presence of a deep chlorophyll maximum at some stations in the TNA study area. Chlorophyll *a*: POC ratios were also higher (average 134 ± 80 µmol mol^{-1}) in the TNA compared to the IB (Table 1). A significant correlation between heme *b* and chl *a* was observed in the TNA samples (Table 2). Chlorophyll *a*: heme *b* ratios in the TNA were below 500, except for four isolated samples (Fig. 3C). The frequency of samples at depth with high chl *a*: heme *b* ratios makes it difficult to identify a cause, although the heme *b* concentrations detected in these samples were likely to be subject to greater error as they were close to the detection limit of the heme *b* technique. Integrated mixed layer depth chl *a*: heme *b* ratios averaged 124 ± 45 and were considerably lower than those observed in the IB. Nitrate and phosphate concentrations were very low in surface waters in the TNA (3-50 nM nitrate, 2-90 nM phosphate) and are likely to limit growth in the region (Moore et al. 2009). Despite this we found no relationships between heme *b*: POC, heme *b*: PON or chl *a*: heme b and dFe, nitrate or phosphate concentrations.

On fourteen days in the TNA, samples were collected both at dawn and mid afternoon (Table 1). Although these samples were not collected from the same waters, afternoon (1500 – 1700 GMT) mixed layer depth chl *a*: heme *b* ratios were higher than dawn (0700 GMT) ratios on eleven of the fourteen days (Fig. 4). These results indicate that diurnal variation in the production of chl and heme may be occurring, with heme *b* production lower during the day relative to chl *a* as a result of optimisation of the chl *a*/ heme *b* biosynthetic pathway (Papenbrock et al. 1999, Tanaka and Tanaka 2007). The lack of concurrent POC/PON data does not allow for examination of potential diurnal cycling of the overall abundance of heme *b* proteins, which has been reported in laboratory cultures (Saito et al. 2011).

4.3 Surface heme b and chlorophyll a in the Scotia Sea

Heme *b* concentrations in the Scotia Sea varied from 0.6 to 21 pM with an average of 1.9 ± 1.7 pM and were thus higher than those determined in the IB (Fig. 5). Particulate organic carbon and nitrogen were not determined for the Scotia Sea samples. However, phytoplankton counts were undertaken at a depth of 20 m at each station (Korb et al. 2010) and heme b concentrations were therefore compared to the calculated phytoplankton carbon biomass (phyC), although it should be noted that these calculations do not include the biomass from nano- or picoeukaryotes, and are thus likely to overestimate actual heme *b*: POC ratios. Results of the comparison are reported in Table 3. Heme *b*: phyC ratios observed at SSC2, SSC4 and SSP3 were similar to heme *b*: C ratios observed in nutrient replete phytoplankton grown in the laboratory (Honey et al. in press). Bioassay experiments carried out close to C2 and P3 indicated that phytoplankton were not iron limited (Hinz et al. 2011). The low heme *b*: phyC ratio observed at stations SSP24, SSP28 and SSR3 to the northwest of South Georgia and in the Scotia Sea indicates that the phytoplankton community were growing under low nutrient conditions at these stations. Iron bioassay experiments near station SSP24 indicated that the phytoplankton community was iron limited in this area (Hinz et al. 2011). The estimates of heme *b*: PhyC determined for stations in the Scotia Sea are broadly compatible with changes in F_v/F_m recorded in the region (Table 3). F_v/F_m was highest around station SSR3, where we observed our highest heme *b*: PhyC ratio. Furthermore south of South Georgia at stations SSP24 and SSP28 F_v/F_m was also observed to be lower (<0.3, Table 3), consistent with the depleted heme *b*:PhyC ratios. However, at other stations (SSC2, SSC4 and SSP3) with similar F_v/F_m values, we observed a wide variability in heme *b*: PhyC ratios. This could have been a result of underestimation of the heme *b*:PhyC ratio due to omission of C from nano- and picoeukaryotes, likely to be especially important at SSC2 and SSC4, as these areas were dominated by small phytoplankton species (Korb et al. 2011). In addition comparison between F_v/F_m and heme *b*: PhyC in the region is also likely influenced by changes in the community composition (Suggett et al. 2009) as the dominant taxanomic groups varied from cryptophytes at station SSC2, dinoflagellates at SSC4 and diatoms at

SSP24, SSP28, SSP3 and SSR3 (Korb et al. 2010; 2011). It was notable that chlorophyll *a*: phyC ratios at stations SSP24, SSP28 and SSR3 were close to the average observed for all the stations (252, 265 and 590 µmol mol^{-1} respectively), showing that while heme *b* was depleted relative to biomass at these stations, chl *a* was not. Integrated mixed layer depth values for chl *a* and heme *b* calculated for the SS are given in Table 1. Chlorophyll *a*: heme b ratios ranged between 80 and 1940, with a mean value of value of 533 (Fig. 5). As with the IB, no significant correlation between heme *b* and chl *a* was observed (Table 2). Integrated chl *a*: heme *b* ratios were below 500 north of the South Orkney Islands, and increased going north across the Scotia Sea to a value of 528 just south of South Georgia. West of South Georgia mixed layer chl *a*: heme *b* ratios decreased to 240. This region is strongly influenced by iron inputs from the South Georgia Ridge and the station sampled was close to an area reported to be iron replete at the time of sampling (Fig. 6, (Hinz et al. 2011)). North West of South Georgia, however, we observed high chl *a*: heme *b* ratios (> 1400), combined with low heme *b*: phyC ratios. This station (R3) was characterized by high chl *a* (ca ~ 5 µg L^{-1}), complete drawdown of Si (<0.15 µM) and relatively depleted N concentrations (ca ~ 14 µM). The phytoplankton community at both stations was dominated by diatoms (Korb et al. 2010; 2011), however F_v/F_m was lower at R3 than at P3 (Table 3). Dissolved iron concentrations were not recorded at the station itself, however comparison of dFe and nutrient data showed that the closest underway dFe samples (situated 15 and 27 km to the southwest of the station; upstream in the ACC) had dFe concentrations of 0.16 ± 0.01 nM and 0.61 ± 0.1 nM respectively (Fig. 6). The phytoplankton community at R3 was dominated by centric diatoms over 10 µm in size (Korb et al. 2010) which are thought to have relatively high iron requirements (Ho et al. 2003, Sunda and Huntsman 1995). It is thus possible that the phytoplankton at this station have exhausted the nutrient supply to the extent that they have reduced their hemoprotein content.

4.4 Implications of changes in heme b and chlorophyll a for variations in the composition of the photosynthetic electron transport chain in marine phytoplankton

This study reports the first investigation into the distribution of heme *b* in the marine environment. In the Atlantic and Southern Oceans, we have observed variations in heme *b* concentrations from <0.2 to 21 pM. Heme *b* distributions reflected changes in phytoplankton biomass, with higher heme *b* concentrations observed in regions of higher biomass. However the concentration of heme *b* relative to the organic carbon and nitrogen concentration and to chl *a* varied considerably between the three areas surveyed. Variations of heme *b*: POC ratios reflect changes in the abundance of heme *b* proteins such as $cytb_6f$ and PSII in particulate material while variations in chl *a*: heme *b* ratios will reflect changes in both the relative abundance of the photosystem complexes and in the number of chl *a* containing antenna complexes associated with PSI and/ or PSII. Thus in this study the observed distributions of heme *b*: POC and chl *a*: heme *b* are likely to

reflect changes in the relative abundance of the photosystem complexes coupled to increases in light harvesting antenna complexes. Laboratory studies have shown that heme *b*: POC decreases when marine phytoplankton are grown under low nutrient conditions. Species specific increases in chl *a*: heme *b* ratios were also observed in phytoplankton grown under low nutrient and low light conditions (Honey et al. in press). In the IB and SS to the south of South Georgia, chl *a*: heme *b* ratios over > 500 were observed at stations with low dFe concentrations (Fig. 7). Although dFe concentrations in the SS to the north west of South Georgia were not as low as those in the IB and south of South Georgia, we suggest that the low Si concentrations coupled to the higher Fe demand of the dominant large centric diatoms led to the enhanced chl *a*: heme *b* ratios. In this study we have highlighted increases in the chl *a*: heme *b* ratio to values >500, which are in excess of chl *a*: heme *b* ratios we have observed in the laboratory (Honey et al. in press). Observed increases increases in chl *a*: heme *b* to values > 500 were associated with particular stations (e.g. IB285 and SSR3) which were not observed to have major shifts in species composition when compared to other nearby stations (Korb et al. 2010, Poulton et al. 2010). The heme *b* content of nutrient replete phytoplankton species investigated to date has been shown to be reasonably consistent across eukaryotic phytoplankton species (Honey et al. in press). However as only a limited number of species have so far been investigated, so it is not possible to completely rule out the possibility that shifts in species composition will result in changes in heme *b* abundance and chl *a*: heme *b* ratios.

Our chl *a*: heme *b* ratios are likely consistent with the adaptation of the photosystem to the prevailing light and nutrient conditions. Our results indicate that the abundance of cytb_6f with respect to biomass and other photosystem complexes is likely to change. Cytochrome b_6f connects the two photosynthetic reaction centre complexes and is involved in linear and cyclic electron transfer (Baniulis et al. 2008, Iwai et al. 2010). Cytochrome b_6f potentially plays a contributory role in regulating electron transport through the process of "photosynthetic control" (Eberhard et al. 2008, Peltier et al. 2010). Furthermore, in green algae, cytochrome b_6f regulates state transitions and the switching of light harvesting complexes from PSII to PSI, thus changing the amount of linear versus cyclic electron transport (Lemeille and Rochaix 2010). Gaining insight into cytb_6f abundance in the ocean and its relationship to other photosystem complexes will shed light on fundamental electron transport processes occurring in the ocean, and how these impact on productivity.

Our investigation into heme *b* distributions has shown that heme *b*: POC and heme *b*: chl *a* ratios vary with biomass and nutrient distributions. We have identified stations in the SS and IB where phytoplankton have high chl *a*: heme *b* as a result of low nutrient concentrations. Our study shows that low dFe is the most likely cause of high chl *a*: heme

b ratios in the IB, while a combination of low dFe and Si contributes to high chl *a*: heme *b* ratios in the SS. Our results indicate that there are changes in the structure of photosynthetic electron transport chain in the phytoplankton communities in the IB and the SS as a result of low nutrient concentrations. Changes in the structure of the photosynthetic electron transport chain will influence the efficiency of photosynthesis and thus the productivity of phytoplankton communities. Determination of particulate heme *b* in the ocean and comparison with POC, biomass or chl *a* thus contributes to our understanding of the dynamics of phytoplankton blooms and adaptation of the photosystem of phytoplankton to prevailing growth conditions in the ocean.

5. Acknowledgements

This work was supported by a NERC Advanced Fellowship grant awarded to MG (NE/E013546/1). The authors would like the officers, crew and scientists of the R.R.S. *Discovery* and R.R.S. *James Clark Ross* during cruises D321, D326 and JR177. We are particularly grateful to Matt Patey for the nutrient data from the Tropical North Atlantic, Stephanie Henson and Alex Poulton for providing the satellite images, Alex Poulton for phytoplankton counts and taxanomic data, C. Mark Moore and Mike Lucas for particulate organic matter data and C. Mark Moore and Thomas S. Bibby for supplying the F_v/F_m data.

6. References

Bailey, S., A. Melis, K. R. M. Mackey, P. Cardol, G. Finazzi, G. van Dijken, G. M. Berg, K. Arrigo, J. Shrager, and A. Grossman. 2008. Alternative photosynthetic electron flow to oxygen in marine *Synechococcus*. Biochimica Et Biophysica Acta-Bioenergetics, **1777**(3):269-276.

Baniulis, D., E. Yamashita, H. Zhang, S. S. Hasan, and W. A. Cramer. 2008. Structure-function of the cytochrome b(6)f complex. Photochem. Photobiol. **84**(6):1349-1358.

Behrenfeld, M. J., K. Worthington, R. M. Sherrell, F. P. Chavez, P. Strutton, M. McPhaden, and D. M. Shea. 2006. Controls on tropical Pacific Ocean productivity revealed through nutrient stress diagnostics. Nature **442**(7106):1025-1028.

Bibby, T. S., M. Y. Gorbunov, K. W. Wyman, and P. G. Falkowski. 2008. Photosynthetic community responses to upwelling in mesoscale eddies in the subtropical North Atlantic and Pacific Oceans. Deep-Sea Research II **55**(10-13):1310-1320.

Cardol, P., B. Bailleul, F. Rappaport, E. Derelle, D. Beal, C. Breyton, S. Bailey, F. A. Wollman, A. Grossman, H. Moreau, and G. Finazzi. 2008. An original adaptation of photosynthesis in the marine green alga *Ostreococcus*, *Proc. Natl. Acad. Sci. U. S. A.*, ***105***(22), 7881-7886.

Chapman, S. K., S. Daff, and A. W. Munro. 1997. Heme: The most versatile redox centre in biology? *In*: Metal Sites in Proteins and Models, pp. 39-70.

Chiapello, I., G. Bergametti, L. Gomes, B. Chatenet, F. Dulac, J. Pimenta, and E. S. Suares. 1995. An Additional Low Layer Transport of Sahelian and Saharan Dust over the North-Eastern Tropical Atlantic. Geophysical Research Letters **22**(23):3191-3194.

Doty, M. S., and M. Oguri. 1956. The Island Mass Effect. Journal du Conseil **22**:33-37.

Eberhard, S., G. Finazzi, and F. A. Wollman. 2008. The Dynamics of Photosynthesis, Annual Review of Genetics **42**:463-515.

Erdner, D. L., and D. M. Anderson. 1999. Ferredoxin and flavodoxin as biochemical indicators of iron limitation during open-ocean iron enrichment. Limnology Oceanography **44**(7):1609-1615.

Gledhill, M. 2007. The determination of heme *b* in marine phyto- and bacterioplankton, Marine Chemistry **103**(3-4):393-403.

Hill, P. G., M. V. Zubkov, and D. A. Purdie. 2010. Differential responses of *Prochlorococcus* and SAR11-dominated bacterioplankton groups to atmospheric dust inputs in the tropical Northeast Atlantic Ocean. FEMS Microbiol. Lett. **306**:82-89.

Hinz, D. J., M. C. Nielsdottir, R. E. Korb, M. J. Whitehouse, A. J. Poulton, C. M. Moore, E. P. Achterberg, and T. S. Bibby. 2011. Responses of microplankton community structure to iron addition in the Scotia Sea. Deep Sea Research II, 10.1016/j.dsr2.2011.06.006

Ho, T. Y., A. Quigg, Z. V. Finkel, A. J. Milligan, K. Wyman, P. G. Falkowski, and F. M. M. Morel. 2003. The elemental composition of some marine phytoplankton. Journal of Phycology **39**(6):1145-1159.

Iwai, M., K. Takizawa, R. Tokutsu, A. Okamuro, Y. Takahashi, and J. Minagawa. 2010. Isolation of the elusive supercomplex that drives cyclic electron flow in photosynthesis. Nature **464**(7292):1210-U1134.

Jickells, T. D., Z. S. An, K. K. Andersen, A. R. Baker, G. Bergametti, N. Brooks, J. J. Cao, P. W. Boyd, R. A. Duce, K. A. Hunter, H. Kawahata, N. Kubilay, J. laRoche, P. S. Liss, N. Mahowald, J. M. Prospero, A. J. Ridgwell, I. Tegen, and R. Torres. 2005. Global iron connections between desert dust, ocean biogeochemistry, and climate. Science **308**(5718):67-71.

Kolber, Z. S., O. Prasil, and P. G. Falkowski. 1998. Measurements of variable chlorophyll fluorescence using fast repetition rate techniques: defining methodology and experimental protocols. Biochimica Et Biophysica Acta-Bioenergetics **1367**(1-3):88-106.

Korb, R. E., M. J. Whitehouse, S. E. Thorpe, and M. Gordon. 2005. Primary production across the Scotia Sea in relation to the physico-chemical environment. Journal of Marine Systems **57**(3-4):231-249.

Korb, R. E., M. J. Whitehouse, M. Gordon, P. Ward, and A. J. Poulton. 2010. Summer microplankton community structure across the Scotia Sea: implications for biological carbon export. Biogeosciences **7**(1):343-356.

Korb, R. E., M. J. Whitehouse, P. Ward, M. Gordon, H. J. Venables, and A. J. Poulton. 2011. Regional and Seasonal differences in microplankton biomass, productivity, and structure across the Scotia Sea: Implications for the export of biogenic carbon. Deep Sea Research II, 10.1016/j.dsr2.2011.06.006

Leblanc, K., C. E. Hare, Y. Feng, G. M. Berg, G. R. DiTullio, A. Neeley, I. Benner, C. Sprengel, A. Beck, S. A. Sanudo-Wilhelmy, U. Passow, K. Klinck, J. M. Rowe, S. W. Wilhelm, C. W. Brown, and D. A. Hutchins. 2009. Distribution of calcifying and silicifying phytoplankton in relation to environmental and biogeochemical parameters during the late stages of the 2005 North East Atlantic Spring Bloom. Biogeosciences **6**(10):2155-2179.

Lemeille, S., and J. D. Rochaix. 2010. State transitions at the crossroad of thylakoid signalling pathways. Photosynthesis Research **106**(1-2):33-46.

Mckay, R. M. L., J. La Roche, A. F. Yakunin, D. G. Durnford, and R. J. Geider. 1999. Accumulation of ferredoxin and flavodoxin in a marine diatom in response to Fe. Journal of Phycology **35**(3):510-519.

Moore, C. M., M. M. Mills, A. Milne, R. Langlois, E. P. Achterberg, K. Lochte, R. J. Geider, and J. La Roche. 2006. Iron limits primary productivity during spring bloom development in the central North Atlantic. Global Change Biology **12**(4):626-634.

Moore, C. M., M. M. Mills, E. P. Achterberg, R. J. Geider, J. LaRoche, M. I. Lucas, E. L. McDonagh, X. Pan, A. J. Poulton, M. J. A. Rijkenberg, D. J. Suggett, S. J. Ussher, and E. M. S. Woodward. 2009. Large-scale distribution of Atlantic nitrogen fixation controlled by iron availability. Nat. Geosci. **2**(12):867-871.

Mulitza, S., D. Heslop, D. Pittauerova, H. W. Fischer, I. Meyer, J. B. Stuut, M. Zabel, G. Mollenhauer, J. A. Collins, H. Kuhnert, and M. Schulz. 2010. Increase in African dust flux at the onset of commercial agriculture in the Sahel region. Nature **466**(7303):226-228.

Nielsdottir, M. C., C. M. Moore, R. Sanders, D. J. Hinz, and E. P. Achterberg. 2009. Iron limitation of the postbloom phytoplankton communities in the Iceland Basin. Global Biogeochemical Cycles **23**:GB3001.

Obata, H., H. Karatani, and E. Nakayama. 1993. Automated determination of iron in sea water by chelating resin concentration and chemiluminescence detection. Analytical Chemistry **65**:1524-1528.

Pankowski, A., and A. McMinn. 2009., Development of immunoassays for the iron-regulated proteins ferrodoxin and flavodoxin in polar microalgae. Journal of Phycology **45**(3):771-783.

Papenbrock, J., H. P. Mock, E. Kruse, and B. Grimm. 1999. Expression studies in tetrapyrrole biosynthesis: inverse maxima of magnesium chelatase and ferrochelatase activity during cyclic photoperiods. Planta **208**(2):264-273.

Patey, M. D., M. J. A. Rijkenberg, P. J. Statham, M. C. Stinchcombe, E. P. Achterberg, and M. Mowlem. 2008. Determination of nitrate and phosphate in seawater at nanomolar concentrations. Trac-Trends in Analytical Chemistry **27**(2):169-182.

Peers, G., and N. M. Price. 2006. Copper-containing plastocyanin used for electron transport by an oceanic diatom. Nature **441**(7091):341-344.

Peltier, G., D. Tolleter, E. Billon, and L. Cournac. 2010. Auxiliary electron transport pathways in chloroplasts of microalgae. Photosynthesis Research **106**(1-2):19-31.

Poulton, A. J., P. M. Holligan, A. Hickman, Y. N. Kim, T. R. Adey, M. C. Stinchcombe, C. Holeton, S. Root, and E. M. S. Woodward. 2006. Phytoplankton carbon fixation, chlorophyll-biomass and diagnostic pigments in the Atlantic Ocean. Deep-Sea Research II **53**(14-16):1593-1610.

Poulton, A. J., A. Charalampopoulou, J. R. Young, G. A. Tarran, M. I. Lucas, and G. D. Quartly. 2010. Coccolithophore dynamics in non-bloom conditions during late summer in the central Iceland Basin (July-August 2007). Limnology and Oceanography **55**(4):1601-1613.

Saito, M. A., E. M. Bertrand, S. Dutkiewicz, V. V. Bulygin, D. M. Moran, F. M. Monteiro, M. J. Follows, F. W. Valois, and J. B. Waterbury. 2011. Iron conservation by reduction of metalloenxyme inventories in the marine diazotroph *Crocosphaera watsonii*. Proc. Natl. Acad. Sci. U. S. A. **108**(6):2184-2189.

Sanders, R., and T. Jickells. 2000. Total organic nutrients in Drake Passage. Deep-Sea Research I **47**(6):997-1014.

Shekhawat, G. S., and K. Verma. 2010. Haem oxygenase (HO): an overlooked enzyme of plant metabolism and defence. Journal of Experimental Botany **61**(9):2255-2270.

Stramma, L., P. Brandt, J. Schafstall, F. Schott, J. Fischer, and A. Kortzinger. 2008. Oxygen minimum zone in the North Atlantic south and east of the Cape Verde Islands. Journal of Geophysical Research **113**(C4):C04014.

Strzepek, R. F., and P. J. Harrison. 2004. Photosynthetic architecture differs in coastal and oceanic diatoms. Nature **431**(7009):689-692.

Stuut, J. B., M. Zabel, V. Ratmeyer, P. Helmke, E. Schefuss, G. Lavik, and R. Schneider. 2005. Provenance of present-day eolian dust collected off NW Africa. Journal of Geophysical Research **110**(D4):14.

Suggett, D. J., C. M. Moore, A. E. Hickman, and R. J. Geider. 2009. Interpretation of fast repetition rate (FRR) fluorescence: signatures of phytoplankton community structure versus physiological state. Marine Ecology Progress Series **376**:1-19.

Sunda, W. G., and S. A. Huntsman. 1995. Iron uptake and growth limitation in oceanic and coastal phytoplankton. Marine Chemistry **50**:189-206.

Tanaka, R., and A. Tanaka. 2007. Tetrapyrrole biosynthesis in higher plants, Annual Review of Plant Biology **58**:321-346.

Whitehouse, M. J. 1997. Automated Seawater Nutrient Chemistry, British Antarctic Survey, Cambridge.

Wolfe-Simon, F., V. Starovoytov, J. R. Reinfelder, O. Schofield, and P. G. Falkowski. 2006. Localization and role of manganese superoxide dismutase in a marine diatom. Plant Physiology, **142**(4):1701-1709.

Table 1. Integrated mixed layer depth values for heme *b* (nmol m^{-2}), chlorophyll *a* (µmol m^{-2}), POC (mmol m^{-2}) and PON (mmol m^{-2}) concentration calculated for stations sampled in the Iceland Basin, Tropical North Atlantic and Scotia Sea.

Station	Lat (°N)	Long (°W)	Julian Day	MLD	Integrated heme *b* (nmol m^{-2})	Integrated chl *a* (µmol m^{-2})	Integrated POC (mmol m^{-2})	Integrated PON (mmol m^{-2})
Iceland Basin								
IB204	59.99	19.86	210.04	43	65.3	9.96	356	58.7
IB209	59.69	20.41	211.13	31	102	7.2	365	55.3
IB212	59.71	18.75	212.09	33	67.4	8.1	288	39.7
IB222	58.86	19.88	214.10	31	26.7	7.1	209	27.3
IB226	58.84	21.01	216.97	35	38.5	15.7	368	50.6
IB243	59.86	20.46	221.55	31	39.8	26.9		
IB247	59.99	20.46	221.98	31	61.7	17.8	280	49.8
IB260	59.19	19.10	224.13	33	9.3	6.6	300	40.4
IB274	59.22	19.90	226.14	19	4.8	7.0	48	16.5
IB281	59.68	18.72	228.51	35	23.5	8.6	186	28.1
IB285	59.67	18.72	230.18	45	30.0	37.7	488	64.3
IB286	59.29	19.79	231.57	29	51.6	14.7	239	36.4
Tropical North Atlantic								
TNA389	25.59	24.10	8.83	104	270	26.1		
TNA390	25.95	25.59	9.23	126	106	21.0		
TNA397	22.83	27.19	12.63	107	209	22.2		
TNA398	20.91	26.12	13.29	97	194	25.2	243	24.6
TNA399	20.37	25.82	13.65	99	187	33.5		
TNA400	18.96	25.03	14.30	77	261	19.2		
TNA401	18.48	24.80	14.63	85	307	30.2		
TNA402	17.60	24.29	15.29	70	274	23.5	187	28.8
TNA402A	17.66	24.3	15.60	70	321	24.5		
TNA403	15.55	25.38	16.30	41	142	12.4		
TNA404	15.04	25.49	16.63	51	219	27.1		
TNA405	13.03	25.82	17.28	47	113	10.9		
TNA407	12.67	27.11	18.27	42	89.6	10.5		
TNA408	12.63	27.78	18.63	48	462	13.2		
TNA409	12.60	29.99	19.29	50	150	18.1	139	21.1
TNA410	12.59	30.60	19.64	64	196	23.5		
TNA411	12.55	32.67	20.30	51	150	13.0	159	27.4
TNA412	12.54	33.30	20.66	61	216	21.6		
TNA413	12.51	35.78	21.30	55	171	12.7	109	18.2
TNA414	12.54	35.31	21.65	67	121	18.2		
TNA415	12.61	33.24	22.30	48	111	13.8		
TNA416	12.59	32.61	22.66	70	69	16.1		
TNA417	12.51	30.61	23.41	71	187	16.1		
TNA418	16.12	30.63	24.50	62	89	12.4		
TNA419	16.16	30.63	25.28	56	84	9.5	121	21.2
TNA420	16.19	30.65	25.66	53	69	8.4		
TNA422	16.22	30.66	26.28	48	46	8.2	127	19.5
TNA423	16.20	30.62	26.63	48	37	7.5		
TNA425	16.23	30.65	27.28	43	87	8.5	95	14.3
TNA426	16.21	30.64	27.63	53	60	9.1		
TNA428	17.00	26.50	28.93	65	199	22.7		

Table 1. (continued)

Station	Lat (°N)	Long (°W)	Julian Day	MLD	Integrated heme *b* (nmol m^{-2})	Integrated chl *a* (μmol m^{-2})	Integrated POC (mmol m^{-2})	Integrated PON (mmol m^{-2})
TNA429	21.94	27.08	30.23	114	315	26.6	233	30.4
TNA430	22.82	27.19	30.64	129	208	20.0		
TNA431	25.07	28.47	31.31	126	127	28.5	205	27.7
TNA432	26.16	26.41	32.39	139	324	29.4	201	27.4
TNA433	26.59	23.72	33.27	147	345	35.3	269	38.6
TNA434	26.71	23.01	33.64	150	199	38.2		
TNA435	27.14	20.44	34.25	129	354	24.68		
				Scotia Sea				
SSC2	-60.20	44.41	8.38	21	90	20.6		
SSC4	-58.02	42.98	19.29	42	315	26.2		
SSP24	-55.90	41.72	23.5	63	109	47.1		
SSP28	-54.59	41.00	29.4	67	159	83.7		
SSP3	-52.85	40.10	32.3	63	867	211		
SSR3	-52.63	39.11	35.3	41	138	212		

Table 2. Results of Pearson Product Moment Correlation for heme *b*, chl *a*, particulate organic carbon (POC) and particulate organic nitrogen (PON) in the Iceland basin, Tropical North Atlantic and Scotia Sea. POC/PON data were not collected for the Scotia Sea.

		Chl *a*	POC	PON
			Iceland Basin	
Heme *b*	r (n)	0.19 (84)	0.41 (77)	0.45 (77)
	p	0.08	<0.01	<0.01
Chl *a*	r (n)		0.66 (79)	0.6 (79)
	p		<0.01	<0.01
POC	r (n)			0.99 (79)
	p			<0.01
			Tropical North Atlantic	
Heme *b*	r (n)	0.41 (269)	0.23 (60)	0.43(60)
	p	<0.01	0.07	<0.01
Chl *a*	r (n)		0.19 (60)	0.38 (60)
			0.15	<0.01
POC	r (n)			0.60 (64)
	p			<0.01
			Scotia Sea	
Heme *b*	r (n)	0.27 (34)		
	p	0.13		

Table 3. Comparison of heme *b*:PhyC ratio with F_v/F_m observed in the Iceland Basin and Scotia Sea. [1]Integrated mixed layer heme *b*: PhyC ratios are compared with average mixed layer F_v/F_m values. [2]Values for heme *b*: PhyC ratios and F_v/F_m for samples collected at 20 m.

	Heme *b*: PhyC (µmol mol^{-1})	F_v/F_m
Iceland Basin [1]		
Station		
IB222	0.24	0.27 ± 0.02
IB226	0.33	0.27 ± 0.02
IB260	0.04	0.24 ± 0.01
IB285	0.09	0.29 ± 0.01
Scotia Sea [2]		
Station		
SSC2	2.4	0.39
SSC4	4.1	0.25
SSP24	0.5	0.19
SSP28	0.5	0.28
SSP3	5.5	0.56
SSR3	0.4	0.39

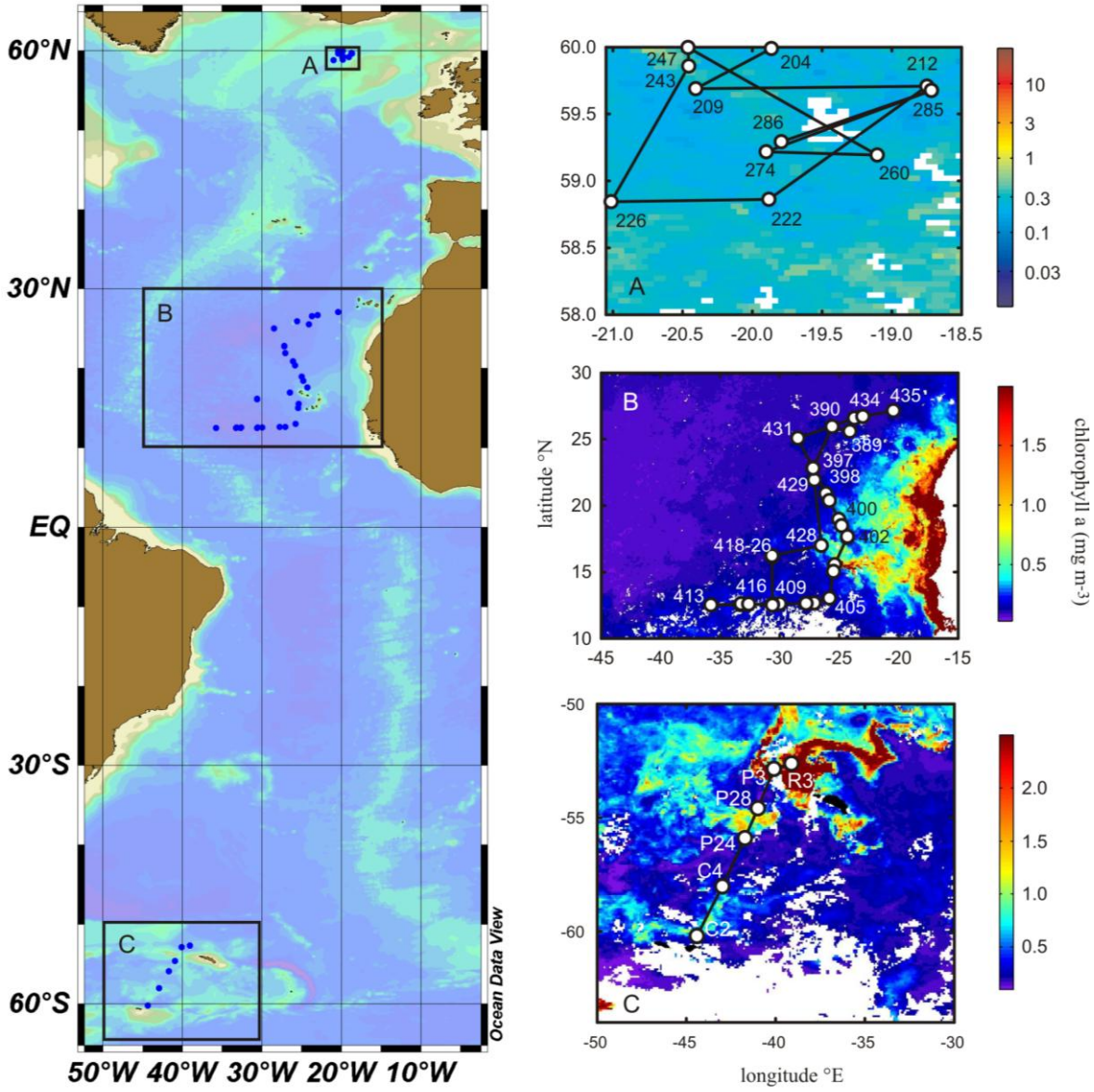

Figure 1. Map of the Atlantic Ocean showing the areas sampled. Inset maps show the sampled stations superimposed on average Sea-WIFS derived chlorophyll a (mg m^{-3}) for the times of the cruises. (**A**) Iceland Basin, (**B**) Tropical North Atlantic and (**C**) Scotia Sea. Note scale changes for chl *a*. Some station numbers have been omitted in B for clarity.

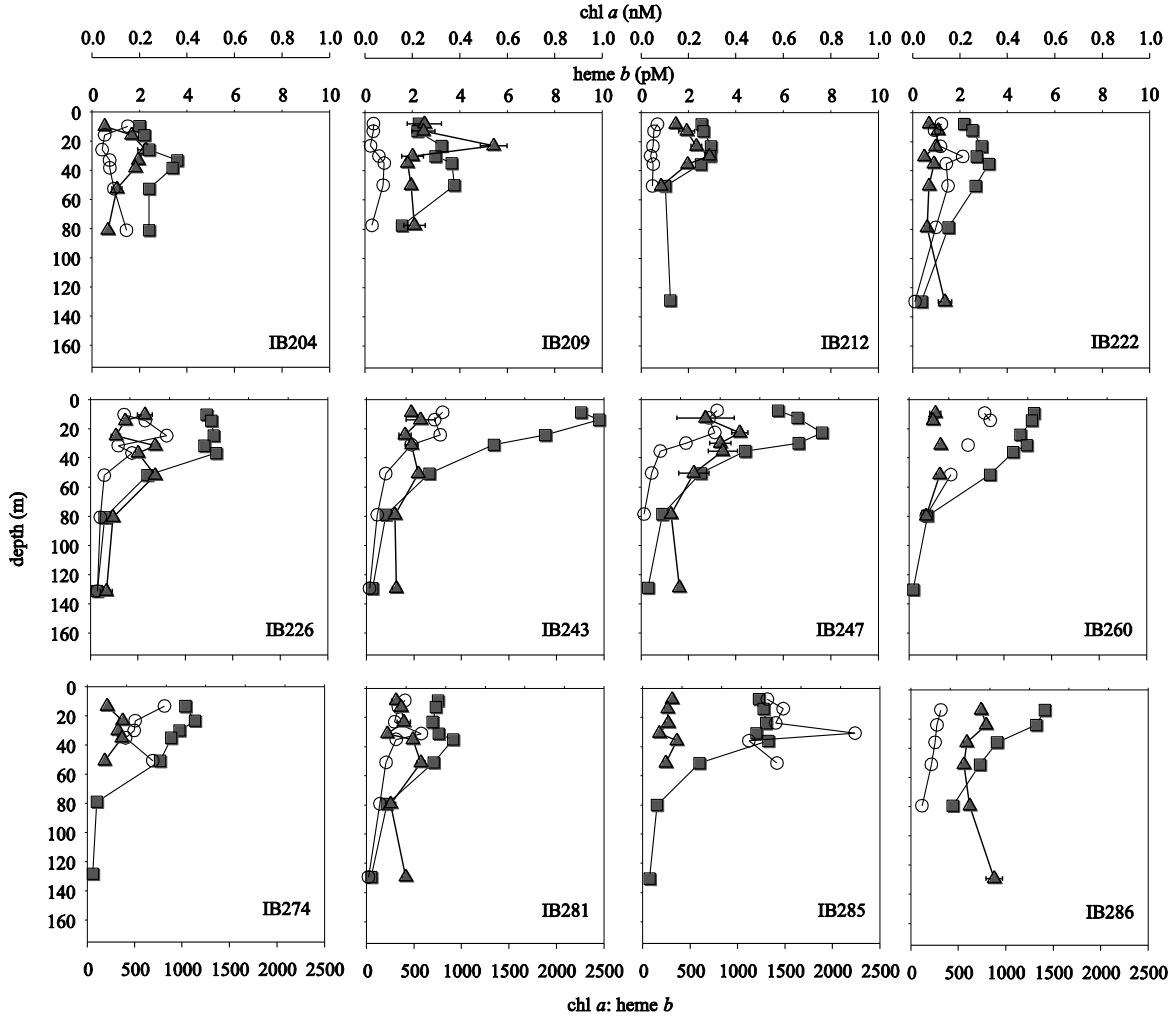

Figure 2. Vertical profiles for heme *b* (triangles), chl *a* (squares) and chl *a*: heme *b* (open circles) determined at stations in the Iceland Basin. Error bars for heme *b* represent the concentration range determined for each sample (n=2).

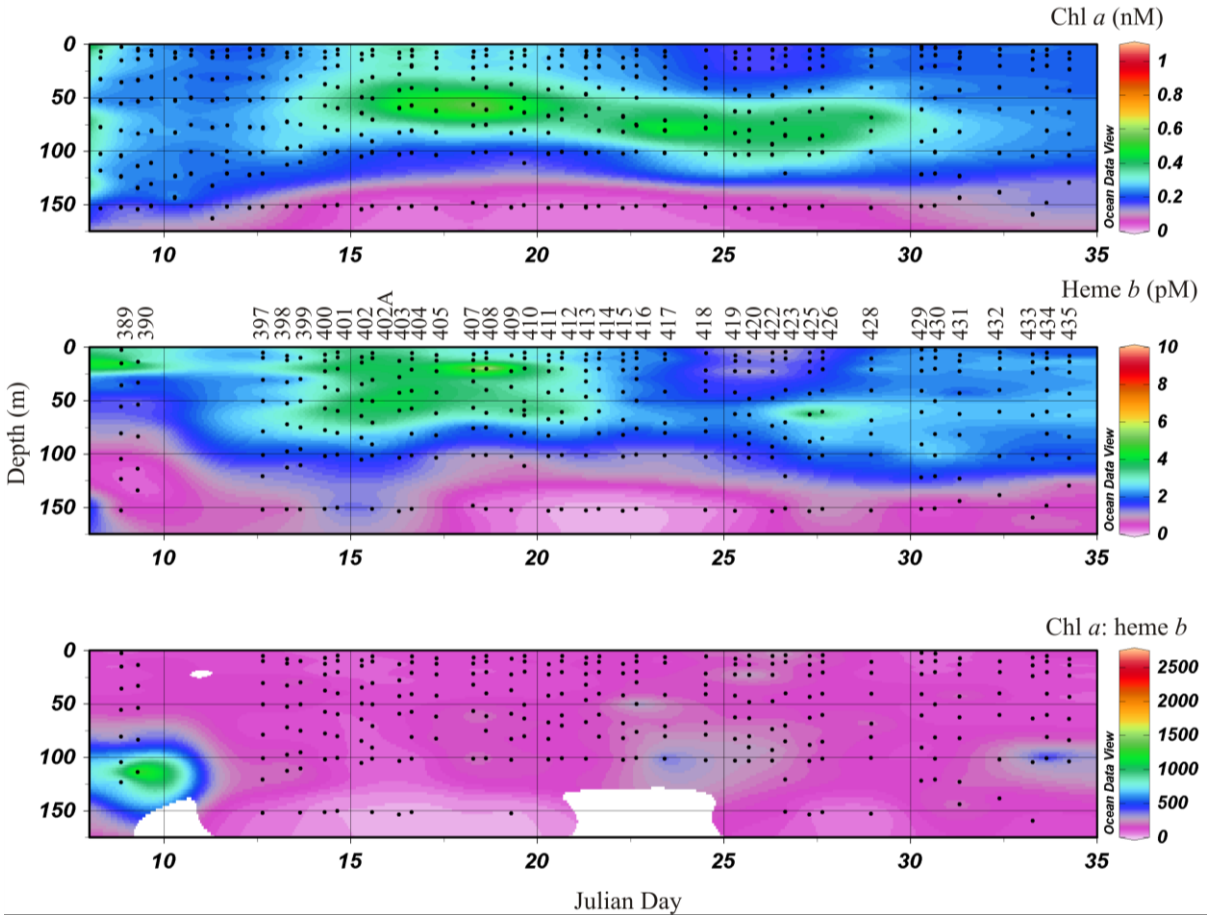

Figure 3. Contour plot for vertical sections of (**A**) chloropyll *a* concentrations (nM), (**B**) heme *b* concentrations (pM) and (**C**) chl *a*: heme *b* determined in the tropical North Atlantic. Station numbers are indicated on B.

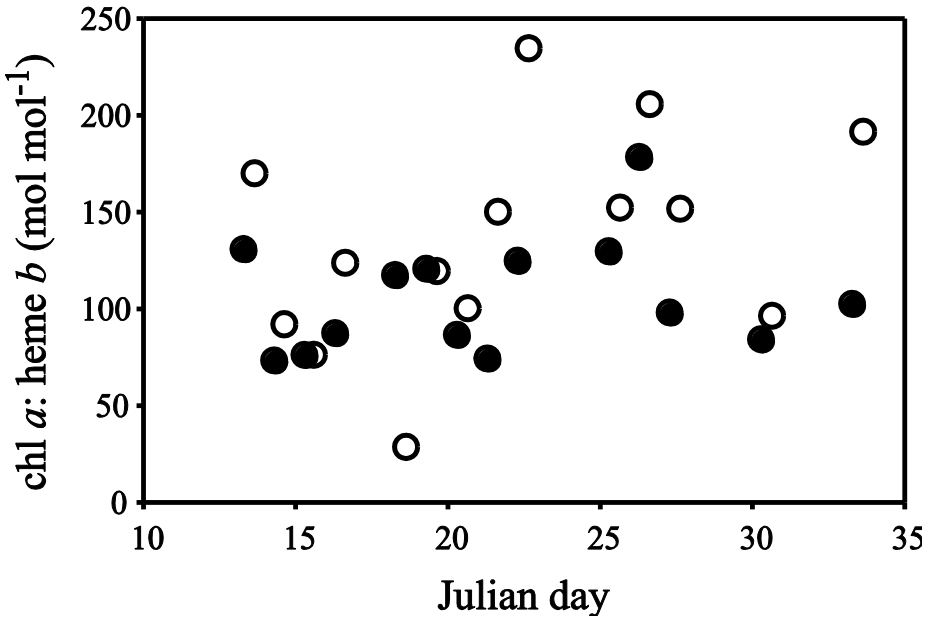

Figure 4. Integrated mixed layer depth chl *a*: heme *b* ratios for days in the Tropical North Atlantic where stations were sampled at dawn (0700 GMT, dark circles) and mid-afternoon (1500–1700 GMT, open circles).

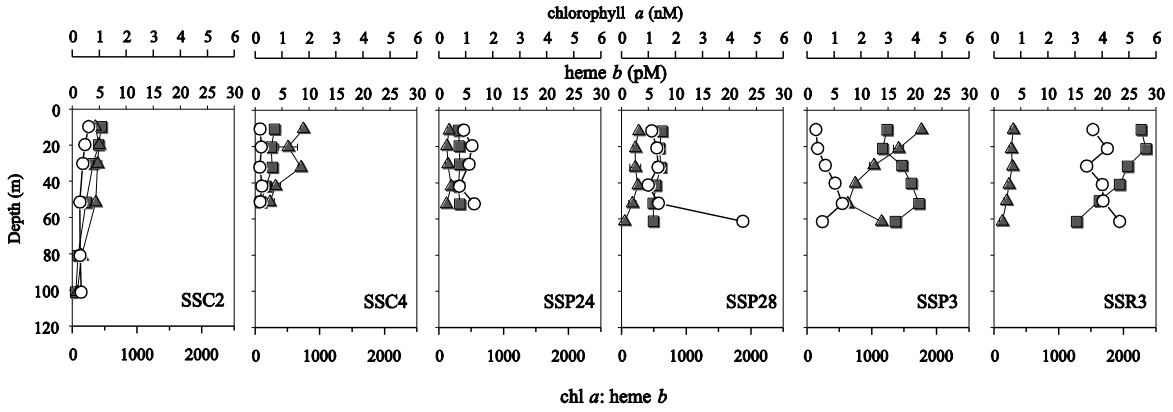

Figure 5. Vertical profiles for heme *b* concentrations (triangles), *c*hl *a* concentrations (squares) and chl *a*: heme *b* ratios (open circles) calculated for stations in the Scotia Sea. Error bars for heme *b* represent the concentration range determined for each sample (n=2).

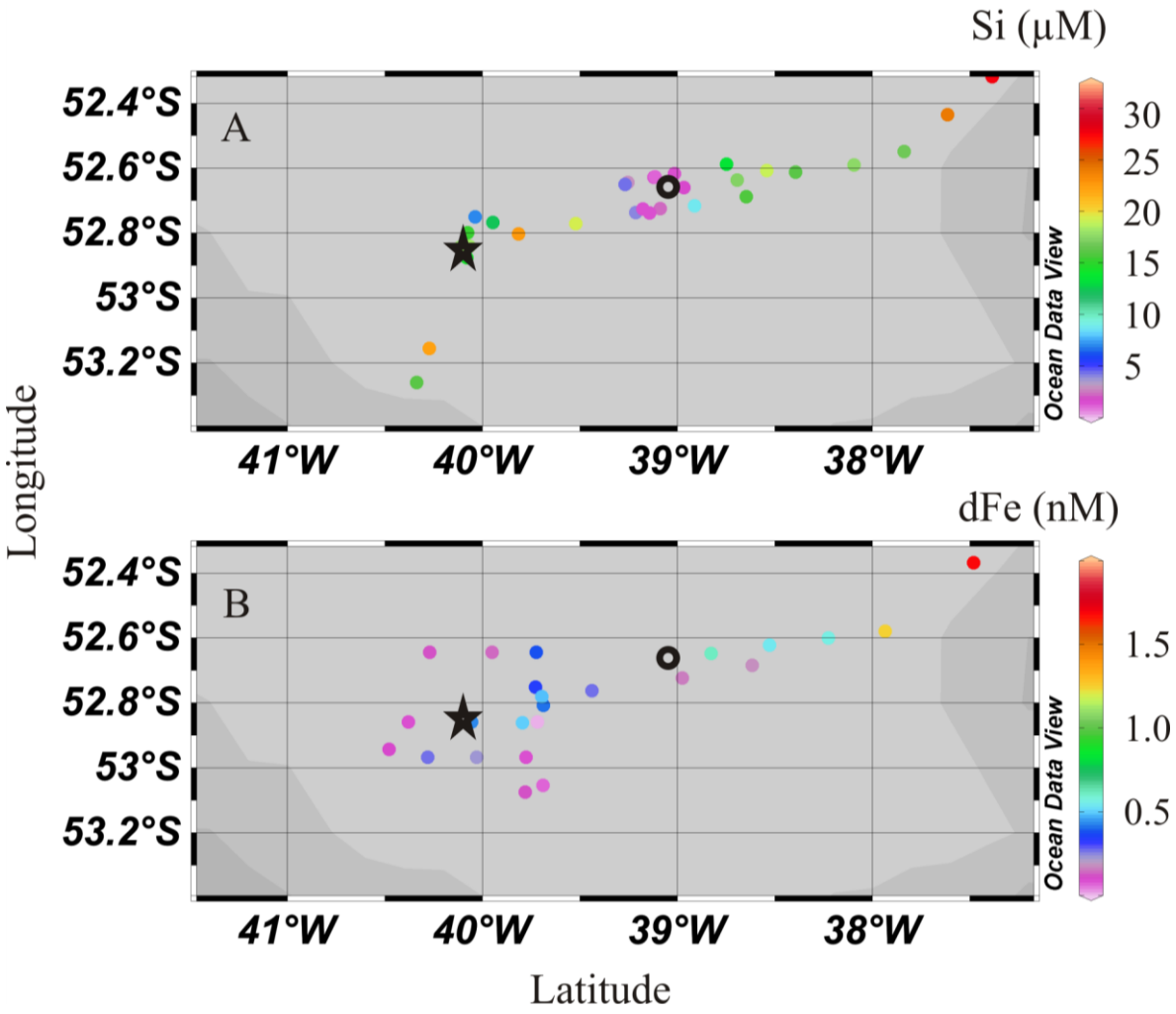

Figure 6. Surface distribution of (**A**) dissolved Si and (**B**) dissolved Fe north west of South Georgia in relation to stations SSP3 (star) and SSR3 (circle).

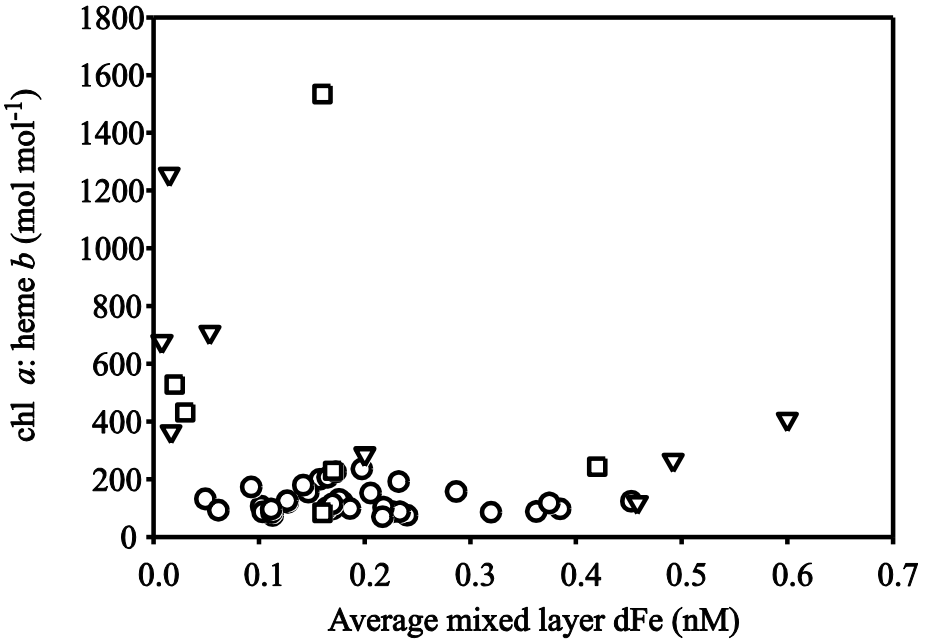

Figure 7. Integrated chlorophyll *a*: heme *b* ratios plotted against average mixed layer dFe concentrations. Iceland basin – inverted triangles, Tropical North Atlantic – circles, Scotia Sea – squares. For the Scotia Sea, the closest dissolved Fe concentrations collected with underway sampling system were used.

Appendix 2

Cruise Metadata

Table 1. D346 - CTD samples (see Chapter 2, Fig. 2.3)
RRS Discovery, 05 Jan - 15 Feb 2010, PI - Brian A. King (NOCS)

Table 2. D361 - CTD samples (see Chapter 2, Fig. 2.4)
RRS Discovery, 07 Feb - 19 Mar 2011, PI - Eric P. Achterberg (NOCS)

Table 3. D361 - FISH samples
RRS Discovery, 07 Feb - 19 Mar 2011, PI - Eric P. Achterberg (NOCS)
Note: Depth approximately 2 - 3 m

Table 1. D346 – CTD samples

Station	Lat (°N)	Long (°W)	Date (dd/mm/yyyy)	Depth (m)	Filtered Volume (L)			Heme *b* (pmol L^{-1})	Chl *a* (nmol L^{-1})	POC (µmol L^{-1})	PON (µmol L^{-1})	N_2 Fixation (nmol N L^{-1} d^{-1})
					Heme *b*	POC/N	Chl *a*					
Florida Straits												
1	27.501	-78.504	06/01/2010	12.5	1.5	1.5	0.5	1.19	0.18	4.09	0.44	
1	27.501	-78.504	06/01/2010	53.1	1.5	1.5	0.5	0.92	0.17	4.99	0.43	
1	27.501	-78.504	06/01/2010	183.2	2	2	0.5	0.83	0.16	1.06	0.06	
2	27.203	-79.569	07/01/2010	7.8	1.5	1.5	0.5	2.46	0.35	3.83	0.46	
2	27.203	-79.569	07/01/2010	52.5	1	1	0.5	4.39	0.58	4.66	0.54	
2	27.203	-79.569	07/01/2010	102.6	1	1	0.5	4.98	0.87			
3	27.207	-79.511	07/01/2010	6.6	1.5	1.5	0.5	2.83	0.37	3.16	0.38	
3	27.207	-79.511	07/01/2010	52.3	1.5	1.5	0.5	3.15	0.43	3.51	0.38	
3	27.207	-79.511	07/01/2010	152.5	1.5	1.5	0.5	0.57	0.03	3.14	0.33	
4	27.211	-79.453	07/01/2010	6.8	2	2	0.5	0.39	0.3	2.87	0.33	
4	27.211	-79.453	07/01/2010	52.1	1.5	1.5	0.5	1.2	0.29	3.51	0.37	
4	27.211	-79.453	07/01/2010	101.9	2	2	0.5	1.62	0.4	2.54	0.32	
5	27.204	-79.405	07/01/2010	6.4	2	2	0.5	2.54	0.25	2.64	0.3	
5	27.204	-79.405	07/01/2010	52	2	2	0.5	2.12	0.23	2.23	0.26	
5	27.204	-79.405	07/01/2010	152.1	2.5	2.5	0.5	0.8	0.09	0.98	0.08	
6	27.206	-79.347	07/01/2010	11.7	2	2	0.5	2.29	0.29	3.06	0.39	
6	27.206	-79.347	07/01/2010	51.5	2	2	0.5	2.6	0.29	2.91	0.4	
6	27.206	-79.347	07/01/2010	202.3	3	3	0.5	0.6		0.95	0.08	
7	27.207	-79.331	07/01/2010	6.1	2.5	2.5	0.5	0.5	0.33	3.06	0.38	
7	27.207	-79.315	07/01/2010	51.2	2.5	2.5	0.5	0.79	0.34	2.56	0.34	
7	27.207	-79.301	07/01/2010	150.9	2.5	2.5	0.5	0.29	0.02	0.67	0.05	
8	27.208	-79.25	07/01/2010	12.1	2	2	0.5	1.68	0.32	3.64	0.42	
8	27.208	-79.25	07/01/2010	51.9	2	2	0.5	2.07	0.38	2.84	0.38	
8	27.208	-79.25	07/01/2010	102	3	3	0.5	1.16	0.17	1.73	0.22	
9	27.2	-79.201	07/01/2010	6.9	2	2	0.5	1.78	0.33	3.61	0.34	
9	27.2	-79.201	07/01/2010	52	2	2	0.5	2.14	0.4	2.58	0.29	
9	27.2	-79.201	07/01/2010	152	1.5	1.5	0.5	0.27		2.58	0.3	

Table 1. (continued)

Station	Lat (°N)	Long (°W)	Date (dd/mm/yyyy)	Depth (m)	Filtered Volume (L)			Heme *b* (pmol L^{-1})	Chl *a* (nmol L^{-1})	POC (µmol L^{-1})	PON (µmol L^{-1})	N_2 Fixation (nmol N L^{-1} d^{-1})
					Heme *b*	POC/N	Chl *a*					
10	27.199	-79.15	07/01/2010	11.1	2	2	0.5	0.68	0.29	4	0.51	
10	27.199	-79.15	07/01/2010	51.2	2	2	0.5	1.34	0.35	2.67	0.33	
10	27.199	-79.15	07/01/2010	101.1	2.5	2.5	0.5	1.31	0.3	2.28	0.31	
11	27.201	-79.125	08/01/2010	5.9	2.5	2.5	0.5	2.78	0.28	3.14	0.3	
11	27.201	-79.125	08/01/2010	50.8	2.5	2.5	0.5	1.56	0.32	2.32	0.27	
11	27.201	-79.125	08/01/2010	151	2.5	2.5	0.5	0.43	0	0.79	0.09	
12	27.203	-79.11	08/01/2010	11.8	2	2	0.5	1.86	0.37	3.22	0.38	
12	27.203	-79.11	08/01/2010	52.2	2	2	0.5	2.08	0.35	2.54	0.34	
12	27.203	-79.11	08/01/2010	102.3	1.5	1.5	0.5	1.46	0.18	2.78	0.41	
13	27.201	-79.105	08/01/2010	6.4	2	2	0.5	2.36	0.37	2.65	0.33	
13	27.201	-79.105	08/01/2010	52.1	2	2	0.5	1.76	0.31	2.16	0.28	
13	27.201	-79.105	08/01/2010	167.6	2	2	0.5	0.47	0.01	1.15	0.11	
Gulf Stream												
14	26.301	-76.561	08/01/2010	6.1	2	2	0.5	0.34	0.16	2.81	0.26	0
14	26.301	-76.561	08/01/2010	25.9	2	2	0.5	1.37	0.16	2.36	0.27	0.05
14	26.301	-76.561	08/01/2010	51.3	1.5	1.5	0.5	1.14	0.17	2.55	0.32	
15	26.299	-76.519	08/01/2010	5.6	2	2	0.5	1.23	0.13	2.76	0.27	
15	26.299	-76.519	08/01/2010	25.9	3	3	0.5	0.99	0.14	2.36	0.23	
15	26.299	-76.519	08/01/2010	50.8	2	2	0.5	1.61	0.16	2.63	0.3	
16	26.32	-76.49	09/01/2010	6.9	2	2	0.5	0.94	0.09	2.28	0.22	
16	26.32	-76.49	09/01/2010	51.8	2	2	0.5	1.47	0.13	2.29	0.24	
16	26.32	-76.49	09/01/2010	102.3	2	2	0.5	1.23	0.14	1.67	0.22	
17	26.302	-76.469	09/01/2010	8.8	2	2	0.5	1.21	0.16	2.3	0.25	
17	26.302	-76.469	09/01/2010	54	2	2	0.5	1.81	0.17	2.43	0.29	
17	26.302	-76.469	09/01/2010	104.4	2	2	0.5	1.21	0.15	1.96	0.24	
19	26.297	-76.457	09/01/2010	5.3	3	3	0.5	1.55	0.15	2.4	0.27	
19	26.297	-76.457	09/01/2010	49.3	2.5	2.5	0.5	1.29	0.17	2.05	0.26	
19	26.297	-76.457	09/01/2010	100.1	2.5	2.5	0.5	1.25	0.13	2.04	0.29	

Table 1. (continued)

Station	Lat (°N)	Long (°W)	Date (dd/mm/yyyy)	Depth (m)	Filtered Volume (L)			Heme *b* (pmol L^{-1})	Chl *a* (nmol L^{-1})	POC (µmol L^{-1})	PON (µmol L^{-1})	N_2 Fixation (nmol N L^{-1} d^{-1})
					Heme *b*	POC/N	Chl *a*					
20	26.3	-76.41	09/01/2010	3	1.5	1.5	0.5	1.63	0.16	2.7	0.28	0.02
20	26.3	-76.41	09/01/2010	50	1.5	1.5	0.5	2.02	0.16	2.51	0.31	0.06
20	26.3	-76.41	09/01/2010	100.8	2	2	0.5	1.61	0.17	2.04	0.27	
21	26.298	-76.378	10/01/2010	5.6	3	2.5	0.5	0.54	0.15	2.14	0.27	
21	26.298	-76.378	10/01/2010	61.7	3	3	0.5	0.9	0.16	2	0.24	
21	26.298	-76.378	10/01/2010	111.8	2.5	2	0.5	1.02	0.16	2.65	0.4	
22	26.298	-76.323	10/01/2010	4.1	3	3	0.5	0.91	0.12	2.42	0.32	
22	26.298	-76.323	10/01/2010	50.3	3	3	0.5	0.83	0.13	2.33	0.31	
22	26.298	-76.323	10/01/2010	120.8	3	3	0.5	1.16	0.24	1.46	0.21	
23	26.29	-76.266	10/01/2010	6.1	2	2	0.5	0.91	0.14	1.87	0.22	0.07
23	26.29	-76.266	10/01/2010	50	3	3	0.5	0.91	0.15	1.81	0.22	
23	26.29	-76.266	10/01/2010	123.2	2.5	2.5	0.5	1.31	0.19	1.24	0.17	0
24	26.298	-76.182	10/01/2010	4.2	2	2	0.5	0.89	0.12	2.17	0.23	
24	26.298	-76.182	10/01/2010	121.1	3.5	3	0.5	0.91	0.2	1.42	0.19	
24	26.298	-76.182	10/01/2010	176.8	3	3	0.5	0.62	0.02	0.93	0.11	
25	26.292	-76.135	11/01/2010	8.2	3	3	0.5	0.89	0.14	1.71	0.24	
25	26.292	-76.135	11/01/2010	54.3	3	3	0.5	1.12	0.14	1.59	0.21	
25	26.292	-76.135	11/01/2010	119.7	3.5	3.5	0.5	1.14	0.19	1.41	0.2	
26	26.298	-76.065	11/01/2010	10.9	2	2	0.5	1.1	0.14	2.06	0.26	0.04
26	26.298	-76.065	11/01/2010	51.2	2.5	2.5	0.5	1.29	0.15			
26	26.298	-76.065	11/01/2010	107.1	2.5	2	0.5	1.13	0.15	2.25	0.33	0.1
27	26.301	-75.545	11/01/2010	11.9	3	3	0.5	0.98	0.13	1.93	0.22	
27	26.301	-75.545	11/01/2010	52.8	3	3	0.5	1.06	0.12	1.74	0.22	
27	26.301	-75.545	11/01/2010	103	3	1.5	0.5	1.06	0.13	7.7	0.49	
28	26.299	-75.436	12/01/2010	11	3	3	0.5	0.76	0.1	1.99	0.25	
28	26.299	-75.436	12/01/2010	52.2	3	3	0.5	0.77	0.1	2.03	0.24	
28	26.299	-75.436	12/01/2010	102.4	3	3	0.5	1.46	0.23	2.32	0.4	

Table 1. (continued)

Station	Lat (°N)	Long (°W)	Date (dd/mm/yyyy)	Depth (m)	Filtered Volume (L)			Heme *b* (pmol L^{-1})	Chl *a* (nmol L^{-1})	POC (µmol L^{-1})	PON (µmol L^{-1})	N_2 Fixation (nmol N L^{-1} d^{-1})
					Heme *b*	POC/N	Chl *a*					
29	26.3	-75.305	12/01/2010	10.4	3	3	0.5	0.98	0.13	1.62	0.22	
29	26.3	-75.305	12/01/2010	50	3	3	0.5	1.1	0.12	1.84	0.23	
29	26.3	-75.305	12/01/2010	121.5	3	3	0.5	1.01	0.23	1.28	0.17	
30	26.298	-75.187	12/01/2010	4.2			0.5		0.09			0.04
30	26.298	-75.187	12/01/2010	50.9	3	3	0.5	0.72	0.13	2.1	0.25	
30	26.298	-75.187	12/01/2010	100.9	2	2	0.5	0.57	0.3	1.62	0.18	0
31	26.302	-75.044	12/01/2010	4.4	3	3	0.5	1.14	0.11	2.19	0.26	
31	26.302	-75.044	12/01/2010	101.2	3	3	0.5	0.81	0.14	1.84	0.22	
31	26.302	-75.044	12/01/2010	178.5	4	3	0.5	0.52	0.03	0.78	0.2	
32	26.298	-74.483	13/01/2010	4	3	3	0.5	0.65	0.1	1.92	0.22	
32	26.298	-74.483	13/01/2010	50.8	3	3	0.5	0.92	0.11	1.7	0.21	
32	26.298	-74.483	13/01/2010	101.3	3	3	0.5	1.37	0.33	1.59	0.27	
33	26.299	-74.31	13/01/2010	4.2	3	3	0.5	0.94	0.13	1.99	0.25	
33	26.299	-74.31	13/01/2010	51.1	3	2.5	0.5	1.01	0.12	2.24	0.29	
33	26.299	-74.31	13/01/2010	101.6	3	3	0.5	0.86	0.25	1.57	0.21	
34	26.299	-74.145	13/01/2010	11.1	3	3	0.5	0.71	0.13	1.81	0.23	
34	26.299	-74.145	13/01/2010	101.8	3	3	0.5	1.09	0.27	1.51	0.22	
34	26.299	-74.145	13/01/2010	177.3	3	3	0.5	0.58	0.06	0.97	0.19	
35	26.302	-73.563	13/01/2010	10.7			0.5		0.15			0.08
35	26.302	-73.563	13/01/2010	100.7			0.5		0.15			0.04
35	26.302	-73.563	13/01/2010	177	3	3	0.5	0.33	0.01	0.66	0.09	
36	26.31	-73.351	14/01/2010	11.5	3	3	0.5	0.82	0.15	1.93	0.26	
36	26.31	-73.351	14/01/2010	51.6	3	3	0.5	0.85	0.15	1.76	0.17	
36	26.31	-73.351	14/01/2010	122.1	3	3	0.5	0.72	0.16	1.08	0.15	
37	26.306	-73.123	14/01/2010	6.3	3	3	0.5	1.04	0.14	1.96	0.26	
37	26.306	-73.123	14/01/2010	52.5	3	3	0.5	0.64	0.15	2.21	0.32	
37	26.306	-73.123	14/01/2010	143.5	3	3	0.5	0.71	0.09	1.25	0.21	

Table 1. (continued)

Station	Lat (°N)	Long (°W)	Date (dd/mm/yyyy)	Depth (m)	Filtered Volume (L)			Heme *b* (pmol L^{-1})	Chl *a* (nmol L^{-1})	POC (µmol L^{-1})	PON (µmol L^{-1})	N_2 Fixation (nmol N L^{-1} d^{-1})
					Heme *b*	POC/N	Chl *a*					
38	26.304	-72.505	14/01/2010	4.4	2.5	2.5	0.5	0.76	0.11	2.08	0.25	
38	26.304	-72.505	14/01/2010	50.1	2.5	2.5	0.5	0.62	0.12	2.12	0.26	
38	26.304	-72.505	14/01/2010	100.7	3	3	0.5	1	0.15	1.83	0.24	
39	26.305	-72.278	14/01/2010	4.9	2.5		0.5	0.81	0.09			0.02
39	26.305	-72.278	14/01/2010	50.2	3	3	0.5	0.79	0.14	2.17	0.23	
39	26.305	-72.278	14/01/2010	80.5	3	3	0.5	1.01	0.26	2.3	0.3	0.03
40	26.308	-72.064	15/01/2010	4.8	3	3	0.5	0.82	0.08	1.84	0.24	
40	26.308	-72.064	15/01/2010	50.7	3	3	0.5	0.58	0.1	2.13	0.29	
40	26.308	-72.064	15/01/2010	111.2	3	3	0.5	1.03	0.18	1.58	0.25	
41	26.308	-71.431	15/01/2010	4.2	3	3	0.5	0.79	0.12	1.7	0.19	
41	26.308	-71.431	15/01/2010	50.3	3	3	0.5	0.93	0.14	2.09	0.28	
41	26.308	-71.431	15/01/2010	120.7	3	3	0.5	0.93	0.21	1.85	0.23	
42	26.298	-71.217	15/01/2010	10.5	1.25		0.5	0.76	0.13			0.04
42	26.298	-71.217	15/01/2010	103.4	3	3	0.5	1.26	0.15	2.05	0.23	0.11
42	26.298	-71.217	15/01/2010	177.1	3	2.5	0.5	0.35	0.02	0.97	0.09	
43	26.285	-71.003	16/01/2010	3.2	3	3	0.5	0.85	0.12	2.35	0.26	
43	26.285	-71.003	16/01/2010	50.2	3	3	0.5	1.19	0.18	1.82	0.22	
43	26.285	-71.003	16/01/2010	105	3	3	0.5	1.13	0.2	2.43	0.3	
44	26.062	-70.38	16/01/2010	5.2	3	3	0.5	0.83	0.1	1.95	0.28	
44	26.062	-70.38	16/01/2010	50.3	3	3	0.5	0.89	0.17	2.03	0.27	
44	26.062	-70.38	16/01/2010	75.4	3	3	0.5	1.4	0.19	2.58	0.37	
45	25.419	-70.159	16/01/2010	5.8	2	2	0.5	0.65	0.08			0.02
45	25.419	-70.159	16/01/2010	50.4	3	3	0.5	0.79	0.09	2.18	0.37	
45	25.419	-70.159	16/01/2010	101	3	3	0.5	1.09	0.29			0.05
46	25.183	-69.542	17/01/2010	5.6	3	3	0.5	0.9	0.1	1.94	0.22	
46	25.183	-69.542	17/01/2010	64.2	3	3	0.5	1.02	0.1	2.26	0.28	
46	25.183	-69.542	17/01/2010	115.2	3	3	0.5	1.24	0.15	2	0.24	

Table 1. (continued)

Station	Lat (°N)	Long (°W)	Date (dd/mm/yyyy)	Depth (m)	Filtered Volume (L)			Heme *b* (pmol L^{-1})	Chl *a* (nmol L^{-1})	POC (µmol L^{-1})	PON (µmol L^{-1})	N_2 Fixation (nmol N L^{-1} d^{-1})
					Heme *b*	POC/N	Chl *a*					
47	24.543	-69.322	17/01/2010	6	3	3	0.5	0.82	0.06	1.89	0.22	
47	24.543	-69.322	17/01/2010	52.2	3	3	0.5	0.89	0.06	1.96	0.21	
47	24.543	-69.322	17/01/2010	115.6	3	3	0.5	0.39	0.02	1.25	0.1	
48	24.303	-69.092	17/01/2010	5.3			0.5		0.06			0.02
48	24.303	-69.092	17/01/2010	50.6	3	3	0.5	0.78	0.06	2	0.22	
48	24.303	-69.092	17/01/2010	101.5	2.5	2.5	0.5		0.31	2.79	0.27	0.03
49	24.306	-68.244	18/01/2010	5.5	3	3	0.5	0.78	0.06	2	0.21	
49	24.306	-68.244	18/01/2010	51.6	3	3	0.5		0.08	2.21	0.25	
49	24.306	-68.244	18/01/2010	111.3	3	3	0.5	1.4	0.28	1.94	0.25	
West Subtropical North Atlantic Gyre												
50	24.305	-67.402	18/01/2010	5	3.5	3.5	0.5	0.95	0.06	1.9	0.24	
50	24.305	-67.402	18/01/2010	51.2	3	3	0.5	0.95	0.13	1.9	0.22	
50	24.305	-67.402	18/01/2010	101.1	3.5	3.5	0.5	1.29	0.31	1.91	0.27	
51	24.3	-66.564	18/01/2010	5.3	2.5	2	0.5	0.88	0.06	2.3	0.26	-0.01
51	24.3	-66.564	18/01/2010	51.6	3	3	0.5	0.8	0.08	2.1	0.27	
51	24.3	-66.564	18/01/2010	102.2	2.5	2.5	0.5	1.6	0.36	1.89	0.24	0.04
52	24.299	-66.126	19/01/2010	4.6	3	3	0.5	0.55	0.05	2.17	0.25	
52	24.299	-66.126	19/01/2010	51.2	2.5	2	0.5		0.08	2.27	0.25	
52	24.299	-66.126	19/01/2010	112.1	3	3	0.5	1.62	0.33	1.51	0.23	
53	24.301	-65.294	19/01/2010	5	3	3	0.5	1.83	0.08	2.28	0.27	
53	24.301	-65.294	19/01/2010	51	3	3	0.5	1.17	0.07	1.8	0.25	
53	24.301	-65.294	19/01/2010	102.2	3	3	0.5	1.5	0.34	1.62	0.21	
54	24.299	-64.461	19/01/2010	5.1	2.5		0.5	1.89	0.14			0.21
54	24.299	-64.461	19/01/2010	100.6	1.5		0.5	2.35	0.37			0.03
54	24.299	-64.461	19/01/2010	177.7	3	3	0.5	0.57	0.01	0.74	0.07	
55	24.308	-64.01	20/01/2010	50.6	3	3	0.5	1.74	0.09	2.24	0.25	
55	24.308	-64.01	20/01/2010	111.1	3	3	0.5	1.12	0.22	1.24	0.15	
55	24.308	-64.01	20/01/2010	176.4	3	3	0.5	0.41	0.02	0.71	0.09	

Table 1. (continued)

Station	Lat (°N)	Long (°W)	Date (dd/mm/yyyy)	Depth (m)	Filtered Volume (L)			Heme *b* (pmol L^{-1})	Chl *a* (nmol L^{-1})	POC (µmol L^{-1})	PON (µmol L^{-1})	N_2 Fixation (nmol N L^{-1} d^{-1})
					Heme *b*	POC/N	Chl *a*					
56	24.297	-63.175	20/01/2010	5.1	3	3	0.5	1.31	0.09	2.29	0.28	
56	24.297	-63.175	20/01/2010	50.1	3	3	0.5	1.83	0.12	2.59	0.25	
56	24.297	-63.175	20/01/2010	100.7	3	3	0.5	2.08	0.31	1.74	0.3	
57	24.301	-62.334	20/01/2010	5.1	2	2	0.5	1.18	0.09	2.7	0.33	4.92
57	24.301	-62.334	20/01/2010	51.8	3	3	0.5	1.07	0.12	2.12	0.25	
57	24.301	-62.334	20/01/2010	102.3	2	2	0.5	2.18	0.37	2.06	0.25	0.05
58	24.305	-61.484	21/01/2010	5.6	3	3	0.5	1.35	0.06	2.19	0.29	
58	24.305	-61.484	21/01/2010	51.3	3	3	0.5	1.78	0.09	2.34	0.32	
58	24.305	-61.484	21/01/2010	110.2	3	3	0.5	2.11	0.38	1.95	0.29	
59	24.301	-61.051	21/01/2010	6.5	3	3	0.5	0.76	0.07			0.79
59	24.301	-61.051	21/01/2010	101.8	3	3	0.5	1.76	0.29			0.05
59	24.301	-61.051	21/01/2010	177.4	3	3	0.5	0.66	0.02	1.97	0.32	
60	24.3	-60.208	21/01/2010	48.9	3	3	0.5	1.04	0.06	2.57	0.29	
60	24.3	-60.208	21/01/2010	114	3	3	0.5	1.6	0.36	1.75	0.25	
60	24.3	-60.208	21/01/2010	176.7	3	3	0.5	0.66	0.03	0.72	0.11	
61	24.304	-59.377	22/01/2010	5.3	3	3	0.5	1.25	0.07	2.51	0.31	
61	24.304	-59.377	22/01/2010	50.6	3	3	0.5	1.1	0.11	2.39	0.32	
61	24.304	-59.377	22/01/2010	111.1	3	3	0.5	1.45	0.28	1.69	0.25	
62	24.299	-58.538	22/01/2010	4.9			0.5		0.05			0.04
62	24.299	-58.538	22/01/2010	49.4	3	3	0.5	1.01	0.09	2.13	0.26	
62	24.299	-58.538	22/01/2010	101.8	3	3	0.5	1.27	0.15	1.6	0.23	0.06
63	24.301	-58.09	22/01/2010	49.8	3	3	0.5	0.75	0.09	2.58	0.28	
63	24.301	-58.09	22/01/2010	117	3	3	0.5	1.31	0.33	1.67	0.25	
63	24.301	-58.09	22/01/2010	175.5	3	3	0.5	0.52	0.03	0.94	0.15	
64	24.301	-57.239	23/01/2010	6.2	3	3	0.5	1.04	0.06	4.54	0.49	
64	24.301	-57.239	23/01/2010	49.6	3	3	0.5	0.93	0.08	1.77	0.25	
64	24.301	-57.239	23/01/2010	116	3	3	0.5	1.77	0.35	1.96	0.28	

Table 1. (continued)

Station	Lat (°N)	Long (°W)	Date (dd/mm/yyyy)	Depth (m)	Filtered Volume (L)			Heme *b* (pmol L^{-1})	Chl *a* (nmol L^{-1})	POC (µmol L^{-1})	PON (µmol L^{-1})	N_2 Fixation (nmol N L^{-1} d^{-1})
					Heme *b*	POC/N	Chl *a*					
65	24.294	-56.414	23/01/2010	4.4	3	3	0.5	0.85	0.07	2.17	0.29	
65	24.294	-56.414	23/01/2010	50.7	3	3	0.5	1.14	0.08	1.92	0.26	
65	24.294	-56.414	23/01/2010	101.1	3	3	0.5	1.18	0.32	1.76	0.24	
66	24.288	-55.566	24/01/2010	11.8	3	3	0.5	0.98	0.07	2.06	0.28	
66	24.288	-55.566	24/01/2010	51.9	3.5	4	0.5	0.54	0.07	1.44	0.2	
66	24.288	-55.566	24/01/2010	102.8	3	3.5	0.5	0.58	0.08	1.21	0.18	
67	24.298	-55.143	24/01/2010	9.5	2.5	0	0.5	1.05	0.06			0.97
67	24.298	-55.143	24/01/2010	50.6	3	3	0.5	1.08	0.07	3	0.34	
67	24.298	-55.143	24/01/2010	99.7	2.5		0.5	1.83	0.38			0.05
68	24.306	-54.272	25/01/2010	5.8	3	3	0.5	1.32	0.09	2.31	0.31	
68	24.306	-54.272	25/01/2010	49.5	3	3.5	0.5	1.26	0.1	1.95	0.27	
68	24.306	-54.272	25/01/2010	102.5	3.5	3.5	0.5	1.46	0.33	1.98	0.31	
69	24.306	-53.563	25/01/2010	5.2	1.75		0.5	1.47	0.09			0.13
69	24.306	-53.563	25/01/2010	102.5	2.5	2.5	0.5	1.61	0.19	2.63	0.35	0.07
69	24.306	-53.563	25/01/2010	175.6	3	3	0.5		0.1	4.42	0.68	
70	24.504	-53.24	26/01/2010	9.6	3	3	0.5	1.26	0.09	2.06	0.27	
70	24.504	-53.24	26/01/2010	52.3	3	3	0.5	1.31	0.1	2.12	0.28	
70	24.504	-53.24	26/01/2010	102.5	3	3	0.5	1.6	0.36	2.14	0.32	
71	25.067	-52.504	26/01/2010	11	2	2	0.5	0.98	0.1	2.55	0.34	
71	25.067	-52.504	26/01/2010	52.6	3	3	0.5	1	0.11	2.65	0.36	
71	25.067	-52.504	26/01/2010	102.6	3		0.5	1.23	0.11			
72	25.048	-52.174	26/01/2010	5.2	3		0.5	1.07	0.08			0.02
72	25.048	-52.174	26/01/2010	51	3	3	0.5	1.36	0.12	2.03	0.28	
72	25.048	-52.174	26/01/2010	126.8	3	3	0.5	1.71	0.34	2.15	0.32	0.03
73	25.013	-51.452	27/01/2010	6.1			0.4		0.08			0.03
73	25.013	-51.452	27/01/2010	50.9	3.5	3.5	0.5	0.91	0.09	1.89	0.23	
73	25.013	-51.452	27/01/2010	102	3		0.5	1.24	0.12			0.02

Table 1. (continued)

Station	Lat (°N)	Long (°W)	Date (dd/mm/yyyy)	Depth (m)	Filtered Volume (L)			Heme *b* (pmol L^{-1})	Chl *a* (nmol L^{-1})	POC (µmol L^{-1})	PON (µmol L^{-1})	N_2 Fixation (nmol N L^{-1} d^{-1})
					Heme *b*	POC/N	Chl *a*					
74	24.562	-51.111	27/01/2010	5.4	3	3	0.5	1.15	0.1	2.55	0.36	
74	24.562	-51.111	27/01/2010	116.7	3	3	0.5	1.2	0.26	1.73	0.24	
74	24.562	-51.111	27/01/2010	175.1	3	3	0.5		0.02	0.88	0.11	
75	24.479	-50.379	28/01/2010	4.4	3	3	0.5	1.47	0.17	2.14	0.3	
75	24.479	-50.379	28/01/2010	48.5	3	3	0.5	1.22	0.13	1.92	0.25	
75	24.479	-50.379	28/01/2010	139.2	3	3	0.5	0.83	0.17	1.88	0.25	
76	24.401	-50.054	28/01/2010	5.3	3	3	0.5	1.1	0.15	1.72	0.22	0.11
76	24.401	-50.054	28/01/2010	52.4	3	3	0.5	1.09	0.15	1.84	0.24	
76	24.401	-50.054	28/01/2010	102.8	2.25		0.5	1.71	0.15			0.02
77	24.312	-49.321	28/01/2010	5.4	3	3	0.5	0.98	0.12	2.08	0.27	
77	24.312	-49.321	28/01/2010	119	3	3	0.5	1.02	0.19	1.93	0.26	
77	24.312	-49.321	28/01/2010	176.4	3	3	0.5	0.77	0.04	0.73	0.1	
78	24.209	-49.005	29/01/2010	5.5	3	3	0.5	1.25	0.16	1.8	0.26	
78	24.209	-49.005	29/01/2010	50.4	3	3	0.5	1.3	0.16	2.06	0.29	
78	24.209	-49.005	29/01/2010	131.5	3	3	0.5	1.35	0.23	1.44	0.21	
79	24.118	-48.284	29/01/2010	4.6	3	3	0.5	0.96	0.13	1.86	0.26	0.05
79	24.118	-48.284	29/01/2010	49.4	3	3	0.5	1.01	0.14	2.11	0.3	
79	24.118	-48.284	29/01/2010	100.2	3	3	0.5	1.52	0.14	2.07	0.26	0.06
80	24.04	-47.566	29/01/2010	3.6	2.5	2.5	0.5	1.24	0.11	2.35	0.28	
80	24.04	-47.566	29/01/2010	24.5	3	3	0.5	0.92	0.11	2.06	0.25	
80	24.04	-47.566	29/01/2010	99.3	3	3	0.5	1.19	0.16	1.96	0.25	
82	23.54	-46.526	30/01/2010	5.4	3	3	0.5	1.27	0.14	1.93	0.25	
82	23.54	-46.526	30/01/2010	25.4	3	3	0.5	1.4	0.14	2.11	0.28	
82	23.54	-46.526	30/01/2010	50.7	3	3	0.5	1.06	0.14	2.34	0.33	
83	23.524	-46.2	30/01/2010	11.4	2	1.75	0.5	1.1	0.12	2.4	0.3	0.01
83	23.524	-46.2	30/01/2010	103	2.25	2	0.5	1.17	0.15	2.21	0.31	0.06
83	23.524	-46.2	30/01/2010	175.7	3	3	0.5	0.96	0.05	1	0.16	

Table 1. (continued)

Station	Lat (°N)	Long (°W)	Date (dd/mm/yyyy)	Depth (m)	Filtered Volume (L)			Heme *b* (pmol L^{-1})	Chl *a* (nmol L^{-1})	POC (µmol L^{-1})	PON (µmol L^{-1})	N_2 Fixation (nmol N L^{-1} d^{-1})
					Heme *b*	POC/N	Chl *a*					
84	23.46	-45.481	31/01/2010	5.2		3	0.5		0.13	1.95	0.3	
84	23.46	-45.481	31/01/2010	27.6	3	3	0.5	1.31	0.13	1.74	0.25	
84	23.46	-45.481	31/01/2010	120.4	2	2	0.5	1.47	0.27	1.96	0.28	
85	23.44	-45.162	31/01/2010	4	3	3	0.5	1.21	0.12	2.41	0.34	
85	23.44	-45.162	31/01/2010	49.4	3	3	0.5	1.1	0.12	2.34	0.32	
85	23.44	-45.162	31/01/2010	124.1	3	3	0.5	1.34	0.33	1.99	0.29	
86	23.381	-44.441	31/01/2010	10.4	3	3	0.5	1.21	0.16			0.1
86	23.381	-44.441	31/01/2010	51.1	3	2.25	0.5	1.28	0.16	2.23	0.34	
86	23.381	-44.441	31/01/2010	100.8	2.5	2	0.5	1.53	0.17			0.09
East Subtropical North Atlantic Gyre												
87	23.321	-44.125	31/01/2010	5.9	3	3	0.5	1.1	0.13	1.91	0.27	
87	23.321	-44.125	31/01/2010	51	3	3	0.5	1.07	0.13	1.8	0.23	
87	23.321	-44.125	31/01/2010	125.6	3	3	0.5	1.4	0.16	1.94	0.27	
88	23.27	-43.403	01/02/2010	4.7	3	3	0.5	1.14	0.12	1.91	0.26	
88	23.27	-43.403	01/02/2010	50.5	3	3	0.5	1.08	0.13	2.11	0.29	
88	23.27	-43.403	01/02/2010	123	3	3	0.5	1.44	0.25	1.28	0.19	
89	23.224	-43.085	01/02/2010	4.7	2.5	2.5	0.5	1.98	0.1	1.8	0.22	0.02
89	23.224	-43.085	01/02/2010	51.5	3	3	0.5	1.61	0.12	1.81	0.24	
89	23.224	-43.085	01/02/2010	101.7	2	2	0.5	2.29	0.14	1.85	0.24	0.15
90	23.15	-42.36	01/02/2010	5	3.5	3.5	0.5	1.44	0.12	2.12	0.25	
90	23.15	-42.36	01/02/2010	50.6	3.5	3.5	0.5	1.44	0.12	2.09	0.26	
90	23.15	-42.36	01/02/2010	115.6	3.5	3.5	0.5	2.31	0.36	1.96	0.32	
91	23.231	-41.461	02/02/2010	5.1	3.5	3.5	0.5	1.58	0.15	2.02	0.32	
91	23.231	-41.461	02/02/2010	51.8	3.5	3.5	0.5	1.28	0.15	1.63	0.22	
91	23.231	-41.461	02/02/2010	116.4	3.5	3.5	0.5	1.9	0.27	1.55	0.22	
92	23.312	-40.567	02/02/2010	5.1			0.5		0.12			0.13
92	23.312	-40.567	02/02/2010	51.5	3.5	3.5	0.5	1.32	0.12	1.89	0.31	
92	23.312	-40.567	02/02/2010	124.6	3.5	3.5	0.5	1.64	0.31	1.85	0.3	0.05

Table 1. (continued)

Station	Lat (°N)	Long (°W)	Date (dd/mm/yyyy)	Depth (m)	Filtered Volume (L)			Heme *b* (pmol L^{-1})	Chl *a* (nmol L^{-1})	POC (µmol L^{-1})	PON (µmol L^{-1})	N_2 Fixation (nmol N L^{-1} d^{-1})
					Heme *b*	POC/N	Chl *a*					
93	23.4	-40.065	02/02/2010	4.9	3.5	3.5	0.5	1.26	0.14	1.84	0.24	
93	23.4	-40.065	02/02/2010	50.5	3.5	2.5	0.5	1.25	0.16	2.09	0.25	
93	23.4	-40.065	02/02/2010	177.7	3.5	3	0.5	0.49	0.03	2.04	0.25	
94	23.48	-39.157	03/02/2010	4.5	3.5	3.5	0.5	1.16	0.12	1.86	0.27	
94	23.48	-39.157	03/02/2010	50.7	3.5	3.5	0.5	1.17	0.12	2.31	0.31	
94	23.48	-39.157	03/02/2010	128.6	3.5	3.5	0.5	1.35	0.24	1.27	0.18	
95	23.561	-38.26	03/02/2010	5.8			0.4		0.13			0.08
95	23.561	-38.26	03/02/2010	51.8	3.5	3.5	0.5	1.27	0.14	1.97	0.26	
95	23.561	-38.26	03/02/2010	138	2		0.5	1.54	0.26			0.08
96	24.054	-37.367	03/02/2010	4.8	3.5	3.5	0.5	1.04	0.09	1.9	0.27	
96	24.054	-37.367	03/02/2010	51.8	3.5	3	0.5	1.06	0.15	1.89	0.26	
96	24.054	-37.367	03/02/2010	120	3.5	3.5	0.5	1.77	0.33	1.7	0.27	
97	24.132	-36.462	04/02/2010	5.3	3.5	3.5	0.5	0.93	0.12	1.9	0.28	
97	24.132	-36.462	04/02/2010	51	3.5	3.5	0.5	1.07	0.13	1.98	0.3	
97	24.132	-36.462	04/02/2010	130	3.5	3.5	0.5	1.52	0.18	1.9	0.3	
98	24.218	-35.556	04/02/2010	6	3	3	0.5	0.74	0.08			0.29
98	24.218	-35.556	04/02/2010	51	3	2.5	0.5	1.04	0.11	2.85	0.49	
98	24.218	-35.556	04/02/2010	132.4	3	3	0.5	1.59	0.29			0.09
99	24.304	-35.051	05/02/2010	4.6	3.5	3.5	0.5	1.14	0.1	2.54	0.38	
99	24.304	-35.051	05/02/2010	49.9	3.5	3.5	0.5	1.41	0.24	2.04	0.31	
99	24.304	-35.051	05/02/2010	108.7	3.5	3.5	0.5	1.52	0.24	2.06	0.33	
100	24.297	-34.25	05/02/2010	7.1	3.5	3.5	0.5	0.83	0.07	2.24	0.31	
100	24.297	-34.25	05/02/2010	53.2	3.5	3.5	0.5	0.8	0.09	1.78	0.25	
100	24.297	-34.25	05/02/2010	179.8	3.5	3.5	0.5	0.48	0.02	0.77	0.12	
101	24.298	-33.437	05/02/2010	4.1	2.5	2	0.5	1.08	0.11	2.52	0.38	0.36
101	24.298	-33.437	05/02/2010	49.8	3.5	3.5	0.5	0.84	0.14	2.2	0.39	
101	24.298	-33.437	05/02/2010	150.9	3	1.75	0.5	1.22	0.17	2.06	0.23	0.11

Table 1. (continued)

Station	Lat (°N)	Long (°W)	Date (dd/mm/yyyy)	Depth (m)	Filtered Volume (L)			Heme *b* (pmol L^{-1})	Chl *a* (nmol L^{-1})	POC (µmol L^{-1})	PON (µmol L^{-1})	N_2 Fixation (nmol N L^{-1} d^{-1})
					Heme *b*	POC/N	Chl *a*					
102	24.3	-33.027	06/02/2010	5.8	3.5	3.5	0.5	1.48	0.09	2.06	0.31	
102	24.3	-33.027	06/02/2010	51.3	3.5	3.5	0.5	0.81	0.11	2.19	0.35	
102	24.3	-33.027	06/02/2010	117.5	3.5	3.5	0.5	1.6	0.3	1.99	0.33	
103	24.296	-32.214	06/02/2010	4.6			0.5		0.1			0.57
103	24.296	-32.214	06/02/2010	51.8	3.5	3.25	0.5	1.43	0.13	2.36	0.35	
103	24.296	-32.214	06/02/2010	121.8	3.5	3	0.5	1.43	0.24	1.91	0.35	0.11
104	24.299	-31.409	06/02/2010	5.5	3.5	3.5	0.5	1.17	0.12	2.04	0.28	
104	24.299	-31.409	06/02/2010	50	3.5	3.5	0.5	0.9	0.1			
104	24.299	-31.409	06/02/2010	91.8	3.5	3.5	0.5	1.78	0.35			
105	24.298	-31.002	07/02/2010	5.4	3.5	3.5	0.5	1.12	0.21	2.13	0.34	
105	24.298	-31.002	07/02/2010	50.4	3.5	3.5	0.5	1.04	0.16	2.25	0.34	
105	24.298	-31.002	07/02/2010	129.9	3.5	3.5	0.5	1.1	0.13	1.99	0.31	
106	24.295	-30.193	07/02/2010	4.5	3.5	3.5	0.5	0.81	0.11			0.48
106	24.295	-30.193	07/02/2010	49.3	3.5	3.5	0.5	0.82	0.13	3.01	0.42	
106	24.295	-30.193	07/02/2010	110.3	3.5	3.5	0.5	1.51	0.24			0.04
107	24.302	-29.395	07/02/2010	5.5	3.5	3.5	0.5		0.1	2.35	0.38	
107	24.302	-29.395	07/02/2010	51.1	3.5	3.5	0.5	1.1	0.12	2.25	0.36	
107	24.302	-29.395	07/02/2010	99.1	3.5	3.5	0.5	1.56	0.38	2.64	0.48	
108	24.301	-28.577	08/02/2010	6.2	3.5	3.5	0.5	1.1	0.13	2.64	0.45	
108	24.301	-28.577	08/02/2010	52.3	3.5	3.5	0.5	1.54	0.16	2.2	0.38	
108	24.301	-28.577	08/02/2010	77.6	3.5	3.5	0.5	2.13	0.38	2.51	0.46	
109	24.301	-28.177	08/02/2010	6	3.5		0.5	1.24	0.11			0.75
109	24.301	-28.177	08/02/2010	52.8	3.5	3.5	0.5	0.98	0.12	2.25	0.34	
109	24.301	-28.177	08/02/2010	128.5	3.5		0.5	0.79	0.16			0.12
110	24.295	-27.36	09/02/2010	3.9	3.5	3.5	0.5	1.1	0.13	2.38	0.38	
110	24.295	-27.36	09/02/2010	51	3.5	3.5	0.5	1.19	0.13	2.44	0.39	
110	24.295	-27.36	09/02/2010	101.7	3.5	3.5	0.5	1.92	0.37	2.1	0.37	

Table 1. (continued)

Station	Lat (°N)	Long (°W)	Date (dd/mm/yyyy)	Depth (m)	Filtered Volume (L)			Heme *b* (pmol L^{-1})	Chl *a* (nmol L^{-1})	POC (µmol L^{-1})	PON (µmol L^{-1})	N_2 Fixation (nmol N L^{-1} d^{-1})
					Heme *b*	POC/N	Chl *a*					
111	24.307	-26.547	09/02/2010	4.4	3.5	3.5	0.5	1.03	0.15	2.16	0.34	
111	24.307	-26.547	09/02/2010	51.1	3.5	3.5	0.5	1.32	0.25	1.8	0.26	
111	24.307	-26.547	09/02/2010	102.1	3.5	3.5	0.5	0.55	0.02	0.72	0.11	
112	24.306	-26.135	09/02/2010	5.7	3.5		0.5	0.93	0.12			4.21
112	24.306	-26.135	09/02/2010	51.3	3.5	3.5	0.5	1.28	0.19	2.57	0.39	
112	24.306	-26.135	09/02/2010	85.2	3.5	3.5	0.5	1.89	0.48	2.15	0.36	0.16
Azores Current												
113	24.307	-25.325	10/02/2010	3.6	3.5	3.5	0.5	1.51	0.19	3.13	0.53	
113	24.307	-25.325	10/02/2010	50.4	3.5	3.5	0.5	1.31	0.21	2.99	0.48	
113	24.307	-25.325	10/02/2010	102.5	3.5	3.5	0.5	1.14	0.26	2.08	0.33	
114	24.309	-24.508	10/02/2010	4.8	2.5	2.25	0.5	0.74	0.17	2.29	0.34	1.92
114	24.309	-24.508	10/02/2010	65.4	3.5	3.5	0.5	1.61	0.2	2.27	0.37	0.55
114	24.309	-24.508	10/02/2010	176.6	3.5	3.5	0.5	0.63	0.02	0.66	0.14	
115	24.3	-24.099	10/02/2010	4.7	3.5	3.5	0.5	0.99	0.17	0.16	0.41	
115	24.3	-24.099	10/02/2010	50	3.5	3.5	0.5	0.92	0.21	3.14	0.48	
115	24.3	-24.099	10/02/2010	99.2	3.5	3.5	0.5	2.04	0.38	2.33	0.36	
116	24.297	-23.301	11/02/2010	5.4	3.5	3.5	0.5	1.66	0.25	2.38	0.34	
116	24.297	-23.301	11/02/2010	70.4	3.5	3.5	0.5	1.54	0.43	4.25	0.65	
116	24.297	-23.301	11/02/2010	101.2	3.5	3.5	0.5	1.53	0.25	2.53	0.42	
117	24.429	-22.531	11/02/2010	3.9	3.5	3.5	0.5	1.27	0.14	2.05	0.29	
117	24.429	-22.531	11/02/2010	49.8	3.5	3.5	0.5	1.63	0.16	2.79	0.37	
117	24.429	-22.531	11/02/2010	111.6	3.5	3.5	0.5	1.17	0.14	1.21	0.19	
118	24.551	-22.159	11/02/2010	50.4	3.5	3.5	0.5	1.97	0.31	3.25	0.48	
118	24.551	-22.159	11/02/2010	101.7	3.5	3.5	0.5	1.23	0.42	3.07	0.4	0.14
119	25.082	-21.391	11/02/2010	2.9	2.5	2.25	0.5	1.24	0.14	4.48	0.67	
119	25.082	-21.391	11/02/2010	25.1	3.5	3	0.5	1.31	0.14	2.87	0.28	
119	25.082	-21.391	11/02/2010	93.9	3.5		0.5	1.41	0.36			

Table 1. (continued)

Station	Lat (°N)	Long (°W)	Date (dd/mm/yyyy)	Depth (m)	Filtered Volume (L)			Heme *b* (pmol L^{-1})	Chl *a* (nmol L^{-1})	POC (µmol L^{-1})	PON (µmol L^{-1})	N_2 Fixation (nmol N L^{-1} d^{-1})
					Heme *b*	POC/N	Chl *a*					
120	25.201	-21.018	12/02/2010	2.9	3.5	3.5	0.5	1.44	0.2	2.58	0.36	
120	25.201	-21.018	12/02/2010	76.1	3.5	3.5	0.5	1.25	0.17	1.82	0.24	
120	25.201	-21.018	12/02/2010	101.8	3.5	3.5	0.5	1.22	0.23	1.8	0.24	
121	25.328	-20.251	12/02/2010	4.4	3.5	3.5	0.5	1.14	0.19	2.5	0.28	0.53
121	25.328	-20.251	12/02/2010	51	3.5	3.5	0.5	1.6	0.24	2.47	0.31	
121	25.328	-20.251	12/02/2010	97.2	2		0.5	0.94	0.22			0.16
122	25.446	-19.478	12/02/2010	4.9	3.5	3.5	0.5	2	0.14	2.66	0.32	
122	25.446	-19.478	12/02/2010	75.9	3	2.25	0.5	2.84	0.2	2.5	0.32	
122	25.446	-19.478	12/02/2010	119.1	3.5	3.5	0.5	1.25	0.2	1.35	0.18	
123	25.577	-19.113	13/02/2010	5.2	3.5	3.5	0.5	0.93	0.13	2	0.27	
123	25.577	-19.113	13/02/2010	25.7	3.5	3.5	0.5	1.93	0.13	2.36	0.34	
123	25.577	-19.113	13/02/2010	94.3	3.5	3.5	0.5	2.01	0.35	1.64	0.24	
124	26.101	-18.344	13/02/2010	4.4	3.5	3.5	0.5	2.07	0.24	3	0.42	
124	26.101	-18.344	13/02/2010	48.3	3.5	3.5	0.5	2.47	0.26	3.12	0.46	
124	26.101	-18.344	13/02/2010	93.7	3.5	3.5	0.5	1.88	0.28	2.21	0.33	
125	26.226	-17.575	13/02/2010	5.3	3.5	3.5	0.5	2.26	0.13	3.12	0.42	1.37
125	26.226	-17.575	13/02/2010	84			0.5		0.23			0.17
125	26.226	-17.575	13/02/2010	175.2	3.5	3.5	0.5	1	0.01	3.1	0.44	
126	26.346	-17.201	13/02/2010	5.5	3.5	3.5	0.5	1.51	0.12	2.77	0.66	
126	26.346	-17.201	13/02/2010	76.2	3.5	3.5	0.5	2.35	0.3	5.15	0.64	
126	26.346	-17.201	13/02/2010	86.4	3.5	3.5	0.5	2.12	0.25	4.42	0.69	
127	26.474	-16.429	14/02/2010	5.4	3.5	3.5	0.5	1.49	0.13	5.02	0.3	
127	26.474	-16.429	14/02/2010	51.3	3.5	3.5	0.5	2.12	0.19	2.31	0.33	
127	26.474	-16.429	14/02/2010	76.2	3.5	3.5	0.5	2.35	0.39	2.82	0.35	
128	26.593	-16.058	14/02/2010	4.8	3.5	3.25	0.5	1.92	0.17	3.1	0.39	
128	26.593	-16.058	14/02/2010	25.7	3.5	3.5	0.5	1.84	0.17	2.42	0.21	
128	26.593	-16.058	14/02/2010	87.5	3.5	3.5	0.5	1.99	0.32	3.07	0.38	

Table 1. (continued)

Station	Lat (°N)	Long (°W)	Date (dd/mm/yyyy)	Depth (m)	Filtered Volume (L)			Heme *b* (pmol L^{-1})	Chl *a* (nmol L^{-1})	POC (µmol L^{-1})	PON (µmol L^{-1})	N_2 Fixation (nmol N L^{-1} d^{-1})
					Heme *b*	POC/N	Chl *a*					
129	27.118	-15.29	14/02/2010	6	3.5	3.5	0.5	1.65	0.13	3.52	0.45	1.49
129	27.118	-15.29	14/02/2010	51.4	3.5	3.5	0.5	1.83	0.23	3.09	0.43	
129	27.118	-15.29	14/02/2010	96.9	3.5	3.5	0.5	2.2	0.4	2.91	0.38	0.18
130	27.249	-14.521	14/02/2010	5.5	3.5	3.5	0.5	2.19	0.18	3.09	0.45	
130	27.249	-14.521	14/02/2010	25.6	3.5	3.5	0.5	2.02	0.18	1.49	0.23	
130	27.249	-14.521	14/02/2010	101.1	3.5	3.5	0.5	1.66	0.17	3.11	0.38	
131	27.374	-14.142	15/02/2010	5.3	3.5	3.5	0.5	3.44	0.26	3.11	0.38	
131	27.374	-14.142	15/02/2010	63	3.5	3.5	0.5	3.24	0.5	2.19	0.4	
131	27.374	-14.142	15/02/2010	176.1	3.5	3.5	0.5	0.77	0.01	3	0.39	
132	27.474	-13.466	15/02/2010	5.5	3	3	0.5	2.49	0.19			1.97
132	27.474	-13.466	15/02/2010	69.6	2.5	2.25	0.5	4.25	0.59			0.54
132	27.474	-13.466	15/02/2010	99	3	3	0.5	1.6	0.09	3.16	0.46	
133	27.52	-13.334	15/02/2010	5.3	3	3	0.5	2.85	0.26	1.48	0.26	
133	27.52	-13.334	15/02/2010	63.8	3	3	0.5	1.69	0.38	1.95	0.41	
133	27.52	-13.334	15/02/2010	104.1	3	3	0.5	2.08	0.16	2.05	0.4	
134	27.547	-13.246	15/02/2010	6.2	3	3	0.5	2.48	0.28	1.94	0.34	
134	27.547	-13.246	15/02/2010	41.7	3	3	0.5	3.11	0.42	2.49	0.35	
134	27.547	-13.246	15/02/2010	100.9	3	3	0.5	2	0.06	2.39	0.37	
135	27.557	-13.222	15/02/2010	7.2	3	3	0.5	1.9	0.22	2	0.28	3.79
135	27.557	-13.222	15/02/2010	63.4	3	3	0.5	2.07	0.44	1.85	0.25	0.33
135	27.557	-13.222	15/02/2010	102.6	3	3	0.5	2.05	0.11	2.06	0.34	

Table 2. D361 – CTD samples

Station	Lat (°N)	Long (°W)	Date (dd/mm/yyyy)	Depth (m)	Filtered Volume (L)			Heme *b* (pmol L^{-1})	Chl *a* (nmol L^{-1})	POC (µmol L^{-1})	PON (µmol L^{-1})	N_2 Fixation (nmol N L^{-1} d^{-1})
					Heme *b*	POC/N	Chl *a*					
Coastal TNA												
2	12.587	-17.913	22/02/2011	2.4	2	2	0.2	15.71	2.02	18.24	2.32	
2	12.587	-17.913	22/02/2011	10.5	2	2	0.2	7.7	1.63	10.08	1.25	
2	12.587	-17.913	22/02/2011	20.9	2	2	0.2	0.89	1.42	4.61	0.71	
2	12.587	-17.913	22/02/2011	30.6	2	2	0.2	14.2	2.23	9.56	1.13	
2	12.587	-17.913	22/02/2011	41	3	3	0.2	12.19	1.97	10.23	1.43	
2	12.587	-17.913	22/02/2011	50.8	3	3	0.2	12.14	1.31	7.79	0.86	
3	12.591	-17.713	22/02/2011	1.7	2	2	0.2	2.74	2.33	12.05	1.72	0.2
3	12.591	-17.713	22/02/2011	11.3	2	2	0.2	3.24	2.1	11.87	1.48	0.2
3	12.591	-17.713	22/02/2011	21.2	2	2	0.2	4.65	1.6	7.36	1.17	0.2
3	12.591	-17.713	22/02/2011	31.1	2	2	0.2	8.8	1.33	4.94	0.75	0.2
3	12.591	-17.713	22/02/2011	51.3	2	2	0.2	0.63	0.81	6.42	0.57	0.45
3	12.591	-17.713	22/02/2011	70.5	3	3	0.2	5.58	0.45	2.09	0.27	
4	12.587	-17.569	22/02/2011	2.6	3	2	0.2	5.4	6.61	22.37	2.72	
4	12.587	-17.569	22/02/2011	2.6	2	2		3.61		22.61	2.52	
4	12.587	-17.569	22/02/2011	10.8	3	2	0.2	4.11	3.37	15.17	2	
4	12.587	-17.569	22/02/2011	20.6	3	2	0.2	2.44	2.32	8.25	1.15	
4	12.587	-17.569	22/02/2011	40.4	3	3	0.2	1.61	0.49	2.64	0.53	
4	12.587	-17.569	22/02/2011	84.8	3	3	0.2	1.82	0.68	4.21	0.61	
6	12.567	-18.824	23/02/2011	1.4	2	2	0.2	4.22	3.11	20.38	2.11	
6	12.567	-18.824	23/02/2011	8.1	2	2	0.2	11.02	3.51	19.09	2.48	0.2
6	12.567	-18.824	23/02/2011	15.1	2	2	0.2	1.35	2.86	15.12	1.74	0.2
6	12.567	-18.824	23/02/2011	21.1	2	2	0.2	5.7	2.72	16.14	2.29	0.2
6	12.567	-18.824	23/02/2011	26.2	2	2	0.2	1.15	2.52	11.5	1.59	0.2
6	12.567	-18.824	23/02/2011	36.5	2	2	0.2	5.83	2.85	9.37	1.27	

Table 2. (continued)

Station	Lat (°N)	Long (°W)	Date (dd/mm/yyyy)	Depth (m)	Filtered Volume (L)			Heme *b* (pmol L^{-1})	Chl *a* (nmol L^{-1})	POC (µmol L^{-1})	PON (µmol L^{-1})	N_2 Fixation (nmol N L^{-1} d^{-1})
					Heme *b*	POC/N	Chl *a*					
Central TNA												
7	12.577	-21.818	24/02/2011	1.4	4	3	0.2	0.4	0.52	2.03	0.33	0.65
7	12.577	-21.818	24/02/2011	20.4	4	3	0.2		0.57	1.74	0.25	1.61
7	12.577	-21.818	24/02/2011	30.6	4	3	0.2		0.23	1.2	0.19	0.66
7	12.577	-21.818	24/02/2011	40.4	4	3	0.2	0.27	0.26			3.53
7	12.577	-21.818	24/02/2011	50.6	3	3	0.2	0.43	0.75	3.08	0.45	0.35
7	12.577	-21.818	24/02/2011	71		3				0.73	0.29	
8	12.585	-23.557	25/02/2011	2	3	3	0.2	0.8	0.23	3.02	0.41	3.25
8	12.585	-23.557	25/02/2011	15.2	3	3	0.2	1	0.3	2.17	0.28	8.94
8	12.585	-23.557	25/02/2011	30.4	3	3	0.2	1.18	0.23	2.39	0.3	
8	12.585	-23.557	25/02/2011	45.3	3	3	0.2	1.21	0.29	1.91	0.25	3.42
8	12.585	-23.557	25/02/2011	55.8	3	3	0.2	2.95	0.62	2.73	0.39	3.04
9	12.3	-25.128	26/02/2011	3.2	4	3	0.2	0.87	0.16	2.14	0.17	6.17
9	12.3	-25.128	26/02/2011	21.6	4	3	0.2	0.69	0.18	1.95	0.21	4.64
9	12.3	-25.128	26/02/2011	31.8								1.81
9	12.3	-25.128	26/02/2011	51.8	4	2	0.2	2.75	0.22	2.52	0.2	0.42
9	12.3	-25.128	26/02/2011	81.6	4	3	0.2	3.29	0.36	1.55	0.19	0.62
9	12.3	-25.128	26/02/2011	91		2				2.01	0.18	
17	10.627	-28.731	11/03/2011	2.2	4	4	0.2	2.99	0.21	1.23	0.19	3.87
17	10.627	-28.731	11/03/2011	22.2	4	4	0.2		0.24	1.25	0.16	6.22
17	10.627	-28.731	11/03/2011	31.8	4	4	0.2		0.21	1.32	0.18	1.26
17	10.627	-28.731	11/03/2011	51.4	4	4	0.2	0.3	0.24	1.34	0.18	10.88
17	10.627	-28.731	11/03/2011	61.7	4	4	0.2	0.37	0.42	2	0.3	1.03
17	10.627	-28.731	11/03/2011	81.8	4	4	0.2	0.56	0.29	0.92	0.16	
18	12.054	-28.98	12/03/2011	2.1	4	4	0.2		0.14	1.22	0.11	0.65
18	12.054	-28.98	12/03/2011	21	4	4	0.2	0.43	0.14	1.41	0.16	0.75
18	12.054	-28.98	12/03/2011	41.4	4	4	0.2		0.22	1.48	0.21	2.02
18	12.054	-28.98	12/03/2011	57.4	4	4	0.2		0.3	1.35	0.18	1.87

Table 2. (continued)

Station	Lat (°N)	Long (°W)	Date (dd/mm/yyyy)	Depth (m)	Filtered Volume (L)			Heme *b* (pmol L^{-1})	Chl *a* (nmol L^{-1})	POC (µmol L^{-1})	PON (µmol L^{-1})	N_2 Fixation (nmol N L^{-1} d^{-1})
					Heme *b*	POC/N	Chl *a*					
18	12.054	-28.98	12/03/2011	69.3	4	4	0.2	1.43	0.82	2.54	0.36	0.29
18	12.054	-28.98	12/03/2011	76.3	4	4	0.2		0.58	1.39	0.21	
Tropical South Atlantic												
10	-7.218	-24.993	04/03/2011	3.9	4	4	0.2		0.05			0.2
10	-7.218	-24.993	04/03/2011	31.6	4	4	0.2		0.07			0.24
10	-7.218	-24.993	04/03/2011	60.7	4	4	0.2	0.6	0.1			0.2
10	-7.218	-24.993	04/03/2011	81.5	4	4	0.2	0.78	0.13	1.29	0.17	0.2
10	-7.218	-24.993	04/03/2011	111.4	4	4	0.2	0.61	0.35	1.36	0.22	0.44
10	-7.218	-24.993	04/03/2011	121.6	4	4	0.2	0.68	0.3	0.69	0.1	
Equatorial Upwelling												
11	-3.261	-25.52	05/03/2011	1.8	4	4	0.2	0.33	0.13	1.08	0.12	6.11
11	-3.261	-25.52	05/03/2011	21.6	4	4	0.2	0.22	0.12	1.14	0.13	4.93
11	-3.261	-25.52	05/03/2011	41.5	4	4	0.2	0.59	0.23	1.53	0.21	0.79
11	-3.261	-25.52	05/03/2011	61.6	4	4	0.2	0.56	0.3	1.3	0.21	0.25
11	-3.261	-25.52	05/03/2011	76.4	4	4	0.2	2.6	0.55	2.09	0.3	1.98
11	-3.261	-25.52	05/03/2011	121.5	4	4	0.2	1.16	0.14	0.58	0.09	
12	-1.173	-25.794	06/03/2011	1.9	4	4	0.2	0.73	0.11	1.07	0.15	2.6
12	-1.173	-25.794	06/03/2011	19.6	4	4	0.2	0.25	0.12	1.22	0.14	
12	-1.173	-25.794	06/03/2011	40.1	4	4	0.2	0.69	0.17	0.99	0.1	0.21
12	-1.173	-25.794	06/03/2011	49.7	4	4	0.2	3.49	0.3	1.67	0.23	0.21
12	-1.173	-25.794	06/03/2011	60.3	4	4	0.2	0.59	0.56	1.66	0.23	0.64
12	-1.173	-25.794	06/03/2011	69.8	4	4	0.2	1.07	0.25	1	0.15	
13	1.157	-26.046	07/03/2011	2.6	4	4	0.2		0.14	0.88	0.09	3.33
13	1.157	-26.046	07/03/2011	21.6	4	4	0.2		0.16	0.94	0.09	2.82
13	1.157	-26.046	07/03/2011	41.4	4	4	0.2	0.64	0.23	1.24	0.19	0.44
13	1.157	-26.046	07/03/2011	51.5	4	4	0.2	0.37	0.37	1.5	0.23	0.2

Table 2. (continued)

Station	Lat (°N)	Long (°W)	Date (dd/mm/yyyy)	Depth (m)	Filtered Volume (L)			Heme *b* (pmol L^{-1})	Chl *a* (nmol L^{-1})	POC (µmol L^{-1})	PON (µmol L^{-1})	N_2 Fixation (nmol N L^{-1} d^{-1})
					Heme *b*	POC/N	Chl *a*					
13	1.157	-26.046	07/03/2011	60.7	4	4	0.2	0.71	0.6	1.92	0.28	0.33
13	1.157	-26.046	07/03/2011	75.9	3.5	4	0.2	0.82	0.32	0.99	0.15	
14	3.33	-26.81	08/03/2011	3.4	4	4	0.2	0.38	0.3	2.15	0.33	2.42
14	3.33	-26.81	08/03/2011	21.3	4	4	0.2	0.81	0.29	2	0.27	4.92
14	3.33	-26.81	08/03/2011	36.4	4	4	0.2	0.72	0.35	1.97	0.27	3.24
14	3.33	-26.81	08/03/2011	46.2	4	4	0.2	0.61	0.47	1.77	0.25	1.09
14	3.33	-26.81	08/03/2011	56.3	4	4	0.2	0.83	0.48	1.48	0.2	0.48
14	3.33	-26.81	08/03/2011	61.7	4	4	0.2	0.56	0.29	0.81	0.13	
15	5.662	-27.499	09/03/2011	1.4	4	4	0.2		0.18	1.42	0.22	4.17
15	5.662	-27.499	09/03/2011	21.5	4	4	0.2	0.27	0.16	2.04	0.23	3.12
15	5.662	-27.499	09/03/2011	31.6	4	4	0.2	0.72	0.19	1.43	0.22	5.38
15	5.662	-27.499	09/03/2011	31.9	4	4	0.2	0.58	0.18	1.97	0.3	5.51
15	5.662	-27.499	09/03/2011	38.8	4	4	0.2	1.52	0.4	1.99	0.29	6.12
15	5.662	-27.499	09/03/2011	71.6	4	4	0.2	0.38	0.28	0.97	0.15	
16	8.339	-28.332	10/03/2011	3.1	4	4	0.2		0.22	1.6	0.22	4.35
16	8.339	-28.332	10/03/2011	20.7	4	4	0.2	0.42	0.2	1.31	0.2	0.6
16	8.339	-28.332	10/03/2011	31	4	4	0.2	0.25	0.21	1.15	0.16	8.66
16	8.339	-28.332	10/03/2011	50.1	4	4	0.2	0.44	0.32	1.77	0.28	3.86
16	8.339	-28.332	10/03/2011	58.1	4	4	0.2	1	1.43	4.98	0.7	0.49
16	8.339	-28.332	10/03/2011	70.9	4	4	0.2	1.19	1.26	3.1	0.41	
East STNA gyre												
19	15.509	-28.786	13/03/2011	1.7	4	4	0.2		0.11	1.22	0.16	0.61
19	15.509	-28.786	13/03/2011	21.5	4	4						3.56
19	15.509	-28.786	13/03/2011	51.2	4	4	0.2	2.25	0.17	0.73	0.13	1.41
19	15.509	-28.786	13/03/2011	68.2	4	4	0.2		0.27	1.34	0.15	0.93
19	15.509	-28.786	13/03/2011	79.3	4	4	0.2		0.43	1	0.16	0.2
19	15.509	-28.786	13/03/2011	96.1	3.5	4	0.2		0.18	0.6	0.1	

Table 2. (continued)

Station	Lat (°N)	Long (°W)	Date (dd/mm/yyyy)	Depth (m)	Filtered Volume (L)			Heme *b* (pmol L^{-1})	Chl *a* (nmol L^{-1})	POC (µmol L^{-1})	PON (µmol L^{-1})	N_2 Fixation (nmol N L^{-1} d^{-1})
					Heme *b*	POC/N	Chl *a*					
13	1.157	-26.046	07/03/2011	60.7	4	4	0.2	0.71	0.6	1.92	0.28	0.33
13	1.157	-26.046	07/03/2011	75.9	3.5	4	0.2	0.82	0.32	0.99	0.15	
14	3.33	-26.81	08/03/2011	3.4	4	4	0.2	0.38	0.3	2.15	0.33	2.42
14	3.33	-26.81	08/03/2011	21.3	4	4	0.2	0.81	0.29	2	0.27	4.92
14	3.33	-26.81	08/03/2011	36.4	4	4	0.2	0.72	0.35	1.97	0.27	3.24
14	3.33	-26.81	08/03/2011	46.2	4	4	0.2	0.61	0.47	1.77	0.25	1.09
14	3.33	-26.81	08/03/2011	56.3	4	4	0.2	0.83	0.48	1.48	0.2	0.48
14	3.33	-26.81	08/03/2011	61.7	4	4	0.2	0.56	0.29	0.81	0.13	
15	5.662	-27.499	09/03/2011	1.4	4	4	0.2		0.18	1.42	0.22	4.17
15	5.662	-27.499	09/03/2011	21.5	4	4	0.2	0.27	0.16	2.04	0.23	3.12
15	5.662	-27.499	09/03/2011	31.6	4	4	0.2	0.72	0.19	1.43	0.22	5.38
15	5.662	-27.499	09/03/2011	31.9	4	4	0.2	0.58	0.18	1.97	0.3	5.51
15	5.662	-27.499	09/03/2011	38.8	4	4	0.2	1.52	0.4	1.99	0.29	6.12
15	5.662	-27.499	09/03/2011	71.6	4	4	0.2	0.38	0.28	0.97	0.15	
16	8.339	-28.332	10/03/2011	3.1	4	4	0.2		0.22	1.6	0.22	4.35
16	8.339	-28.332	10/03/2011	20.7	4	4	0.2	0.42	0.2	1.31	0.2	0.6
16	8.339	-28.332	10/03/2011	31	4	4	0.2	0.25	0.21	1.15	0.16	8.66
16	8.339	-28.332	10/03/2011	50.1	4	4	0.2	0.44	0.32	1.77	0.28	3.86
16	8.339	-28.332	10/03/2011	58.1	4	4	0.2	1	1.43	4.98	0.7	0.49
16	8.339	-28.332	10/03/2011	70.9	4	4	0.2	1.19	1.26	3.1	0.41	
East STNA gyre												
19	15.509	-28.786	13/03/2011	1.7	4	4	0.2		0.11	1.22	0.16	0.61
19	15.509	-28.786	13/03/2011	21.5	4	4						3.56
19	15.509	-28.786	13/03/2011	51.2	4	4	0.2	2.25	0.17	0.73	0.13	1.41
19	15.509	-28.786	13/03/2011	68.2	4	4	0.2		0.27	1.34	0.15	0.93
19	15.509	-28.786	13/03/2011	79.3	4	4	0.2		0.43	1	0.16	0.2
19	15.509	-28.786	13/03/2011	96.1	3.5	4	0.2		0.18	0.6	0.1	

Table 2. (continued)

Station	Lat (°N)	Long (°W)	Date (dd/mm/yyyy)	Depth (m)	Filtered Volume (L)			Heme *b* (pmol L^{-1})	Chl *a* (nmol L^{-1})	POC (µmol L^{-1})	PON (µmol L^{-1})	N_2 Fixation (nmol N L^{-1} d^{-1})
					Heme *b*	POC/N	Chl *a*					
20	17.399	-28.395	14/03/2011	2.7	4	4	0.2	0.25	0.11	1.24	0.15	1.66
20	17.399	-28.395	14/03/2011	25.3	4	4	0.2		0.1	1.13	0.14	2.27
20	17.399	-28.395	14/03/2011	54.7	4	4	0.2	0.24	0.14	1.07	0.1	0.73
20	17.399	-28.395	14/03/2011	73.9	4	4	0.2		0.3	1.33	0.2	0.2
20	17.399	-28.395	14/03/2011	90.5	4	4	0.2	0.42	0.48	1.15	0.16	0.2
20	17.399	-28.395	14/03/2011	105	3.2		0.2		0.43			
20	17.399	-28.395	14/03/2011	129.4	3.4	4	0.2	0.67	0.18	0.71	0.12	
21	19.115	-28.131	15/03/2011	6.6	4	2	0.2	0.24	0.12			1.64
21	19.115	-28.131	15/03/2011	21.3	4	4	0.2	2.24	0.13	1.05	0.08	3.65
21	19.115	-28.131	15/03/2011	41.9	3.7	2	0.2	0.23	0.12			2.43
21	19.115	-28.131	15/03/2011	61	4	4	0.2	0.59	0.15	1.02	0.1	1.86
21	19.115	-28.131	15/03/2011	76	4	4	0.2	1.16	0.22	1.11	0.16	0.24
21	19.115	-28.131	15/03/2011	111.6	3.3	2	0.2	0.61	0.48	1.18	0.33	
21	19.115	-28.131	15/03/2011	145		4				1.12	0.16	
21	19.17	-28.115	15/03/2011	12.3	4	4	0.2		0.14	1.08	0.1	
21	19.17	-28.115	15/03/2011	22.2		4				1.59	0.15	
21	19.17	-28.115	15/03/2011	31.9	4	4	0.2		0.15	0.95	0.07	
21	19.17	-28.115	15/03/2011	41	4	4	0.2		0.16	1.02	0.1	
21	19.17	-28.115	15/03/2011	51	4	4	0.2		0.21	1.11	0.14	
21	19.17	-28.115	15/03/2011	62	4	4	0.2		0.2	1.2	0.15	
21	19.17	-28.115	15/03/2011	81.8	4	4	0.2		0.26	0.95	0.12	
21	19.17	-28.115	15/03/2011	102.3	4	4	0.2	0.42	0.34	1.15	0.16	

Table 3. D361 - FISH samples

FISH	Lat (°N)	Long (°W)	Date (dd/mm/yyyy)	Filtered Volume (L)		Heme *b* (pmol L^{-1})	Chl *a* (nmol L^{-1})
				Heme *b*	Chl *a*		
5	26.6826	-16.5349	18/02/2011	4	0.2	0.1	0.17
7	25.9329	-16.751	18/02/2011	4	0.2	0.44	0.25
12	24.1798	-17.249	19/02/2011	4	0.2	0.25	0.48
14	23.52	-17.4242	19/02/2011	4	0.2	0.17	0.54
18	22.0716	-17.819	19/02/2011	4	0.2	1.1	0.87
19	21.7355	-17.9068	19/02/2011	4	0.2	0.47	3.41
23	19.8912	-18.1576	20/02/2011	4	0.2	0.69	2.58
27	18.5464	-18.1556	20/02/2011	4	0.2	0.77	1.12
29	17.8645	-18.1544	20/02/2011	3	0.2	2.02	1.29
35	15.3806	-18.1656	21/02/2011	3	0.2	1.7	3.59
40	13.967	-18.0702	21/02/2011	3	0.2	0.08	12.67
42	13.2025	-17.981	21/02/2011	2	0.2	2.87	4.99
55	12.5936	-19.1654	23/02/2011	4	0.2	1.33	0.37
58	12.5843	-20.253	23/02/2011	4	0.2	0.08	0.14
73	12.2037	-25.6426	26/02/2011	5	0.2	0.15	0.13
75	11.6025	-25.741	26/02/2011	5	0.2	0.18	0.15
81	9.5333	-25.6579	27/02/2011	4	0.2	0.07	0.17
85	8.2626	-25.6113	27/02/2011	5	0.2	0.11	0.14
93	5.4448	-25.4951	28/02/2011	5	0.2	0.41	0.15
97	4.0025	-25.4369	28/02/2011	5	0.2	0.11	0.13
105	1.2354	-25.3367	01/03/2011	5	0.2	0.27	0.16
111	-0.7128	-25.263	01/03/2011	4	0.2	0.11	0.15
123	-3.8958	-25.1331	02/03/2011	4	0.2	0.38	0.11
127	-4.1753	-25.1201	02/03/2011	5	0.2	0.11	0.09
136	-4.8006	-25.0836	02/03/2011	5	0.2	0.16	0.06
148	-6.3558	-25.0209	03/03/2011	5	0.2	0.06	0.07
150	-6.9561	-25.0027	03/03/2011	5	0.2	0.06	0.06
157	-5.3317	-25.1887	04/03/2011	5	0.2	0.04	0.06
166	-2.605	-25.6623	05/03/2011	5	0.2	0.18	0.16
173	-0.2732	-25.8809	06/03/2011	4	0.2	0.11	0.13
178	1.3417	-26.1162	07/03/2011	4	0.2	0.18	0.24
180	1.9413	-26.3442	07/03/2011	3	0.2	0.33	0.23
212	12.449	-28.9708	12/03/2011	4	0.2	0.07	0.14
216	13.8032	-28.9023	12/03/2011	4	0.2	0.07	0.14
232	19.3843	-27.9149	15/03/2011	4	0.2	0.06	0.11